National Library of Canada
Bibliothèque nationale du Canada

Canadian Theses Service
Service des thèses canadiennes

Ottawa, Canada
K1A 0N4

NOTICE

The quality of this microform is heavily dependent upon the quality of the original thesis submitted for microfilming. Every effort has been made to ensure the highest quality of reproduction possible.

If pages are missing, contact the university which granted the degree.

Some pages may have indistinct print especially if the original pages were typed with a poor typewriter ribbon or if the university sent us an inferior photocopy.

Reproduction in full or in part of this microform is governed by the Canadian Copyright Act, R.S.C. 1970, c. C-30, and subsequent amendments.

AVIS

La qualité de cette microforme dépend grandement de la qualité de la thèse soumise au microfilmage. Nous avons tout fait pour assurer une qualité supérieure de reproduction.

S'il manque des pages, veuillez communiquer avec l'université qui a conféré le grade.

La qualité d'impression de certaines pages peut laisser à désirer, surtout si les pages originales ont été dactylographiées à l'aide d'un ruban usé ou si l'université nous a fait parvenir une photocopie de qualité inférieure.

La reproduction, même partielle, de cette microforme est soumise à la Loi canadienne sur le droit d'auteur, SRC 1970, c. C-30, et ses amendements subséquents.

NL-339 (r. 88/04) c

Canada

UNIVERSITY OF ALBERTA

INVESTIGATIONS OF ELECTROSPRAY IONIZATION MASS SPECTROMETRY

BY

MICHAEL GEORGE IKONOMOU

A THESIS SUBMITTED TO

THE FACULTY OF GRADUATE STUDIES AND RESEARCH

IN PARTIAL FULFILLMENT OF THE REQUIREMENTS FOR THE

DEGREE OF DOCTOR OF PHILOSOPHY

DEPARTMENT OF CHEMISTRY

EDMONTON, ALBERTA

FALL 1990

National Library of Canada
Bibliothèque nationale du Canada

Canadian Theses Service
Service des thèses canadiennes

Ottawa, Canada
K1A 0N4

The author has granted an irrevocable non-exclusive licence allowing the National Library of Canada to reproduce, loan, distribute or sell copies of his/her thesis by any means and in any form or format, making this thesis available to interested persons.

The author retains ownership of the copyright in his/her thesis. Neither the thesis nor substantial extracts from it may be printed or otherwise reproduced without his/her permission.

L'auteur a accordé une licence irrévocable et non exclusive permettant à la Bibliothèque nationale du Canada de reproduire, prêter, distribuer ou vendre des copies de sa thèse de quelque manière et sous quelque forme que ce soit pour mettre des exemplaires de cette thèse à la disposition des personnes intéressées.

L'auteur conserve la propriété du droit d'auteur qui protège sa thèse. Ni la thèse ni des extraits substantiels de celle-ci ne doivent être imprimés ou autrement reproduits sans son autorisation.

ISBN 0-315-65037-0

University of Alberta
Edmonton
Canada T6G 2G2

Department of Chemistry
Faculty of Science
F3-44 Chemistry Bldg. Tel. (403) 492-3254 Fax (403) 492-8231

March 20, 1990

From: Dr. J. W. Lown; Dr. A. Naghipur. Dr. P. Kebarle

To: M. G. Ikonomou.

Dear Michael:

This is a letter of permission by which we fully authorize you to reproduce in your Ph.D thesis material from our co-authored publications:

(a) Naghipur, A.; Ikonomou, M. G.; Kebarle, P.; Lown, J. W. Mechanism of Action of (2-Haloethyl)nitrosoureas on DNA: Discrimination between Alternative Pathways of DNA-Base Modification by 1, 3-Bis(2-fluorogthy)-1-nitrosourea Using Specific Deuterium Labelling: Reaction Product Identification by HPLC/Tandem Mass Spectrometry. *J. Amer. Chem. Soc.* (In Press, Manuscript No. JA891672R-20-7-150).

(b) Ikonomou, M. G.; Naghipur, A.; Lown, J. W.; Kebarle, P. Characterization of the Reaction Products of Deoxyguanosine with the Anticancer Agent BFNU and BFNU-1,1,1',1'-d4 in Different Buffers by HPLC/API-MS/MS. *Biom. & Envir. Mass Spectrom.* (In Press, Manuscript No. F/1040)

Yours sincerely,

J. W Lown (Professor)

A. Naghipur (PDF)

P. Kebarle (Professor)

University of Alberta
Edmonton
Canada T6G 2G2

Department of Chemistry
Faculty of Science
F3-44 Chemistry Bldg. Tel. (403) 492-3254 Fax (403) 492-8231

May 20, 1990

To: M. G. Ikonomou.

From: Dr. P. Kebarle; Dr. A. T. Blades;. Dr. P. Jayaweera.

Dear Michael:

This is a letter of permission by which we fully authorize you to reproduce in your Ph.D thesis material from our co-authored publications:

1. Ikonomou, M. G.; Blades, A. T.; Kebarle, P. Investigations of the Electrospray Interface for Liquid Chromatography -- Mass Spectrometry. *Anal. Chem.* **1990**, *62*, 957-967.

2. Jayaweera, P.; Blades, A.T.; Ikonomou, M. G.; Kebarle, P. Production and Study in the Gas Phase of Multiply Charged Solvated or Coordinated Metal Ions. *J. Amer. Chem Soc.* **1990**, *112*, 2452-2454.

3. Blades, A.T.; Jayaweera, P.; Ikonomou, M. G.; Kebarle, P. First Studies of Alkaline Earth Transition Metal Ions, M^{++}, Gas Phase Ion Chemistry. *J. Chem. Phys.* (In Press).

4. Blades, A.T.; Jayaweera, P.; Ikonomou, M. G.; Kebarle, P. Ion-Molecule Clusters Involving Doubly Charged, M^{++}, Metal Ions. *Int. J. Mass Spectrom. Ion Processes* (In Press).

5. Blades, A.T.; Jayaweera, P.; Ikonomou, M. G.; Kebarle, P. First Studies of M^{+3} Metal ion Ligands, Gas Phase Ion Chemistry. *Int. J. Mass Spectrom. Ion Processes* (In Press).

Yours sincerely,

P. Kebarle (Professor) A. T. Blades P. Jayaweera

UNIVERSITY OF ALBERTA

RELEASE FORM

NAME OF AUTHOR: MICHAEL GEORGE IKONOMOU

TITLE OF THESIS: INVESTIGATIONS OF ELECTROSPRAY IONIZATION MASS SPECTROMETRY

DEGREE FOR WHICH THESIS WAS PRESENTED: Ph.D.

YEAR THIS DEGREE GRANTED: 1990

PERMISSION IS HEREBY GRANTED TO THE UNIVERSITY OF ALBERTA LIBRARY TO REPRODUCE SINGLE COPIES OF THIS THESIS AND TO LEND OR SELL SUCH COPIES FOR PRIVATE, SCHOLARLY OR SCIENTIFIC RESEARCH PURPOSES ONLY.

THE AUTHOR RESERVES OTHER PUBLICATION RIGHTS, AND NEITHER THE THESIS NOR EXTENSIVE EXTRACTS FROM IT MAY BE PRINTED OR OTHERWISE REPRODUCED WITHOUT THE AUTHOR'S WRITTEN PERMISSION.

SIGNED: 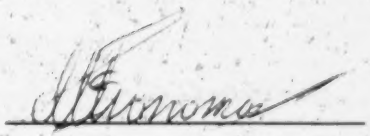

PERMANENT ADDRESS: Profitou Ilia 18
Erythres, Attikis
GREECE

DATED: September 20, 1990

THE UNIVERSITY OF ALBERTA

FACULTY OF GRADUATE STUDIES AND RESEARCH

THE UNDERSIGNED CERTIFY THAT THEY HAVE READ, AND RECOMMENDED TO THE FACULTY OF GRADUATE STUDIES AND RESEARCH FOR ACCEPTANCE, A THESIS ENTITLED **INVESTIGATIONS OF ELECTROSPRAY IONIZATION MASS SPECTROMETRY** SUBMITTED BY **MICHAEL GEORGE IKONOMOU** IN PARTIAL FULFILLMENT OF THE REQUIREMENTS FOR THE DEGREE OF **DOCTOR OF PHILOSOPHY.**

Supervisor _____
Dr. P. Kebarle

Committee Chairman _____
Dr. G. Horlick

Committee Member _____
Dr. N. Dovichi

Committee Member _____
Dr. L. Hepler

Committee Member _____
Dr. F. Pasutto

External Examiner _____
Dr. R. K. Boyd
Senior Research Officer
NRC Halifax, Nova Scotia
CANADA

DATED: September 20, 1990

To my parents Georgios and Eleni (Nitsa),

and to my wife Vasiliki

ABSTRACT

Electrospray (ESP) is one of the most modern Mass Spectrometric ionization methods that provides abundant yields of intact gas phase ions from large non-volatile and thermally labile species in solution. In the present study the positive ions produced by electrospray from solutions of various analytes in methanol were detected with an atmospheric pressure triple quadrupole mass spectrometer. Analytes studied included: NH_4^+, Na^+, K^+, Cs^+, Ca^{++} and the onium ions BH^+ of some 30 organic nitrogen bases B. The analyte ion sensitivities decrease with analyte ion concentration and presence of foreign electrolyte in the solution, at concentrations above 10^{-5} mol/L. At low concentrations, sensitivities are very high such that ions at 10^{-8} mol/L concentration can be detected easily. Detection limits in the sub-femtomol-attomol range have been achieved. The sensitivity of the organic bases B is pH dependent and increases as the BH^+ concentration in solution increases. However, the effect is obscured by the depression of the ion signal caused by foreign electrolyte. It is also shown that above 10^{-5} mol/L B in solution, gaseous B at sufficient pressure can be generated and gas phase proton transfer to higher gas phase basicity coanalytes can occur. Dimers, B_2H^+, may also be formed in the gas phase. The gas phase ion reaction time is estimated as ~ 2 ms.

A comparative study between ESP and Ion Spray (pneumatically assisted electrospray) was undertaken. High yields of positively charged droplets and gas phase ions ($\approx 10^{-7}$ A) are produced with both ESP and Ion Spray when the capillary is exposed to high voltages. Ion Spray, however, produces ions even in the absence of any electric field between the sprayer and the counter electrode, with yields $\approx 10^{-11}$ A. In either case (i.e. high field versus zero-field conditions) charge separation, or droplet charging, takes place at the sprayer's tip and not during the droplets' travel to the counter electrode. Differences between the two techniques depend mostly on their operational characteristics. For a specific application, one can choose between the two on the basis of their performance according to the requirements of the application.

By electrospraying solutions of metal salts in methanol-water, high yields of doubly and triply charged metal-ion-ligand (L) clusters, $M^{z+}(L)_n$ where M (Mg, Ca, Sr, Ba, Mn, Fe,

Co, Ni, Cu, Zn, Y, La, Ce, Nd, Sm), could be produced in the gas phase and detected with the mass spectrometer. The relative distribution of water clusters for some ions were close to the predicted gas phase equilibrium values. The clusters have n ≈ 10 and the binding energies are in the 15 kcal/mol range. Bonding of the ligands at n < 6 is much stronger. The ion-ligand interactions can be studied by collisional-induced dissociation (CID) in the triple quadrupole. Single ligand loss at high n values gives way to charge reduction at low n values upon CID of $M^{z+}(L)_n$. The water clusters undergo the charge reduction: $M^{2+}(H_2O)_n = MOH^+(H_2O)_{n-2} + H_3O^+$. Different ligands may accelerate (NH_3, pyridine) or retard (DMF, DMSO) the onset of charge reduction. Charge reduction with DMF and DMSO occurs by simple charge transfer: $M^{2+}(DMSO)_n = M^+(DMSO)_{n-1} + DMSO^+$. Polydentate cage type ligands protect ions from charge reduction. Thus the only triply charged M^{3+} so far observed was Co^{3+} sepulchrate where the ion is coordinated to six nitrogens.

The heated nebulizer / corona discharge combination is a complementary method to electrospray and has been used successfully to couple HPLC to mass spectrometry. In this combination the total effluent from the HPLC column is introduced into the atmospheric pressure ionization (API) source of the triple quadrupole mass spectrometer via a heated nebulizer. The gasified mixture produced from the heated nebulizer is exposed to corona discharge ionization which leads to ionization of analytes via gas phase chemical ionization. In Chapter 5 a practical application utilizing the heated nebulizer / corona discharge HPLC/MS interface is described. The products of the reaction of the anticancer agent 1,3-bis(2-fluoroethyl)-1-nitrosourea (BFNU), and of its labelled form BFNU-1,1,1',1'-d_4, with the DNA base deoxyguanosine, were characterized by HPLC/MS/MS. The ions formed by LC/API-MS, and their MS/MS spectra, allowed unambiguous identification of the products of the reaction under a variety of experimental conditions, and also assignment of positions of the deuterium atoms. The identification and characterization of a variety of 7-(2'-haloethyl)guanine derivatives among the reaction products provides confirmation of a proposed mechanism for the action of BFNU on DNA bases.

ACKNOWLEDGEMENTS

I would like to express my sincere gratitude to my advisor, Professor Paul Kebarle, for providing me the opportunity and encouragement to perform the research described in this dissertation.

I especially thank my friend and co-worker, Dr. Arthur T. Blades, for providing helpful suggestions and valuable comments during those endless discussions concerning interpretation of the mysterious electrospray data.

The assistance and advice of Dr. Allan Hogg on mass spectrometric related issues is greatly appreciated.

I would also like to thank members of Dr. Kebarle's group, in particular, Gary J. C. Paul for his daily amusement, and Dr. Lou S. Crocker for proof reading parts of this manuscript.

Thanks are extended to members of the Chemistry Department, Machine, Electronics, and Glassblowing workshops, the Physical Sciences Library, and to staff of the Analytical Mass Spectrometry laboratory, for their contributions and advice.

The financial assistance provided by the Chemistry Department, University of Alberta, and the Natural Science and Engineering Research Council of Canada is acknowledged.

TABLE OF CONTENTS

Page

CHAPTER 1. GENERAL INTRODUCTION 1

INTRODUCTION 2

a. Electrospray Atomization 2

b. Electrospray Ionization Mass Spectrometry 5

c. The Present Work 9

REFERENCES 14

CHAPTER 2. INVESTIGATIONS OF THE ELECTROSPRAY INTERFACE FOR LIQUID CHROMATOGRAPHY / MASS SPECTROMETRY 19

INTRODUCTION 20

EXPERIMENTAL SECTION 21

The Atmospheric Pressure Mass Spectrometer 21

RESULTS AND DISCUSSION 25

a. The Electrospray Ionization Total Ion Currents and Spatial Distribution 25

b. Sensitivities for Mass Analyzed Ions: pH Dependence of Nitrogen Bases from Electrosprayed Solutions 32

c. Coanalyte Interference: Proton Transfer in Solution and in the Gas Phase 47

d. Residence Time of Electrosprayed Ions in the Atmospheric Pressure Region 53

CONCLUSIONS 57

APPENDIX 2-I. Partial Pressures of Compounds Evaporating from Electrosprayed Droplets 59

APPENDIX 2-II. Evaluation of BH^+ Concentrations in Methanol 60

APPENDIX 2-III. Drift Time of Ions in the Electrospray Field 61

REFERENCES 65

CHAPTER 3. A COMPARATIVE STUDY OF ELECTROSPRAY AND ION SPRAY IONIZATION MASS SPECTROMETRY IN THE POSITIVE ION MODE 68

INTRODUCTION 69

EXPERIMENTAL SECTION 71

a. The Atmospheric Pressure Ion Source Mass Spectrometer 71

b. Intermediate Electrode Experiments 74

RESULTS AND DISCUSSION 77

a. Pneumatically Assisted Electrospray (Ion Spray) Operation 77

b. Effect of Ionization Voltage on Analyte Ions Generated by ESP, HYP-ESP, and Ion Spray 86

c. Mass Spectrometric Ion Sampling Efficiency Under HYP-ESP and Ion~Spray Ionization Conditions 95

d. Origin of Ions Generated by Ion Spray Under No-Field Conditions 99

CONCLUSIONS 105

APPENDIX 3-I. Diagrams of Ion Spray (B) and (C) Type Experiments 107

APPENDIX 3-II. Summary and Conclusions of the Performance Comparison Between Electrospray and Ion Spray 108

a. General 108

b. Sensitivity and Stability as a Function of Flow Rate 108
c. Relative Sensitivities of Organic Bases 109
d. Dependence of Analyte Signal on Ion Concentration 109
e. Sensitivities of Organic Bases at Various MeOH-H_2O Compositions 110
f. Sensitivities of Organic Bases in Different Solvents 110
g. Analyte Signal in Presence of Buffer 111

REFERENCES 112

CHAPTER 4. PRODUCTION AND STUDY IN THE GAS PHASE OF MULTIPLY CHARGED SOLVATED OR COORDINATED METAL IONS BY ELECTROSPRAY MASS SPECTROMETRY 114

INTRODUCTION 115

EXPERIMENTAL SECTION 119

RESULTS AND DISCUSSION 120

a. Features of Electrospray-Generated-Multiply-Charged Metal Ion Mass Spectra 120

b. Metal Ion Hydration Equilibria Measurements 125

c. Collision Induced Dissociation (CID) Mass Spectra of $M^{2+}(L)_n$ and $M^{3+}(L)_n$ Complexes. Ligand Loss Versus Charge Reduction 131

I. $M^{2+}(L)_n$ Complexes 131

II. $M^{3+}(L)_n$ Complexes 141

CONCLUSIONS 148

REFERENCES 149

CHAPTER 5. CHARACTERIZATION OF THE REACTION PRODUCTS OF DEOXYGUANOSINE WITH THE ANTICANCER AGENT BFNU AND BFNU-1,1,1',1'-d_4 IN DIFFERENT BUFFERS BY HPLC/API-MS/MS *152*

INTRODUCTION *153*

a. Action of Haloethylnitrosoureas on DNA Bases *153*

b. Description of LC/MS/MS Methodology Used to Identify the Reaction Products *154*

EXPERIMENTAL SECTION *157*

a. Reaction of Deoxyguanosine with BFNU *157*

b. Chromatography *157*

c. Mass Spectrometry *158*

RESULTS AND DISCUSSION *161*

a. API and CAD Mass Spectra of Authentic 7-(2'-Hydroxyethyl)-guanine and 7-(2'-Haloethyl)guanine Samples *161*

b. Characterization of 7-(2'-Fluoroethyl)guanine and 7-(2'-Hydroxyethyl)guanine Resulting from the Reaction of Deoxyguanosine with BFNU in TRIS *166*

c. Characterization of Dideuterated 7-(2'-Fluoroethyl)guanine Resulting from the Reaction of BFNU 1,1,1',1'-d_4 with Deoxyguanosine in TRIS *169*

d. Characterization of Dideuterated 7-(2'-Bromoethyl)guanine Resulting from the Reaction of Deoxyguanosine with BFNU in TRIS and in the Presence of KBr *175*

e. Characterization of Monodeuterated 7-(2'-Bromoethyl)guanine, the only Bromo-Derived Product, Resulting from the Reaction of Deoxyguanosine with BFNU 1,1,1',1'-d_4 in TRIS in the Presence of KBr 179

f. Characterization of 7-(2'-Hydroxyethyl)guanine and 7-(2'-Haloethyl)guanines and their Deuterium-Labeled Counterparts from the Reaction of Deoxyguanosine with BFNU or BFNU 1,1,1',1'-d_4 in Different Buffers....182

CONCLUSION....183

APPENDIX 5-I. Outline of Proposed Mechanism of DNA Base Modification by the Anticancer Alkylator BFNU....184

APPENDIX 5-II Calculation of Reaction Time Required for the CH_2-CH_2F Pyrolytic Bond Cleavage....186

APPENDIX 5-III. CAD Spectral Characteristics of Protonated 7-(2'-Haloethyl)guanines and Pathways of $(BH + H)^+$ Formation from 7-(2'-Haloethyl)guanines under LC/API-MS Conditions....186

APPENDIX 5-IV. Experimental Parameters that Cause Uncertainties in Quantifying the Reaction Products with the Present LC/MS/MS Instrumentation....189

REFERENCES....193

CHAPTER 6. CONCLUDING SUMMARY....196

a. The ESP/MS Study (Chapter 2)....197

b. The ESP Versus Ion Spray Study (Chapter 3)....199

c. Multiply Charged Metal-Ion-Ligand Complexes, $M^{z+}(L)_n$, Produced in the Gas Phase by ESP (Chapter 4)....200

d. The Combined HPLC/MS/MS Study (Chapter 5)....201

REFERENCES....203

LIST OF TABLES

Page

Table 2.1. Nitrogen Bases Used in Electrospray Experiments *42*

Table 3.1. Ion Sampling Efficiency with the Mass Spectrometer Under Standard HYP-ESP and HYP-ESP(A) Ionization Conditions..... *96*

Table 3.2. Ion Sampling Efficiency with the Mass Spectrometer Under Standard Ion Spray and Ion Spray(A) Ionization Methods..... *96*

Table 3.3. Summary of Selected HYP-ESP and Ion Spray Data..... *106*

Table 4.1. Thermochemical Data for Reactions $M^{z+}(H_2O)_{n-1} + H_2O = M^{z+}(H_2O)_n$ where z = 1 or 2..... *127*

Table 4.2. Ligand Number at which Charge Reduction from M^{2+} to M^+ Occurs in Preference to Neutral Ligand Expulsion..... *136*

Table 5.1. Guanosine Modification by BFNU or BFNU-1,1,1',1'-d_4. Hydroxyethyl-N-dG and Haloethyl-N7-dG Products Analyzed by HPLC/MS and HPLC/MS/MS *170*

LIST OF FIGURES

Page

Figure 1.1. Exponential increase in the number of papers, related to ESP/MS, presented at the annual meetings of the American Society of Mass Spectrometry 7

Figure 2.1. Schematic diagram of electrospray mass spectrometric apparatus 22

Figure 2.2. (A) Detailed diagram of ESP tip assembly. (B) Experimental arrangement used to measure total ion currents produced by electrospray ionization. 24

Figure 2.3. Total ion current produced by ESP as a function of NaCl concentration in methanol. 27

Figure 2.4. log-log plot of total ion current versus NaCl concentration 28

Figure 2.5. Total ion currents versus concentration for several electrolytes in a linear current versus log concentration plot. 29

Figure 2.6. Electrospray-produced ion currents to a 0.5 cm diameter area moved in a straight line across a plane electrode 31

Figure 2.7. Mass spectrum from electrosprayed 3×10^{-4} M solution of KNO_3 in methanol 33

Figure 2.8. Mass analyzed ion intensities: (A) electrosprayed $CsNO_3$ solution in methanol. (B) electrosprayed KNO_3 solution in methanol 35

Figure 2.9. (A) Mass spectrum from electrosprayed 10^{-5} M solution of cocaine hydrochloride in methanol. (B) 10^{-5} M cocaine hydrochloride in 1.6×10^{-4} M HCl solution in methanol 36

Figure 2.10. Ion intensities for protonated base BH^+ from electrosprayed cocaine hydrochloride in methanol solution 38

Figure 2.11. Effect of electrolytes on intensities of BH^+ ions 39

Figure 2.12. Observed ion intensities for BH^+ ions obtained by electrospray of 10^{-5} M solutions in methanol of the free bases B. Bases are identified in Table 2.1 ..... *41*

Figure 2.13. Observed ion intensities for BH^+ ions, same as in Figure 2.12, but 10^{-5} M solutions of the BHCl were used *43*

Figure 2.14. Effect of acidification of electrosprayed solutions on BH^+ ion intensity; (A) strong base; (B) weaker base *46*

Figure 2.15. Intensities of BH^+ ions from electrosprayed solutions of base pairs with equimolar concentrations in methanol *48*

Figure 2.16. Measured intensities of BH^+ ions from electrosprayed solutions of base pairs with equimolar concentration in methanol: (A) pure bases; (B)base hydrochlorides *49*

Figure 2.17. (A) Ion intensities of BH^+ and $B'H^+$, where B is tripropylamine added to the gas phase and B' is 4-methoxyaniline from electrosprayed solution containing 10^{-5} M of B'. (B) Ion intensities of BH^+ and $B'H^+$ where both ions originate from electrosprayed solutions which have constant concentration of $[B'] = 10^{-5}$ M and variable [B] *51*

Figure 2.18. Gas phase proton transfer between ions $B'H^+$ from electrosprayed base B' and a stronger base B added to the gas phase *55*

Figure 2.19. Electric field strength as function of distance between electrospray capillary tip and plane electrode *62*

Figure 3.1. Detailed schematic diagram of the Ion Spray ionization assembly *72*

Figure 3.2. Ion Spray arrangements used to investigate the effect of field and nebulization on Ion Spray ionization *75*

Figure 3.3. (A) Multiple ion monitoring spectrum of m/z 304 (BH^+ of cocaine) and m/z 33 ($CH_3OH_2^+$) as a function of Ion Spray nebulization pressure. (B) Ion intensity of m/z 304 as a function of

nebulization pressure from ion sprayed cocaine/HCl solutions in methanol and in buffer 78

Figure 3.4. (A) HYP-ESP mass spectrum of 10^{-5} M cocaine/HCl in methanol,. (B) Ion Spray mass spectrum of the same solution as in (A) 80

Figure 3.5. Same as Figure 3.4 but 10^{-5} M purine/HCl in methanol..... 82

Figure 3.6. Same as Figure 3.5 but 10^{-5} M $CsNO_3$ in methanol 83

Figure 3.7. BH^+ intensity as a function of curtain gas (ultrapure N_2) flow rate, ●, Ion Spray, ❑, HYP-ESP..... 85

Figure 3.8. (A) Total ion current to interface plate,TIC(IN), as a function of electrospray (ESP) ionization voltage, 10^{-11} mol/min cocaine/HCl in methanol. (B) Same as in (A) but for mass analyzed BH^+. (C) Single ion monitoring of BH^+, m/z 304, at different voltages and spray conditions as a function of time..... 87

Figure 3.9. (A) Same as in Figure 3.8A and 3.8B, respectively. ❑ HYP-ESP, ● Ion Spray, 60 psi 89

Figure 3.10. (A) Ion Spray generated positive ion mass spectrum, tip at zero volts, 10^{-11} mol/min cocaine/HCl solution in methanol, 60 psi. (B) Negative ion mass spectrum obtained under the same conditions as in (A) 91

Figure 3.11. (A) TIC(IN) as a function of ionization voltage. ❑ HYP-ESP (A), ● Ion Spray (A) conditions, 10^{-11} mol/min cocaine/HCl, 60 psi. (B) Same as in (A) but mass analyzed BH^+ dependence on ionization voltage 94

Figure 3.12. (A) i_1, ▲, TIC(IN), ●, and i_2, ○, dependence on ionization voltage from Ion Spray (B) type experiments, 10^{-11} mol/min cocaine/HCl. Ionization tip on line with intermediate electrode and interface plate orifices. (B) Same as in (A) but ionization tip 1 cm off axis. (C) Same as in (A) but mass analyzed BH^+ dependence on ionization voltage 101

Figure 3.13. (A) TIC(IN) dependence on ionization voltage from Ion Spray (C) type experiments, 10^{-11} mol/min cocaine/HCl, 60 psi. Ionization tip on line with the intermediate electrode and interface plate orifices. (B) Same as in (A) but mass analyzed BH^+ dependence on ionization voltage *103*

Figure 4.1. Electrospray mass spectrum of 10^{-4} M $CoBr_2$ in MeOH, with 1% H_2O at 10 μL/min *123*

Figure 4.2. (A) Electrospray mass spectrum of 10^{-4} M $CoBr_2$ in MeOH, with 10^{-2} M DMSO at 10 μL/min. (B) Same as in A but OR to CB voltage difference has been reduced to 5 V *124*

Figure 4.3. Relative intensities of alkali cation $M^+(H_2O)_n$ and isoelectronic alkaline earth $M^{2+}(H_2O)_n$ observed with the mass spectrometer *128*

Figure 4.4. (A) CID mass spectrum of $Mn^{2+}(H_2O)_6$ in Q2. (B) CID of $Mn^{2+}(H_2O)_4$ *132*

Figure 4.5. CID mass spectrum of $Ca^{2+}(H_2O)_3$ *133*

Figure 4.6. CID mass spectrum of $Ni^{2+}(H_2O)_5$ *134*

Figure 4.7. CID mass specrum of $Cu^{2+}(DMSO)_3$ *140*

Figure 4.8. Elements whose M^{II} salts led to $M^{2+}(L)_n$ shown in small circles. Elements whose M^{III} salts led to $M^{3+}(L)_n$ shown with shadowed circles. These led also to doubly charged ions. *142*

Figure 4.9. CID mass spectrum of $Y^{2+}OH(H_2O)_6$ *144*

Figure 4.10. CID mass spectrum of $La^{3+}(DMSO)_6$ *145*

Figure 5.1. Schematic of the triple quadrupole mass spectrometer with the heated nebulizer LC/MS interface *159*

Figure 5.2. (A) HPLC/UV (254 nm) chromatogram of a standard mixture of 1 nmol (authentic compounds were dissolved in 10% MeOH, 0.1 M NH_4Ac) each of 7-(2'-hydroxyethyl)guanine, 7-(2'-fluoroethyl)guanine, 7-(2'-chloroethyl)guanine.

(B) Reconstructed ion chromatograms for peaks corresponding to compounds listed in (A) *162*

Figure 5.3. (A) Positive ion API mass spectrum of authentic 7-(2'-fluoroethyl) guanine . (B) LC/MS/MS CAD daughter ion spectrum of protonated 7-(2'-fluoroethyl)guanine. (C) LC/MS/MS CAD spectrum of protonated guanine..... *163*

Figure 5.4. (A) HPLC/UV (254 nm) chromatogram of the products resulting from the reaction of BFNU with deoxyguanosine in TRIS buffer. (B) Reconstructed ion chromatogram for peaks corresponding to MH^+ and characteristic fragments of 7-(2'-fluoroethyl)guanine. (C) Background subtracted LC/API mass spectrum deduced from the peak maxima at 13.5 min, shown in (B)..... *167*

Figure 5.5. (A) Reconstructed ion chromatograms for peaks corresponding to MH^+ and characteristic fragments of dideuterated 7-(2-fluoroethyl) guanine. (B) Background subtracted LC/API mass spectrum deduced from the peak maxima at 13.5 min, shown in (A). (C) LC/MS/MS CAD spectrum of MH^+ of dideuterated 7-(2'-fluoroethyl)guanine *171*

Figure 5.6. (A) Reconstructed ion chromatograms for peaks corresponding to MH^+ and characteristic fragments of 7-(2'-bromoethyl)guanine. (B) Background subtracted LC/API mass spectrum deduced from the peak maxima at 28.5 min, shown in (A). (C) LC/MS/MS CAD spectrum of MH^+ of 7-(2'-bromoethyl)guanine..... *176*

Figure 5.7. (A) Reconstructed ion chromatograms for peaks corresponding to non-deuterated 7-(2'-bromoethyl)guanine, mono-deuterated 7-(2'-bromoethyl)guanine, dideuterated 7-(2'-bromoethyl)guanine, and characteristic fragments. (B) Background subtracted LC/API mass spectrum deduced from the peak maxima at 28.5 min, shown in (A) *180*

Figure 5.8. LC/MS/MS CAD spectrum of MH^+ of 7-(2'-chloroethyl)guanine *187*

ABBREVIATIONS

API	Atmospheric Pressure Ionization
α	Polarizability
b	Total axial distance between tip and plate
B	Base
BCNU	1,3-Bis(2-Chloroethyl)-1-Nitrosourea
BFNU	1,3-Bis(2-Fluoroethyl)-1-Nitrosourea
C_A	Concentration of analyte A
CAD	Collision activated decomposition
CB	Cluster Buster electrode
CCNU	1-(2-Chloroethyl)-3-Cyclohexyl-1-Nitrosourea
CEM	Detector
CID	Collision Induced Dissociation
CZE	Capillary Zone Electrophoresis
D	Bond dissociation energy
DMF	Dimethylformamide
DMSO	Dimethylsulfoxide
EHD	Electrohydrodynamic
EHI	Electrohydrodynamic ionization
E_{COU}	Coulomb energy
ESP	Electrospray ionization
FAB	Fast Atom Bombardment
FD	Field Desorption
GB	Gas phase Basicity
h	Height
HENU	(2-Haloethyl)nitrosourea
HPLC	High Performance Liquid Chromatography
HYP	Hypodermic needle tip
i	Ion current in amperes
I	Intensity in cps
i.d.	Inside diameter
IE	Ionization Energy
IN	Interface plate
k	Rate constant
K_A	Acidity constant

K_B	Basicity constant
K_S	Autoprotonation constant
L	Left
LC	Liquid Chromatography
LD	Laser Desorption
MS	Mass Spectrometry
μ	Mobility of the ions
μ_o	Zero field mobility
MeCCNN	1-(2-Chloroethyl)-3-(4-Methylcyclohexyl)-1-Nitrosourea
m_i	Mass of ion
m_r	Reduced mass
m/z	Mass/charge ratio
n_M	Rate of an electrosprayed compound M
o.d.	Outside diameter
OR	Orifice
ρ	Slope
PD	Plasma Desorption
P_M	Partial pressure of compound M
PPM	Parts Per Million
Py	Pyridine
Q	Quadrupole
r	Radius
R	Right
R.T.	Retention Time
S_1	Solvent molecule 1
SIM	Single Ion Monitoring
SIMS	Secondary Ion Mass Spectrometry
S.S.	Stainless Steel
t	Drift time
T	Temperature
TIC(IN)	Total Ion Current to interface plate
TNEB	Temperature of nebulizer
t_r	Total reaction (residence) time
TRIS	Tris(hydroxymethyl)aminomethane
TS	Thermospray
V_c	Volume of cone

$\overline{V}_c$	Rate of change of V_c with time
$V_{(S)}$	Ion drift velocity
V_T	Total volume
$\overline{V}_t$	Total rate of volume flow

CHAPTER 1

GENERAL INTRODUCTION

INTRODUCTION

The work described in this dissertation is concerned with electrospray ionization mass spectrometry, one of the most recent soft ionization techniques that has revolutionized the field of analytical mass spectrometry and has inspired unique applications in biochemistry and medicine.

Electrospray is the technical term used to describe the disruption of a liquid surface into a spray of charged droplets when subjected to an intense electric field. Electrospraying can be achieved very easily. Simply by applying a potential to a metal capillary, through which a liquid is flowing at a relatively low flow rate, a spray can be generated. Under the action of a small electric field the liquid emerging from the capillary assumes a conical shape and the rate of detachment from the capillary tip increases relative to what is observed when there is no field applied. An increase in the electric field causes the liquid to form a single steady jet having a conical base at the capillary tip. A few millimeters beyond the capillary tip, the jet breaks up into a brush of small droplets. This is referred to as single spray. A further increase in the electric field causes two or more jets to develop until finally many smaller symmetrically arranged jets form at the rim of the capillary, producing a monodisphere cloud spray. This mode is referred to as multispray.

a. Electrostatic Atomization.

Electrospraying, or electrostatic atomization, has been known for more than two centuries since George Mathius Bose (*1*) recorded the phenomenon in 1745. It was ascribed at the time to the reduction of surface tension by the electric field. In 1914, John Zeleny (*2*) rediscovered the phenomenon and investigated it from the point of view of an electrical discharge from a liquid point. Since then the phenomenon has attracted considerable interest from both a fundamental and an applied point of view. On the applied side, the process has been utilized in paint spraying, crop spraying, electrostatic printing, electrostatic emulsification, fuel

atomization in combustion systems, in space vehicle propulsion systems, and more recently as an ionization method for mass spectrometry.

Following Zeleny's experiments the mechanisms responsible for electrical dispersion of liquids (electrostatic atomization) and charged droplet formation have received considerable attention and have been studied extensively (*3-16*). However, no satisfactory quantitative mechanism explaining the phenomenon has been suggested to date. Some of the parameters that have been found to effect the electrospray process are the magnitude of the applied voltage and the field geometry, the flow rate of the liquid and its physical properties, such as the electrical conductivity, viscosity, surface tension, and dielectric constant.

Although the detailed processes involved in electrostatic atomization remain uncertain, the following conclusions can be derived from the findings of the investigations to date (*3-16*). When an electrolyte solution is emerging from a capillary which is held at positive voltage relative to a counter electrode located a few centimeters from the capillary tip, an enrichment of positive ions in the liquid near the liquid-gas interface of the capillary tip is expected to take place. The excess positive charge reduces the stability of the liquid surface, leading to liquid dispersion and consequently to the formation of positively charged droplets. Experiments from the Kebarle group (*16, 17*) have indicated that, with such an electrospray arrangement, a continuous positive current is measured at the counter electrode. This means that the electric field promotes separation of the electrosprayed electrolytic solution. If charge balance requirements are to be met, negative ions from the solution should be discharging or positive ions should be released into the solution at the wall of the capillary, i.e. an electrochemical oxidation process should be occuring at a liquid-metal interface. This means that the electrospray experiment operates as a special kind of electrolysis cell. The positive electrode, where a conventional oxidation occurs, is the capillary wall in contact with the liquid, while the negative half cell is of a special kind where excess positive ions in solution are carried away by charged droplets.

The charged droplets formed at the capillary tip lose solvent due to evaporation as they drift through the atmospheric pressure gas. The charge to mass ratio of the droplets increases and the droplets become more and more prone to undergo electrohydrodynamic (EHD) disintegration. Good experimental evidence for the disintegration of larger droplets into smaller ones has been presented by Doyle et al. (*4*) and Davis et al. (*15*). The observed process is emission from the charged droplet of one or several much smaller droplets which carry off only a small fraction of the mass (~5%), but a relatively large fraction of the charge (~20%). As further solvent evaporation reduces the size of the remaining large drop, disintegrations occur again and again (*4*). It is also observed that the disintegrations occur fairly close to the Rayleigh limit (*4, 15*), which can be considered as a threshold for the onset of EHD instability.

One of the most credible theoretical models in the literature (*3-15*), one that can explain certain features of experimentally observed charged droplet behavior, is that of Hendrick and Pfeifer (*13a,b*). The model deals with events in the region where charged droplet formation occurs, i.e. presumably at the tip of the liquid cone just past the end of the capillary. When the capillary is of positive polarity, charging of the liquid surface occurs by positive ions present in the liquid which are driven by the imposed field. Electrospray is observed only with dipolar liquids (*3*), and such liquids even when believed completely pure contain dissolved ions due to contamination from the wall of the vessels used, or electrolytic impurities, or autoprotolysis of the given liquid. The concentrations of these ions vary with conditions, but often reaches the 10^{-5} M range. It is also observed that deliberate addition of electrolytes leads to larger currents, although this current increases with the ion concentration only up to about 10^{-4} M (*13a, 17*). It is therefore very likely that the charging of the droplets in electrospray is due to a separation of the positive ions from the negative ions in the solution by the action of the imposed electric field (*16*). However, it should be mentioned here that charged droplets can be created by a variety of mechanisms even in the absence of an external

electric field (*13d, 18*). The currents measured in the absence of an electric field however are orders of magnitude lower compared to those obtained with electrospray.

The theoretical understanding of the process involved in electrospray becomes even more complicated when one examines the formation of gas phase ions from charged droplets. Iribarne and Thomson (*19*) have described a detailed model which predicts that direct evaporation of solvated ions can occur before the droplet becomes disrupted due to electrohydrodynamic (EHD) instability. On the basis of this work a model in which the larger and more highly charged droplets disintegrate via EHD instabilities into smaller charged droplets and these ultimately evaporate ions by the Iribarne-Thomson mechanism, has become widely accepted (*20, 21, 22*).

Direct experimental evidence for the Iribarne-Thomson ion evaporation is not available, because experiments dealing with this phenomenon would be much more difficult to design. The evaluation of the activation barrier for ion evaporation (*19*) involves some questionable assumptions as pointed out by Rollgen et al (*23*). These authors have proposed an alternative mechanism in which the formation of gaseous ions takes place by solvent evaporation from very small droplets, ~1 nm in diameter, which contain only one ion. These very small droplets are presumably by-products of consecutive droplet disintegrations due to EHD instability.

The processes envisaged above are also supported by experiments which indicate the occurrence of corrosion of the capillary (*24, 25*), which imply electrochemical reactions, and the mass spectrometric identification of the gaseous ions which show that the majority of the detected ions are chemically the same as the ions present in the solution (*20, 21, 17*).

b. Electrospray Ionization Mass Spectrometry

Electrospray ionization for mass spectrometry has its roots in the pioneering work of Malcolm Dole and his colleagues (*26*). Their approach was to electrospray dilute solutions of polystyrene and a number of other polymers into a bath gas of nitrogen at atmospheric

pressure. The resultant mixture of ions and neutral molecules was sampled into vacuum through a nozzle-skimmer system. A supersonic molecular beam was formed upon passage of this mixture into a vacuum chamber which in turn was energy analyzed by means of a repeller grid-Faraday cage ion collector system. By estimating the velocity of the beam it was possible to calculate the mass to charge ratio, m/z, of the macroions in the beam (*26b*).

Following Dole's work, Fenn and coworkers (*20*) assembled an apparatus like Dole's and obtained similar results. A short time thereafter they realized that the Dole method could only give rough estimates of m/z values, and so they searched for alternative methods to determine the mass of electrospray-produced gas phase ions more accurately. Instead of macromolecules they used solute species with molecular weights that could be analyzed by mass spectrometers. In 1984, they demonstrated the successful coupling of electrospray ionization, both in the positive (*20a*) and negative ion mode (*20b*), to mass spectrometry. In the same year, the Soviet researchers Aleksandrov et al. (*27*) first demonstrated the extraordinary potential of electrospray ionization as an interface for liquid chromatography with mass spectrometry. In their first publications, they also demonstrated the ability of the technique for oligosaccharide (*28a*) and polypeptide (*28b*) analysis with molecular weights up to 1500, and methods for polypeptide sequence determinations (*28c*).

Bruins and Henion (*21*) in 1987, using a modified version of the electrospray method which they called Ion Spray (pneumatically assisted electrospray), described a number of exciting applications of the technique. The same year Smith and coworkers (*22*) demonstrated the successful coupling of capillary zone electrophoresis to mass spectrometry utilizing electrospray as the interface. To date some 25 research groups are involved in electrospray mass spectrometry research and the number of reports present in the annual meeting of the American Society of Mass Spectrometry, as shown in Figure 1.1, has increased exponentially from the time the subject was first introduced by Fenn in 1984.

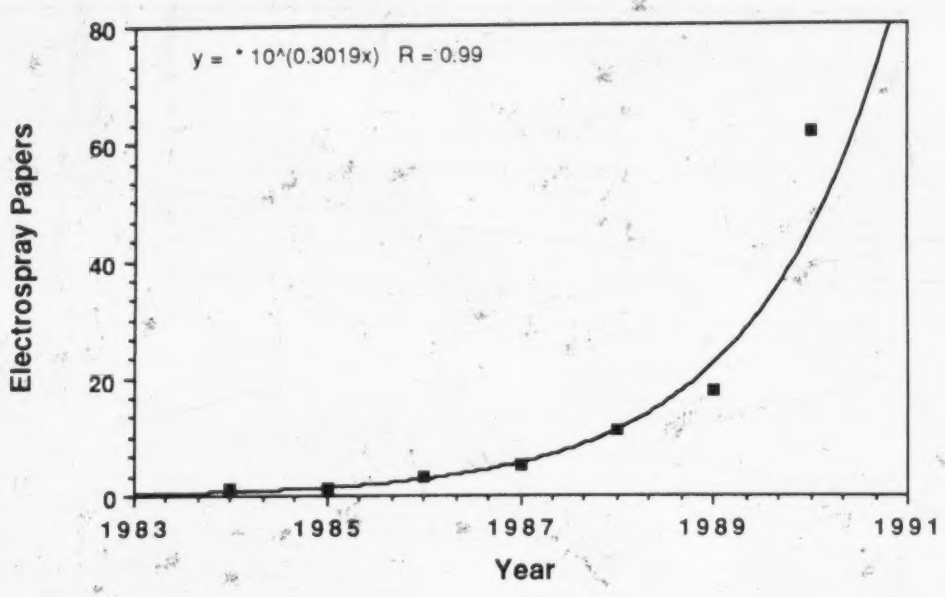

Figure 1.1. Exponential increase in the number of papers, related to ESP/MS, presented at the annual meetings of the American Society of Mass Spectrometry.

In the last 20 years a number of "soft" ionization techniques for mass spectrometry has been developed extending the power of mass spectrometric methods to the analysis and characterization of large, nonvolatile and thermally labile molecules. Combined with the new advances in mass spectrometric hardware, interfaces with separation methods, and computer interfacing, mass spectrometry has become a widely used tool in many areas of science and technology, especially biology and medicine.

Ionization with all the modern methods is achieved via desorption, i.e. direct formation of ions from liquid or solid surfaces. In this way there is no need for neutral molecule volatilization, a process responsible for thermal decomposition of the neutral species, prior to ionization. Among the "soft" ionization techniques that have been practised most are fast atom bombardment (FAB), and secondary ion mass spectrometry (SIMS) (*29*), thermospray ionization (TS) (*30*), field desorption (FD) (*31*), plasma desorption (PD) (*32*), laser

desorption (LD) (*33*), and very recently, electrospray ionization (ESP) (*17, 20-22*). In a recent review (*34*) Fenn has divided these techniques into two categories: energy sudden methods (FAB, SIMS, PD, LD), and field desorption methods (FD, TS, ESP, Ion Spray), and has provided a summary of the operational characteristics and their capabilities for the analysis of large and complex molecules. Although the general features of these techniques are similar, i.e. the ability to analyze high molecular weight biopolymers with minimal or no fragmentation and high detection efficiency, the much greater degree of charging induced on biomolecules upon electrospray is a feature unique to electrospray ionization.

Electrospray multiple charging is of the form $(M+nH)^{+n}$, $(M+nNa)^{+n}$ or $(M-nH)^{-n}$. It has been shown (*35*) that electrospray ionization can deposit as many as 175 positive charges on biomolecules. Electrospray mass spectra of multiply charged biomolecules contain a sequence of peaks with an intensity distribution that is near Gaussian, has a width of ~500 on the m/z scale, and is generally centered between 800 and 1200. Each ion differs by one charge from those of adjacent neighbors in the sequence. This high degree of charging facilitates the ESP analysis of very high-mass proteins and other biomolecules with mass spectrometers of limited mass range, e.g. quadrupoles with m/z limit of 1000 to 2000. In this respect proteins such as the bovine albumin dimer with a molecular weight of ~133,000, which acquires some 90 to 110 protons (a distribution of peaks) upon electrospray ionization, can be analyzed with mass spectrometers of m/z limit of ~1500 (*35*), i.e. $(M+100H)^{+100}$ has an m/z value of 1331.

These features of electrospray ionization mass spectrometry have inspired unique applications of the technique, including peptide sequencing utilizing tandem mass spectrometry (*36, 37*), molecular mass determination of proteins using spectra showing a sequence of peaks due to ions with varying number of charges and implementing specially developed algorithms (*38*), and analysis of oligonucleotides and proteins with as yet no evidence of an upper molecular weight limit (*39*). A summary of the biochemical applications of ESP/MS, including capillary zone electrophoresis / mass spectrometric applications using

ESP as an interface, has been published recently by Smith (*40*). Reports from Henion's laboratory (*41*) have demonstrated the successful coupling of high performance liquid chromatography (HPLC) and ion chromatography to mass spectrometry, utilizing the Ion Spray (pneumatically assisted electrospray) as the LC/MS interface, for the analysis of drugs and a number of industrially important compounds. The success of the first ESP/MS applications has initiated a tremendous growth in the utilization of the technique, and exciting advances in the field are expected in the future.

c. The Present Work.

As was pointed out above, electrospray is performed at atmospheric pressure and its utilization requires a mass spectrometer which can sample ions present in gas at atmospheric pressure. Since part of the M.Sc. thesis work of the author (*42*) was associated with atmospheric pressure ionization mass spectrometry, the transition to ESP ionization evolved quite naturally. The instrumentation used was a SCIEX TAGA 6000E triple quadrupole mass spectrometer equiped with an atmospheric pressure ion source. The open configuration of the ion source housing of this instrument made the design and adaptation of the electrospray assembly to these apparatus convenient. Electrospray work from other laboratories at the time (*20, 21, 22*) was focused mostly on specific analytical applications although important information concerning the method was also given. The aim of my work was to obtain more general information concerning both the physico-chemical aspects of the ESP process itself and the applicability of the method to a wide range of analytes.

Using our own version of the ESP/MS interface, fundamental studies involving a large variety of analytes were undertaken in order to establish factors affecting the yield of positive ions in the gas phase from electrosprayed solutions. Analytes studied included NH_4^+, Na^+, K^+, Cs^+, Ca^{++} and the onium ions BH^+ of some 30 organic nitrogen bases B. The effect of parameters such as field gradient, electrolyte concentration, solvent composition, analyte solution flow rate, and ion source temperature on electrospray performance were investigated.

The objective was to obtain information on the efficiency of charge separation of positive and negative ions in the electrospray process under various conditions, and thereby gain a better understanding on factors influencing the emission of positive ions of a given kind from charged droplets into the gas phase. Search for optimum analyte sensitivity conditions, the sensitivity dependence of organic nitrogen bases (detected as BH^+) on solution pH, and the role (from the point of view of analyte sensitivity) of ion-molecule reactions such as proton transfer in the gas phase, in the electrospray ion source, were also among the elements of interest. The results obtained are described and discussed in Chapters 2 and 3.

As was pointed out in the previous section Ion Spray (*21*) is a modified version of electrospray in which a nebulizing gas is used in addition to high electric field to assist with liquid dispersion. Although the reports of Fenn (*20*) and Henion (*21*) describe in detail the two interfaces (electrospray and Ion Spray) a systematic comparison between the two techniques has not been made. For this reason a direct comparison of the two techniques was undertaken in order to reveal any fundamental differences between the ionization processes, and differences in the operational procedures of the techniques. In this study experiments were designed in such a way as to qualitatively and quantitatively examine the importance of the electric field, and nebulization pressure (in the case of Ion Spray) on the ion yields produced by the two techniques, using solutions of various analytes. Once optimum Ion Spray operational conditions were achieved an investigation parallel to that described above for electrospray was undertaken. The results obtained are described and discussed in Chapter 3.

During the course of the electrospray investigations the capability of the technique to produce multiply charged metal ions in the gas phase was realized. Doubly and triply charged gaseous ions were formed when solutions of metal salts were electrosprayed. Hydrates and other ligand complexes $M^{z+}(L)_n$ (where L is a ligand) were observed as major ions for the alkaline earths (Mg^{2+}, Ca^{2+}, Sr^{2+}, Ba^{2+}) and the transition metals (Mn^{2+}, Fe^{2+}, Co^{2+}, Ni^{2+}, Zn^{2+}). A variety of M^{2+} ion-ligand complexes with the above metal ions and Cr^{2+}, Cu^{2+},

Co^{3+} with ligands dimethylsulfoxide, dimethylformamide, ammonia, pyridine and the polydentate peptides, di- and poly-ketones, cyclic tetramines (cyclams), and the polycyclic hexamine-sepulchrate, could also be prepared and observed. This exciting variety of species leads to the question: How can one study these ions?

These findings were revolutionary considering that species of the type described above are not easy to produce in the gas phase. Multiply charged "naked" metal ions are not difficult to produce in the dilute gas phase. This is illustrated by the availability of experimental higher ionization potentials for the elements. The difficulties arise when other chemical matter is near the multiply charged ion. The general method used for singly-charged ion-clusters like $M^+(H_2O)_n$, is to generate M^+ in a gas phase in which ligand molecule vapor is present. The formation of $M^+(H_2O)_n$ then proceeds spontaneously by third-body-dependent association reactions corresponding to eq 1.1. This method may not work for M^{2+} species when the

$$M^+(H_2O)_{n-1} + H_2O = M^+(H_2O)_n \qquad (1.1)$$

second ionization energy of M, I.E.(M^+), is much larger than the ionization energy of the ligand, as is the case for Mg where I.E.(Mg^+) = 15.0 and I.E.(H_2O) = 12.6 eV. Little information is available on the outcome of the gas phase reactions of M^{2+} and L where I.E.(M^+) > I.E.(L). Change transfer to the ligand, leading to M^+ and L^+ and formation of $M^+OH + H_3O^+$ for cases where the ligand and the third body are H_2O, are reaction channels that could compete with formation of stabilized $M^{2+}(L)_n$.

Since Electrospray ionization was the first method to produce such a large variety of the species described above, it was decided to mount a systematic investigation in order to get a better understanding of the behavior of these species. At first the electrospray-generated multiply-charged metal ion mass spectra, as well as the collision induced dissociation (CID) mass spectra of metal ion-ligand complexes, were investigated in detail and examined for trends common to different groups of metal compounds. The influence of experimental parameters, such as conditions under which the atmospheric pressure-vacuum interface of the

TAGA is operated (see Chapters 2, and 4) on spectral appearance were also investigated. Furthermore investigations into the use of the present ESP/MS arrangement (see Chapter 2), to obtain thermochemical data for ion-molecule reactions between singly and multiply charged metal ions with ligands, were also undertaken. The results obtained are described and discussed in Chapter 4.

In recent years rapid progress has been made in overcoming the substantial technical problems associated with the coupling of HPLC to mass spectrometry (*43, 44*). This marriage has produce a powerful analytical technique, and has opened an alternative route of analysis for many mixtures of biological origin. A review outlining new advances in LC/MS has been published lately by Arpino (*45*).

Nucleic acids (nucleotide bases, nucleosides, nucleotides and derivatives) are one of the most important classes of biological compounds, and a large body of research has been dedicated to them. The use of mass spectrometric methods, such as FAB-MS, PD-MS, and LC/MS (with interfaces such as TS, direct liquid introduction (DLI), and heated nebulizers), for the analysis of mixtures of nucleic acids has been well established (*46-48*). Although these LC/MS interfaces and "soft" ionization methods produce abundant molecular ion (MH^+) peaks, fragment ions are usually not existent or lost in the background of conventional mass spectra. This inherent lack of information can be overcome by the use of tandem mass spectrometry (MS/MS) (*49*). Combined LC/MS/MS systems therefore can be very effective for the analysis and characterization of complex mixtures of thermally labile and non-volatile biological compounds.

(2-Haloethyl)nitrosoureas (HENUs) have an established place in the clinical treatment of a range of human malignancies, including Hodgkin's disease, Burkitt's lymphoma and cerebral neoplasms (*50-52*). HENUs decompose spontaneously under physiological conditions to give rise to electrophiles which react with sensitive cellular macromolecules (*50, 51*). Several lines of evidence indicate that DNA is one of the principal cell targets (*50, 51*) and specific lesions have been identified (*53*). Determining the mechanism of reaction of

HENUs with DNA bases is essential in order to understand the details of the mechanism of action of these valuable clinical agents. In a collaborate project with Dr. J.W. Lown (Chemistry Department), reactions of BFNU and BFNU-1,1',1'',1''' d_4 with the DNA base deoxyguanosine, under various *in vitro* experimental conditions, were performed and the products were analyzed by HPLC/MS/MS. In this study the heated nebulizer / corona discharge combination, a method complementary to electrospray, was used as the HPLC/MS interface. The procedures and methods used to analyze and characterize the reaction products are described in Chapter 5. Based on the structures of the identified reaction products a pathway mechanism for the *in vitro* alkylation of the DNA base deoxyguanosine by the anticancer agent BFNU was elucidated.

REFERENCES

1. Bose, G.M. "Recherches sur la cause et sur a veritable theorie de l'electricite". Wittenberg **1745**.
2. (a) Zeleny, *J. Phys. Rev.* **1914**, *3*, 69. (b) *Ibid.* **1917**, *10*, 1. (c) *Ibid.* **1920**, *16*, 102. (d) Zeleny, J. *Proc. Cambridge Phil. Soc.* **1915**, *18*, 71.
3. Drozin, V.G. *J. Colloid Sci.* **1955**, *10*, 158.
4. (a) Doyle, A.; Moffett, D.; Vonnegut, B. *J. Colloid Sci.* **1964**, *19*, 136. (b) Vonnegut, B.; Neubauer, R. *Ibid.* **1952**, *7*, 616. (c) *Ibid.* **1953**, *8*, 551.
5. Taylor, G. *Proc. Roy. Soc.* **1964**, *280*, 383. (b) *Ibid.* **1969**, *A313*, 453.
6. Melcher, J.R.; Warren, E.P. *J. Fluid Mech.* **1971**, *47*, 127.
7. English, W.N. *Phys. Rev.* **1948**, *74*, 179.
8. Ryce, S.A. *J. Colloid Sci.* **1964**, *19*, 249.
9. DeShon, W.E.; Carson, R.S. *J. Colloid Interface Sci.* **1968**, *28*, 161.
10. Huberman, M.N. *J. Appl. Phys.* **1970**, *41*, 578.
11. Bollini, R.; Sample, S.B. *J. Colloid Interface Sci.* **1976**, *3*, 291.
12. Kelly, A.J. *J. Appl. Phys.* **1978**, *49*, 2621.
13. (a) Pfeifer, R.J.; Hendricks, C.D. *AIAA Journal* **1968**, *6*, 496. (b) Pfeifer, R.J.; Hendricks, C.D. *Phys. Fluids* **1967**, *10*, 2149. (c) Hendricks, C.D. *J. Colloid Sci.* **1962**, *17*, 249. (d) Hendricks, C.D. "Charging Macroscopic Particles". *In Electrostatics and Applications*; Moore, A.D., Ed.; John Willey: New York, **1973**.
14. Hayati, I.; Bailey, A.I.; Tadros, TH. F. *J. Colloid Interface Sci.* **1987**, *117*, 205.
15. Taflin, D.C.; Zhang, S.H.; Allen, T.; Davis, E. *J. Am. Inst. Chem. Eng. (AIChE) Journal*, **1988**, *34*, 1310.
16. Juhasz, P.; Kebarle, P. *Int. J. Mass Spectrom. Ion Proc.* (in press).
17. Ikonomou, M.G.; Blades, A.T.; Kebarle, P. *Anal. Chem.* **1990**, *62*, 957.
18. Loeb, L.B. *Science* **1945**, *102*, 573.

19. (a) Iribarne, J.V.; Thomson, B.A. *J. Phys. Chem.* **1976**, *64*, 2287. (b) *Ibid.* **1979**, *71*, 4451. (c) Iribarne, J.B.; Dziedzic, P.J.; Thomson, B.A. *Int. J. Mass Spectrom. Ion Phys.* **1983**, *50*, 331.

20. (a) Yamashita, M.; Fenn, J.B. *J. Phys. Chem.* **1984**, *88*, 4451. (b) *Ibid.* **1984**, *88*, 4671. (c) Whitehouse, C.M.; Dreyer, R.N.; Yamashita, M.; Fenn, J.B. *Anal. Chem.* **1985**, *57*, 675.

21. (a) Bruins, A.P.; Covey, T.R.; Henion, J.D. *Anal. Chem.* **1987**, *59*, 2642. (b) Bruins, A.P.; Weidolf, L.O.G.; Henion, J.D.; Buddy, W.L. *Anal Chem.* **1987**, *59*, 2647.

22. Olivares, J.A.; Nguyen, N.T.; Yonker, C.R.; Smith, R.D. *Anal. Chem.* **1987**, *59*, 1232.

23. Schmeltzeisen-Redeker, G.; Butfering, L.; Rollgen, F.W. *Int. J. Mass Spectrom. Ion Proc.* **1989**, *90*, 139.

24. Zolotoi, N.B.; Karpov, G.B.; Talroze, V.L.; Skurat, V.E.; Ramendik, V.; Vasyuta, Y. V. *Zh. Anal. Khim.* **1980**, *35*, 1461.

25. (a) Simons, D.S.; Colby, B.N.; Evans, C.A. *Int. J. Mass. Spectrom. Ion Phys.* **1974**, *15*, 291. (b) Stimpson, B.P.; Simons, D.S.; Evans, C.A. *J. Phys. Chem.* **1978**, *82*, 660.

26. (a) Dole, M.; Mach, L.L.; Hines, R.L.; Mobley, R.C.; Ferguson, L.P.; Alice, M.B. *J. Chem. Phys.* **1968**, *49*, 2240. (b) Mach, L.L.; Kralik, P.; Rheude, A.; Dole, M. *J. Chem. Phys.* **1970**, *52*, 4977; (c) Clegg, G.A.; Dole, M. *Biopolymers* **1971**, *10*, 821. (d) Teer, D.; Dole, M. *J. Polym. Sci.* **1975**, *13*, 985.

27. (a) Aleksandrov, M.L.; Gall, L.N.; Krasnov, V.N.; Nikolaev, V.I.; Pavlenko, V.A.; Shkurov, V.A. *Dokl. Akad. Nauk SSSR* **1984**, *277*, 379. (b) Aleksandrov, M.L.; Gall, L.N.; Krasnov, V.N.; Nikolaev, V.I.; Pavlenko, V.A.; Shkurov, V.A.; Baram, G.I.; Gracher, M.A.; Knorre, V.D.; Kusner, Y.S. *Bioorg. Khim.* **1984**, *10*, 710.

28. (a) Aleksandrov, M.L.; Besuklandnikov, P.V.; Grachev, M.A.; Elyakova, L.A.; Zyyaginsteva, T.N.; Kondratsev, V.M. Kusner, Y. S.; Mirgorodskaya, O.A.; Fridiyansky, G.V. *Bioorg. Khim.* **1986**, *12*, 1689. (b) Aleksandrov, M.L.; Gall, L.N.; Krasnov, V.N.; Nikolaev, V.I.; Kusner, Y.S.; Baram, G.I.; Shkurov, V.A.; Mirgorodskaya, O.A. *Bioorg. Khim.* **1985**, *11*, 700. (c) Aleksandrov, M.L.; Gall, L.N.; Krasnov, V.N.; Nikolaev, V.I.; Kusner, Y.S.; Baram, G.I.; Shkurov, V.A.; Mirgorodskaya, O.A.; Grachev, M.A.; Knorre, V.D. *Bioorg. Khim.* **1985**, *11*, 705.

29. (a) Barber, M.; Bordoli, R.S.; Elliot, G.J.; Sedgwick, R.D.; Tyler, A.N. *J. Chem Soc. Chem. Commun.* **1981**, 325. (b) Barber, M.; Bordoli, R.S.; Elliot, G.J.; Sedgwick, R.D.; Tyler, A.N. *Anal. Chem.* **1982**, *54*, 645A.

30. Vestal, M.L. *Mass Spectrom. Rev.* **1983**, *2*, 447.

31. Beckey, H.D. Principles of Field Ionization and Field Desorption Mass Spectrometry; Pergamon: Oxford, **1977**.

32. (a) Sundquvist, B.; Macfarlane, R.D. *Mass Spectrom. Rev.* **1985**, *4*, 421. (b) Roepstorff, P.; Sundquvist, B. *In Mass Spectrometry in Biomedical Research*; Gaskell, S.J. Ed.; Wiley: London, **1986**, 269.

33. (a) Karas, M.; Hillenkamp, F. *Anal. Chem.* **1986**, *60*, 2299. (b) Karas, M.; Hillenkamp, F.; Bahr, U.; Ingendoh, A. *Angew. Chem.* **1989**, *101*, 805.

34. Fenn, J.B.; Mann, M.; Meng, C.K.; Wong, S.F.; Whitehouse, C.M. *Mass Spectrom. Rev.* **1990**, *9*, 37.

35. Loo, J.A.; Udseth, H.R.; Smith, R.D. *Anal. Biochem.* **1989**, *179*, 404.

36. Covey, T.R.; Bonner, R.F.; Shushum, B.I.; Henion, J.D. *Rapid Commun. Mass Spectrom.* **1988**, *2*, 249.

37. (a) Loo, J.A.; Edmonds, C.G.; Smith,. R.D. *Science* **1990**, *248*, 201. (b) Barinaga, C.J.; Edmonds, C.G.; Smith, R.D.; Udseth, H.R. *Rapid Commun. Mass Spectrom.* **1989**, *3*, 160.

38. Mann, M.; Meng, C.K.; Fenn, J.B. *Anal. Chem.* **1989**, *61*, 1702.

39. Fenn, J.B.; Mann, M.; Meng, C.K.; Wong, S.F.; Whitehouse, C.G. *Science* **1989**, *246*, 64.

40. Smith, R.D.; Loo, J.A.; Edmonds, C.G.; Barinaga, C.J.; Udseth, H.R. *Anal. Chem.* **1990**, *62*, 882.

41. (a) Lee, F.D.; Henion, J.D.; Budde, W.L.;Edland, P.O. *Biomed.Envirom. Mass Spectrom.* **1989**, *18*, 233. (b) Conboy, J.J.; Henion, J.D.; Martin, M.W.; Zweigenbaum, J.A. *Anal Chem.* **1990**, *62*, 800.

42. Sunner, J.; Ikonomou, M. G.; Kebarle, P. *Anal. Chem.* **1988**, *60*, 1308.

43. Vestal, M.L. *Mass Spectrom. Rev.* **1983**, *2*, 447.

44. Covey, T.R.; Lee, E.D.; Bruins, A.P.; Henion, J.D. *Anal. Chem.* **1986**, *58*, 1451A.

45. Arpino, P. *Mass Spectrom. Rev.* **1989**, *8*, 35.

46. Fenselau, C.A. *In Photochemistry and Photobiology of Nucleic Acids*; Wang, S.Y., Ed.; Academic Press: New York, **1976**; pp 419.

47. McCloskey, J.A. *In Mass Spectrometry in the Health and Life Sciences*; Burlingame, A.L., Castagnoli, N.,Jr., Eds.; Elsevier: Amsterdam, **1985**; pp 521.

48. McCloskey, J.A. *In Mass Spectrometry in Biomedical Research*; Gaskell, S.J., Ed.; John Wiley and Sons: New York, **1986**; pp75.

49. McLafferty, F.W., Ed. "*Tandem Mass Spectrometry*", John Wiley and Sons: New York, **1983**.

50. Ludlum, D. B. In *Cancer, a Comprehensive Treatise*; F.F. Becker, F. F., Eds.; Plenum Press: New York, 1978; p 285.

51. Wheeler, G. P. A Review of Studies on the Mechanism of Action of Nitrosoureas; American Chemical Society Symp. Series No. 30; American Chemical Society: Washington, DC, 1976.

52. (a) Weinkam, S. J.; H-S Liu, H-S. *Adv. Pharmacol. Chemother.* **1982**, *19*, pp 1-33. (b) Hemminki, K.; Ludlum, D. B. *J. Natl. Cancer Inst.* **1984**, *73*, 1021. (c)

Proceedings of the 7th New Drug Symp. on Nitrosoureas. In *Cancer Treat. Ref.* **1976**, *60*, 651.

53. (a) Brundrett, R. B.; Cowens, J. W.; Colvin, M. *J. Med. Chem.* **1976**, *19*, 1958. (b) Lown, J. W. In *New Approaches to the Design of Antineoplastic Agents*; Bardos, T. J., Kaslman, T. I., Eds.; Elsevier, 1982; p 61.

CHAPTER 2

INVESTIGATIONS OF THE ELECTROSPRAY INTERFACE FOR LIQUID CHROMATOGRAPHY/MASS SPECTROMETRY*

* A version of this Chapter has been published: Ikonomou, M. G.; Blades, A. T.; Kebarle, P. *Anal. Chem.* **1990**, *62*, 957 - 967.

INTRODUCTION

Recent work by Fenn et al. (*1-3*) has demonstrated the extraordinary potential of electrospray ionization (ESP) as an interface for capillary liquid chromatography mass spectrometry. Henion et al. (*4-6*) using a modification of the electrospray method, which they called ion-spray, have also described a number of exciting applications of the technique. Smith et al. (*7-10*), using electrospray as the interface in capillary zone electrophoresis, have reported impressive results. The above work and more recent results presented at a meeting on ion desorption mechanisms (*11a*) led to the perception that electrospray is a technique whose importance may in the near future equal that of outstanding methods such as fast atom bombardment (FAB) and laser desorption.

Electrospray is performed at atmospheric pressure, and its utilization requires a mass spectrometer that can sample ions present in gas at atmospheric pressure. Research on electrospray in the present laboratory evolved quite naturally out of our previous investigations of atmospheric pressure ionization (*12*). The results to be described here are based on work extending over the past two years. A preliminary report was presented at a recent symposium (*11b*).

The previous work on electrospray (*1-10*) has mostly emphasized specific analytical applications, although important information concerning the method was also given. The aim in the present work was to obtain somewhat more general information concerning both the physicochemical aspects of the process itself and the applicability of the method to a wide range of analytes.

EXPERIMENTAL SECTION

The Atmospheric Pressure Mass Spectrometer

The instrument was a SCIEX TAGA 6000E atmospheric pressure triple quadrupole mass spectrometer (*13*), which was used also in the earlier atmospheric pressure ionization (API) work in this laboratory (*12*). Instead of the corona discharge needle employed in the API work, an electrospray capillary was mounted as shown in Figure 2.1. The capillary is easily installed and its position easily optimized since the large lid of the atmospheric pressure chamber of the TAGA makes that region very accessible.

The stainless steel capillary (0.065 in. o.d., 0.005 in. i.d.) ≈1 in. long, was supplied with solution, generally 20 μL/min, by means of a motor-driven syringe connected to the capillary by means of silica capillary tubing. Typically, the spray capillary was at +9 kV and the distance between the capillary tip and interface gas entrance was ≈4 cm; see Figure 2.1.

A flow of 1 L/s of air is maintained through the atmospheric pressure ion source. The flow continually removes solvent vapor produced by the electrospray. Ions produced in the atmospheric pressure chamber drift under the influence of the electric field toward the interface plate (650 V) and enter the interface gas chamber through a hole (≈4 mm) in the interface plate. The interface chamber contains ultrapure N_2 gas through which the ions are made to drift under the influence of an electric field. Some of the ions come to the vicinity of the interface chamber exit orifice OR, 0.1 mm diameter, 60 V, through which interface gas and ions enter the vacuum of the triple quadrupole mass analysis chamber.

The interface gas flows slowly through the interface chamber (0.2 L/min) and enters the atmospheric pressure ionization chamber through the aperture in the interface plate. This current keeps gases from the atmospheric ionization region out of the interface chamber but is slow enough to allow the drifting ions to enter. The interface gas has three major beneficial effects: (a) It keeps the mass analysis region clean. (b) The ions in the atmospheric pressure ionization chamber are clustered with solvent molecules, H_2O present in the air or CH_3OH from the evaporating electrospray solution. An equilibrium solvent-molecule distribution

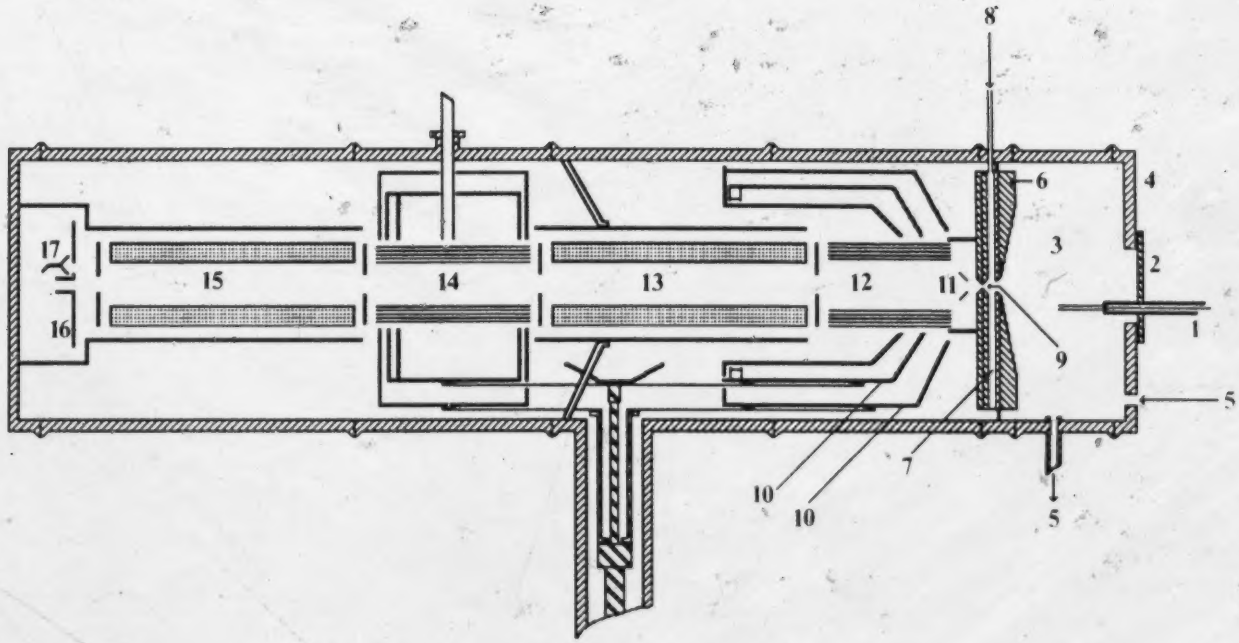

Figure 2.1. Front end of apparatus (1) electrospray tip assembly (see Figure 2.2A for detailed diagram); (2) holder plate movable in x and y direction; (3) atmospheric pressure ion source chamber; (4) transparent (Lucite) lid; (5) atmospheric air "in" and "out"; (6) interface plate, IN; (7) interface gas chamber; (8) interface gas (N_2) inlet; (9) orifice-entrance into mass analysis vacuum region, OR; (10) cryopumping surfaces; (11) cluster buster electrode, CB; (12) Brubaker lens, Q_0; (13) first quadrupole, Q_1; (14) collision quadrupole, Q_2; (15) third quadrupole, Q_3; (16) faraday plate; (17) detector, CEM.

$M^+(Sl)_n$ where Sl is the solvent molecule and M^+ the ion, centered around n ≈3-10, is generally present (*12a*). In the dry interface chamber consecutive dissociation of solvent molecules occurs, bringing n down to ≈2 (*12a*). This process is beneficial since it concentrates the analyte ion signal into only a few m/z values. (c) The adiabatic expansion into the vacuum chamber through the interface orifice OR leads to a large temperature drop. However N_2, due to its lack of dipole and low polarizability, has a very low tendency to cluster with the ions. Whatever N_2-containing clusters are formed are very weakly bonded. The presence of electric fields in the initial stages of the expansion leads to collision-induced declustering such that no N_2 adducts are detected (*12a, 13*). The magnitude of these fields, which can be controlled by the voltage of the first electrode past the orifice 9, see Figure 2.1, has also an effect on the ion-solvent molecule cluster average size; i.e. a higher field reduces the size of the observed clustered ions. This means that only strongly bound clusters are generally observed, and the solvent molecule number in the observed clusters is not at all representative of the ion clusters present in the atmospheric pressure ion source.

Mass analysis is obtained in the first quadrupole Q_1 (300 resolution) and tandem mass spectrometry (MS/MS) spectra can be obtained by collisional activation in Q_2 with argon as collision gas and daughter ion scans in Q_3. Ion counting was used for determination of the intensities of mass analyzed ions. The counter becomes nonlinear above ≈7 x 10^5 counts/s. Therefore for quantitative measurements, when the signal obtained with Q_1 exceeded 7 x 10^5 counts/s, both quadrupoles Q_1 and Q_3 were used in the resolving mode, in this manner reducing the ion signal. The intensities obtained were then adjusted to the intensity that would have been observed with only Q_1 in the resolving mode.

The total ESP ion currents were measured not in the API mass spectrometer, but with the arrangement shown in Figure 2.2B, using a Keithley 610B microampmeter.

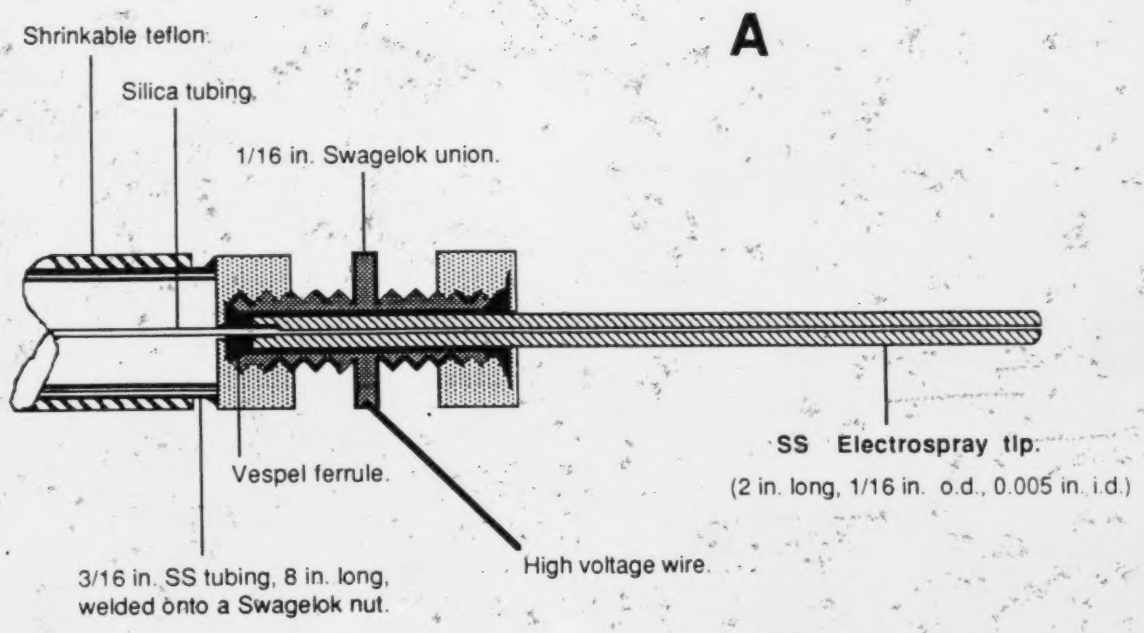

- The back side of the SS ESP capillary is drilled out to 0.015 in. i.d. to accept the silica tube (zero volume fitting).
- Edges of ESP tip are rounded with emery cloth in order to minimize initiation of corona discharge when high voltage is applied to the tip.
- SS Swagelock union appropriately enlarged to allow the ESP tip to seal against the vespel ferrule.
- The 3/16 in. SS tubing, covered with Teflon, is mounted into a 1/4 in. Swagelock fitting affixed to the X-Y positioner.

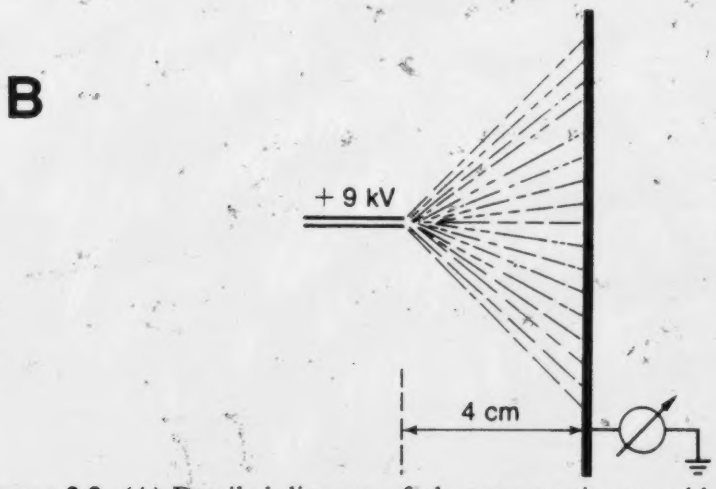

Figure 2.2 (A) Detailed diagram of electrospray tip assembly. (B)Arrangement used for measurement of total ion current produced by electrospray. Distance of 4 cm and voltage 9kV are typical values used.

RESULTS AND DISCUSSION

a. The Electrospray Ionization. Total Ion Currents and Spatial Distribution.

The electrospray capillary tip was kept at ≈9 kV and some 4 cm back from the interface plate aperture of the API mass spectrometer, see Figure 2.1. These conditions are somewhat different to those used under API corona discharge where the discharge needle tip is ≈2 cm away from the interface plate aperture at ≈5 kV and constant discharge current of 2.0 μA. With the present ESP arrangement no corona discharge occurs. When a suitable liquid is present in the capillary, held at a positive potential, the liquid at the tip of the capillary forms a cone under the influence of the electric field, and a stream of fine droplets, i.e. a mist, is generated from the tip of the liquid. The droplets are positively charged and drift toward the negative electrode, i.e., the interface plate. At higher electric fields, the liquid cone shrinks and is replaced by a crown of several much smaller tips which lie along the rim of the capillary electrode, as visually observed through the ion source view port with suitable illumination. An increase of the total ion current by a factor of 3 or more occurs at this changeover. The ions detected with the mass spectrometer for both of the above conditions are largely the electrolyte ions present in the solution. Typically if the solution (methanol) contains 10^{-5} M Na salts, the dominant positive ions observed will be Na^+ and Na^+H_2O. If the voltage is increased further, the emitting multiple liquid cones disappear and the detected ions change drastically. A 20-fold increase in ionization current (current "leaving" the ESP tip) is observed when this transition occurs. Solution electrolyte ions are no longer seen, the new ions being almost exclusively $CH_3OH_2^+(CH_3OH)_n$, when clean air is present in the ion source. These ions are most likely due to electric gas discharge which leads to ionization of gas molecules and a sequence of gas-phase ion-molecule reactions that result in the formation of the ion clusters $H_3O^+(H_2O)_n$, in the presence of water vapor (*14a*), and $CH_3OH_2^+(CH_3OH)_n$ in the presence of methanol vapor (*14b*). All experimental results that will be described in the subsequent text were obtained under true electrospray conditions, i.e. in the absence of an electric gas discharge. (See also Fenn (*1-3*).)

Typical total ion currents measured with a separate test rig, see Figure 2.2B, consisting of the electrospray electrode held at a positive potential and a large metal plate at ground voltage as the counter electrode, are shown in Figure 2.3. The current, for a given liquid flow-rate through the capillary is seen to increase with the electrolyte (NaCl) concentration. The current is initially proportional to the concentration, but at higher concentrations a leveling is observed. This leveling occurs earlier for the higher capillary flow-rate experiments.

The approximate linearity of current versus electrolyte concentration at low concentrations, i.e. less than 10^{-5} M, cannot be well demonstrated by total ion current plots, due to the presence of electrolyte impurities in the solvent at these concentrations. However the linearity at low concentrations can be inferred from the mass analyzed signal, as will be shown later.

A wider range of concentrations (NaCl) is shown in the log current vs log concentration plot of Figure 2.4. Formation of charged fine droplets, i.e. electrospray ionization, does not occur above $\approx 10^{-2}$ M electrolyte concentration.

The total ion currents observed with six different electrolytes (NaCl, NaBr, KBr, $CsNO_3$, $NH_4CH_3CO_2$, $CaCl_2$) are shown in Figure 2.5. The currents, and their dependences on the equivalent electrolyte concentrations, are seen to be very similar.

The total ion results indicate that the positive-negative ion separation occurring in the electrosprayed droplets can be very efficient. For example for a liquid flow of 3×10^{-5} M NaCl at 15 μL/min, the total Na^+ ions in the solution delivered for electrospray are 4.5×10^{12} ions/s. The measured total ion current, see Figure 2.3, is 3×10^{-7} A, and this corresponds to 1.8×10^{12} positive ions/s or a yield of ≈40% of the total positive ions available. This suggest that the average electrosprayed droplet for these conditions contains 40% excess of positive ions, with the remaining positive ions counterbalanced by negative ions. At this point, we do not make the distinction whether the total ion current measured in Figure 2.2B consists largely of gas-phase positive ions arriving at the counter (grounded) electrode or of multiply charged positive droplets or a mixture of both. It is also assumed that no negative ions are emitted from the counter electrode.

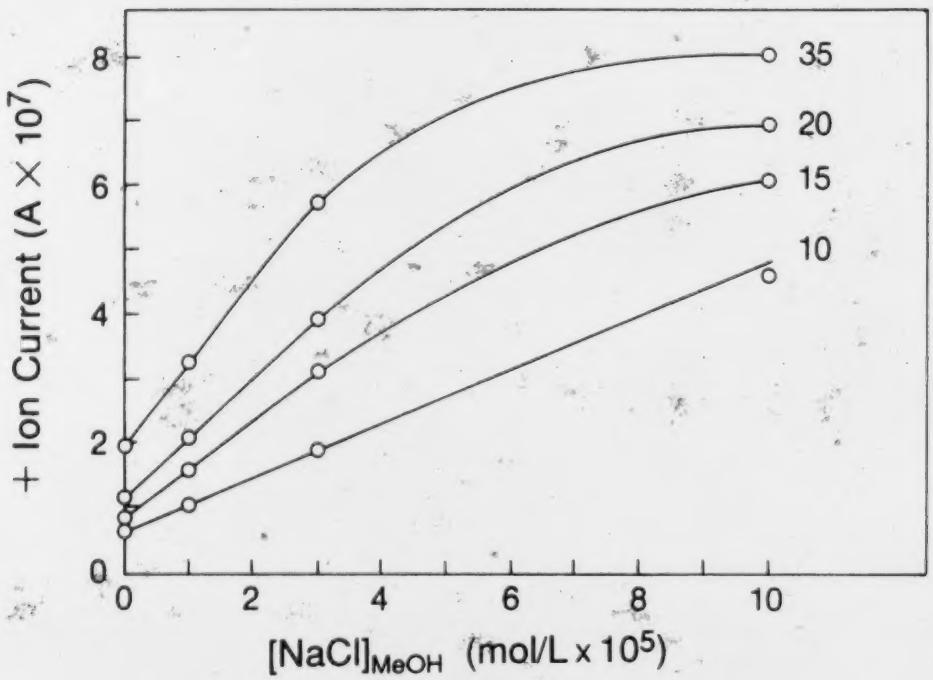

Figure 2.3 Total ion currents measured as a function of NaCl concentration in methanol. Values given besides curves give solution flow in microliters per minute.

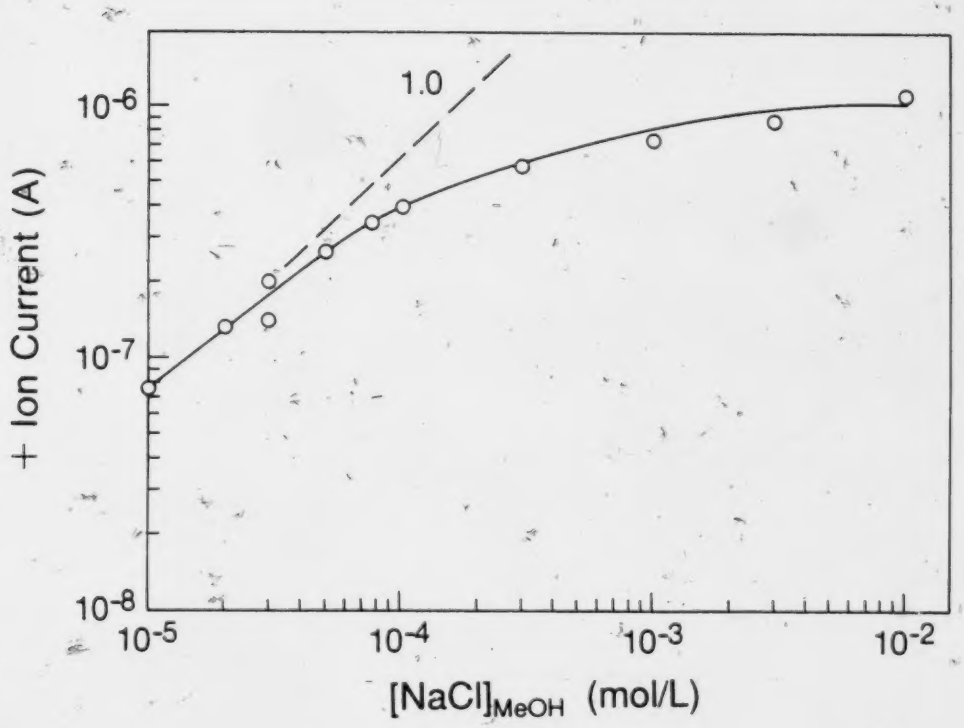

Figure 2.4. log-log plot of total ion current versus NaCl concentration. Dashed line gives slope equal to unity. Methanol solution, flow-rate 20 μL/min.

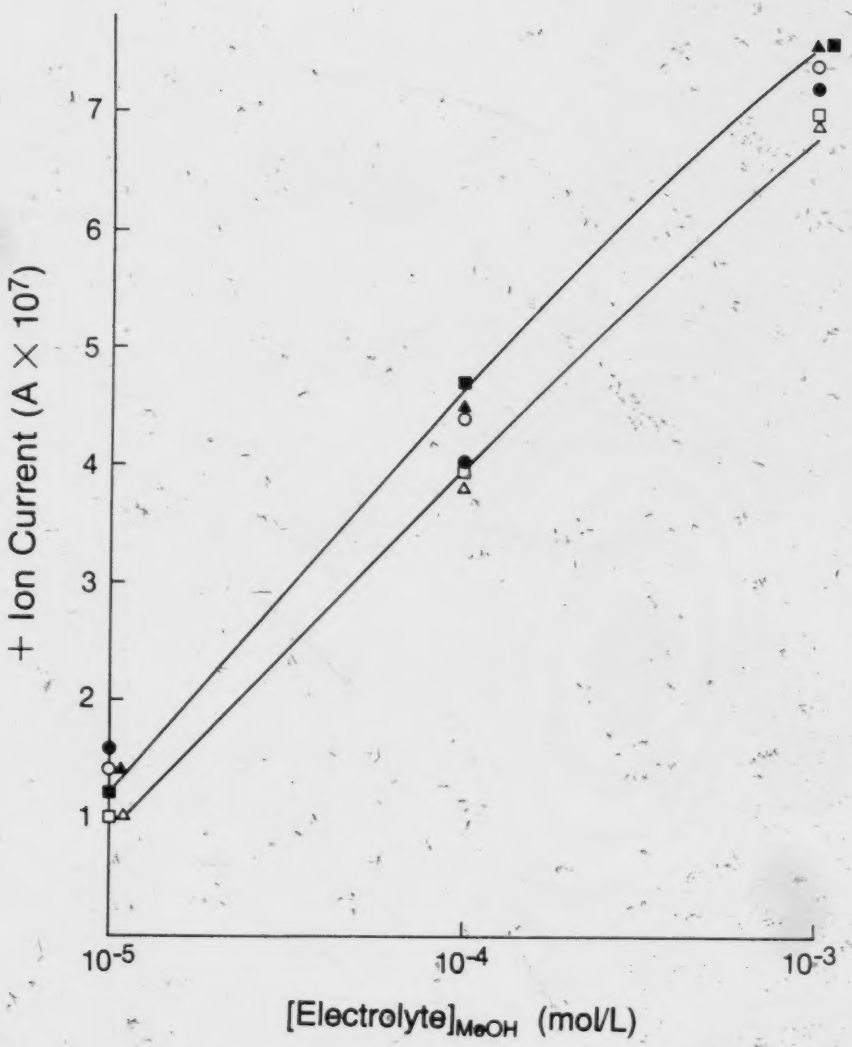

Figure 2.5. Total ion currents versus concentration for several electrolytes in a linear current versus log concentration plot. Concentration of divalent $CaCl_2$ divided by two. Key: ○, NaBr; ●, KBr; ❑, NaCl; ■, $CaCl_2$; Δ, $CsNO_3$; ▲, $NH_4^+ \cdot CH_3CO_2^-$. Methanol solution, liquid flow-rate 20 μL/min.

It should be noted that the high (≈40%) charge separation yield is present only at low electrolyte concentrations where the current is proportional to concentration, i.e. below ≈3 x 10^{-5} M (see Figures 2.3 and 2.4). At higher concentrations rapid decrease of yield occurs. Thus for an electrolyte concentration of 10^{-2} M a total ion current of only 10^{-6} A is obtained (Figure 2.4) which corresponds to a yield of only 0.3%. This decrease of yield may be expected to lead to a corresponding decrease of sensitivity for analyte detection with the mass spectrometer. This expectation is verified in the next section which deals with mass analyzed ions.

Spatial profiles of the total ion current arriving at the counter electrode, Figure 2.2B, are shown in Figure 2.6. These results were obtained through use of two thin brass plates stacked one above the other. The upper, much larger plate had a 0.5 cm diameter hole in its center. The lower smaller plate was insulated from the upper plate. The current profiles shown were obtained by displacing the upper plate horizontally and measuring the electrospray current to the lower plate. The current corresponds to the current passing through the hole in the upper plate. The single maximum profile shown corresponds to electrospray from a single central tip of the liquid, which occurs when lower potentials are applied to the ESP capillary. The double maximum profiles seen at the bottom of Figure 2.6 correspond to spray from a crown of several small liquid tips, which occurs at higher capillary potentials. Thus, the current profiles follow the spray pattern observed visually. Furthermore, the broadness of the ion current profiles appears to be caused, in single and multiple tip spray, by the mutual electrostatic repulsion of the positively charged droplets.

On the basis of Figure 2.6 one might have expected that the maximum ion intensities obtained with the single cone and multiple cone spray should be approximately equal. However, in general, much better sensitivity and signal stability for mass spectrometric detection were obtained with the multiple spray pattern at higher fields. For this condition, the capillary was offset by approximately 1 cm from the central axis of the interface plate of the API interface (Figure 2.1). This position corresponds to the maximum current observed with

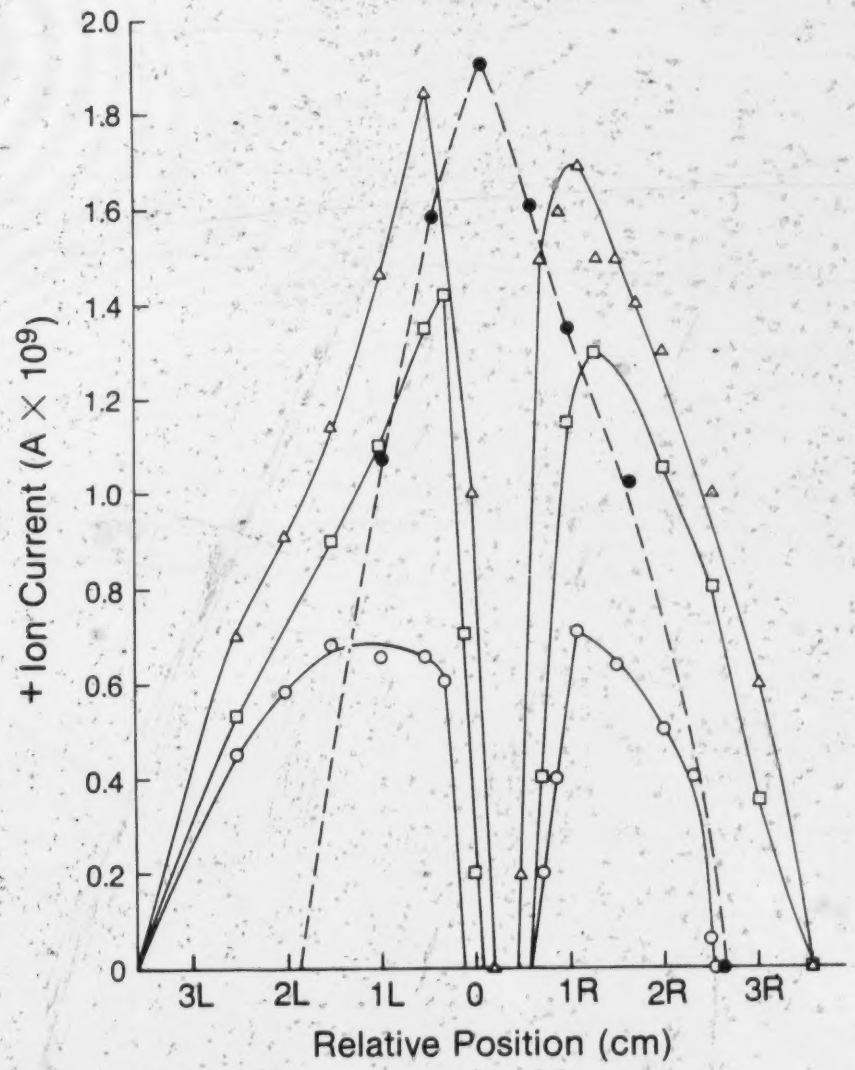

Figure 2.6. Electrospray ion currents to a 0.5 cm diameter area moved in a straight line across the plane electrode, see Figure 2.2B. The 0 cm point designates the position when the ESP capillary tip is on-axis with the 0.5 cm area, L and R represent left and right axial movements relative to the ESP tip. Key: (dashed line) electrospray liquid forms a single cone, 3×10^{-5} M solution, ≈6 kV applied to the ESP capillary; (full lines) electrospray liquid forms a crown of multiple small cones; (○) 10^{-6} M, (❑) 10^{-5} M, (Δ) 10^{-4} M NaCl solutions, ≈9 kV applied to the ESP capillary. Distance between electrospray capillary and electrodes was 3.8 cm.

multiple spray, see Figure 2.6. Once the multiple-tip spray has been generated, and its position relative to the interface plate aperture has been optimized, the ESP interface components do not need to be readjusted. The multiple spray regenerates every time the high voltage (≈9 kV) is applied to this ESP capillary; the ion signal, as monitored by the mass spectrometer, is very reproducible, better than 5% for many months of operation.

As the charged droplets travel downfield through the atmospheric gas, evaporation shrinks the droplet size and this results in an increase of the electric field strength at the surface of the drops. At a certain critical field strength at the droplet surface formation of positive ions occurs either by escape of single, but partially solvated positive ions (*15*), or by the expulsion of smaller highly charged droplets that ultimately lead to formation of gaseous ions (*16*). The nature of the gaseous ions is considered in the next section.

b. Sensitivities for Mass Analyzed Ions: pH Dependence of Nitrogen Bases from Electrosprayed Solutions.

The most suitable class of compounds for positive-ion reverse-phase HPLC/ESP-MS are nitrogen bases, such as nucleosides and nucleotides, polypeptides and proteins, biogenic amines, and alkaloids including narcotics. The ESP sensitivities of these are, as will be shown, pH dependent. It is therefore of interest to consider first the sensitivities of simpler systems such as the alkali ions, for which pH is expected to be less important.

A typical mass spectrum, obtained for a 3 x 10^{-4} M solution of KNO_3 in methanol, is shown in Figure 2.7. The potassium ions K^+, $K^+(H_2O)$, and $K^+(H_2O)_2$ represent 80% of the total ions. The main "extraneous" ions are $Na^+(H_2O)_n$, which are due to sodium ions present as impurity in the methanol solution. This means that more than 90% of the observed ions are due to ions present in the solution. Similar results are obtained with the other alkali ions. The hydrates rather than the methanol solvated ions are generally observed. The vapor pressures of methanol and water in the atmospheric pressure ionization region are estimated, see Appendix 2-I, to be approximately equal. K^+ shows a small preference for H_2O (*17*),

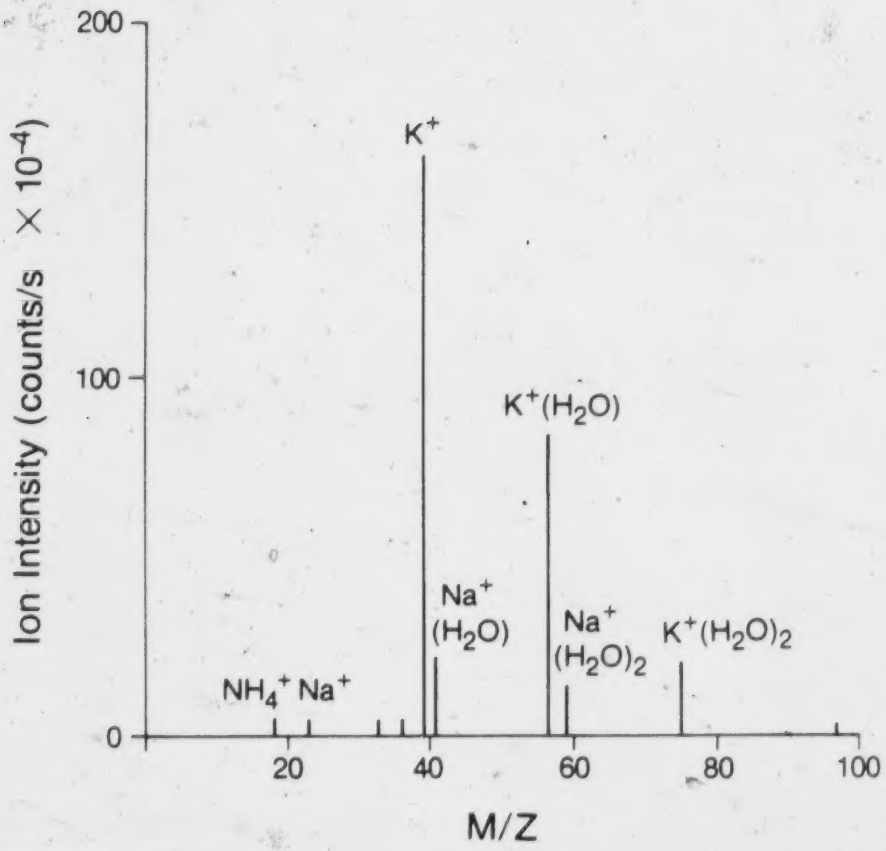

Figure 2.7 Mass spectrum obtained with electrospray. 3×10^{-4} M solution of KNO_3 in methanol; liquid flow 24 μL/min; 9 kV; 4 cm distance to interface plate. The two low intensity ions between Na^+ and K^+ are $CH_3OH_2^+$ and $NH_4^+(H_2O)$.

furthermore, an exchange of CH_3OH for H_2O occurs in the interface region since the "ultrapure"" N_2 gas used contains traces (2 ppm) of water. Experiments in which the water present in the interface gas was decreased or increased, at the parts-per-million level, demonstrated that the observed hydration of the ions is due to the presence of water in the interface gas. It could be shown that ion-hydration equilibria established in the interface chamber. Details of the equilibria measurements are not included in this thesis but will be given in a future publication.

The dependence of ion intensity on concentration of the ions in methanol solution is shown in Figure 2.8 for KNO_3 and $CsNO_3$. Logarithmic scales are used in order to accommodate a wide range of data. The slopes of the plots are close to unity in the linear range, which occurs at low concentrations up to10^{-5} M. This means that the ion intensity in this range is close to proportional to the ion concentration in the bulk (analyte) solution. The sensitivity for K^+ in the linear range is seen to be about 2 times higher than that for Cs ions (see ion intensities at 10^{-5} M, Figure 2.8).

At concentrations above 10^{-5} M the ion intensities are seen to flatten out. This feature is similar to the total ion current-concentration dependence observed in Figure 2.4; however, the flattening out and decrease of the mass analyzed ion current occur earlier, i.e. at lower concentrations.

As an example of dependence of ESP sensitivity of nitrogenous bases, the ESP mass spectrum obtained with a solution of a nitrogen base salt, cocainehydrochloride, 10^{-5} M in methanol, is given in Figure 2.9A. There is only one peak representing the analyte and that corresponds to BH^+, where B is the cocaine base. Protonation without decomposition of the base is the typical result of ESP (*1-11*). Correcting for mass dependent transmission of the quadrupole (*12a*), one finds that more than 90% of the total ion intensity in Figure 2.9A is due to BH^+. Addition of 1.4×10^{-4} mol/L HCl to the above solution leads to the spectrum shown in Figure 2.9B. The BH^+ peak is significantly reduced; the high intensity ions now are protonated methanol $MeOH_2^+$ and $MeOH_2^+ \cdot MeOH$. These ions should be due to protonation

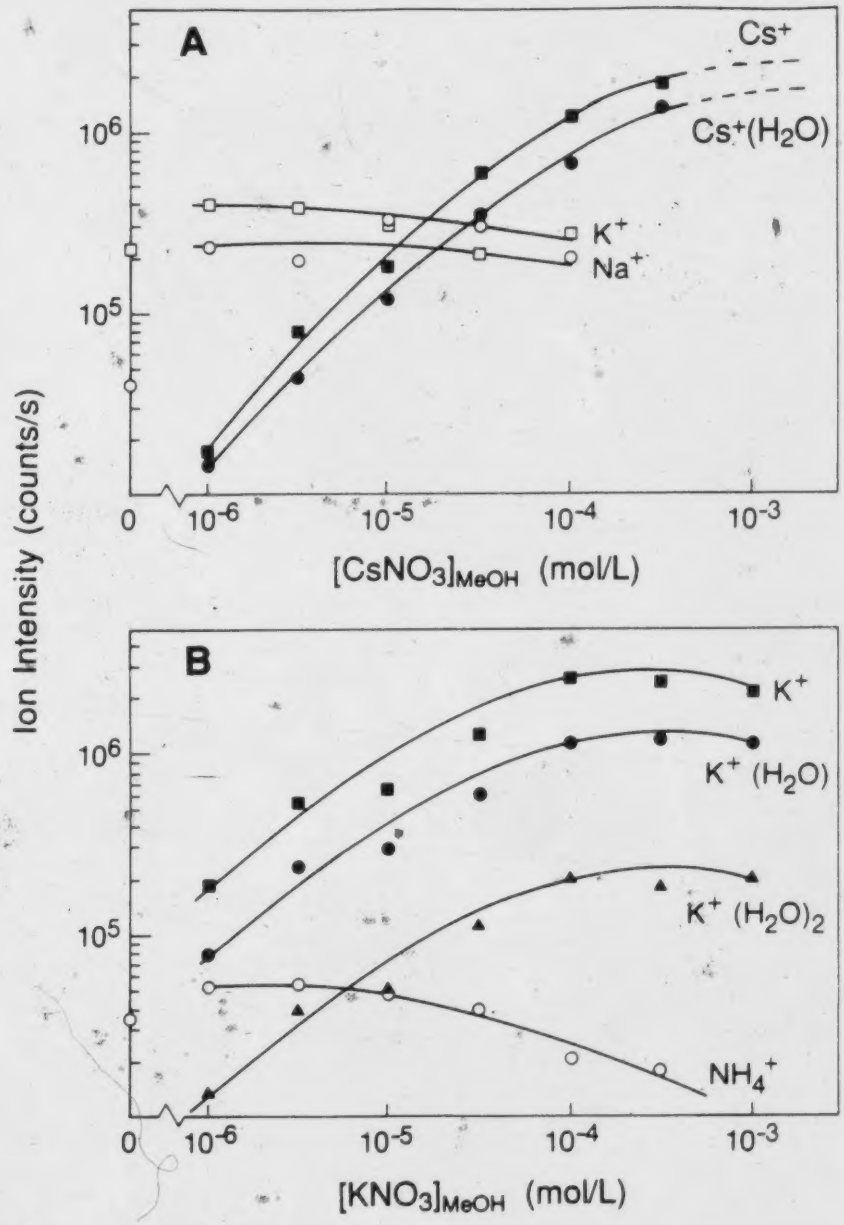

Figure 2.8. Mass analyzed ion intensities: (A) electrosprayed $CsNO_3$ solution in methanol, ions due to Cs^+ and major impurities K^+ and Na^+; (B) ions from KNO_3 solution in methanol. Ions due to K^+ and major impurity ion NH_4^+. Na^+ was also present as impurity and had the same profile as in Figure 2.8A. Ion intensities corrected for mass dependent transmission.

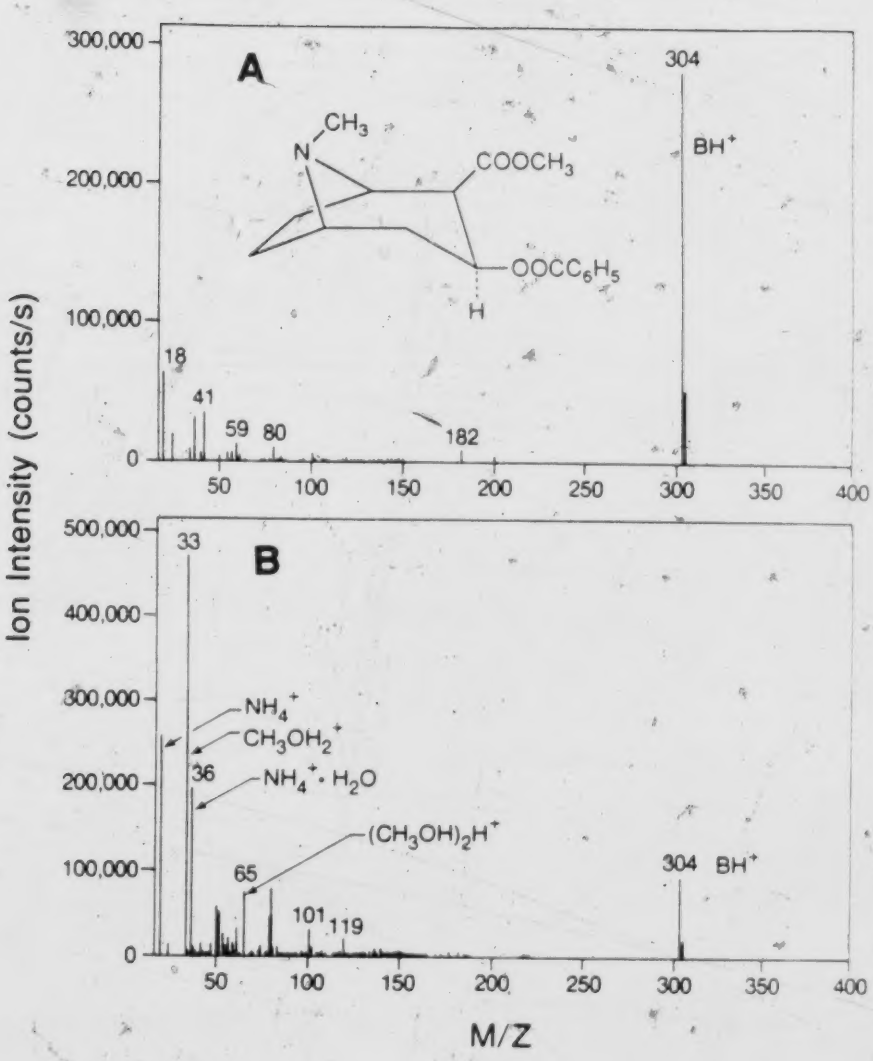

Figure 2.9. (A) Mass spectrum from electrosprayed 10^{-5} M solution of cocaine hydrochloride in methanol. BH^+ stands for the protonated base. (B) 10^{-5} M cocaine hydrochloride in 1.6 x 10^{-4} M HCl solution in methanol. Neither spectrum is corrected for mass dependent transmission of the quadrupole. All instrumental conditions identical for (A) and (B).

of methanol in the acidified solution. However some of the background ions, e.g. NH_4^+, have also increased. The cause for the NH_4^+ increase was not investigated.

The dependence of the BH^+ signal on the concentration of BHCl (B = cocaine) in methanol is shown in Figure 2.10. The results illustrate the impressive concentration range, 10^{-8} - 10^{-3} M, over which the alkaloid can be readily detected. As was observed for Cs^+, the slope in the linear region of the log-log plot is close to unity; i.e. the BH^+ intensity is close to proportional to the BHCl concentration. The background at the m/z value characteristic of BH^+ signal (*m/z* 304) is some 50 counts/s when neat methanol is run through the system.. Extrapolating from the data of Figure 2.10 a BH^+ signal 3 times higher than that of the background can be obtained from 1.5 x 10^{-9} M concentrations. Under single ion monitoring conditions detection requires ≈5 s, which for a 20 μL/min solution flow corresponds to a detection limit of 1 x 10^{-15} mol of analyte in solution. Furthermore, the detection limit can be lowered by an order of magnitude on adjusting the quadrupoles for maximum transmission in a higher mass range. The results in Figure 2.9 were obtained with maximum transmission adjusted to *m/z* 80.

A decrease of sensitivity, below the linear extrapolation from lower concentrations, begins to occur above 10^{-6} M, close to but somewhat *earlier* than was the case for the alkali salts. The decrease of BH^+ intensity at a higher HCl concentration is also illustrated in Figure 2.10.

The decrease of ion intensity of BH^+ on addition of electrolyte, ammonium acetate or HCl, for the analytes cocaine and tripropylamine, is illustrated by the data in Figure 2.11. Decreases by a factor of 10-20 result when the foreign electrolyte is present at concentrations in the 10^{-2} - 10^{-1} M range. Decreases of analyte ion intensities on addition of foreign electrolyte above 10^{-5}M were always observed. Obviously, these are related to the observed saturation and decrease of total ion signal at high electrolyte concentrations, see Figures 2.3-2.5. The actual causes responsible for these phenomena cannot be described here due to the absence of a reliable model of the electrospray and gas phase ion formation mechanism.

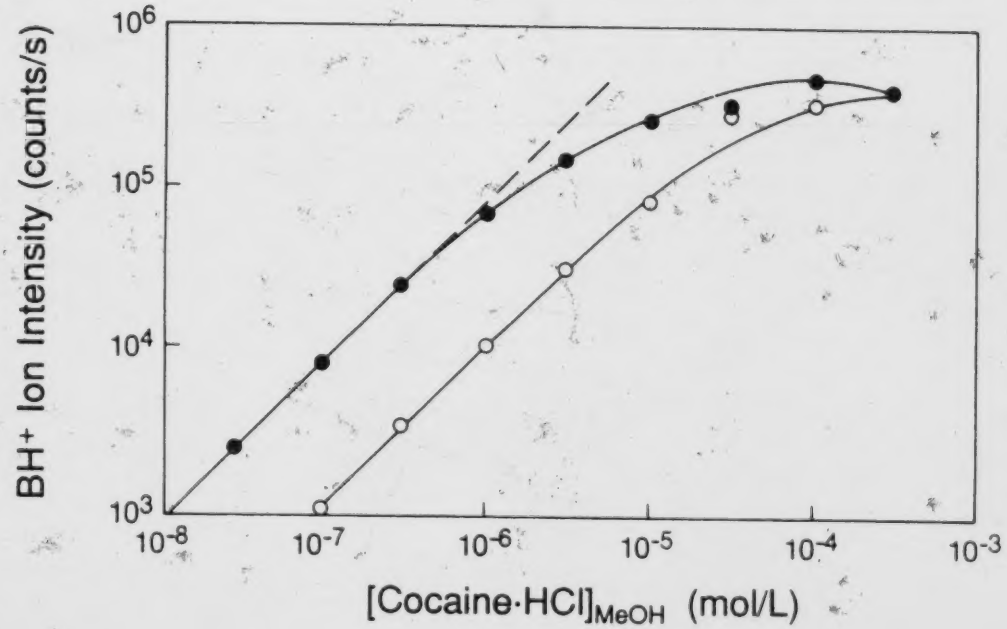

Figure 2.10. Ion intensities for protonated base BH^+ from electrosprayed cocaine hydrochloride in methanol solution: ●, pure methanol; ○, methanol with 10^{-4} M HCl. Ion intensities not corrected for mass dependent transmission. Dashed line gives slope equal to unity. Liquid flow-rate 20 μL/min. Capillary potential 9 kV.

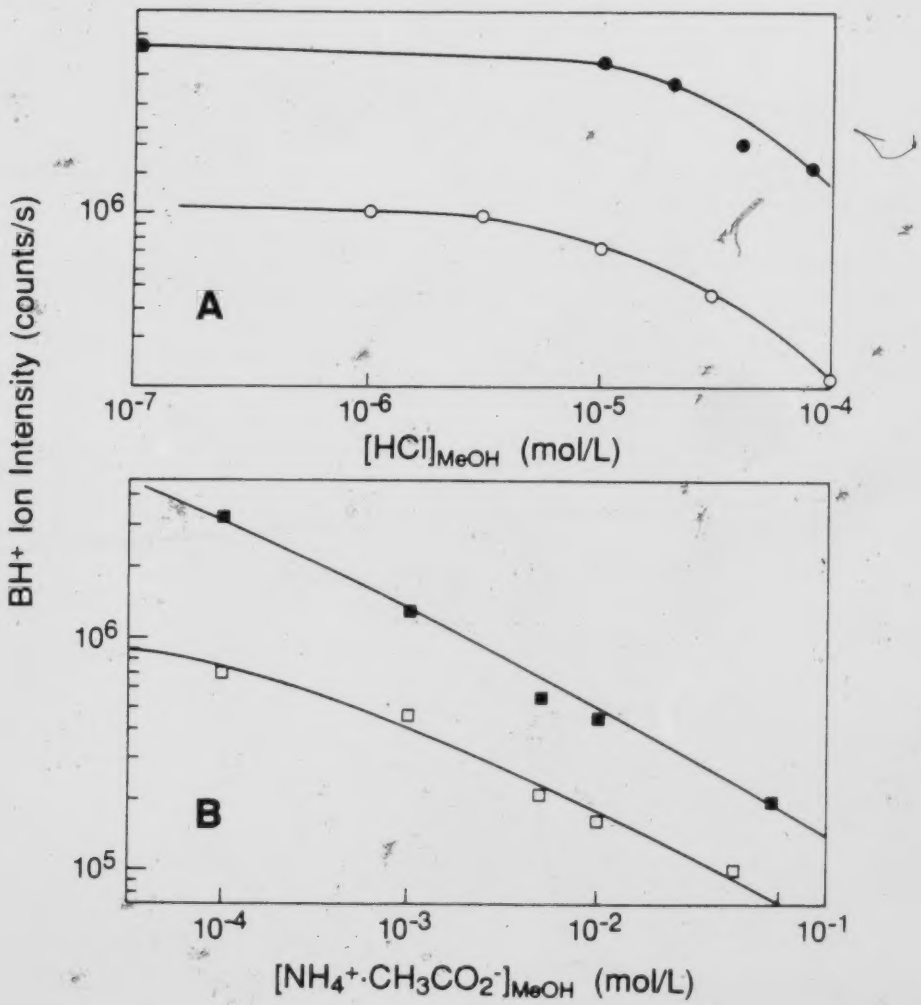

Figure 2.11. Effect of electrolytes on intensities of BH^+ ions: (A) (●) 10^{-5} M of cocaine hydrochloride in methanol solutions with increasing HCl concentration; (○) 10^{-6} M cocaine hydrochloride. (B) (■) 10^{-5} M cocaine hydrochloride in methanol solutions with increasing ammonium acetate concentrations; (❑) same but BH^+ from 10^{-5} M solution of tripropylamine. BH^+ intensities corrected for mass dependent transmission. Liquid flow-rate 20 μL/min. Capillary potential 9 kV.

Cocaine and tripropylamine are strong bases which are essentially completely protonated in methanol solution. For these bases, the addition of acidic electrolyte will have the same effect as the addition of *any electrolyte* to ions like Cs^+ or K^+ and a decrease of the BH^+ ion intensity will result (see Figure 2.11). For bases B that are weak, and thus little ionized in methanol, the addition of acidic electrolyte will lead to an increase of BH^+ concentration in solution. This will lead to an increase of BH^+ ion intensity, but the situation will be complicated by the fact that too much (acidic) electrolyte will also cause a decrease of ion intensity in a fushion similar to that observed for the stronger bases.

First we examine the sensitivities observed for a variety of bases B with known aqueous basicity constants K_B. The observed BH^+ intensities obtained from 10^{-5} M solutions of the pure bases in methanol are shown in Figure 2.12 plotted versus the aqueous pK_B values. As discussed in Appendix 2-II, the expected pK_B values in methanol are approximately 1.4 pK units higher. While there is a considerable scatter in the data, a decrease of BH^+ intensity with increasing pK_B is definitely observed and that trend should reflect the decreasing solution concentration of BH^+ with increasing pK_B. Some of the scatter is undoubtedly due to our use of the aqueous rather than the methanol pK_B values since an exactly parallel shift of all pK_B values cannot be expected. Additional scatter is expected, since the ion intensities for different BH^+ that were electrosprayed need not be the same even when the solution BH^+ concentrations are the same. This would be due to different desorption efficiences from the charged droplets to the gas phase for BH^+ with different molecular structure. The alkali ions showed very similar sensitivities relative to each other (see Figure 2.8); however the bases B used have widely different structural features and volatilities which may lead to different desorption efficiencies for the BH^+ ions.

The sensitivities observed with 10^{-5} M hydrochlorides BHCl in methanol are shown in Figure 2.13. Again, a decrease of sensitivity with increasing pK_B is observed. However the intensities for some of the BH^+, lying in the pK_B range 7-8, are seen to be significantly higher relative to Figure 2.12 results. Thus, the BH^+ intensities of the methyl pyridines ($pK_B \approx 8$)

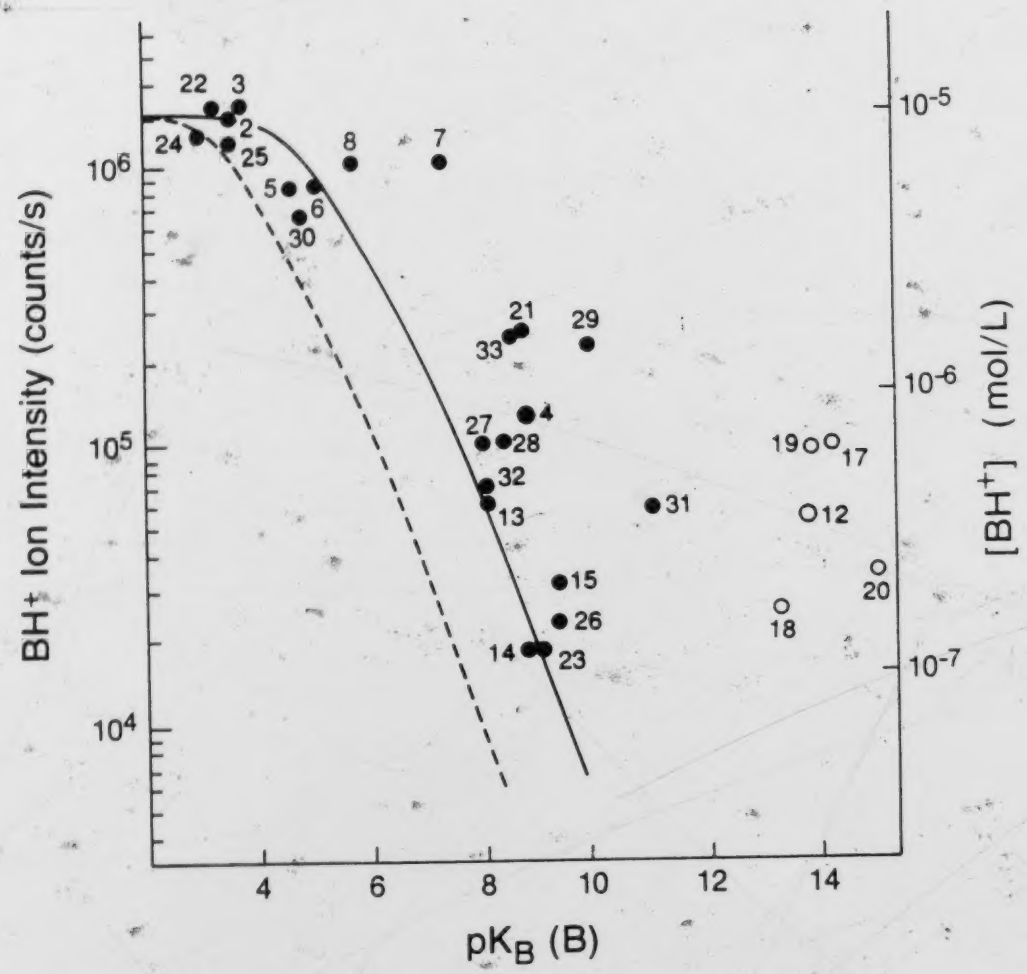

Figure 2.12. Observed ion intensities for BH^+ ions obtained by electrospray of 10^{-5} M solutions in methanol of the free bases B. Bases are identified in Table 2.1. pK_B values are for aqueous solution (*28*). The two curves shown give calculated BH^+ concentrations in methanol solution. Solid line pK_B in MeOH is assumed to be the same as in HOH. Dashed line pK_B in MeOH = pK_B in H_2O + 1.4. Vertical coordinate axis on the right side gives calculated $[BH^+]$ in solution. All BH^+ intensities corrected for mass dependent transmission. For distinction between full and open circles see page 44.

Table 2.1. Nitrogen Bases B Used in Electrospray Experiments.

No	base B	*m/z* of BH^+	pK_B	No	base B	*m/z* of BH^+	pK_B
1	cytosine	112	9.4	18	acetamide	61	13.5
2	n-propylamine	60	3.5	19	urea	61	13.8
3	tripropylamine	144	3.6	20	thiourea	61	15.0
4	adenine	136	9.9	21	4-methoxyaniline	124	8.6
5	ethanolamine	62	4.5	22	triethylamine	102	3.2
6	4-aminopyridine	95	4.9	23	N,N-dimethylaniline	122	8.9
7	2-aminopyridine	95	7.2	24	piperidine	86	2.9
8	morpholine	88	5.6	25	n-butylamine	74	3.4
9	cocaine	304	5.6	26	4-methylaniline	108	9.5
10	codeine	300	6.0	27	4-methylpyridine	94	8.0
11	morphine	286	6.1	28	3-methylpyridine	94	8.3
12	theophylline	181	13.7	29	3-methoxyaniline	124	9.8
13	2-methylpyridine	94	8.0	30	benzylamine	108	4.7
14	pyridine	80	8.8	31	4-aminobenzoic acid	138	11.0
15	aniline	94	9.3	32	3-aminopyridine	110	8.0
16	guanine	152	10.7	33	4-aminopyridine	110	8.5
17	caffeine	195	14.0				

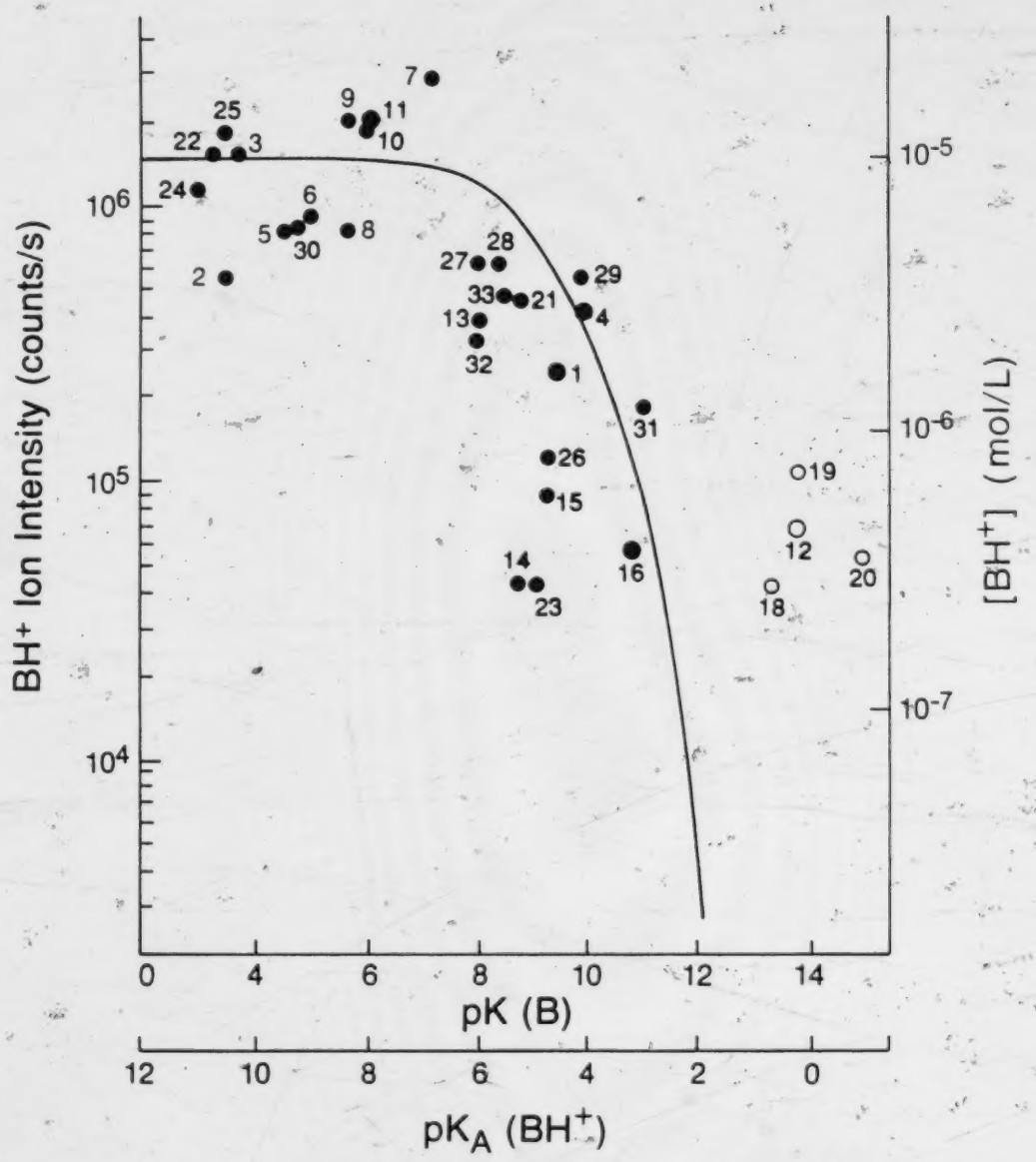

Figure 2.13 Observed ion intensities for BH^+ ions, same as in Figure 2.12, but 10^{-5} M solutions of the BHCl were used. Curve shown gives calculated $[BH^+]$ in solution assuming that $pK_A(BH^+)$ in MeOH = $pK_A(BH^+)$ in H_2O + 0.6. All BH^+ intensities are corrected for mass dependent transmission.

are higher by a factor of 6. It is shown below that a large increase of $[BH^+]$ in solution on conversion from the free bases to the hydrochlorides is expected exactly in this pK_B range. Calculated concentrations in solution of the protonated bases are also shown in Figures 2.12 and 2.13. Unfortunately, pK_B and pK_A values in methanol are not available for most of the compounds used. Therefore, the calculations were made by assuming that the pK_B values in methanol, required for Figure 2.12, are equal to those in H_2O (solid line Figure 2.12) or equal to those in H_2O but increased by 1.4 pK units (dashed curve). The pK_A values required for the calculations relating to Figure 2.13 were assumed equal to the aqueous pK_A but increased by 0.6 pK units. For details of these approximations see Appendix 2-II.

The mass spectrometrically detected BH^+ intensity scale and the calculated solution concentration $[BH^+]$ scale in Figures 2.12 and 2.13 were adjusted relative to each other by assuming that the average base when fully protonated in solution, such that $[BH^+] = 10^{-5}$ M, should give 1.5×10^6 counts/s ion intensity. This choice corresponds to an approximate best fit of the experimentally determined intensities with the calculated $[BH^+]$ at low pK_B values where the bases are fully protonated (see Figures 2.12 and 2.13).

The experimental points in the Figures were divided into two groups. A much larger group shown as full black circles, and a small group shown as open circles. For the larger group, there is a fair correspondence between the observed ion intensities and the calculated values of solution $[BH^+]$. Thus, these data confirm the expected approximate proportionality of ion signal to $[BH^+]$ and the dependence of the ion intensity on the pK_B of the bases and the pH of the solution. The results for the pure bases, Figure 2.12, show that only the strongest bases with $pK_B < 5$ are nearly completely ionized, i.e. $[BH^+] \approx 10^{-5}$ M. For the hydrochlorides near-complete ionization extends up to $pK_B \approx 9$. The observed BH^+ ion intensities show rapid downturns at $pK_B \approx 5$ for the pure bases and $pK_B \approx 9$ for the hydrochlorides, and the calculated $[BH^+]$ concentrations take downturns in much the same pK_B range.

The observed large deviations from the above relationships exhibited by the compounds shown as open circles in Figures 2.12 and 2.13 may be due to special causes. Thus, the compounds (*18-20*), acetamide, urea, and thiourea, are strongly soluble in water but are weak nitrogen bases which may have pK_B and pK_A values in methanol significatly different from those assumed.

It is interesting to note that the best fit relationship which for $[BH^+] = 10^{-5}$ M leads to a BH^+ ion intensity of 1.5×10^6 counts/s is close to the intensities observed for the alkali ions, see Figure 2.8, where $[K^+] = 10^{-5}$ M produces $\approx 0.8 \times 10^6$ counts/s ion signal.

Changes of BH^+ ion signal of a strong base, tripropylamine, and a somewhat weaker base, 4-methylpyridine, from electrosprayed solutions where the base is 10^{-5} M and the HCl concentration is gradually increased, are shown in Figure 2.14. The strong base tripropylamine, which is 100% ionized even in the absence of HCl, cannot further increase its $[BH^+]$ in solution. Therefore, addition of HCl leads only to an increase of $CH_3OH_2^+$ and the intensity of BH^+ decreases with increasing foreign electrolyte concentration. On the other hand, the weaker pyridine base increases its solution value of $[BH^+]$ as the HCl concentration is increased, and this leads to increased BH^+ ion intensity. After the base in solution is fully ionized, which happens at $\approx 5 \times 10^{-5}$ M HCl, further addition of HCl decreases the BH^+ ion signal since the additional HCl leads to an increase of foreign electrolyte. These changes are completely consistent with the observations in Figures 2.12 and 2.13 and the preceding discussion.

We conclude that the electrospray intensities of BH^+ ions do exhibit solution pH dependence, i.e. increase as the solution $[BH^+]$ increases, but the trends are obscured by different desorption efficiencies of BH^+ and the adverse effect of extraneous electrolytes on the mass-selected sensitivity.

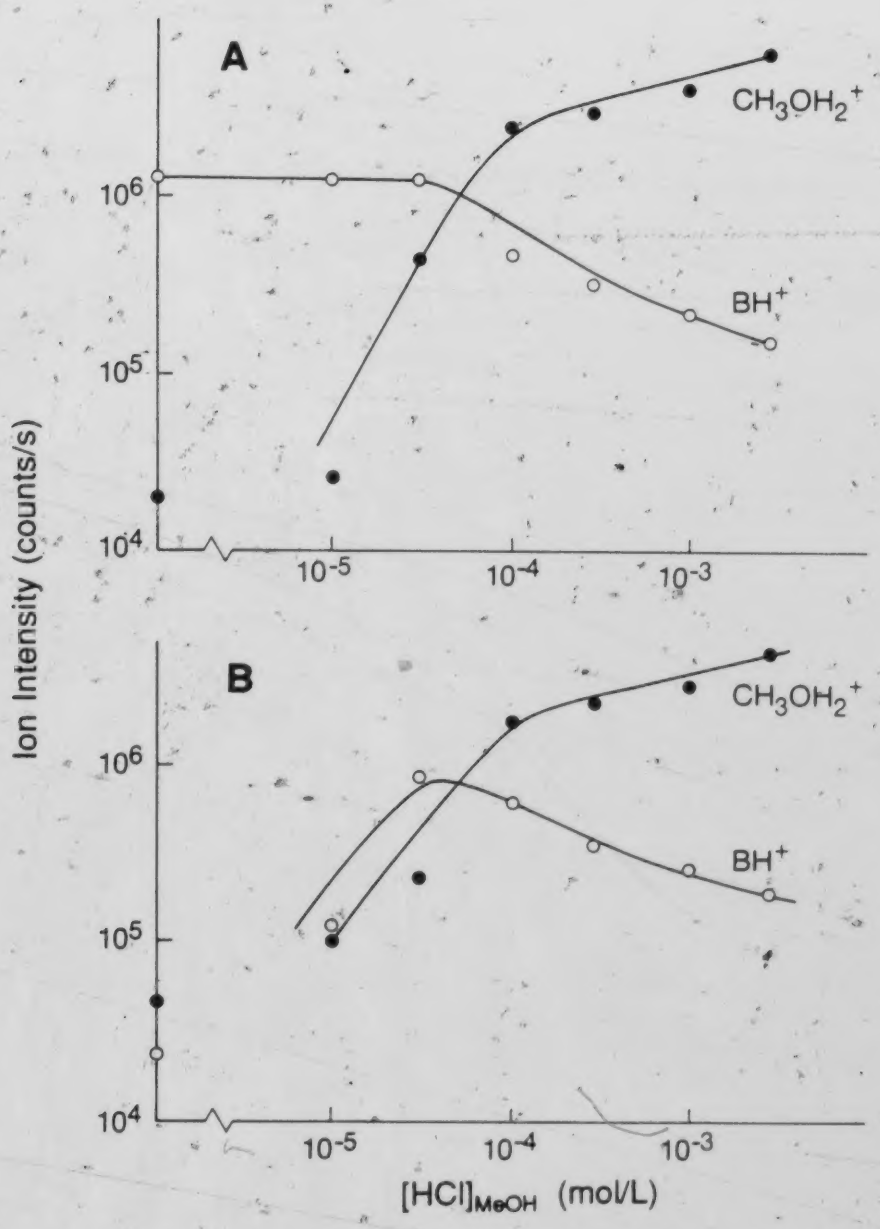

Figure 2.14. Effect of acidification of electrosprayed solutions on BH^+ ion intensity; (A) strong base B (tripropylamine), which is fully ionized in solution, does not profit from acidity increase; (B) weaker base 4-methylpyridine becomes fully ionized in solution only after addition of HCl. Bases in both figures have constant concentration of 10^{-5} M in methanol. Ion signal shown as $CH_3OH_2^+$ corresponds to total ions $H^+(CH_3OH)_n$.

c. Coanalyte Interference: Proton Transfer in Solution and in the Gas Phase.

The effects of coanalytes in solution are illustrated by the results shown in Figures 2.15 and 16. Measured BH^+ ion intensities are given in Figure 2.15A for increasing equimolar concentrations of two coanalytes with reversed solution and gas phase basicity order, 4-aminopyridine (pK_B = 4.89, GB = 222 kcal/mol) and n-butylamine (pK_B = 3.4, GB = 211 kcal/mol). All gas phase basicities GB quoted in this section are from the compilation of Lias et al. (*18*). The BH^+ intensity of 4-aminopyridine, the analyte with the lower solution basicity but higher gas-phase basicity, is seen to become higher than that of its coanalyte at high concentrations. Similar behavior is also observed for the pair tripropylamine (pK_B = 3.6, GB = 226 kcal/mol) and n-propylamine (pK_B = 3.46, GB = 210 kcal/mol), i.e. the BH^+ of the stronger gas phase base and weaker solution base tripropylamine is smaller at low concentrations but becomes higher at large concentrations, the crossover for this pair occurring at lower concentrations (see Figure 2.15B). The dominance of the higher *gas-phase* basicity analyte at high concentrations suggests that this effect may be due to gas-phase proton transfer. Thus, evaporation of the free bases from the solvent droplets may be leading to sufficiently high gas-phase base concentrations for gas-phase proton transfer to occur as shown in eq 2.1, where $B'H^+$ is due to electrospray-produced gas-phase ions and B is the

$$B'H^+ + B = B' + BH^+ \qquad (2.1)$$

evaporated molecule of the stronger gas-phase base. However this interpretation is made somewhat uncertain by the fact that the quoted solution basicities are for water and not methanol. Because the solution basicities are fairly close, it is possible that the basicity order in methanol may be the reverse to that in water. In that case, the observed BH^+ changes in Figure 2.15 could be due to expected changes of relative BH^+ concentrations in *solution*; i.e. at high concentrations, the stronger base will increase the basicity of the solution and suppress the ionization of the weaker base.

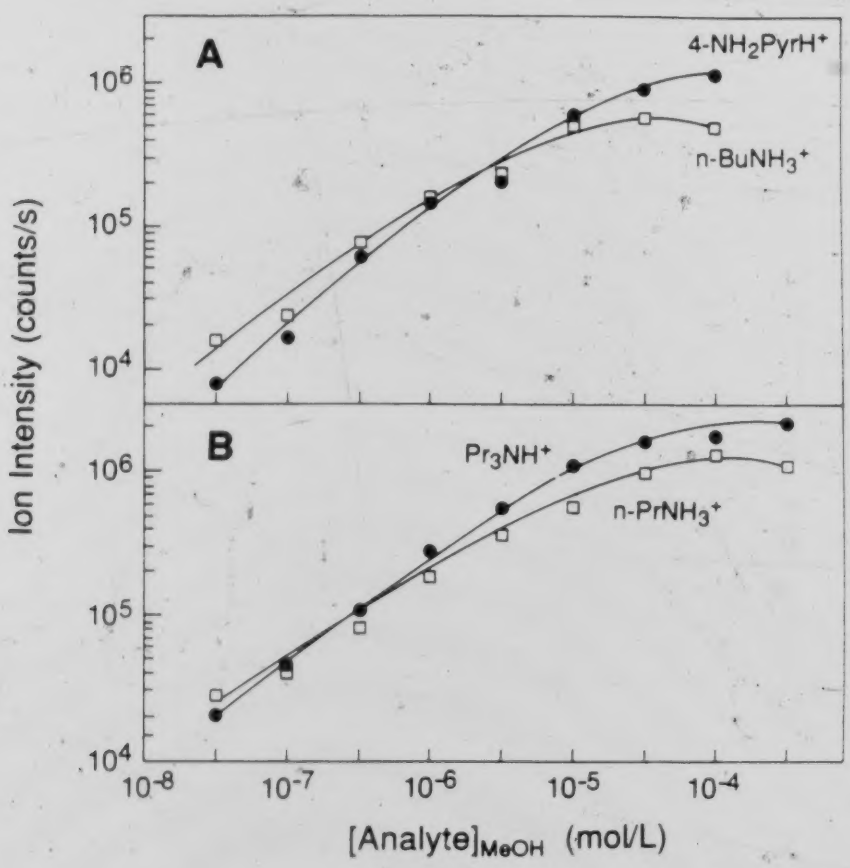

Figure 2.15 Intensities of BH^+ ions from electrosprayed solutions of two bases with equimolar concentrations in methanol. (A) ●, 4-aminopyridine (4-NH_2Pyr); ❑, n-butylamine (n-$BuNH_2$); (B) ●, tripropylamine (Pr_3N); ❑, n-propylamine (n-$PrNH_2$). All ion intensities are corrected for mass dependent transmission.

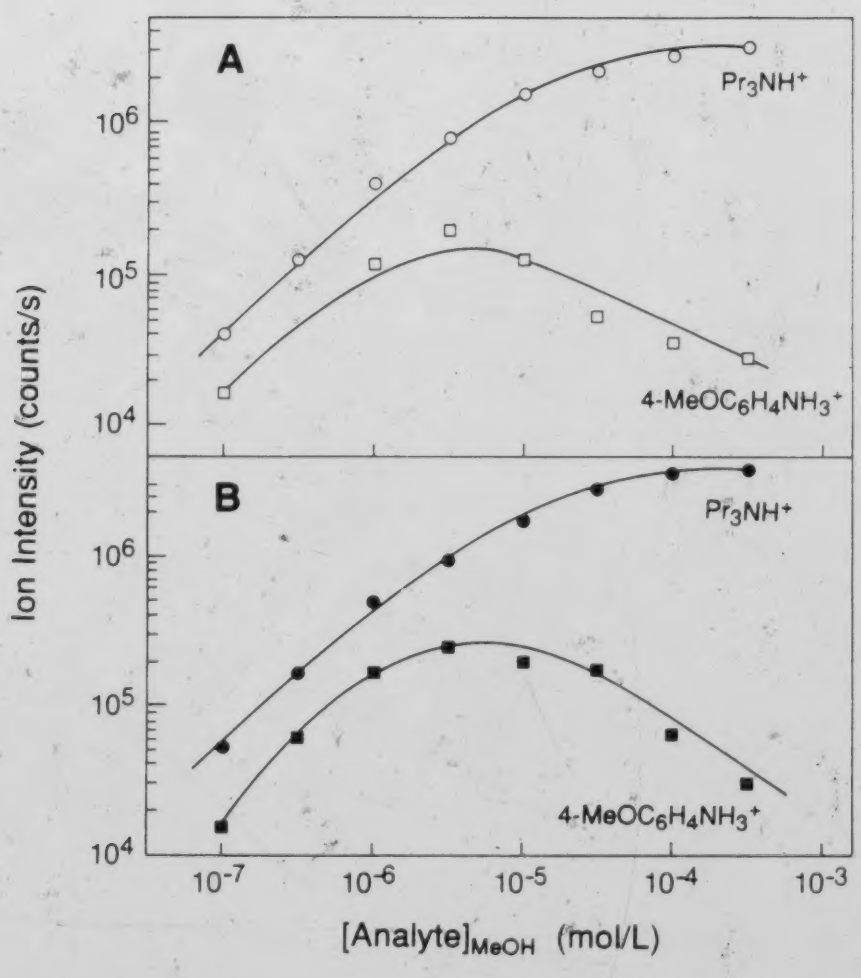

Figure 2.16 Measured intensities of BH^+ ions from electrosprayed solutions of two bases with equimolar concentration in methanol: (A) ○, tripropylamine (Pr_3N); ❑, 4-methoxyaniline ($4\text{-}MeOC_6H_4NH_2$); (B) ●, tripropylamine hydrochloride; ■, 4-methoxyaniline hydrochloride. All ion intensities are corrected for mass dependent transmission.

Results for two bases with a very large pK_B difference are shown in Figure 2.16. Unfortunately two suitable bases with a large pK_B difference in solution and reversed basicity order in the gas phase could not be found. The pair used, tripropylamine (pK_B = 3.6, GB = 226 kcal/mol) and 4-methoxyaniline (pK_B = 8.6, GB = 206 kcal/mol), has the same basicity order in both phases. The observed BH^+ intensities show a large decrease of the protonated 4-methoxyaniline at high concentrations. This suppression could be due to corresponding protonated base changes in solution and calculations of the concentrations in solution show that such changes will occur in the concentration range used. However the same interpretation cannot be sustained for the results where equimolar concentrations of the hydrochlorides of the bases are used, see Figure 2.16B. The BH^+ ion curves obtained with the free bases and with the hydrochlorides are seen to be essentially identical. This would not be the case had solution BH^+ concentrations been determining the BH^+ intensities, since in solution the suppression of the weaker base should not occur when the hydrochlorides are used. The close similarity of the two sets of results suggests that gas-phase proton transfer to the stronger gas-phase base, tripropylamine, is involved.

Experiments were performed in which gaseous bases B were mixed at known partial pressures into the air supplied to the atmospheric ionization chamber. Simultaneously methanol solutions containing known concentrations of a second base B' of lower gas phase basicity were electrosprayed. The observed BH^+ and $B'H^+$ intensity changes as the partial pressure of B was increased are shown in Figure 2.17A. The stronger gas-phase base, tripropylamine, added to the gas phase is seen to cause a decrease of the intensity of electrospray produced $B'H^+$ obtained with a constant concentration 10^{-5} M 4-methoxyaniline in methanol. Very similar results, not shown, were observed also for tripropylamine, in the gas phase, and $B'H^+$ from electrosprayed n-butylamine solution.

The results in Figure 2.17A must be due to gas phase proton transfer eq 2.1. Intensities for BH^+ from tripropylamine and $B'H^+$ from 4-methoxyaniline where both originate from the same electrosprayed solution are shown in Figure 2.17B. In these experiments solutions

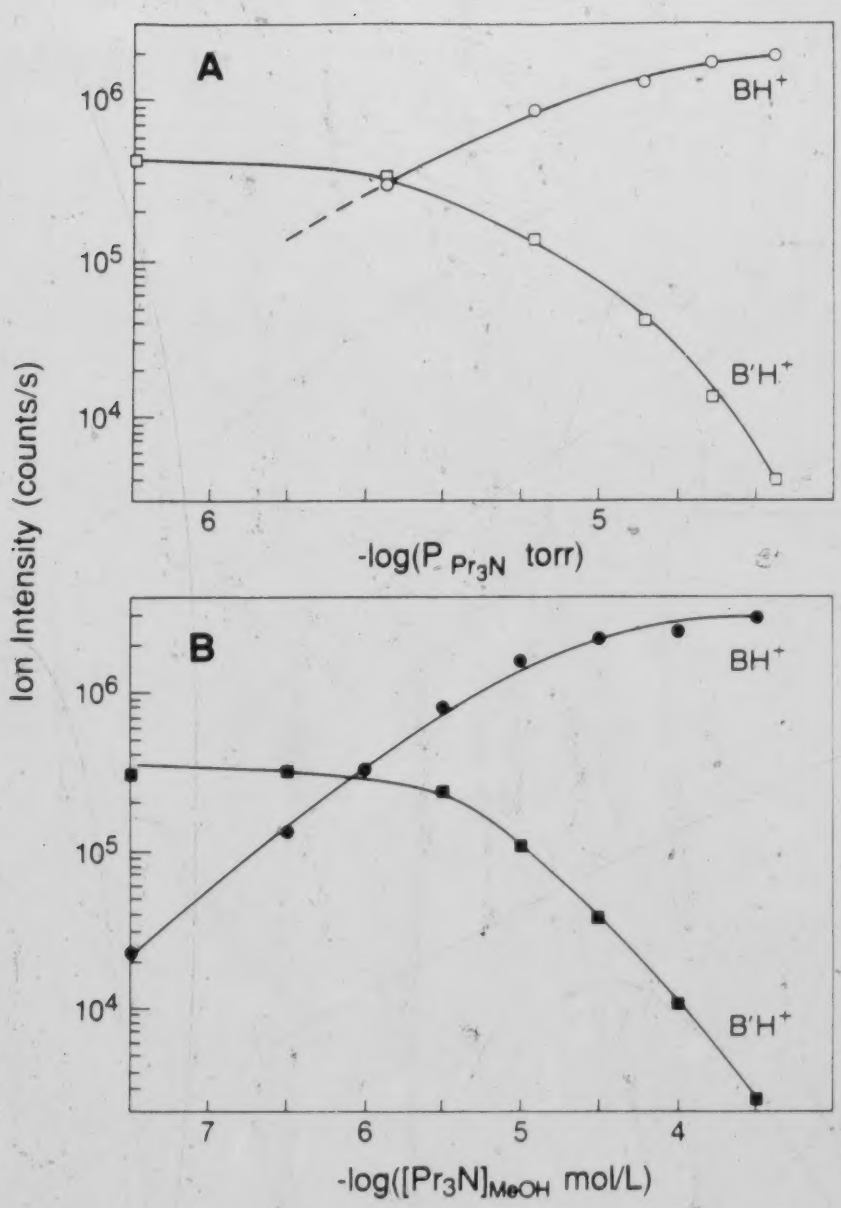

Figure 2.17 (A) Ion intensities of BH^+ and $B'H^+$, where B is tripropylamine added to the gas phase and B' is 4-methoxyaniline from electrosprayed solution containing 10^{-5} M of B'. (B) Ion intensities of BH^+ and $B'H^+$ where both ions originate from electrosprayed solutions which have constant concentration of $[B'] = 10^{-5}$ M and variable concentration of [B]. All ion intensities are corrected for mass dependent transmission.

were used in which the 4-methoxyaniline concentration was kept constant at 10^{-5} M and the tripropylamine concentration was gradually increased. The shapes of the BH^+ intensities in Figure 2.17B are seen to be very similar to those in Figure 2.17A. This similarity supports the assumption that gas phase proton transfer is involved in both cases and also in Figure 2.16. From the two sets of results in Figure 2.17 taking corresponding decreases of $B'H^+$ (4-methoxyanilinium) intensity one can establish the approximate proportionality shown in eq 2.2 where P_B is the effective pressure of B produced in the gas phase from electrosprayed

$$P_B \text{ (Torr)} \approx 0.6 \text{ (Torr mol}^{-1} \text{ L)} [B] \text{ (mol L}^{-1}) \qquad (2.2)$$

methanol solution containing [B] (flow rate 20 μL/min). Equation 2.2 is valid for concentrations above $\approx 10^{-5}$ M. For example, 1.8×10^{-5} M electrosprayed tripropylamine according to eq 2.2 produces 10^{-5} Torr tripropylamine in the gas phase.

An estimate based on assumed near complete evaporation of electrosprayed B, given in Appendix 2-I, also leads to an equation of the same form as eq 2.2, but with the proportionality factor 0.4 (Torr mol^{-1} L). The agreement, considering the uncertainties in the gas flow conditions, see Appendix 2-I, must be considered as very good and provides additional evidence for the importance of gas phase proton transfer when analytes at solution concentrations above 10^{-5} M are coelectrosprayed. Above 10^{-5} M concentrations, only a very small fraction of ions BH^+ present in solution enter the gas phase (see total ionization results, Figure 2.3, and associated discussion of ion yield). Therefore, most of the B present in the droplets can evaporate as B provided that it is sufficiently volatile. Even when B is largely present as BHCl in solution, assuming that Cl^- is the typical counterion, B and HCl escaping in the gas phase can lead to a fairly complete conversion of BH^+ to gas-phase B. The present interpretation of the results should be valid only for bases of relatively high volatility as used in the present experiments.

Buffers which can produce nitrogen bases in the gas phase, such as ammonium acetate, can also lead to gas-phase proton transfer. Fortunately, ammonia is a relatively weak nitrogen base in the gas phase (*18*); however the proton transfer eq 2.1 in the gas phase actually involves solvated (hydrated) $B'H^+$ ions and solvent transfer can occur to BH^+. Under such conditions, ammonia becomes a relatively stronger base due to the relatively strong solvation interactions of the ammonium ion (*12a, 19a*).

The presence of proton held dimers B_2H^+ was observed in electrospray mass spectra by Smith (*8*) at high B concentrations in solution. B_2H^+ ions were observed also in the present work. For example, high intensities of B_2H^+ were seen for B = cytosine. It is known that this dimer is held in the gas phase by very strong bonding forces (*17*). The presence of relatively high pressures of bases B evaporated from the solution demonstrated above suggests that the dimers are formed by the well-known reaction of BH^+ with B in the gas phase. The B_2H^+ are not so frequently observed, because often the bonding is weak and the B_2H^+ ions do not survive the collision-induced decomposition occurring past the orifice. While gas-phase formation of B_2H^+ can be expected for relatively volatile bases B, the origin of such ions from the solution can by no means be excluded provided that there is appreciable B_2H^+ ion concentration in solution. The present findings show only that the observation of B_2H^+ ions with the mass spectrometer is no proof that these species are present in the solution.

d. Residence Time of Electrosprayed Ions in the Atmospheric Pressure Region.

The experiment in which a base B is added to the air stream at a known partial pressure, while a base B' at constant concentration in solution is electrosprayed, and gas-phase proton transfer between the electrospray produced gaseous $B'H^+$ and the gaseous B is observed (see eq 2.1 and Figure 2.17A), can be used to obtain estimates of the residence time of

electrosprayed ions in the atmospheric pressure region, where the reaction occurs. The integrated rate equation for reaction 2.1 is shown in eq 2.3, where $I(B'H^+)$ is the detected

$$-\ln(I(B'H^+)/I(B'H^+)_o) = k[B]t_r \qquad (2.3)$$

ion intensity at different gas-phase concentrations [B]. Equation 2.3 is for a pseudo-first-order reaction, as is appropriate for the present conditions where the concentration of the ions is very much lower than the concentration of the neutral reactant so that [B] remains constant. t_r is the total reaction (residence) time, which is assumed to be the same for all ions. The ions are also expected to diffuse to the walls where they discharge. This ion loss is not included in eq 2.3. It can be shown that eq 2.3 will still be approximately valid, provided that the diffusion loss is first order in the ion concentration and the diffusion rate constants for the two ions, $B'H^+$ and BH^+, are approximately the same (*19b*).

Logarithmic plots of measured $I(B'H^+)$ versus the given constant pressure of B used in a given experiment are shown in Figure 2.18. The plots are seen to be good straight lines, confirming the validity of eq 2.3.

Three series of experiments were performed in which the B (tripropylamine) was used in the gas phase and three different bases, B', were electrosprayed. Since the slopes ρ of the lines correspond to: $\rho = kt_r$, see eq 2.3, the different slopes indicate either different residence times or different rate constants for the ions $B'H^+$. The mobilities of the different $B'H^+$ even when clustered with solvent molecules are expected to be quite similar (*20*), and therefore probably the rate constants are the ones that change. It was shown in earlier work (*19a*) that the rate constants for proton transfer reactions involving ions that are clustered by solvent molecules generally increase as the exothermicity of the proton transfer reaction increases. The slopes obtained in Figure 2.18 are seen to increase with increasing exothermicity, evaluated from the gas-phase basicity difference ΔGB (*18*). This result also suggests that it is the rate constants which change. Assuming that the reaction with the largest slope proceeds at

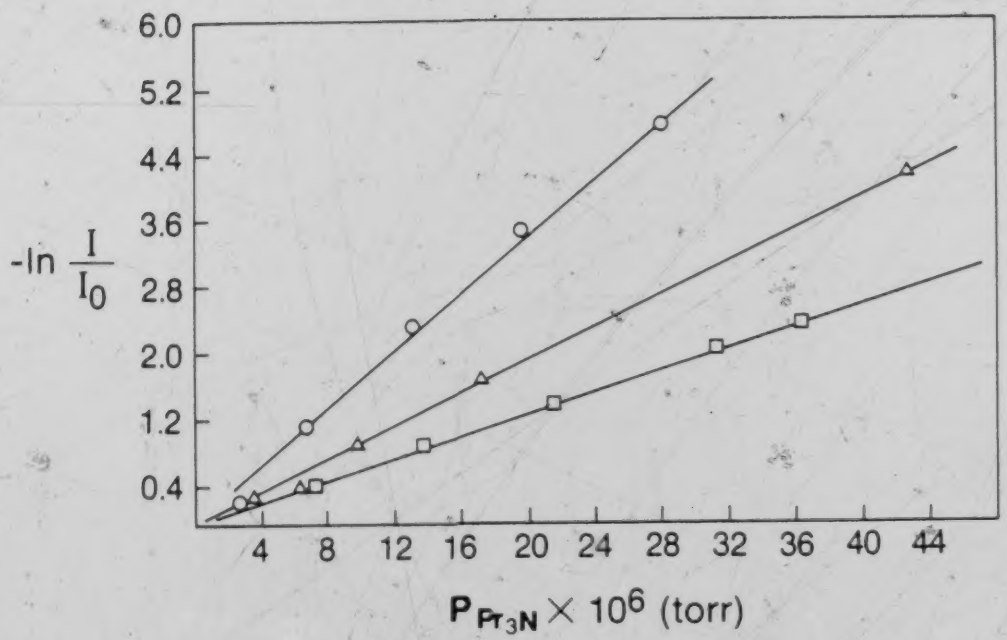

Figure 2.18 Gas phase proton transfer between ions $B'H^+$ from electrosprayed base B' and a stronger base, B = tripropylamine added to the gas phase. I is intensity of $B'H^+$ when pressure of B is P_B. I_o is intensity when $P_B = 0$. Slope of straight lines leads to product of rate constant and residence time: ○, B' = 4-methoxyaniline, exothermicity of proton transfer ΔGB = 19.7 kcal/mol; △, B' = n-butylamine ΔGB = 15.6 kcal/mol; □, B' = 4-aminopyridine, ΔGB = 4.2 kcal/mol.

the collision limit (*19*), $k = 2 \times 10^{-9}$ (molecules^{-1} cm^3 s^{-1}), one evaluates a reaction time $t_r \approx 2.6 \times 10^{-3}$ s.

The millisecond reaction time for the gas phase ions produced by electrospray, evaluated above, appears to be of the right order of magnitude. A similar residence time was evaluated on the basis of the mobility of the ions in atmospheric air, the electric field strength present, and the distance between the electrospray tip and the interface plate; see Appendix 2-III. Considering that both methods used for obtaining t_r are approximate, an agreement within a factor of 2 as obtained, see Appendix 2-III, can be considered as good. In actual electrospray conditions, a good fraction of the distance may involve travel with the ions still inside the droplets, so that they cannot participate in gas-phase reactions (*21*). This fact was not taken into account in the Appendix 2-III calculation. However, as it turns out, the electric field is weakest in the vicinity of the interface plate, see Figure 2.19, and consequently the calculated residence time is mostly due to ion drift in this region. Assuming that most of the gas phase ions were generated roughly in the first half of this low field region, an approximate correspondence between the residence time evaluated on the basis of the reaction kinetics and ion drift velocities can be accounted for.

CONCLUSIONS

(a) When electrospray is operated in the positive ion mode, a partial separation of positive and negative ions of electrolytes present in the solution occurs near the capillary tip and the electrosprayed droplets contain excess positive ions. At low electrolyte concentrations, 10^{-5} M or less, the ion separation can be very efficient such that the positive ions exceeded the negative ions by a factor of 2 (50% yield).

(b) The ion separation yield decreases as the electrolyte concentration is increased.

(c) For alkali ions, Ca^{2+} and NH_4^+, and organic nitrogen bases, BH^+, the efficiencies of emission of positive ions of the given kind, from the droplets into the gas phase, seem to be fairly similar.

(d) When the total electrolyte concentration in the solution is less than 10^{-4} M, extremely high analyte detection sensitivities can be obtained; i.e. ions in the 10^{-9} - 10^{-7} M range can be easily detected with the mass spectrometer. The detection limit for ions BH^+ in solution can be as low as 10^{-16} mol.

(e) Because the positive ion-negative ion separation yield decreases as the total electrolyte concentration is increased, and the emission of ions from the droplets is relatively nonselective, ionic analyte detection sensitivities decrease with increasing total electrolyte concentration in the electrosprayed solution.

(f) The sensitivities for organic nitrogen bases B are pH dependent; i.e. the detected BH^+ ion signal is approximately proportional to the BH^+ concentration in solution. However these trends are obscured when high concentrations of external electrolyte are used for the pH control.

(g) The residence time of the average electrosprayed gas phase ions in the atmospheric gas region is $\approx 2 \times 10^{-3}$ s. Ion-molecule reactions in the gas phase such as proton transfer to

stronger gas-phase base coanalyte can occur in this region and may degrade the sensitivity of the given ionic analyte. This effect is important only at high analyte or buffer concentrations.

(h) The decrease of analyte ion sensitivity at high foreign electrolyte concentration may be considered as a weakness of the method, for reverse phase HPLC applications, where buffers in the 10^{-2} M range or higher are used in order to improve the separation. However, the very high sensitivity of ESP which allows analytes in the 10^{-9} - 10^{-5} M range to be easily detected, means that much smaller quantities of mixtures can be used in the LC separations and the buffer concentration can be dropped accordingly to 10^{-4} - 10^{-3} M levels, where its effect on the sensitivity will be very small. Considering also the low effluent flow requirement, it becomes clear that ESP shows its greatest promise for micro LC/MS applications.

Appendix 2-I. Partial Pressures of Compounds Evaporating from Electrosprayed Droplets.

Of interest is the partial pressure in the electrosprayed region where the gases may engage in ion-molecule reactions with the electrosprayed ions. Assume that the rate of introduction of an electrosprayed compound M (which could also be the solvent) is: $\overline{n}_M$ (mol s^{-1}). The solution when sprayed forms a cone with radius at the base r = 4 cm and height h = 4 cm, whose volume is $V_c = \pi r^2 h/3 = 67$ cm^3; see Figure 2.2B. Complete evaporation of the solvent and components is assumed. The evaporation occurs into atmospheric air. The complete cylindrical atmospheric pressure container, see Figure 2.1, has the dimensions: radius = 11 cm and length 11 cm, corresponding to a volume $V_t = 4200$ cm^3. The air out of that volume is removed at a total rate $\overline{V}_t = 1$ Ls^{-1}. Since the moles of air per unit volume in the electrosprayed cone region is very much larger than the moles of the electrosprayed vapor, the assumption is made that the evaporated solvent and analytes diffuse very slowly past the cone volume, i.e., remain confined to the cone volume. The rate $\overline{V}_c$ at which the cone volume is exhausted, due to $\overline{V}_t = 1L\ s^{-1}$ overall flow, is assumed to be:

$$\overline{V}_c = \frac{V_c}{V_t} \times \overline{V}_t = \frac{67}{4200} \times 1 = 1.6 \times 10^{-2} Ls^{-1} \qquad (2.4)$$

Now, P_M the partial pressure of the compound M can be obtained via the ideal gas law, eq 2.5,

$$P_M \overline{V}_c = \overline{n}_M RT \qquad (2.5)$$

$$P_M(\text{Torr}) = (1.17 \times 10^6)\overline{n}_M \qquad (2.6)$$

where eq 2.6 is obtained for a temperature T = 300 K and the numerical values quoted above. Using eq 2.6 and an LC flow of 20 μL min^{-1}, one evaluates the partial pressure of methanol (density methanol 0.8 g/cm^3), $P(CH_3OH)$ = 12 Torr. Thus, methanol is present at only a fraction of its saturation pressure (≈120 Torr). Assuming a 25% humidity of the air used, the water pressure in the same volume will be ≈5 Torr. A volatile analyte, present at a concentration of C_A (mol L^{-1}) in the electrosprayed solution, will lead according to eq 2.6 to a pressure:

$$P_A(\text{Torr}) = 0.4\ (\text{Torr mol}^{-1}\ \text{L})\ x\ C_A\ (\text{mol L}^{-1}) \qquad (2.7)$$

Appendix 2-II. Evaluation of BH^+ Concentrations in Methanol.

Unfortunately pK_B (or pK_A) values for many of the bases used in the present work in methanol solution are not available in the literature. Bell (*23*) provides data for a number of primary ammonium ions which show that the pK_A increases by ≈1.2 pK units from water to methanol. Grunwald (*24*) has provided data which indicate that the pK_A for tertiary ammonium ions increase by less than 0.5 pK unit and Ritchie (*25*) has shown that the pK_A for methyl-substituted pyridinium ions increases by only 0.2 pK unit from water to methanol. The autoprotonation constant (*26*) K_s for methanol, equivalent to $K_w = 10^{-14}$ for water, is much smaller; see eq 2.8. This value reflects the relatively poorer solvation of the $CH_3OH_2^+$

$$K_s(CH_3OH) = 10^{-16.7} = [CH_3OH_2^+][CH_3O^-] \qquad (2.8)$$

and CH_3O^- ions by methanol when compared to H_3O^+ and OH^- in water.

In order not to introduce additional trends in the data by arbitrary assumptions on *selective* changes of pK_A for the different groups of compounds, we have assumed that all the pK_A values increase by 0.6 pK_A unit from water to methanol. Furthermore since the methanol

used in our electrospray is not completely dry, the autoprotolysis constant was assumed equal to $pK_S = 16$, which makes the pK_B increases equal to 1.4 pK units.

The protonated base concentrations $[BH^+]$ in solution were evaluated by using the conventional acid-base equilibria equations. The concentrations when the pure bases were dissolved in methanol were obtained from eq 2.9,where $x = [BH^+] = [MeO^-]$ and C_B is the

$$K_B(MeOH) = \frac{[BH^+]\,[MeO^-]}{[B]} = \frac{x^2}{C_B - x} \qquad (2.9)$$

initial concentration of the base; x was evaluated by solving the quadratic equation.

The concentrations of $[BH^+]$, when the base hydrochlorides were dissolved, were obtained from eq 2.10,where $x = [B] = [MeOH_2^+]$, C_{BHCl} is the initial concentration of the

$$K_A(MeOH) = \frac{[B]\,[MeOH_2^+]}{[BH^+]} = \frac{x^2}{C_{BHCl} - x} \qquad (2.10)$$

base hydrochloride, and K_A is the acidity constant of BH^+.

Appendix 2-III. Drift Time of Ions in the Electrospray Field.

The drift time t for ions drifting from the capillary tip to the plane electrode, see Figure 2.2B, and remaining on the axis of the rotationally symmetric electrical field $\varepsilon(s)$ was evaluated. The axial field as a function of the distance s from the tip to the plate, evaluated in ref 22, is shown in Figure 2.19. Given the ion drift velocity v(s), the drift time t is obtained from eq 2.11 where b = 4 cm is the total axial distance between tip and plane electrode and

$$t = \int_0^b \frac{ds}{v(s)} = \frac{1}{\mu}\int_0^b \frac{ds}{\varepsilon(s)} \qquad (2.11)$$

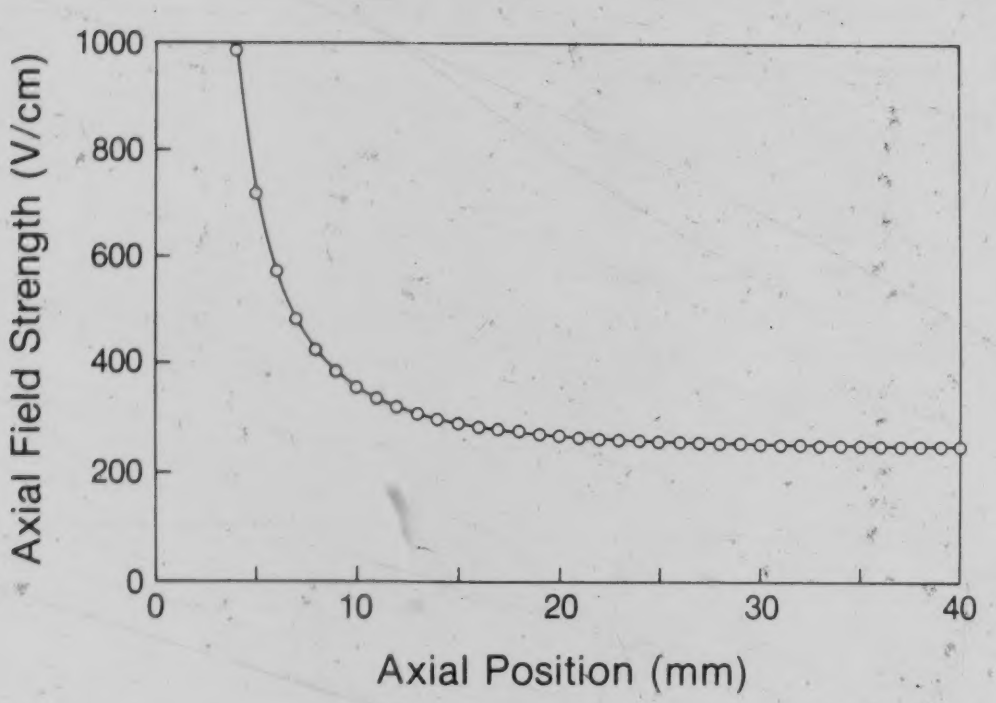

Figure 2.19 Electric field strength as function of distance between electrospray capillary tip and plane electrode. Space charge effects neglected. (Figure is based on modeling calculations described in ref 22.)

μ is the mobility of the ions, see eq 2.12. The mobility μ was obtained from the reduced zero field mobility μ_o, see eq 2.13, where P (Torr) and T(K) are pressure and temperature (*20*).

$$v = \mu\varepsilon \tag{2.12}$$

$$\mu = \frac{760}{P}\frac{T}{273}\mu_o \tag{2.13}$$

The zero field mobility μ_o for ions moving in gases, which have polarizability α but no dipole moments, can be evaluated to a good approximation (*20*) with eq 2.14, where α is in

$$\mu_o = 13.876/(\alpha m_r)^{1/2} \text{ cm}^2 \text{ V}^{-1} \text{ s}^{-1} \tag{2.14}$$

Å^3 and the reduced mass m_r is in atomic units. The mass m_r selected for the drifting solvated ion was 300. This leads to a reduced mass in air of 26.6 amu. It should be noted that μ_o shows only a very small dependence on the ion mass so long as $m_{ion} >> m_{air}$. The polarizability of air was taken as 1.718 Å^3, see ref 27. The mobility $\mu = 2.2 \text{ cm}^2 \text{ V}^{-1} \text{ s}^{-1}$ was evaluated with eqs 2.13 and 2.14 and a drift time $t = 7 \times 10^{-3}$ s was obtained with eq 2.10 where the integral was evaluated for $\varepsilon(s)$, from Figure 2.19, with the trapezium rule.

The electric field is smallest near the plane electrode, Figure 2.19, and remains approximately constant over three fourths of the distance to the capillary. This means that the gas phase ions will spend ≈90% of their total drift time in this region.

The present calculations neglect the effect of space charge. Busman, Sunner, and Vogel (*29*) have shown that the presence of space charge increases the electric field in the above region. The increase is dependent on the current density and geometric parameters. The increased electric field leads to a decrease of the ion residence time. A decrease of ion residence time relative to that in the absence of space charge by a factor of 2 to 4 can be estimated for the present conditions. Thus, an ion drift time of 1-2 ms appears to be the best

estimate. This is close to the ion residence time obtained in section 2.d on the basis of proton transfer kinetics.

REFERENCES

1. Yamashita, M.; Fenn, J. B. *J. Phys. Chem.* **1984**, *88*, 4451; **1984**, *88*, 4671.
2. Whitehouse, C. M.; Dreyer, R. N.; Yamashita, M.; Fenn, J. B. *Anal. Chem.* **1985**, *57*, 675.
3. Wong, S. F.; Menz, C. K.; Fenn, J. B. *J. Phys. Chem.* **1988**, *92*, 546.
4. Brunis, A. P.; Weidorf, L. O. G.; Henion, J. D. *Anal. Chem.* **1987**, *59*, 2647.
5. Brunis, A. P.; Covey, T. R.; Henion, J. D. *Anal. Chem.* **1987**, *59*, 2642.
6. Covey, T. R.; Bonner R. F.; Shushan, B. I.; Henion, J. D. *Rapid Commun. in Mass Spectrom.* **1988**, *2*, 249.
7. Olivares, J. A.; Nguyen, J. A.; Yonker, C. R.; Smith, R. D. *Anal. Chem.* **1987**, *59*, 1230.
8. Smith, R. D.; Olivares, J. A.; Nguyen, N. T.; Udseth, H. R. *Anal. Chem.* **1988**, *60*, 436.
9. Smith, R. D.; Barinaga, C. J.; Udseth, H. R. *Anal. Chem.* **1988**, *60*, 1948.
10. Udseth, H. R.; Loo, J. A.; Smith, R. D. *Anal. Chem.* **1989**, *61*, 228.
11. (a) Talks by Fenn, J. B. and by Henion, J. D. at meeting on *Mechanisms in Desorption Ionization Mass Spectrometry*; Sanibel Island, FL, Jan 1989. (b) Alexander, A. J.; Kebarle, P. Mass Spectrometric Identification of Nucleosides and Nucleotides Separated by HPLC Presented at *Ion Separation Methods Symposium 3rd Chemical Congress of the North American Continent*, Toronto, ON. Canada June 1988.
12. (a) Sunner, J.; Nicol, G.; Kebarle, P. *Anal. Chem.* **1988**, *60*, 1300. (b) Sunner, J.; Ikonomou, M. G.; Kebarle, P. *Anal. Chem.* **1988**, *60*, 1308.
13. Reid, N.; Buckley, J. A.; French, J. B.; Poon, C. C. *Adv. Mass Spectrom.* **1979**, *8B*, 1843.
14. (a) Good, A.; Durden, D. A.; Kebarle, P. *J. Chem. Phys.* **1970**, *52*. 222. (b) Grimsrud, E. P.; Kebarle, P. *J. Am. Chem. Soc.* **1973**, *95*, 7939.

15. (a) Iribarne, J. V.; Thomson, B. A. *J. Chem. Phys.* **1976**, *64*, 2287. (b) Thomson, B. A.; Iribarne, J. V. *J. Chem. Phys.* **1979**, *71*, 4451. (c) Iribarne, J. V.; Dziediz, P. J.; Thomson, B. A. *J. Mass Spectrom. Ion. Phys.* **1983**, *50*, 331.

16. Taflin, D. C.; Zhang, S. H.; Allen, T.; Davis, J. E. *AIChE.* **1988**, *34*, 1310.

17. (a) Searles, S. K.; Kebarle, P. *Can. J. Chem.* **1969**, *47*, 3638. (b) Keesee, R. G.; Castleman, A. Q., Jr. *J. Phys. Chem. Ref. Data* **1986**, *15*, 1011.

18. Lias, S. G.; Liebman, J. F.; Levin, R. D. *J. Phys. Chem. Ref. Data* **1984**, *13*, 695.

19. (a) Nicol, G.; Sunner, J.; Kebarle, P. *Int. J. Mass Spectrom. Ion Processes* **1988**, *84*, 135. (b) Kebarle, P. Pulsed Electron High Pressure Mass Spectrometer. In Weissberger *Techniques for the Study of Ion-Molecule Reactions*; Farrar, J. H., Saunders, W. Eds.; Wiley-Interscience: New York, 1988, p 255.

20. Lindinger, A. A.; Albritton, D. L. *J. Chem. Phys.* **1975**, *62*, 3517.

21. Ikonomou, M. G.; Blades, A. T.; Kebarle, P., unpublished results.

22. Juhasz, P.; Kebarle, P. *Int. J. Mass Spectrom. Ion Processes* (in press).

23. Bell, R. P. *The Proton in Chemistry*; Cornell University Press: Ithaca, NY, 1959; Chapters IV and V.

24. (a) Guthbezahl, B.; Grunwald, E. *J. Am. Chem. Soc.* **1953**, *75*, 559. (b) Bacarella, A. L.; Grunwald, E.; Purlee, E. L.; Marshall, H. P. *J. Org. Chem.* **1955**, *20*, 749.

25. Ritchie, C. D.; Heffley, P. D. *J. Am. Chem. Soc.* **1965**, *87*, 5404.

26. (a) Covington, A. K.; Dickinson, T. *Physical Chemistry of Organic Solvent Systems*; Plenum Press: London & New York , 1973. (b) O. Popovich, O.; Tomkins, R. P. T. *Nonaqueous Solution Chemistry*; Wiley Interscience: New York, 1981.

27. Radzig, A. A.; Smirnov, B. M. *Reference Data on Atoms Molecules and Ions*; Springer: New York, 1985; p.444.

28. (a) Albert, A.; Serjean, E. P. *The Determination of Ionization Constants*; Chapman and Hall: London and New York, 1984. (b) TSO, P.O.P. *Basic Principles in Nucleic Acid Chemistry*; Academic Press: New York and London, 1974; Vol. 1,pp 453-471.

29. Busman, M.; Sunner, J.; Vogel, C.R., unpublished results.

CHAPTER 3

A COMPARATIVE STUDY OF ELECTROSPRAY AND ION SPRAY IONIZATION MASS SPECTROMETRY IN THE POSITIVE ION MODE.

INTRODUCTION

Electrospray (ESP) is emerging as one of the most powerful ionization methods for liquid chromatography mass spectrometry for the analysis of peptides, proteins and many other classes of biologically important molecules. Its operational capabilities as an LC/MS interface were first demonstrated by Fenn et al. in 1984 (*1, 2*) and subsequent developments have been described in a recent review (*3*). Henion et al. (*4, 5*), using a modification of the electrospray method which they termed "" and later "pneumatically assisted electrospray" (*6*), have also described a number of exciting applications of this technique. Smith et al. have also used electrospray successfully as an interface for capillary zone electrophoresis (CZE) with mass spectrometry and a summary of work in that laboratory has been published recently (*7*). Some of the processes involved in electrospray ionization, and the capability of electrospray to produce multiply charged metal ions in the gas phase were examined in studies undertaken in our laboratory, see Chapters 2 and 4 (*8, 10-13*).

Although the reports of Fenn and Henion describe in detail the two interfaces (electrospray and) a systematic comparison between the two techniques has not been made. For this reason a direct comparison of the two techniques was undertaken in order to reveal any fundamental differences between the ionization processes, and differences in the operational procedures of the techniques. Experiments were designed in such a way as to qualitatively and quantitatively examine the importance of the electric field, and nebulization pressure in the case of , on the ion yields produced by the two techniques using solutions of various analytes.

It was pointed out in Chapter 2 that optimum electrospray operation is obtained only when the capillary thickness (ESP tip), voltage applied to the tip, tip-counter electrode distance, solution composition, and solution flow rate are chosen so that the liquid emerging from the electrospray tip forms a multispray, i.e. a mist of fine droplets produced from a crown of several liquid tips which lie along the rim of the electrospray capillary. Even though Ion Spray relative to electrospray involves one extra variable, nebulization gas flow-rate, optimum performance can be achieved very easily. The assistance of nebulization for liquid dispersion

makes parameters like solution composition and solution flow rate not as crucial in achieving good performance (*14*). Therefore under certain conditions Ion Spray performs better, but in others ESP is a superior performer.

Since the differences between the two techniques depend mostly on their operational characteristics for a specific application, one can choose between the two on the basis of their performance according to the requirements of the application.

The data presented here represent only a small part of the wide range of experiments that were designed to fully optimize and characterize the two systems from the perspective of their utilization as HPLC/MS interfaces (*14*).

EXPERIMENTAL SECTION

a. The Atmospheric Pressure Ion Source Mass Spectrometer

The instrument was a SCIEX TAGA 6000E atmospheric pressure ion source triple quadrupole mass spectrometer operated in the positive ion mode, Figure 2.1. Detailed schematic diagrams for the electrospray and Ion Spray assemblies utilized in the study are shown in Figures 2.2A and 3.1, respectively. The electrospray assembly is that described in Chapter 2 (see Figure 2.2 and Experimental) while that providing Ion Spray is a similar device to that first introduced by Henion et al. (*4*). Solution was supplied to either of the above at 20 μL/min by a motor driven syringe (SAGE Instruments Model 341A, Cambridge, MA).

The front end of the assemblies was held at approximately 4 cm from the interface orifice and 1.5 cm off axis, see Figure 2.1. The voltage applied to the tip varied with respect to the device used and the desired experiment, as will be discussed later. However, optimum voltages were about 9 kV for the electrospray and 5.5 kV for the . A nebulization pressure of 60 psi (N_2) was found as the optimum pressure with the present arrangement, (Figure 3.1), for good signal stability and sensitivity for all systems studied, see Results and Discussion. Without nebulization gas, and with the outer tube removed, or pulled ≈1 cm back relatively to the inner, the Ion Spray assembly becomes a Fenn-type electrospray (*1-3*), capillary dimensions: 0.004 in i.d., 0.018 in o.d..

The electrospray tip used by Fenn et al. has an outer diameter which is ≈3.5 times smaller than the one used in this laboratory. A thick walled capillary which allowed the tip to be smooth and round was chosen here in order to prevent an early onset of corona discharge ionization, and particularly a mixture of electrospray with corona discharge conditions. The thicker capillary leads to a weaker field gradient and thus higher voltages needed to be applied to the tip. With this configuration and with a 4 cm tip-counter electrode distance, best sensitivity was obtained with ≈9 to 9.5 kV applied to the tip. Corona onset voltage was ≈10.5 kV. On the other hand, experiments with finer capillaries have indicated that optimum electrospray operation and corona discharge onset voltage differ by only 100 to 400 V, which

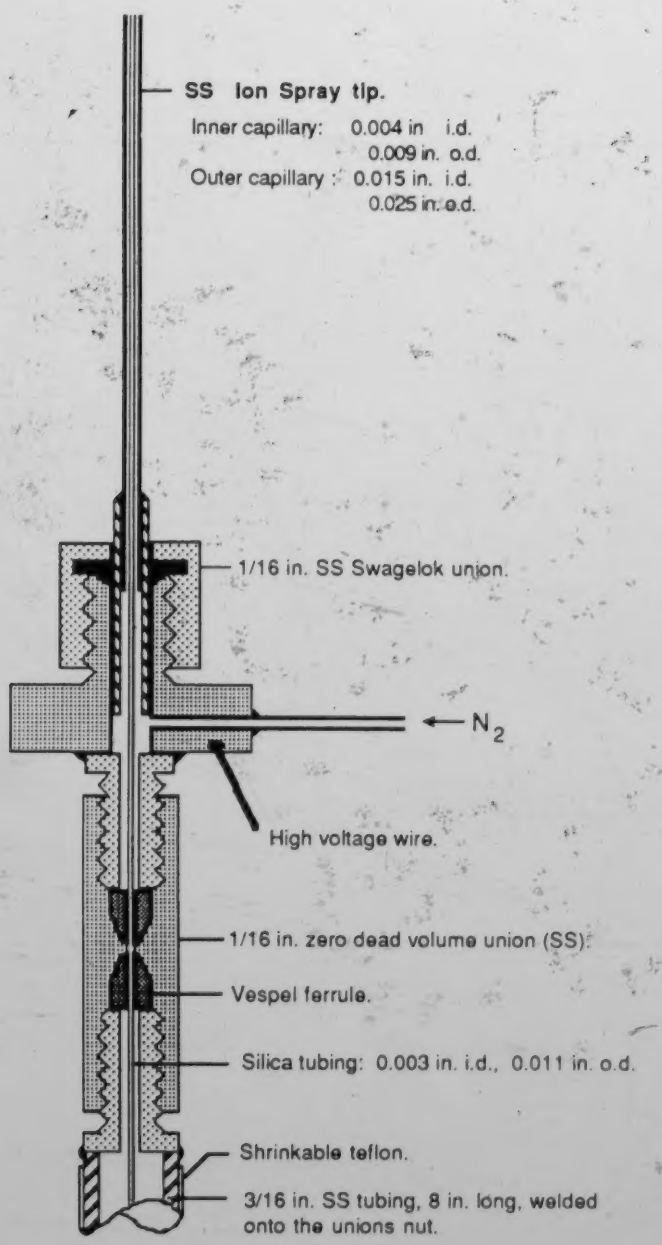
SS Ion Spray tip.
Inner capillary: 0.004 in i.d.
0.009 in. o.d.
Outer capillary : 0.015 in. i.d.
0.025 in. o.d.
1/16 in. SS Swagelok union.
N_2
High voltage wire.
1/16 in. zero dead volume union (SS).
Vespel ferrule.
Silica tubing: 0.003 in. i.d., 0.011 in. o.d.
Shrinkable teflon.
3/16 in. SS tubing, 8 in. long, welded onto the unions nut.

Figure 3.1. Detailed schematic diagram of the Ion Spray ionization assembly.

makes optimum "clean" electrospray operation somewhat delicate to achieve. Investigations performed with the thicker capillary will be referred to as ESP, and those with the thin capillary wall as HYP-ESP in the following sections (HYP for hypodermic needle tip dimensions as used by Fenn (*1-3*)).

A flow of 0.5 L/s of air is maintained through the atmospheric pressure ion source. The flow continually removes solvent vapor produced by the electrospray and/or . Ions produced in the atmospheric pressure chamber drift under the influence of the electric field towards the interface plate (650 V) and enter the interface gas chamber through a hole (d = 3.7 mm) in the interface plate. The interface chamber contains ultrapure N_2 gas through which the ions are made to drift under the influence of an electric field. Some of the ions come to the vicinity of the interface chamber exit orifice OR, 0.1 mm diameter, 60 V, through which interface gas and ions enter the vacuum of the triple quadrupole mass analysis chamber (Figure 2.1).

The interface gas flows slowly (0.5 L/min) through the interface chamber (curtain gas region) and enters the atmospheric pressure ionization chamber through the aperture in the interface plate. A small fraction of the gas undergoes adiabatic expansion into the vacuum chamber through the interface orifice (OR). The electric fields in the initial stages of the expansion are adjusted by the voltages applied to the OR, CB, and Q_0 electrodes (see Figure 2.1) so as to induce maximum declustering and obtain maximum analyte ion sensitivity: more details are given in Chapters 2, 4 and (*15-17*). Typical voltages were: OR = 60 V, CB = 33 V, Q_0 = 30 V. Under these conditions only strongly held clusters are generally observed and the solvent molecule number in the observed clusters is not at all representative of the ion clusters present in the atmospheric pressure ion source (*15,16*).

Mass analysis was obtained with the third quadrupole Q_3 resolving (300 resolution) and Q_1 in the drain pipe mode. Ion counting was used for determination of the intensities of the mass analyzed ions. The counter becomes nonlinear above $\approx 7 \times 10^5$ counts/s. Therefore, for the quantitative measurements, when the signal obtained with Q_3 exceeded 7×10^5 counts/s, both quadrupoles Q_1 and Q_3 were used in the resolving mode, reducing in this manner the ion

signal. The intensities obtained were then adjusted to the intensity that would have been observed with only Q_3 in the resolving mode.

b. Intermediate Electrode Experiments

A schematic representation of the experimental arrangements used to determine the effect, wherever applicable, of the nebulization and ionization voltage on HYP-ESP and Ion Spray generated mass spectra is shown in Figure 3.2. The setup of Figure 3.2A is that of standard Ion Spray operation with the tip of the assembly beeing 12 cm, rather than 4 cm as is in ESP, away from the interface plate and the tip is aligned on axis with the interface plate orifice. The experiments performed with this experimental arrangement will be referred to as Ion Spray (A) and/or HYP-ESP (A)..

In Figure 3.2B the Ion Spray tip is 8.7 cm back and on line with the interface orifice while a 12 cm diameter stainless steel disk intermediate electrode, with a 1.5 mm orifice at the disk's center, is placed between the interface plate and the . Experiments where the disk voltage was equal to that applied to the Ion Spray capillaries are designated as Ion Spray (B).

Similarly, in Figure 3.2C the sprayer is 8.7 cm back and on line with the interface orifice but the intermediate electrode is of different configuration. The arrangement consists of a sandwich of two disk electrodes, each of 12 cm diameter, electrically insulated from each other, and 1.6 cm apart. A 2.54 cm o.d., 1.5 cm long stainless steel tube is attached to the front disk, see Figure 3.2C. Both disks and sprayer were maintained at the same voltage, however the current to each disc could be measured separately. Experiments with this arrangement will be identified as Ion Spray (C) in the following sections.

The positive ion currents: (i_1), current leaving the sprayer; (i_2), current arriving at the intermediate electrode, and TIC(IN), current arriving at the interface plate, were measured with floating microammeters as shown in Figure 3.2. (Note: in the Results and Discussion section we also deal with a total ion current that is quoted in counts per second (cps).

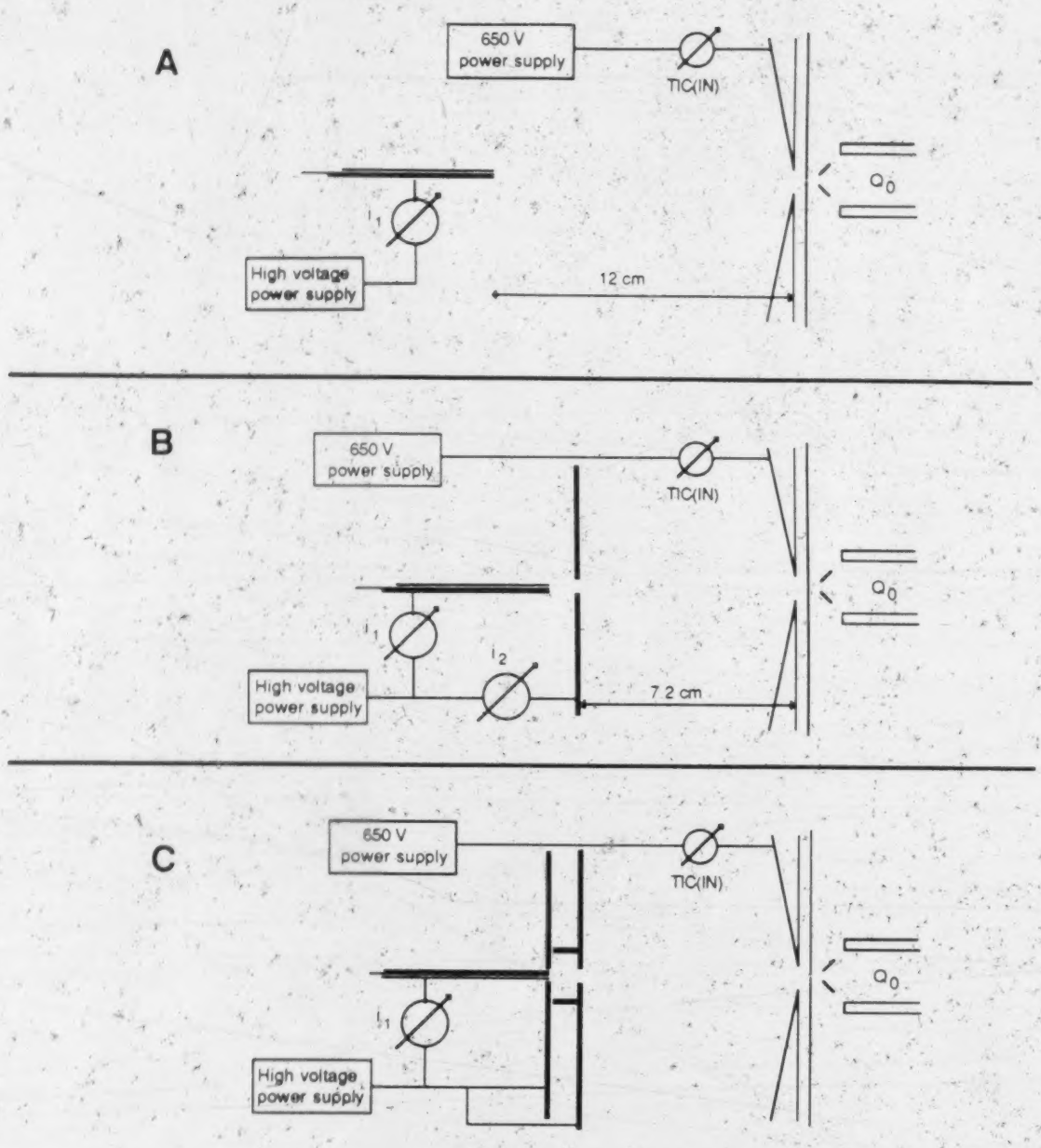

Figure 3.2. Ion Spray arrangement used to investigate the effect of field and nebulization on Ion Spray ionization. (A) Standard Ion Spray operation but distance from interface plate is 12 rather than 4 cm used in all other experiments. (B) The electrode between the sprayer and the IN plate is at the same potential as the sprayer. (C) Same as (B) but a different type of intermediate electrode arrangement. More details about relative distances and other design specifications are given in Appendix 3.I.

This current represents the sum of the mass analyzed ion currents arriving at the detector, while TIC(IN) quoted in amperes represents the total ion current due to charged droplets as well as gas phase ions arriving at the interface plate.)

RESULTS AND DISCUSSION

a. Pneumatically Assisted Electrospray (Ion Spray) Operation

The Ion Spray tip was kept at 5.5 kV, ≈4 cm back from the interface orifice and ≈1.5 cm off center. These are the standard (optimal) conditions for the HYP-ESP and Ion Spray operation. The 5.5 kV ionization voltage, as will be shown below, was found to be the optimum voltage with this experimental setup providing maximum signal intensity and stability for analyte ions.

The dependence of the BH^+ intensity and stability, for a 10^{-5} M cocaine hydrochloride solution in methanol, on Ion Spray nebulization pressure is shown in Figure 3.3A. The 0 psi condition depicts that of HYP-ESP operation. Maximum sensitivity is obtained at 60 psi. The ion of m/z 33 ($CH_3OH_2^+$) is also monitored in this experiment for two reasons: a) large increases of $CH_3OH_2^+$ intensity relative to that of ions like Na^+ (impurity in methanol), indicates the onset of corona discharge, and b) it serves as an indicator in establishing the degree of solvent penetration into the interface region (ultrapure N_2 chamber) due to nebulization. Yet a better indicator ion to monitor the latter is m/z 50 (NH_4^+MeOH), see discussion below. Penetration of the curtain gas by methanol and/or water from the electrospray region leads to ion molecule clustering reactions (*15, 16*). It was observed that when the intensity of the ions m/z 33, m/z 23 (Na^+), m/z 41 (Na^+H_2O) decreased with nebulization pressure, the intensities of the ions m/z 50 (NH_4^+MeOH), and m/z 55 (Na^+MeOH), increased. These trends are due to the equilibrium reactions 3.1 and 3.2 being

$$Na^+ + nMeOH = Na^+(MeOH)_n \qquad (3.1)$$

$$NH_4^+ + nMeOH = NH_4^+(MeOH)_n \qquad (3.2)$$

shifted to the right with high concentrations of MeOH in the interface chamber. Notice that these conclusions are valid only when the HYP-ESP and Ion Spray experiments are performed under identical interface conditions, i.e. same IN, OR, CB, and Q_0 lens voltages,

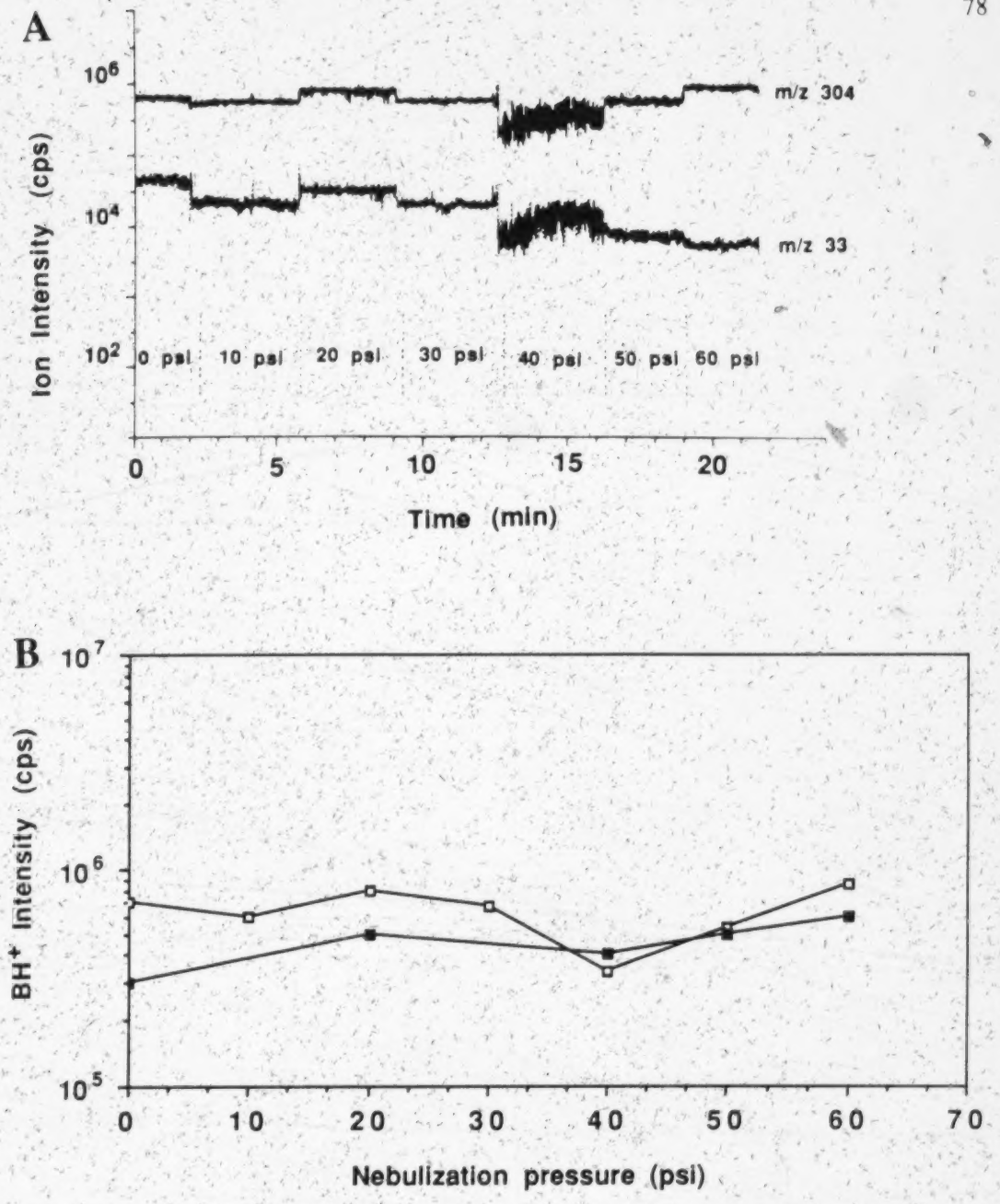

Figure 3.3. (A) Multiple ion monitoring spectrum of m/z 304 (BH^+ of cocaine) and m/z 33 ($CH_3OH_2^+$) as a function of Ion Spray nebulization pressure. Solution sprayed: 10^{-5} M cocaine/HCl at 20 μL/min. (B) Ion intensity of m/z 304 as a function of nebulization pressure from ion sprayed cocaine/HCl solutions. ❑ 10^{-5} M cocaine/HCl in methanol, ■ $3x10^{-4}$ M cocaine/HCl in buffer, buffer composition: 0.02 M NH_4Ac, 75% H_2O, pH=4.

see Figure 2.1. As has been shown in Chapter 4 one can adjust these lens voltages so as to induce declustering and thus shift reactions 3.1 and 3.2 to the left. However trends presented here are strictly due to nebulization since all the other interface variables were kept the same for all experiments.

The mass spectra obtained with and without nebulization resulting from 10^{-5} M cocaine hydrochloride solution at 20 μL/min flow rate are shown in Figure 3.4. Although there are changes in the ion distribution of the non-analyte-related ions this does not seem to affect the sensitivity of m/z 304 (BH^+ of cocaine). In fact somewhat better sensitivity is obtained with nebulization. The same features were observed with all the investigated analytes (mostly strong organic bases) whether the analyte was dissolved in methanol or in a buffered solution, see Figure 3.3B for a representative example. Notice from the data in Figure 3.3B that both the BH^+ sensitivities obtained with HYP-ESP (i.e. zero nebulization pressure) and Ion Spray are significantly reduced when the analyte is present in a buffer. The same type of behavior was also observed with ESP, i.e. suppression of analyte ion production with increasing overall electrolyte content in solution, see Chapter 2. Therefore, the fact that Ion Spray and electrospray show similar sensitivity decreases with increasing electrolyte concentration suggests that a similar mechanism for ion production operates, when the Ion Spray is operated under optimum conditions. Extensive studies investigating such similarities were also performed, and a summary of the findings is presented in Appendix 3.II.

From the data presented in Figures 3.3B and 3.4 it appears that Ion Spray provides somewhat better overall sensitivity than ESP. However, this is not always the case. The performance of the two techniques is dependent on factors such as solution flow rate, solvent composition, etc., and there are conditions where ESP is superior, see for example Appendix 3.II. The selection of this particular set of data for presentation here is to demonstrate the effect of nebulization on Ion Spray ion production.

It is important to note here, that if the Ion Spray assembly is not carefully positioned relative to the interface plate orifice, nebulization can drastically alter the appearance of the

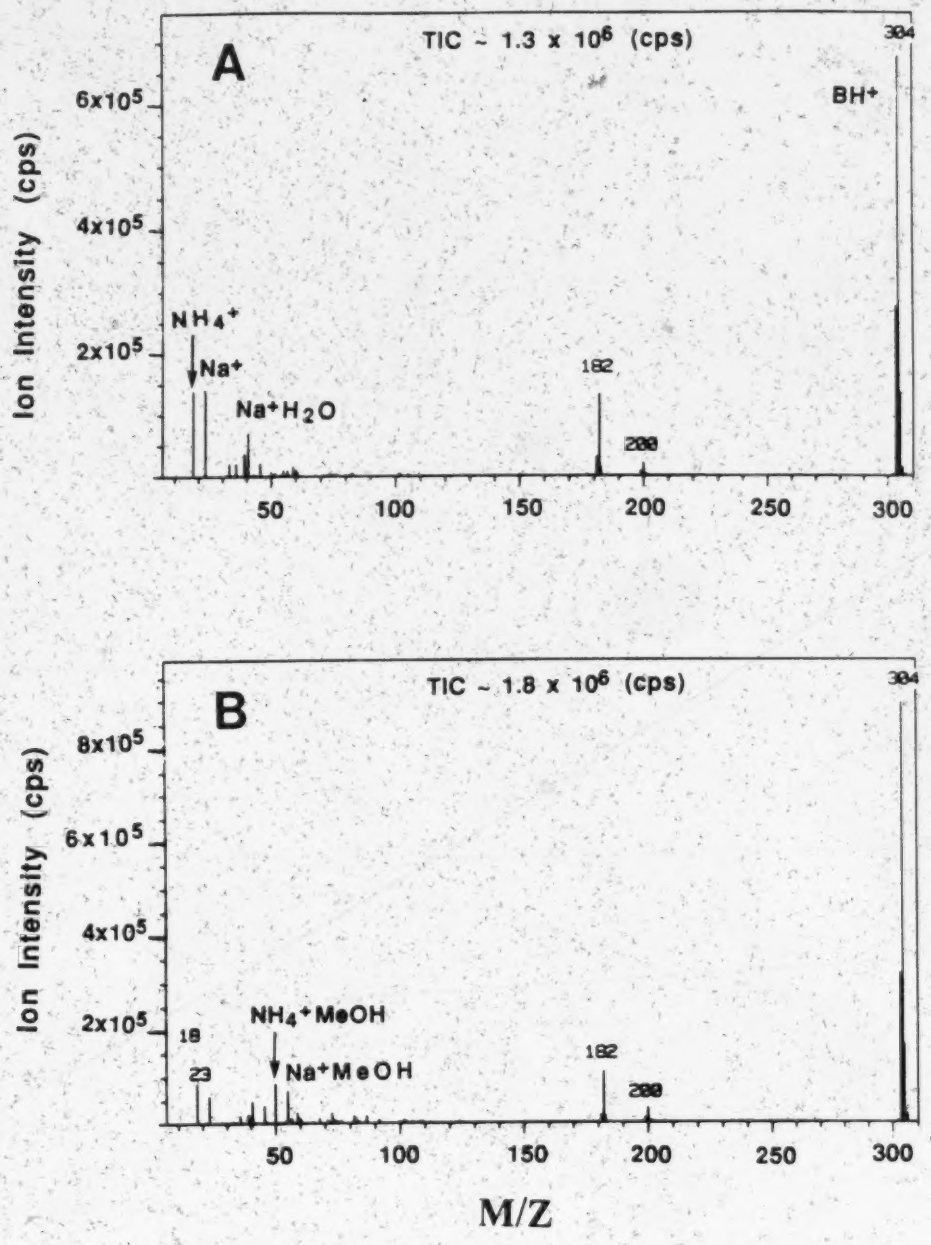

Figure 3.4. (A) HYP-ESP mass spectrum of 10^{-5} M cocaine/HCl in methanol, 20 μL/min. (B) Ion Spray mass spectrum of the same solution as in (A), Nebulization pressure: 60 psi. The Ion Spray tip is 4 cm away from the interface orifice and ≈1.5 cm off center.

mass spectra, for example see Figures 3.5 and 3.6. In Figures 3.5B and 3.6B the "extra" ions are due to ion molecule clustering reactions taking place in the interface region, but as in Figure 3.4B, the overall sensitivity of the analyte-related ions is higher with nebulization. Data of Figures 3.5 and 3.6 were obtained with the Ion Spray tip 4 cm away from the interface orifice but a little less than 1.5 cm off center. The higher degree of clustering observed in the Ion Spray spectra, Figures 3.5B and 3.6B, could either be due to solvent MeOH and/or H_2O being introduced into the interface chamber by the N_2 nebulization gas current, or possibly the Ion Spray producing more solvated BH^+ and M^+ species relative to HYP-ESP. If the latter was the case, the extent of clustering should have been the same for all experiments, Figures 3.4B, 3.5B, and 3.6B. However, since the degree of clustering increases as the Ion Spray tip is directed more and more towards the interface orifice, and since none of the other experimental parameters (nebulization pressure, voltage applied to the interface lenses, etc.) is altered, the present findings imply that the former mechanism is the more likely cause of the higher degree of clustering. This conclusion is further justified in the following discussions. Closer alignment of the Ion Spray tip with the interface orifice at the 4 cm clearance and at 60 psi leads to much larger growth of ion clusters. Evidently the interface is penetrated even more sharply by the nebulization gas current and the increase of solvent vapour eventually leads to analyte signal loss.

Another interesting observation that is extracted from the spectra of Figures 3.5 and 3.6 is that the TIC in the B spectra (Ion Spray conditions) is much higher than those in A. A set of ion mobility experiments was performed in order to investigate the reason for this TIC increase. As described elsewhere (*9*) the interface gas chamber assembly of the mass spectrometer was modified from its original SCIEX configuration. In brief, the ultrapure N_2 (curtain gas) instead of being passed in a broad flow through the interface chamber is now introduced as a directed flow across the incoming ion beam. The linear velocity of the gas is varied by adjusting its flow rate. At high flow rates (2.5 L/min) the ion intensity, as monitored by the mass analyzer, is observed to decrease which is attributed to deflection of the

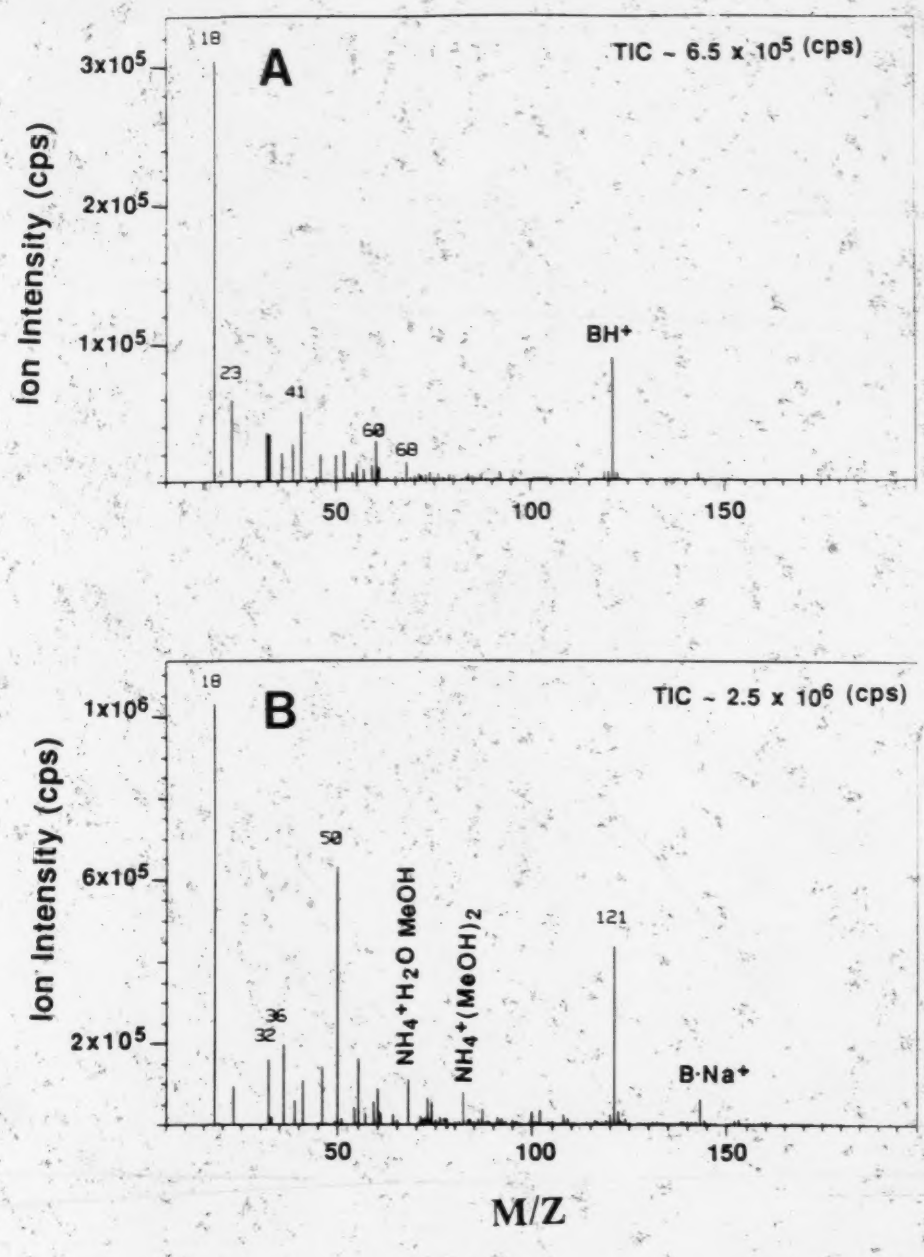

Figure 3.5. Same as Figure 3.4 but 10^{-5} M purine/HCl in methanol was used instead, B here denotes purine. Ion Spray tip is a little less than 1.5 cm off center.

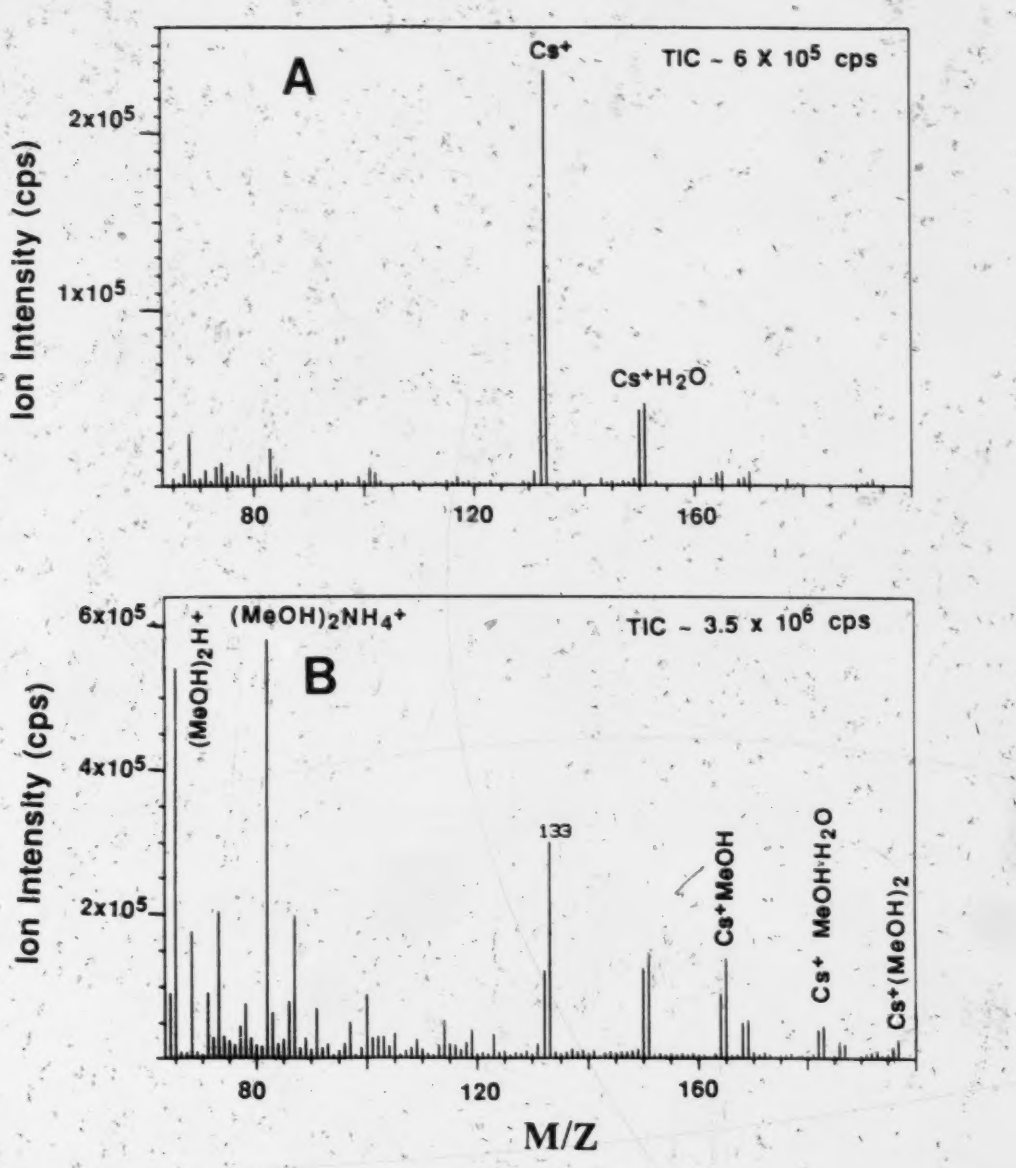

Figure 3.6. Same as Figure 3.5 but 10^{-5} M $CsNO_3$ in methanol was used as analyte.

incoming ion beam from its path by the curtain gas. By monitoring the intensity of desired ions by the mass spectrometer as a function of curtain gas flow rate, one can obtain qualitative information about the drift velocities of the ions under investigation. The results of such an experiment are shown in Figure 3.7. The intensity of m/z 304 (BH^+ of cocaine) was monitored as a function of curtain gas flow rate. In one experiment BH^+ was generated by ion spraying 10^{-5} M cocaine/HCl solution at 20 μL/min and in the other BH^+ was generated by electrospraying (HYP-ESP) of the same solution. The assembly's tip voltage and the voltages of all electrodes of the mass spectrometer were kept the same in the two experiments.

The results of Figure 3.7 show that the Ion Spray-generated ions survive the curtain gas counter flow much better. Thus at the highest flow the Ion Spray ion intensity is approximately seven times higher than that of the HYP-ESP ions. Since both Ion Spray and HYP-ESP generate the same amount of total ion current, TIC(IN) $\approx 2 \times 10^{-7}$ A, and since the voltage drop between the device's tip and the counter electrode is the same in both instances then the higher ion throughput with Ion Spray must be due to nebulization. This could either be due to the possibility that HYP-ESP produces more solvated BH^+ ions than Ion Spray, and thus lower drift velocities for the same field gradient, or due to nebulization gas current giving rise to higher velocities along the z axis to the Ion Spray-produced ions relative to those produced by the field alone (drift velocities). If the HYP-ESP generated BH^+ ions were more solvated than those from Ion Spray, this should have been in evidence in the spectra of Figures 3.4A, 3.5A, and 3.6A. Since these spectra indicated minimum or no clustering of the analyte ions relative to the spectra of Figures 3.4B, 3.5B, and 3.6B spectra, it is concluded that, in the extreme case, the degree of solvation of the HYP-ESP ions is not greater than those of the Ion Spray. Based on these arguments it appears that the latter mechanism (higher ion velocities) is more reasonable in explaining the trends of Figure 3.7.

The proposition that Ion Spray does not produce more solvated BH^+ ions than HYP-ESP can also be argued in view of the data presented so far. If one assumes that the Ion Spray ions are more solvated than the HYP-ESP ones, then lower drift velocities would have been

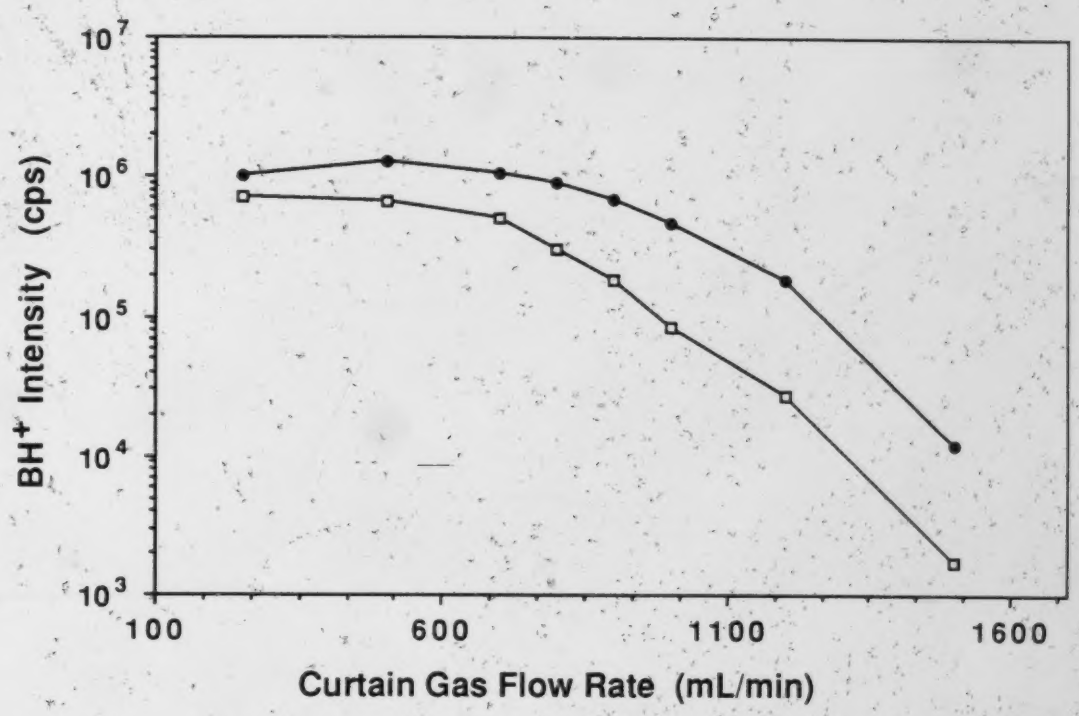

Figure 3.7. BH^+ intensity as a function of curtain gas (ultrapure N_2) flow rate, in transverse flow mode. ●, Ion Spray, ❑, HYP-ESP. Conditions: 10^{-5} M cocaine/HCl in MeOH, 20 μL/min, Ioniz. volt.: 5.5 kV, Interface orifice tip clearance 4 cm and 1.5 cm off center, Nebulization pressure: 60 psi.

expected, and thus the experiment of Figure 3.7 should have indicated a higher effect on the Ion Spray generated ions relative to those of HYP-ESP, provided that the field where the ions travel is maintained the same in both experiments. Since the opposite is observed, and because Ion Spray mass spectra obtained under optimum conditions are very similar to those of HYP-ESP, see (Figure 3.4), the present findings suggest that Ion Spray BH^+ ions are not solvated more than those of HYP-ESP. Considering that the experiments of Figure 3.7 were conducted under optimal conditions, the higher ion throughput with Ion Spray is clearly due to nebulization gas current giving rise to higher velocities along the z axis for the Ion Spray produced ions, relative to those produced by the field alone.

Increases in analyte ion sensitivity and TIC's with nebulization have been observed throughout under the present experimental conditions, see for example Figures 3.4B, 3.5B, and 3.6B. Additional explanations relating to the higher sensitivities obtained with pneumatically assisted electrospray relative to those of HYP-ESP (i.e. no nebulization), under certain experimental conditions, are given in following sections.

b. Effect of Ionization Voltage on Analyte Ions Generated by ESP, HYP-ESP, and Ion Spray.

The effect of ionization voltage (voltage applied to the ESP tip) on the total ion current TIC(IN), arriving at the interface plate (Figure 3.2) and on BH^+ intensity generated from electrospraying (ESP) 10^{-11} mol/min of cocaine/HCl, is shown in Figure 3.8. The trends were characteristic for all the examined organic base hydrochlorides in methanol. As has been shown elsewhere (9) TIC(IN) is equal in magnitude to the current leaving the ESP tip and represents the net positive charge of droplets and gas phase ions leaving the ESP tip. The TIC(IN) changes with experimental parameters were also found to parallel the TIC reconstructed from the mass spectra.

TIC(IN), Figure 3.8A, was measured with the arrangement shown in Figure 3.2A but now the ESP tip was only 4 cm away from the interface orifice and 1.5 cm off center. The

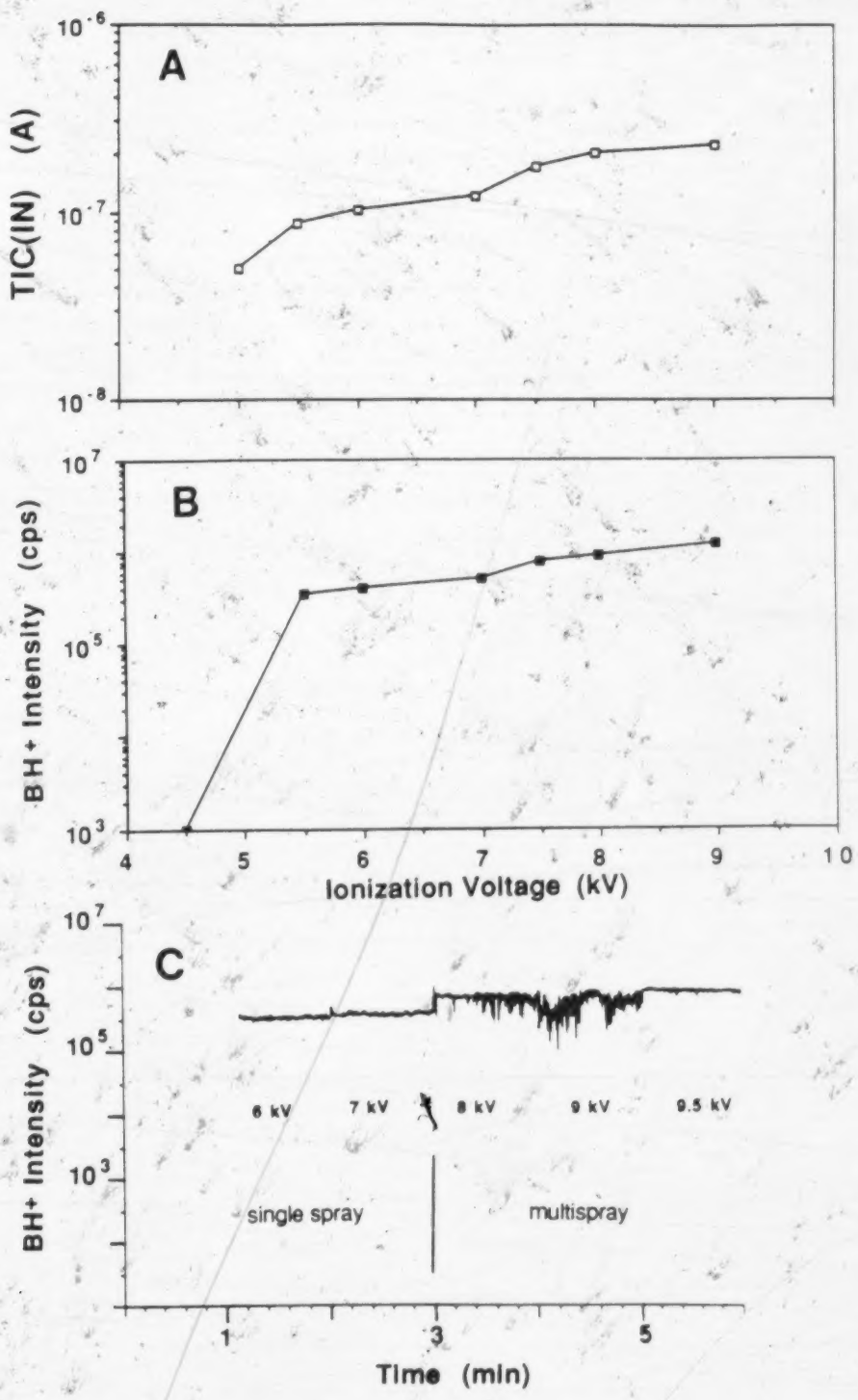

Figure 3.8. (A) Total ion current to interface plate,TIC(IN), as a function of electrospray (ESP) ionization voltage, 10^{-11} mol/min cocaine/HCl in methanol. (B) Same as in (A) but for mass analyzed BH^+, m/z 304. (C) Single ion monitoring of BH^+, m/z 304, at different voltages and spray conditions as a function of time. Time dependence illustrates signal stability for the various conditions.

voltage below which ion generation cuts off with this setup is ≈4.5 kV. At lower voltages there is no visible spray nor any measurable ionization current. Corona discharge is initiated at ≈10.5 kV, 1.5 kV above the voltage at which optimum electrospray conditions are obtained.

When analyte solutions in methanol are used, the liquid at the tip of the capillary forms a cone (at ≈ 5.5 kV-) and a stream of fine droplets, i.e. a mist, is generated from the tip of the liquid cone. At higher electric fields, the liquid cone is replaced by a crown of several much smaller tips which lie along the rim of the capillary electrode. An increase of the total ion and BH^+ current occurs at this change over, see Figure 3.8. Best sensitivity and signal stability (≈3% fluctuation) is obtained at ≈ 9.5 kV, and solution flow rates between 10 and 30 μL/min, see Figure 3.8C for typical performance at 20 μL/min. Under these conditions this device provides better sensitivity and signal stability compared to that obtained with HYP-ESP and Ion Spray. However this electrospray arrangement suffers large sensitivity losses, relative to the other two, at high electrolyte concentrations and when the water content of the methanol solvent is increased , see Chapter 2 and Appendix 3.II. When the analyte is present in 100% MeOH, the total electrolyte content of the solution is less than 10^{-3} M, and the flow rate is between 10 and 30 μL/min, this electrospray arrangement is the best choice.

Identical experiments to those of ESP, Figure 3.8, were also performed with HYP-ESP and Ion Spray, Figure 3.9. Notice that the ionization voltage used here spans only up to 6 kV. The thinner capillary used with these devices (see experimental section) does not allow electrospray operations above 6 kV. Corona discharge occurs at voltages higher than 6 kV and this leads to a decrease of electrospray generated ion intensities.

A very interesting feature of the data of Figure 3.9 is that the ion production cut off voltage, with the present arrangement, is ≈ 2.5 kV for HYP-ESP, while Ion Spray still produces ions at lower voltages. Actually ions are detected even when there is no voltage applied to the tip, see Figure 3.9B. Furthermore since the interface plate is at 650 V, see

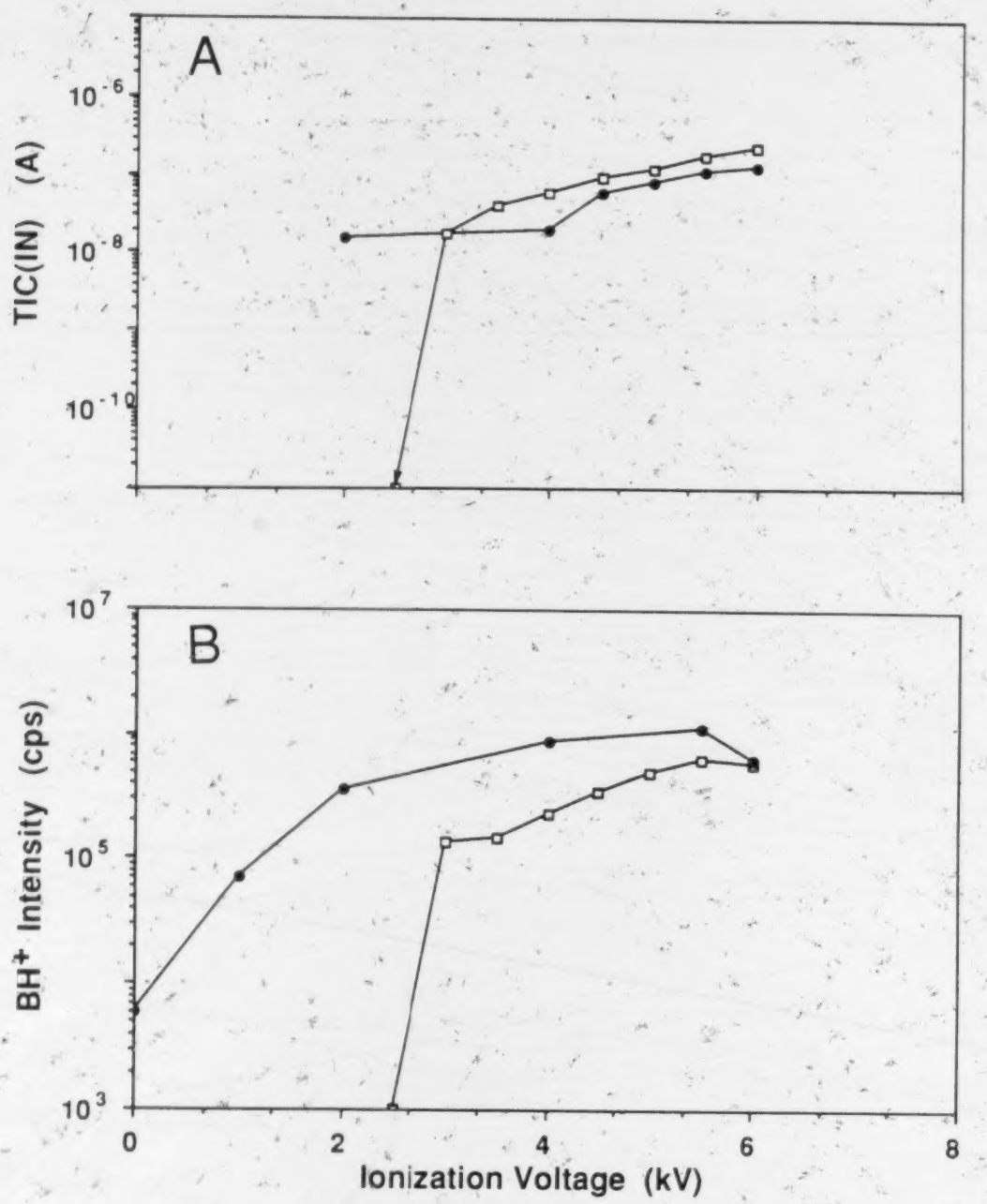

Figure 3.9. (A) Same as in Figure 3.8A and 3.8B, respectively. ❑ HYP-ESP, ● Ion Spray, 60 psi.

Figure 2.1, under these "no field-nebulization only" conditions the ions have to travel uphill by close to 650 V in order to make it into the sampling orifice of the mass spectrometer.

Total ion currents, TIC(IN), generated by either HYP-ESP or Ion Spray are approximately the same when the ionization voltage is higher than 2.5 kV, see Figure 3.9A, suggesting that a similar droplet charging mechanism is taking place. The present findings, along with those of Chapter 2, have indicated that charge separation and subsequent formation of unipolar charged droplets are field-dependent processes in electrospray ionization. Because electrospray stops producing ions below a certain field gradient (Refs. *1-3*, and Chapter 2), the gradient being a function of voltage applied to the tip, tip-counter electrode distance, and tip thickness, the feature of ion production in the absence of any voltage applied to the tip is therefore unique to Ion Spray. Even though the ion intensities recorded under these conditions are orders of magnitude lower than those recorded under optimal conditions, they are still impressive. Since these ion currents are produced in the absence of any field, and because electrospray cannot operate under such conditions, the mechanism of ion production in this case cannot be the same as that of electrospray ionization.

The effect of ionization voltage on BH^+ sensitivity over the 0 to 6 kV range is shown in Figure 3.9B. Ion Spray sensitivity is consistently higher throughout. The higher sensitivity is attributed to nebulization and spray quality, see following discussions. Signal stability is between 3 and 10% with both techniques at all voltages.

Although the recorded BH^+ intensity, with no voltage applied to the tip, is some 250 times lower than that obtained at 5.5 kV, it is strong enough that a no-field Ion Spray mass spectrum can be recorded, Figure 3.10A. The analyte ions m/z 304, 182 (cocaine fragment), and m/z 50 ($NH_4^+CH_3OH$) represent more than 95% of the total ions. This means that almost all of the observed ions are due to ions present in solution. Similar results were obtained with all the base hydrochloride solutions tested. On reversing the instrument polarity a negative ion mass spectrum could also be recorded, Figure 3.10B (the Ion Spray tip is again at 0 V). Even though identification of all the ions present in this spectrum (on the basis of the m/z values

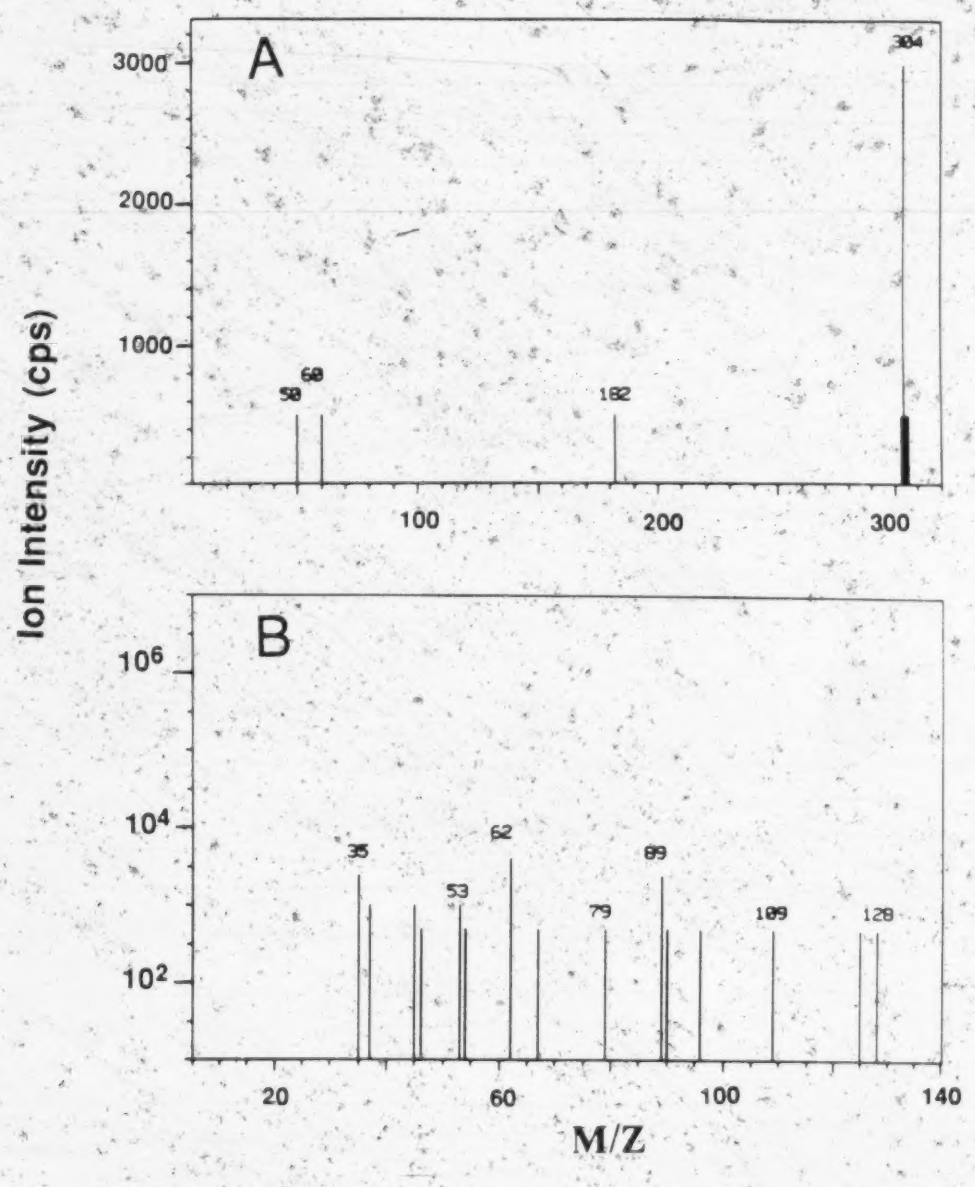

Figure 3.10. (A) Ion Spray generated positive ion mass spectrum, tip at zero volts, 10^{-11} mol/min cocaine/HCl solution in methanol, 60 psi. (B) Negative ion mass spectrum obtained under the same conditions as in (A).

alone) is not trivial, it is certain that chloride is indeed present (m/z 35, 37). Since the sprayed solution was a 10^{-5} M chloride salt (cocaine/HCl) the presence of chloride ions in this spectrum is not accidental. Because both positive and negative ions are produced under zero-field-nebulization only conditions, the present data imply that the droplets (solvated ions) produced in this manner do not all carry the same charge polarity. Although the net charge of these droplets, as will be shown below (Figure 12B), is slightly positive this does not mean that all droplets have the same nett charge. Unfortunately though, the currents recorded in these experiments are extremely weak and reliable quantitative information cannot be obtained.

Apart from the observations on zero-field Ion Spray, results from a companion systematic comparative study of HYP-ESP and Ion Spray (60 psi) suggest that the mechanism of ion production, at 5.5 kV ionization voltage, is probably the same for both techniques, see Appendix 3.II. These studies were based on the ESP work of Chapter 2, and both HYP-ESP and Ion Spray, from a qualitative standpoint, were found to respond very similarly to the various tests at 5.5 kV ionization voltage. These tests however cannot be applied when ions are produced under zero-field nebulization-only conditions since the two techniques are not comparable then. In order to obtain some information on the mechanism(s) involved in ion production under such conditions a number of specially designed experiments needed to be performed, see following discussions.

To determine whether or not the above reported trends occur with other experimental arrangements, a set of HYP-ESP(A) and Ion Spray (A) experiments were performed with the arrangement shown in Figure 3.2A. The 12 cm clearance was chosen because the Ion Spray could be operated on-axis with the interface orifice without any indications of nebulization gas (60 psi) penetration into the curtain gas chamber. Maximum ionization voltage that could be applied to the tip, without initiating a corona discharge, was 10 kV. The dependence of TIC(IN) and BH^+ sensitivity (cps) on ionization voltage, for a 10^{-5} M cocaine/HCl solution flowing at 20 μL/min, is shown in Figure 3.11.

The trends of TIC(IN) and BH^+ are very similar to the ones obtained with the standard HYP-ESP and Ion Spray setup, Figure 3.9. Although the voltage is higher in the present experiments, similar trends were also observed with a number of other base hydrochlorides investigated in this manner. Even though absolute values of TIC(IN) and BH^+ varied from one analyte solution to the other, depending on factors such as total electrolyte content in solution and absolute sensitivity for BH^+ , the overall voltage dependences were very similar to those presented here. The wider voltage range available with this experimental setup has provided a better overall picture of the voltage dependence. The cut-off voltage for HYP-ESP(A) is ≈4 kV while Ion Spray (A), as with the standard arrangement, still produces ions without voltage applied to the tip.

The magnitude of TIC(IN) at 0 V , $2x10^{-11}$ A (Figure 3.11A), is of interest and needs to be discussed. Notice that this positive ion current is induced strictly by nebulization of the analyte solution. A 100 fold increase in TIC(IN) is obtained when a relatively low voltage, 1 kV, is applied to the tip, see Figure 3.11A. In this case the voltage drop between the tip and the interface plate is only 350 V, IN held at 650 V, yet the TIC(IN) increase is substantial. The $2x10^{-11}$ A current was recorded with IN at 650 V, however there were no observable current changes when IN was set to 0V also. Thus, the 100 fold increase in TIC(IN) must be due the field that the liquid emerging from the capillary is exposed to. Raising the voltage from 1 to 4kV, which is the cut-off voltage of HYP-ESP operation, causes a TIC(IN) increase of only by a factor of ≈8, a moderate increase relative to the previous 100 fold increase.

These results indicate that, with relatively moderate voltages applied to the tip, the net positive charge produced by Ion Spray is substantial compared to what is obtained under zero-field-nebulization only conditions. This suggests that charge separation can be accomplished even when the electrolyte solution is exposed to relatively moderate fields. However, unless Ion Spray is utilized this phenomenon cannot be realized. This is because electrospray does not occur under these conditions; the field is not strong enough to bring about atomization.

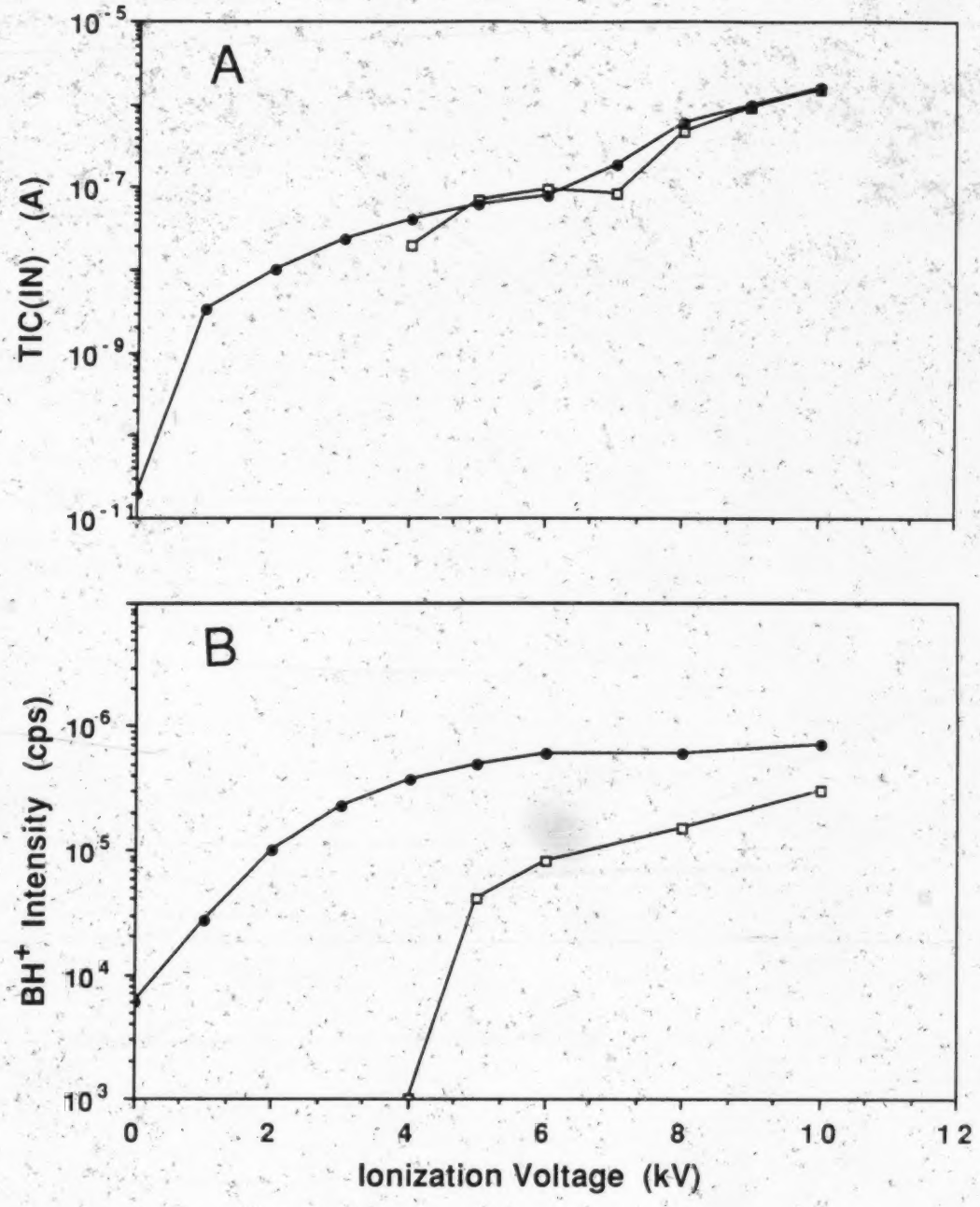

Figure 3.11. (A) TIC(IN) as a function of ionization voltage. ❑ HYP-ESP (A), ● Ion Spray (A) conditions, see Figure 3.2, 10^{-11} mol/min cocaine/HCl, 60 psi nebulization pressure. (B) Same as in (A) but mass analyzed BH^+ dependence on ionization voltage. See Figure 3.2A for experimental setup.

Ion spray on the other hand does not depend on the field for atomization. With this technique atomization is induced principally by nebulization, especially under low field conditions.

Total ion currents, which are independent of spray quality, indicate that the same amount of current reaches the interface plate with both HYP-ESP and Ion Spray, at voltages higher than 4 kV (see Figure 3.11A). Yet, the BH^+ sensitivity is much higher with Ion Spray, 10 fold at 5 kV and double at 10 kV, see Figure 3.11B. In addition, the electrospray BH^+ sensitivity is increased 10 fold by increasing the ionization voltage from 5 to 10 kV while only a 25% gain is observed with Ion Spray. The improved electrospray sensitivity is due to the better spray (multispray) available at high voltages. With Ion Spray however the spray quality is taken care of by nebulization, and thus only a moderate increase in BH^+ sensitivity is obtained with the same increase in ionization voltage. Optimal sensitivity with both techniques is obtained at 10 kV ionization voltage. The somewhat better sensitivity obtained with Ion Spray is consistent with the data presented in the the previous section, where the device was operated under standard conditions. Possible explanations as to why nebulization improves sensitivity, under certain conditions, are given below.

c. Mass Spectrometric Ion Sampling Efficiency under HYP-ESP and Ion Spray Ionization Conditions.

In addition to the effects discussed so far, the ion sampling efficiency of the mass spectrometer with HYP-ESP and Ion Spray as ion sources needs to be considered. Selection of representative sets of data, Tables 3.1 and 3.2 from Figures 3.4, 3.9, and 3.11, revealed additional features of the two techniques especially when they are utilized as ion sources for mass spectrometry.

Data for Table 3.1 were chosen for conditions where HYP-ESP operation is optimum, i.e. multispray, and maximum ionization voltage is applied to the tip without the presence of a corona discharge. Under the conditions presented in the Table, TIC(IN) is some 20 times higher at 10 kV relative to what is available at standard conditions, 5.5 kV. On the basis of

Table 3.1. Ion sampling efficiency with the mass spectrometer under standard HYP-ESP, and HYP-ESP(A) ionization conditions.[a]

	HYP-ESP (5.5 kV, 4 cm)[b]	HYP-ESP(A) (10 kV, 12 cm)[b]
TIC(IN), A	8×10^{-8}	1.6×10^{-6}
BH^+ sensitivity, cps	6×10^5	4×10^5

[a] 10^{-5} M cocaine/HCL in MeOH, 20 μL/min.

[b] Ionization voltage and clearance between the tip and the interface plate orifice.

Table 3.2. Ion sampling efficiency with the mass spectrometer under standard Ion Spray and Ion Spray(A) ionization conditions.[a]

	Ion Spray (A) (10 kV, 12 cm)[b]	Ion Spray (A) (6 kV, 12 cm)[b]	Ion Spray (5.5 kV, 4 cm)[b]
TIC(IN), A	1.6×10^{-6}	9×10^{-8}	8×10^{-8}
BH^+ sensitivity, cps	7×10^5	6×10^5	9×10^5
TIC[c], cps	1.5×10^6	1.4×10^6	1.8×10^6

[a] 10^{-5} M cocaine/HCL in MeOH, 20 μL/min, 60 psi (nebulization pressure).

[b] Ionization voltage and clearance between the tip and the interface plate orifice.

[c] From full mass spectra scans taken under the respective conditions.

this observation, one would have expected a 20 times higher BH^+ intensity in the 10 kV experiment. This however is not observed. BH^+ sensitivities are very similar in both instances. These trends indicate that a much smaller fraction of the overall electrospray-generated ion current is sampled by the mass spectrometer in the 10 kV case. Because this conclusion is based on the mass analyzed BH^+ intensities, it requires the assumption that the same percentage of BH^+ relative to the total ion current is produced in both experiments. In other words, since the BH^+ intensity is about 1/2 of the TIC in the 5.5 kV experiment, Figure 3.4A, then it would have to represent only about 1/40 of the TIC in the 10 kV experiment in order to compensate for the 20 fold differences in TIC(IN)'s between the two experiments. However this is not so. The 10 kV spectrum (not shown) was very similar to that of Figure 3.4A. BH^+ was the base peak and the same impurity ions, although in different relative intensities, were present.

Similar trends were observed with the Ion Spray experiments as well. Data from Table 3.2, columns 1 and 2, indicate that in the 6 kV experiment TIC(IN) is ≈20 times lower than that at 10 kV, yet BH^+ intensities and mass spectrometric TIC's are approximately the same in both cases. These apparent discrepancies are not due to variations in nebulization since identical conditions were used for both experiments, neither are they due to variations in BH^+ intensities relative to TIC. As indicated in the table, the BH^+ intensity corresponds to approximately the same fraction of TIC in both experiments. It seems from these data that the total number of ions sampled by the mass spectrometer is governed by the ion concentration in the ion source, rather than by the ion drift velocities. Notice that for both experiments the tip-counter electrode distance was the same, 12 cm. Therefore the ion drift velocities, and thus the ion throughput, are expected to be higher with the 10 kV experiment assuming that equally solvated BH^+ ions are produced in either case. On the contrary, a much larger fraction of the overall Ion Spray-generated ion current is sampled by the mass spectrometer in the 6 kV experiment.

Similar sensitivity limitations, i.e. non linear relationships between total ion currents produced by electrospray or by corona discharge ionization, and ion currents sampled by the mass spectrometers via the atmospheric pressure-vacuum interface, were also experienced in previous studies utilizing the TAGA mass spectrometer system (*9*). Specially designed experiments led to the conclusion that the ion sampling efficiency of the mass spectrometer is influenced by space-charge. Sunner et al., in a theoretical study (*21*), have also shown that atmospheric pressure ion sources of the TAGA type are space-charge dominated. Since the trends observed here are consistent with previous investigations, the poor ion sampling efficiencies with HYP-ESP and Ion Spray as ion sources are probably caused by space-charge.

Two other operational characteristics of these systems can be illustrated from the data in Tables 3.1 and 3.2. Firstly, by comparing data from columns 1,2, and 3 in Table 3.2, it is evident, in terms of analyte sensitivity, that the (5.5 kV, 4 cm) set represents the preferred operational conditions. Although TIC(IN) at 5.5 kV is similar to that at 6 kV, see Table 3.2, the BH^+ intensity and TIC are much higher when the clearance between the tip and the interface plate is 4 cm. Similar values for TIC(IN) imply similar overall ion concentrations in the ion source, i.e. in the space between the Ion Spray tip and the interface plate. It appears from the data that the smaller the separation, the higher the fraction of the ions sampled. Considering that the same amount of current is produced by both experiments these data suggest that the longer the ions have to travel before they reach the interface orifice (see Figure 2.1) the more they tend to diffuse. Therefore, for the 12 cm clearance condition the charge density at the sampling orifice level is decreased resulting in a lower BH^+ intensity and TIC.

Secondly, comparison of the data of Table 3.1 (column 1, HYP-ESP), to those of Table 3.2 (column 3, Ion Spray), which have been obtained using identical ionization voltage and distance between tip and interface plate, indicates a higher BH^+ sensitivity with Ion Spray. With both devices operating under optimum conditions, this appears to be the case with all the data collected so far at 20 μL/min, see for example Figures 3.4, 3.5, and 3.6. The enhanced

sensitivity is strictly due to increased nebulization efficiency. TIC(IN) values are similar for both spray systems because the drift velocities are the same in both instances, and furthermore TIC(IN) measurements are not space-charge limited. BH^+ sensitivity however is determined by the ion concentration in the IN-OR region (see Figure 2.1 for definition of the IN-OR region). This concentration is determined by TIC(IN), and the conditions which determine what fraction of TIC(IN) enters the ion sampling orifice (OR). Space-charge will tend to spread the ion beam, while the nebulizing gas current will reduce the ion residence time (spray tip to OR), thereby decreasing beam spreading due to ion diffusion and unipolar ion repulsion. Nebulization therefore appears to enhance BH^+ sensitivity not only due to better spray quality available but also by enhancing the ion concentration in the ion sampling orifice region. It should be mentioned at this point that increases in BH^+ sensitivity with Ion Spray are not due to overcoming the curtain gas resistance with nebulization. The curtain gas flow rate is very low, 0.5 L/min, and reducing the flow to 0.1 L/min does not effect the analyte sensitivity nor the TIC with either HYP-ESP or Ion Spray.

d. Origin of Ions Generated by Ion Spray Under Zero-Field Conditions.

The experiments discussed thus far indicate very clearly that charge separation can be induced by nebulization only, and without the presence of any field between the Ion Spray tip and the counter electrode (IN). However, a fundamental question still remains unanswered: Where does charge separation take place under such conditions? One possibility is at the sprayer's tip. Other possibilities are that the sprayer produces neutral droplets and/or droplets of both polarities, and charge separation occurs during the droplets flight in the region between the sprayer and the interface plate. In order to explore the origin of these ions, the Ion Spray (B) and (C) type of experiments were configured, see Figure 3.2B and C.

In the (B) type experiments, identical voltages were applied to both the Ion Spray tip and to the intermediate electrode, i.e. zero-field gradient. Changes in i_1, i_2, TIC(IN), and BH^+ intensity were monitored simultaneously as a function of voltage applied to this assembly. It

was assumed that this experimental setup will lead to field free conditions between the Ion Spray tip and the intermediate electrode, in the presence of a field between this electrode and the interface plate which is changed from 0 to 1400 V/cm. In this fashion if ions did not originate from the tip, but formed in flight, we expected to see some field dependence on the positive ion current arriving at the interface plate. The sprayer voltage had to be kept the same as that of the intermediate electrode at all times in order to eliminate the possibility of any electrospray-induced ionization, see previous sections.

A typical set of data obtained with this experimental setup is shown in Figure 3.12. Data for Figure 3.12A and C were obtained with the sprayer aligned with the intermediate electrode and interface plate orifices. The results of Figure 3.12A show very clearly, that the profiles of i_1 and TIC(IN) are almost identical and also very similar in magnitude. This implies that the current arriving at the interface plate is originating from the sprayer. A small fraction of this current is also collected at the intermediate electrode level, see Figure 3.12A. When the sprayer is displaced off center then most of the current is collected at the intermediate electrode and very little arrives at the interface plate, see Figure 3.12B. Although the data presented here are very convincing, proving that charge separation indeed takes place at the sprayer, the dependence of i_1, i_2, TIC(IN), and BH^+ intensity on voltage applied to the assembly, Figure 3.12A, and C, can not be accounted for. It should be pointed out, for sake of comparison, that the voltage dependence of these quantities is low compared to what is observed when the sprayer is exposed to high fields, Figures 3.9, and 3.11. The much lower TIC(IN) and BH^+ sensitivity available from the Ion Spray operating in the absence of any field, i.e. zero-field induced ionization, show that such a system will be of little analytical significance.

It has been our experience, in accord with that of earlier work (see Refs. *3, 4* in Chapter 1), that one can generate electrospray in the absence of a counter electrode simply by applying positive high voltage to the electrospray capillary. In this case the surrounding atmosphere must be acting as a counter electrode, i.e. the tip is positively charged relative to the atmospheric space around it and the emitted positive drops and ions are carried away

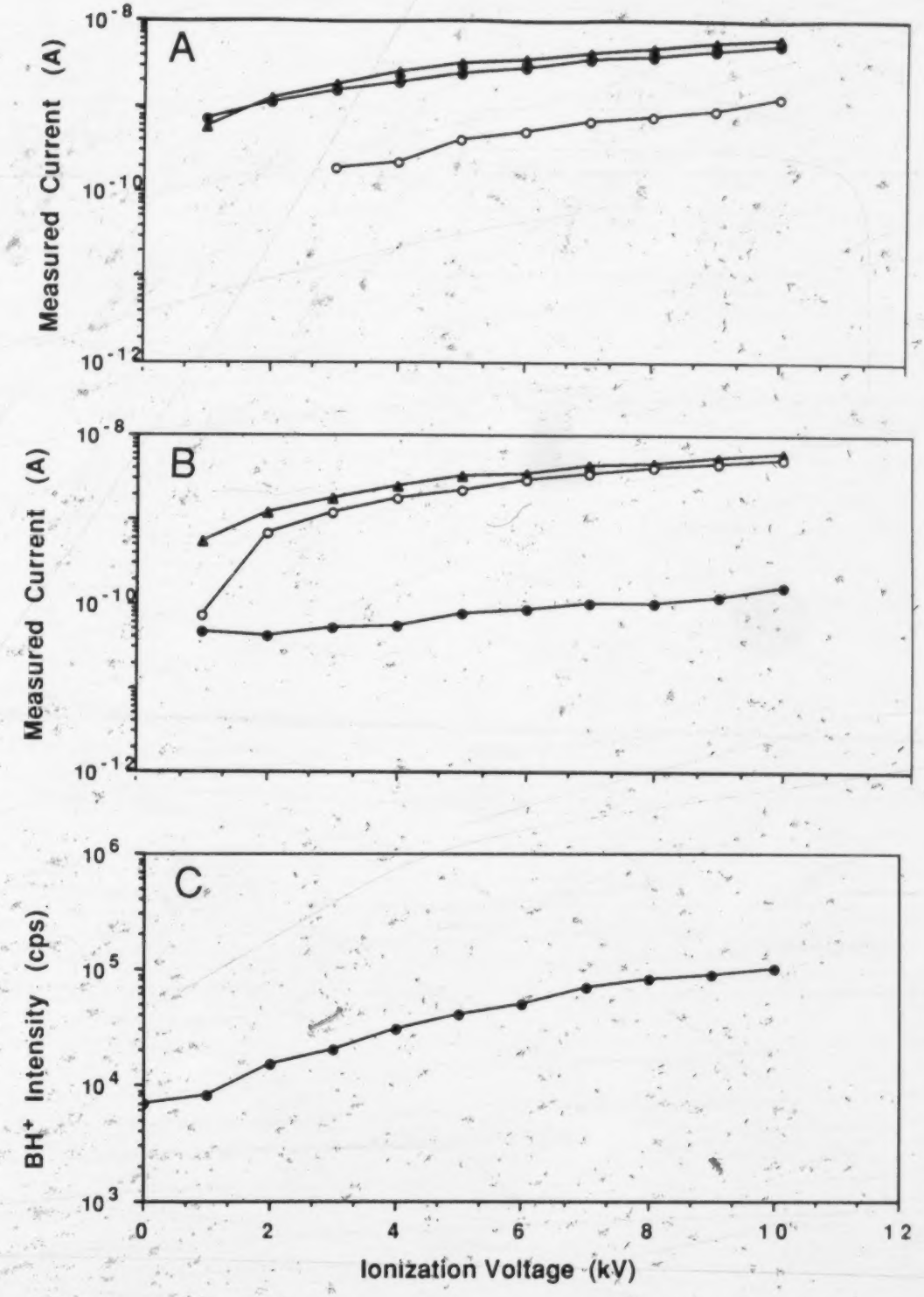

Figure 3.12. (A) i_1, ▲, TIC(IN), ●, and i_2, ○, dependence on ionization voltage from Ion Spray (B) type experiments, 10^{-11} mol/min cocaine/HCl, 60 psi. Ionization tip on line with intermediate electrode and interface plate orifices. (B) Same as in (A) but ionization tip 1 cm off axis. (C) Same as in (A) but mass analyzed BH^+ dependence on ionization voltage. See Figure 3.2B for experimental setup.

ultimately by the convection of the atmospheric gas. Based on this kind of observation, it is possible that when the assembly of Figure 3.2B is exposed to high voltages, a virtual electrospray charge separation is taking place at the sprayer tip. In other words the intermediate electrode (Figure 3.2B) which was to serve as a shield against any field "seeing" the sprayer might not be sufficient. If that were the case then the voltage dependence of i_1 in Figure 3.12A could be accounted for.

In order to examine whether or not the voltage dependence of TIC(IN) in the Ion Spray (B) type experiments was due to the Ion Spray tip being exposed to some field that was not accounted for (see previous discussion), the Ion Spray experiments were re-configured, see Figure 3.2C and Experimental. With this configuration the Ion Spray tip is almost totally shielded while fields as high as 1400 V/cm can be generated in the region between the assembly's intermediate electrode and the interface plate. The dependence of TIC(IN) and BH^+ on voltage applied to the assembly with this experimental setup is shown in Figure 3.13. Because the background level of the i_1 measuring microammeter was $\approx 10^{-10}$ A when floated at high voltages, i_1 measurements were not very reliable and are thus not included in Figure 3.13A. TIC(IN) is totally independent of the voltage applied to the assembly and about four orders of magnitude lower in intensity relative to what is obtained under optimum Ion Spray operation, see Figure 3.9. These data also indicate that, even though the droplets formed under the present conditions are subsequently exposed to fields as high as 1400 V/cm, the amount of positive current arriving at the interface plate is equal in intensity to that obtained when the droplets travel in a field free zone, i.e. in experiments were the intermediate electrode and the interface plate (IN) were kept at the same voltage (650 V).

If charge separation was taking place during the droplets travel between the intermediate electrode and (IN), then the field should have had an effect on the positive ion yield collected at the (IN). As the field increases one would have expected negatively charged droplets and gas phase ions to travel towards the more positive electrode (the intermediate disc in this case), thereby allowing for a higher net positive current to be collected at the (IN). Since this is not

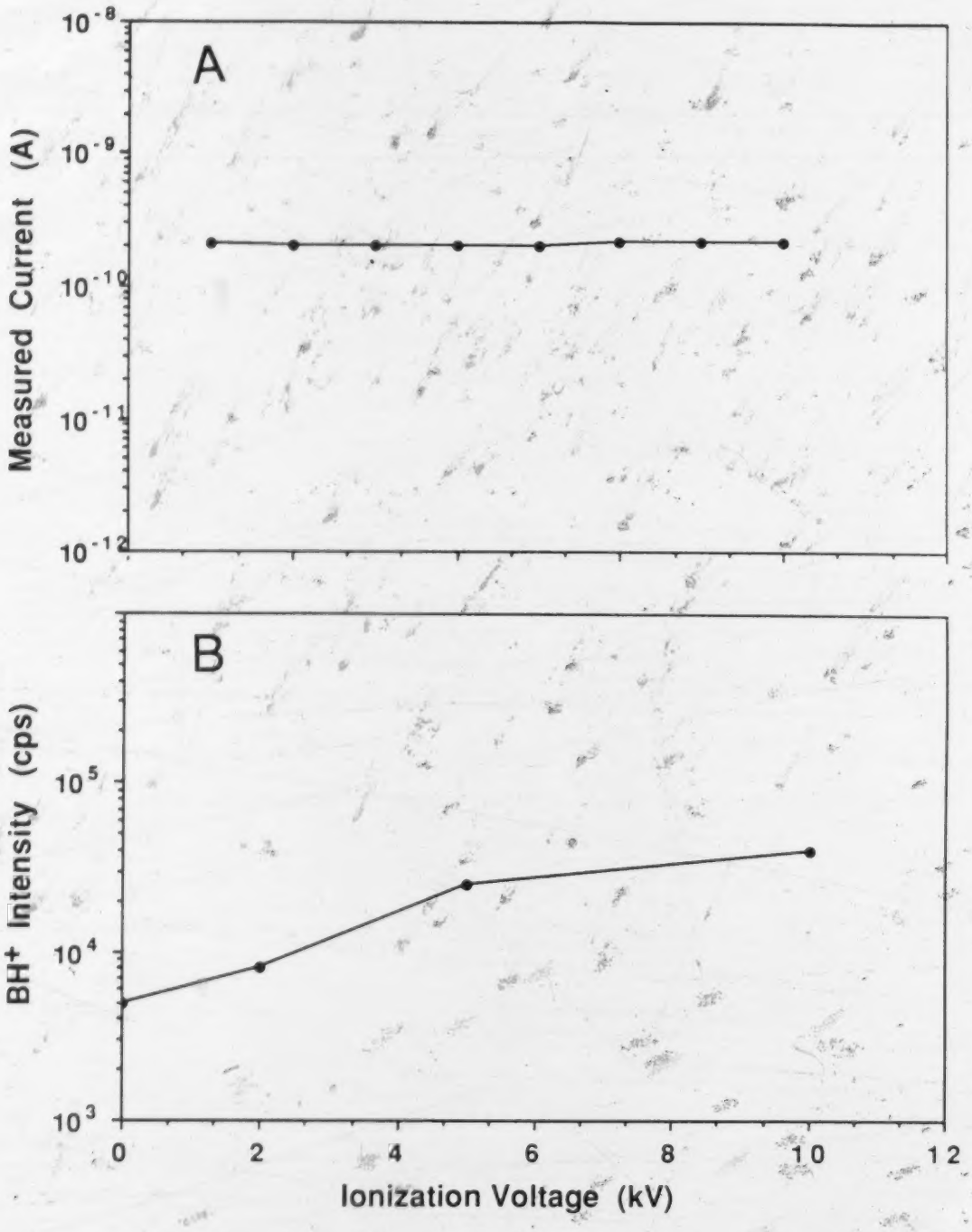

Figure 3.13. (A) TIC(IN) dependence on ionization voltage from Ion Spray (C) type experiments, 10^{-11} mol/min cocaine/HCl, 60 psi. Ionization tip on line with the intermediate electrode and interface plate orifices. (B) Same as in (A) but mass analyzed BH^+ dependence on ionization voltage. SeeFigure 3.2C for experimental setup.

observed, the degree of charge separation and, therefore, the magnitude of the positive current arriving at (IN) must originate from the sprayer.

The present findings, first, justified our speculation of a field induced charge separation in view of the results of Ion Spray (B) experiments, and second, in conjunction with what has been discussed so far, showed that charge separation under zero-field-nebulization only conditions takes place at the sprayer's tip and not during the droplet's travel from the sprayer to the counter electrode.

CONCLUSIONS

1. Pneumatically assisted electrospray (Ion Spray), properly tuned, provides equally good, and at times (depending on operational conditions) better, analyte signal stability and sensitivity relative to electrospray. The conditions of nebulizer gas back-pressure of 60 psi, 5.5 kV voltage at 4 cm tip-counter electrode distance, and ≈1.5 cm off center, appear to be the optimum settings for maximum analyte signal stability and sensitivity.
2. The large ion currents observed with Ion Spray and electrospray are due to charge separation induced by the field at the tip when the capillary is exposed to high voltages. High yields of positively charged droplets and gas phase ions $\approx 10^{-7}$ A are produced under optimal conditions. Ion Spray, however, produces ions under zero-field conditions also. Droplet charging and therefore unipolar ion formation, due to liquid atomization, has been investigated by a number of research groups and a variety of mechanisms have been proposed (*22 - 24*). However, due to the complexity of the phenomenon a consensus in these investigations has not been reached.
3. Ion Spray-generated ions have higher velocities in z direction relative to electrospray due to the nebulization gas current. This overcomes sensitivity limitations due to space-charge and allows for higher total ion currents to be sampled via the mass spectrometer's ion sampling orifice, i.e. the atmospheric pressure / vacuum interface.
4. Although Ion Spray can produce ions in the absence of any field, this mode of operation is of limited analytical significance since the analyte related ion signals are of very low sensitivity. Best analyte sensitivity is obtained under standard Ion Spray conditions; see Table 3.3 for maximum sensitivities available from all the different Ion Spray and electrospray experimental configurations investigated.
5. Results from specially designed experimental setups, Ion Spray B and C type configurations, indicated that charge separation under zero-field conditions (nebulization only) takes place at the sprayer's tip and not during the droplets' flight.

Table 3.3 Summary of selected HYP-ESP and Ion Spray data.

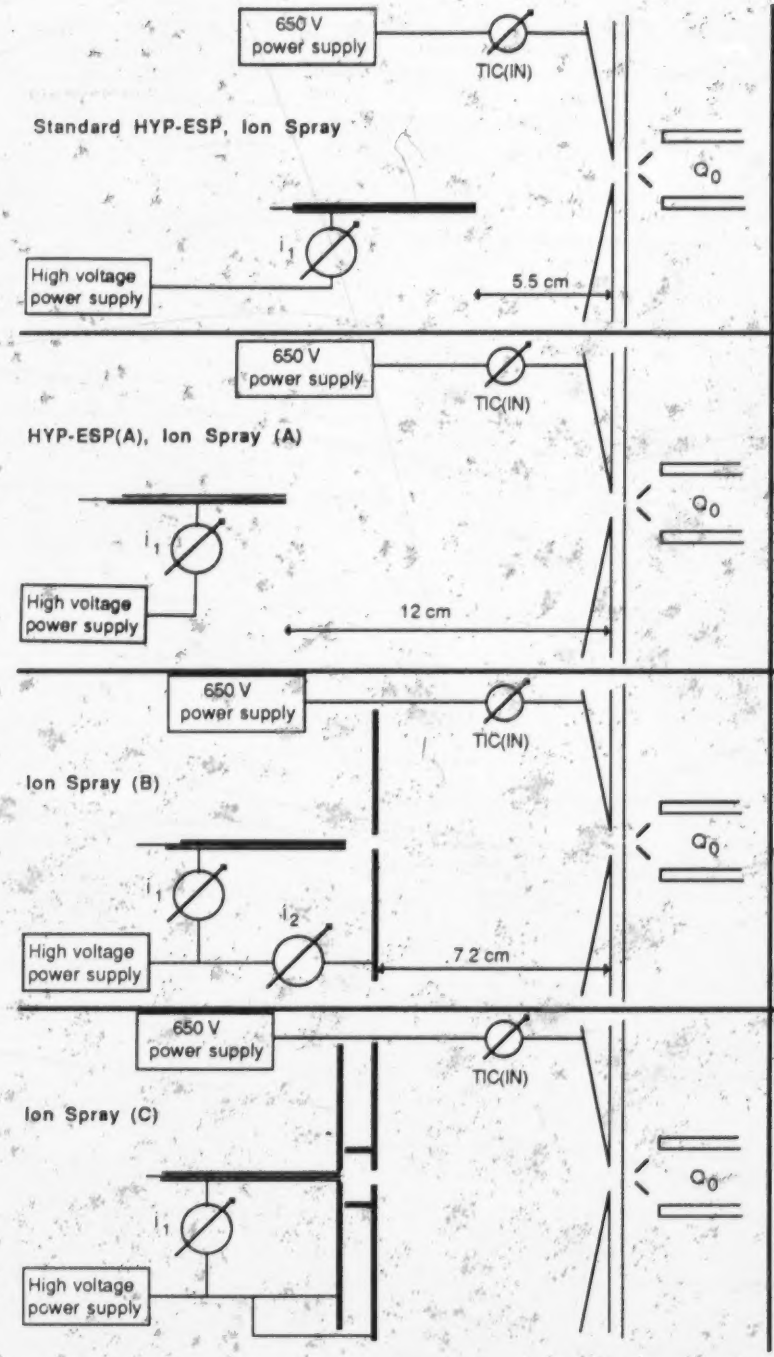

	HYP-ESP		ION SPRAY	
	TIC(IN) (A)	I_{BH^+} (cps)	TIC(IN) (A)	I_{BH^+} (cps)
Standard HYP-ESP, Ion Spray	8×10^{-8}	3×10^5	8×10^{-8}	9×10^5
HYP-ESP(A), Ion Spray (A)	1.6×10^{-6}	4×10^5	1.6×10^{-6}	4×10^5
Ion Spray (B)	NA	NA	4×10^{-9}	1.5×10^5
Ion Spray (C)	NA	NA	2×10^{-10}	4×10^4

APPENDIX 3.I Detailed Diagrams of Ion Spray (B) and (C) Type Experiments.

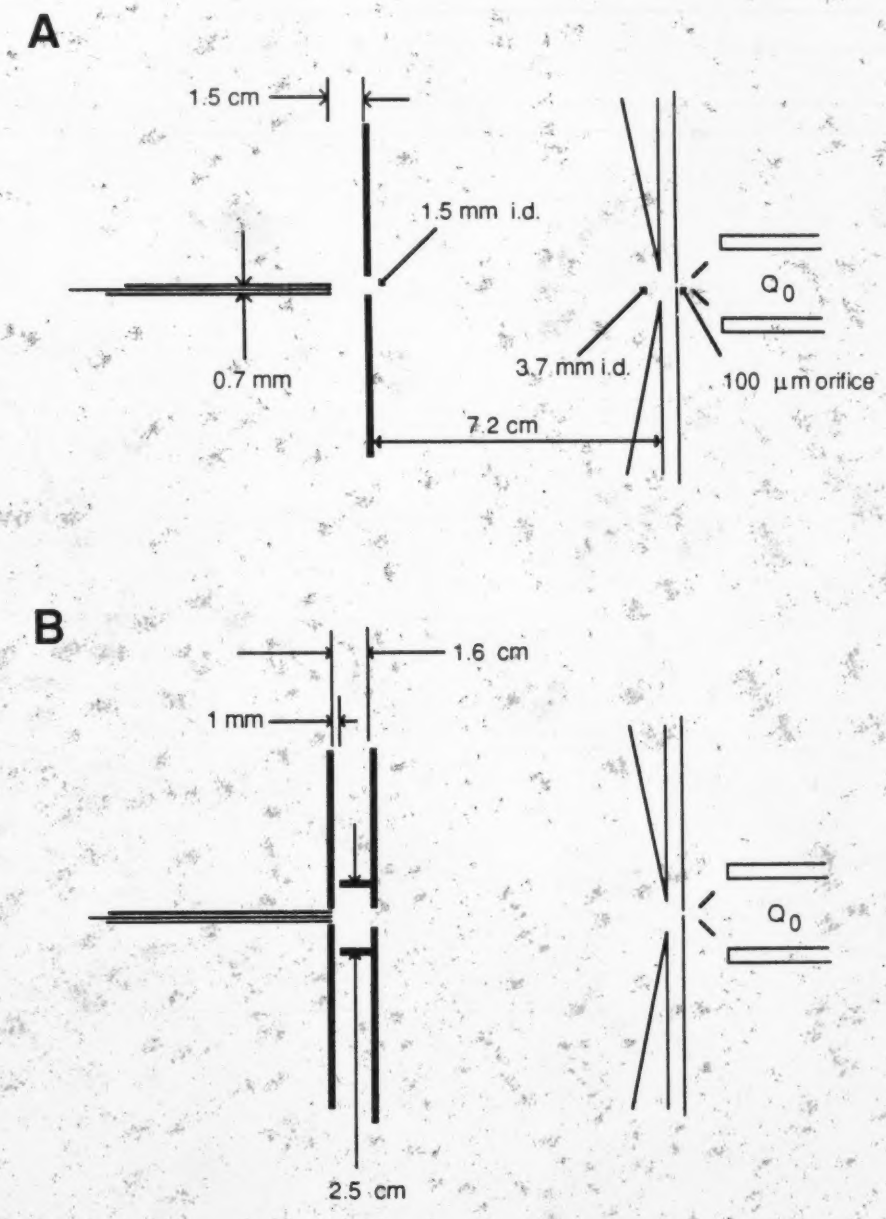

Intermediate plates are of ≈12 cm diameter and ≈1.5 mm thickness.

APPENDIX 3.II Summary and CONCLUSIONS of the Performance Comparison Between Electrospray and Ion Spray (*14*).

a. General.

Two different versions of electrospray were used. In *ESP*, a special version developed at the University of Alberta, a blunt, rounded, smooth tip, obtained from a thicker walled stainless steel capillary is used. In *HYP-ESP* a sharp tip is used from a thin walled capillary, actually a hypodermic needle. This is the device used by Fenn. The inner diameter of the capillary in both cases is the same. Pneumatically assisted electrospray, or *Ion-Spray*, is essentially the same device as that used by Henion et al.

Conditions:

ESP	9 kV, 4 cm distance.
HYP-ESP	5.5 kV, 4 cm distance.
Ion Spray	5.5 kV, 4 cm distance and 1.5 cm off center, 60 psi Nebulization pressure.

Note: Although these Ion Spray conditions provide maximum analyte signal stability and sensitivity, it should be mentioned at this point that, at conditions where HYP-ESP operates well (i.e. low flow rates and methanol or acetonitrile as solvents) nebulization pressures lower than ≈50 psi have no effect on the analyte signal. The nebulization pressure needs to be increased to 60 psi in order to obtain some gain in sensitivity.

b. Sensitivity and Stability as a Function of Flow Rate.

Solutions: All in 100% MeOH.

10^{-5}, 10^{-6}, 10^{-7} M cocaine/HCl.

Conclusions: *ESP* provides best sensitivity at 5-30 µL/min. flow rate. *HYP-ESP* performs best in 1.2-20 µL/min. *Ion Spray* performs well at 1.2 to 20

μL/min, but performs equally well from 30 to 390 μL/min also. Thus sensitivity is 30 times higher than *HYP-ESP* at 390 μL/min.

c. Relative Sensitivities of Organic Bases.

Conditions: Flow rate, 20 μL/min. Some 15 analytes, organic bases in the 2-12 pK_B range, dissolved in 100% MeOH. Both free bases and HCl salts were tested, each as 10^{-5} M solution.

Conclusions: Similar sensitivity trends with all three methods, i.e. low pK_B bases give high sensitivity while poor sensitivity is obtained for those of high pK_B. Sensitivities of high pK_B bases is increased when HCl is added to the solution. Relative sensitivities vary from one method to the other but trends are similar. For more details on trends with *ESP* see Chapter 2.

d. Dependence of Analyte Signal on Ion Concentration.

Conditions: 20 μL/min, MeOH solvent.

Analytes: Triheptylamine, $CsNO_3$, RbCl, cocaine/HCl.

Conclusions: Analyte signal approximately linear with analyte concentration up to 10^{-5} M, at higher concentration intensity flattens out. This behavior was observed for *ESP*, see Chapter 2, and closely similar behavior was observed also with *HYP-ESP* and *Ion Spray*. With *ESP* the spray quality decreased (coarsening of the droplet size) at high concentration. With *Ion Spray* the fine spray quality is maintained even at high concentrations, however the analyte signal shows the same flattening out as for *ESP*. Thus droplet size is not directly responsible for the decrease of sensitivity at high electrolyte concentrations.

e. Sensitivities of Organic Bases at various Methanol-Water solvent compositions.

Conditions: Solvent from 100-10% MeOH, 0-90% H_2O.
Experiments at 4.5 and 20 μL/min flow rate.

Analytes: Triheptylamine, cocaine/HCl, Codeine/HCl each at 10^{-5} M concentration.

Conclusions: *ESP* does not work below 75% MeOH. *HYP-ESP* and *Ion Spray* produce spray right down to 10% MeOH, however analyte sensitivity decreases somewhat with decreasing percentage of MeOH. Sensitivity for analytes is strongly dependent on flow rate. Thus *Ion Spray* gives 3-5 times better sensitivity than *HYP-ESP* at 20 μL/min but the situation reverses in favour of *HYP-ESP* at 4.5 μL/min.

f. Sensitivities of Organic Bases in Different Solvents.

Conditions: 20 μL/min flow.

Solvents: MeOH, Ethanol, 2-Propanol, Acetonitrile, Ethyl Acetate, Acetone, 2-Butanone, Dimethyl sulfoxide (DMSO), Diethyl Ether.

Analyte: Codeine/HCl at 10^{-5} mol/L.

Conclusions: *Ion Spray* gives the best sensitivity. Sensitivity is better by a factor of 2 to 3 relative to *HYP-ESP* and also signal stability is much better with *Ion Spray*. The analyte could not be detected at all with *HYP-ESP* in some solvents while detection with *Ion Spray* was possible although signal was week relative to the good solvents. Best solvents for all three devices: MeOH and Acetonitrile; worst solvent: Diethyl ether.

g. Analyte Signal in Presence of Buffer.

Buffer: 0.02 M ammonium acetate in 3:1 H_2O: MeOH, pH = 3.9, flow rate 20 μL/min.

Analyte: Cocaine.

Conclusions: The cocaine BH^+ ion signal increases with increasing [B] in solution but the relationship is less than linear in buffer, in a concentration range where it is linear in absence of buffer. *Ion Spray* leads to better sensitivity by a factor of ≈2 to 3 relative to *HYP-ESP*.

REFERENCES

1. Yamashita, M.; Fenn, J. B. *J. Phys. Chem.* **1984**, 88, 4451; **1984**, 88, 4671.
2. Whitehouse, C. M.; Dreyer, R. N.; Yamashita, M.; Fenn, J. B. *Anal. Chem.* **1985**, 57, 675.
3. Fenn, J. B.; Mann, M.; Meng, C. K.; Wong, S.F.; Whitehouse, C. M. *Mass Spectrom. Rev.* **1990**, *9*, 37
4. Brunis, A. P.; Covey, T. R.; Henion, J. D. *Anal. Chem.* **1987**, 57, 2642.
5. Brunis, A. P.; Weidorf, L. O. G.; Henion, J. D. *Anal. Chem.* **1987**, 59, 2647.
6. Huang, E. C.; Henion, J. D. *J. Am. Soc. Mass Spectrom.* **1990**, *1*, 158
7. Smith, R. D.;Loo, J. A.; Edmonts, C. G.; Barinaga, C. J.; Udseth, H. R. *Anal. Chem.* **1990**, *62*, 882.
8. Chapter 2. (Ikonomou, M. G.; Blades, A. T.; Kebarle P. *Anal. Chem.* **1990**, *62*, 957.)
9. Ikonomou, M. G.; Blades, A. T.; Kebarle P. (in preparation)
10. Jayaweera, P.; Blades, A.T.; Ikonomou, M. G.; Kebarle, P. *J. Amer. Chem. Soc.* **1990**, *112*, 2452.
11. Blades, A.T.; Jayaweera, P.; Ikonomou, M. G.; Kebarle, P. *J. Chem. Phys.* **1990**, *92*, 5900.
12. Blades, A.T.; Jayaweera, P.; Ikonomou, M. G.; Kebarle, P. *Int. J. Mass Spectrom. Ion Processes* (In Press).
13. Blades, A.T.; Jayaweera, P.; Ikonomou, M. G.; Kebarle, P. *Int. J. Mass Spectrom. Ion Processes* (In Press).
14. Ikonomou, M. G.; Blades, A. T.; Kebarle P. (in preparation).
15. Sunner, J.; Nicol, G.; Kebarle, P. *Anal. Chem.* **1988**, 60, 1300.
16. Sunner, J.; Ikonomou, M. G.; Kebarle, P. *Anal. Chem.* **1988**, 60, 1308.
17. Reid, N.; Buckley, J. A.; French, J. B.; Poon, C. C. *Adv. Mass Spectrom.* **1979**, 8B, 1843.

18. Castleman, A. Q. Jr. *J. Phys. Chem. Ref. Data* **1986**, *15*, 1011.

19. Lias, S. G.; Liebman, J. F.; Levin, R. D. *J. Phys. Chem. Ref. Data* **1984**, *13*, 695.

20. (a) Nicol, G.; Sunner, J.; Kebarle, P. *Int. J. Mass Spec. and Ion Processes* **1988**, *84*, 135. (b) Kebarle, P. "Pulsed Electron High Pressure Mass Spectrometer" in Weissberger "*Techniques for the Study of Ion-Molecule Reactions*", Farrar, J.H. and Saunders, W. Eds. Wiley-Interscience (**1988**).

21. Busman, M.; Sunner, J.; Vogel, C.R., unpublished results.

22. Loeb, L.B. *Science* **1945**, *102*, 573.

23. (a) Pfeifer, R.J.; Hendricks, C.D. *AIAA Journal* **1968**, *6*, 496. (b) Pfeifer, R.J.; Hendricks, C.D. *The Phys. of Fluids* **1967**, *10*, 2149. (c) Hendricks, C.D. *J. Colloid Sci.* **1962**, *17*, 249. (d) Hendricks, C.D. "Charging Macroscopic Particles". *In Electrostatics and Applications*; Moore, A.D., Ed.; John Wiley: New York, **1973**.

24. (a) Iribarne, J. V.; Thomson, B. A. *J. Chem. Phys.* **1976**, *64*, 2287. (b) Thomson, B. A.; Iribarne, J. V. *J. Chem. Phys.* **1979**, *71*, 4451. (c) Iribarne, J. V.; Dziediz, P. J.; Thomson, B. A. *Int. J. Mass Spectrom. Ion. Phys.* **1983**, *50*, 331.

CHAPTER 4

PRODUCTION AND STUDY IN THE GAS PHASE OF MULTIPLY CHARGED SOLVATED OR COORDINATED METAL IONS BY ELECTROSPRAY MASS SPECTROMETRY*

* A version of this Chapter has been published: Jayaweera, P.; Blades, A. T.; Ikonomou, M. G.; Kebarle, P. *J. Am. Chem. Soc.* **1990**, *112*, 2452. Blades, A. T.; Jayaweera, P.; Ikonomou, M. G.; Kebarle, P. *J. Chem. Phys.* **1990**, *92*, 5900. Blades, A. T.; Jayaweera, P.; Ikonomou, M. G.;Kebarle, P. *Int. J. Mass Spectrom. Ion Proc.* (in press). Blades, A. T.; Jayaweera, P.; Ikonomou, M. G.;Kebarle, P. *Int. J. Mass Spectrom. Ion Proc.* (in press).

INTRODUCTION

Studies of gas phase ion-chemistry have been mostly restricted to singly charged positive or negative ions (*1*). Singly charged ions have also been the only ions involved in ion cluster studies (*2,3*). A strong motivation for the study of ion clusters was the realization that the interactions of ions and solvent or other ligand molecules, determined from gas phase measurements, provide unique information regarding ion-solvation and ion-ligand interactions in liquid solutions. Thus, determinations of the gas phase equilibria, eq 4.1, initiated in

$$M^+(H_2O)_{n-1} + H_2O = M^+(H_2O)_n \qquad (4.1)$$

Kebarle's laboratory some 20 years ago (*4, 5*), which led to the sequential enthalpies $\Delta H^{\circ}_{n,n-1}$ and entropies $\Delta S^{\circ}_{n,n-1}$, have provided a wealth of data on ion-solvent and ion-ligand interactions (*2, 6*). Extensive theoretical studies of ion-ligand binding energies (*7*) and molecular dynamics of ion-solutions (*8*) were stimulated by the above results. The quoted work (*1-8*) gives only representative examples of a large number of publications.

The above studies have been limited to singly charged ions M^+, yet doubly and triply charged ions such as Mg^{2+}, Ca^{2+} and Fe^{2+}, Fe^{3+}, Co^{2+}, Co^{3+}, Cu^{2+}, Zn^{2+}, etc., are of paramount importance in condensed phase chemistry and in biochemistry. Thermochemical data for ion-solvent and ion-ligand interactions are also useful from the analytical standpoint. For example, the equilibrium distribution of metal hydrates or other metal ion-ligand clusters can be predicted when the analysis involves mass spectrometric techniques where metal ion formation takes place in the presence of ligand molecules; some of these techniques are described below. In addition, ligand specificity towards different metal ions can also be useful in increasing the selectivity of these techniques.

Multiply charged "naked" metal ions are not difficult to produce in the dilute gas phase. This is illustrated by the availability of experimental higher ionization potentials for the elements. The difficulties arise when other chemical matter is near the multiply charged ion.

The general method used for singly charged ion-clusters like $M^+(H_2O)_n$, is to generate M^+ in a gas phase in which ligand molecule vapor is present. The formation of $M^+(H_2O)_n$ then proceeds spontaneously by third-body-dependent association reactions corresponding to eq 4.1. This method may not work for M^{2+} species when the second ionization energy of M, I.E.(M^+), is much larger than the ionization energy of the ligand; this is the case, for example, for Mg where I.E.(Mg^+) = 15.0 and I.E.(H_2O) = 12.6 eV. Little information is available on the outcome of gas phase reactions: M^{2+}+L where I.E.(M^+) > I.E.(L). Change transfer to the ligand, leading to M^+ and L^+ and formation of $M^+OH + H_3O^+$ for cases where the ligand and the third body are H_2O, are reaction channels that could compete with formation of stabilized $M^{2+}L$.

Some results for reactions of M^{2+}+ L have been reported (*9*). These involved (*9a*) the species Mg, Ca, Ba with relatively low I.E.(M^+) values. Reactions of Ti^{2+} with the lower alkanes have also been examined (*9b*) and similar work has also been reported (*9c*) for Nb^{2+} and La^{2+}. These results are of considerable interest; however, for the above systems, the I.E.(M^+) values are all relatively low. Furthermore, most of the ion-ligand reactions observed led to charge reduction, i.e., among the products were two singly charged ions. It appears also that only a limited range of M^{2+} ions can be produced with the methods used (*9*), and that many low I.E. ligands will lead to charge reduction already in the first collision.

Since doubly and triply charged ions exist in solution, preparation of gas phase ions like $M^{2+}(H_2O)_n$ might be possible by transfer of multiply hydrated ions from the liquid to the gas phase. Until recently this alternative would have been considered impossible. However, recent mass spectrometric techniques developed for analytical purposes, such as Fast Atom Bombardment (FAB) (*8,10,11*), Thermospray (*12,13,14*), Electrohydro-dynamic Ionization (EHI) (*15*), and Electrospray (*16,17*), have demonstrated that singly-charged inorganic ions M^+ attached to ligands, can be produced in the gas phase when the corresponding ions are present as electrolytes in the solution. Due to a longstanding interest in the initiation of M^{2+} gas phase ion chemistry, we became, for this and other reasons, involved in research

involving these techniques (*10,14,17*). Some doubly charged ion-ligand species can be produced with all of these techniques. However, only very low intensities of $M^{2+}(L)_n$ ions are observed with FAB (*11*) and then only when large multidentate complexing agents are used, presumably because these stabilize the charge by extensive charge delocalization. Even then, the dominant process is charge reduction to singly charged ions (*11*). Similar processes dominate (*15*) also in EHI/MS. More promising in this regard is Thermospray, and Röllgen (*13*) has reported the observation of $Ca^{2+}(H_2O)n$ and $Sr^{2+}(H_2O)n$. However, these and the higher alkaline earths should be relatively easy to produce since for these, I.E.(M^+) < I.E.(H_2O).

The multiply charged metal ion studies described in the present work are based on Electrospray ionization mass spectrometry. While Electrospray has been known for many years, it was Fenn (*16*) who first introduced mass spectrometric studies of ions produced by electrospray. Fenn *et al.* (*18*), Smith *et al.* also using electrospray (*19*), and Covey, Bonner, Shushan and Henion (*20*) who used a related technique, "Ion spray", have reported multiply charged ions. However, these were organic systems such as peptides and proteins of molecular weight of well over 100,000 Da containing many basic residues. The basic groups can be protonated and lead to ions with as many as 175 positive charges (*19b*). While the findings are of the greatest analytical interest, the protonated basic groups are far apart on the molecular scale, and the species can be viewed as singly charged ions connected by peptide strings.

Work in our group was focussed on multiply charged metal ions, where the charge is formally located on just one atomic center, the metal ion, even though the multiply charged metal ion cluster may owe its stability to charge delocalization on to the ligands. We found that M^{2+} were formed as major gas phase ions when suitable liquid solutions containing the M^{2+} ions were electrosprayed. This was the case for the alkaline earths, Mg^{2+}, Ca^{2+}, Sr^{2+}, Ba^{2+}, which could be produced as hydrates $M^{2+}(H_2O)_n$ or complexed to other ligands (*21,22,23*). Significantly only $Be(OH)^+(H_2O)_n$ ions were obtained with $Be(NO_3)_2$ salt. It

should be noted that the I.E.(Be^+) = 18.2 eV is the highest in this series; I.E.(Mg^+) = 15 eV, I.E.(Ca^+) = 11.8 eV, etc. The transition metal hydrates $M^{2+}(H_2O)_n$ were also observed for the first row transition metals Mn^{2+}, Fe^{2+}, Co^{2+}, Ni^{2+}, Zn^{2+}, when the corresponding solutions were electrosprayed (*21,22,23*). A variety of M^{2+} ion-ligand complexes with the above metals and from Cr^{2+}, Cu^{2+}, Co^{3+} with ligands such as dimethyl sulfoxide (DMSO), dimethylformamide (DMF), pyridine and polydentate ligands such as peptides, di- and poly-ketones, cyclic tetramines (cyclams), and the polycyclic hexamine (sepulchrate), could also be prepared and observed. Triply charged ion ligand complexes $M^{3+}(L)_n$ could also be produced in the gas phase (*23,24*). Solutions of the M^{3+} salts, M = Y, La, Ce, Nd, Sm, with L = DMSO and DMF, led to M^{3+} complexes; however L = H_2O led only to the charge reduced complexes, $MOH(H_2O)_n^{2+}$.

In this Chapter features of the electrospray-generated multiply-charged metal ion mass spectra, as well as collision induced dissociation (CID) mass spectra of metal ion-ligand complexes will be presented. The influence of the experimental arrangement used on spectral appearance, i.e. the extent of metal ion clustering to ligand molecules, and thus the metal-ion ligand distribution, will be described. Furthermore, details on how this arrangement can be used to obtain thermochemical data of singly and multiply charged metal ions with ligands will be given.

EXPERIMENTAL SECTION

The electrospray ion source and the triple quadrupole mass spectrometer used for the ion detection have been described in detail in the experimental section of Chapter 2. The electrospray source was also operated in much the same way as before, see Chapter 2. The ions produced by the electrospray, driven by an electric field, enter an interface chamber containing ultrapure nitrogen at atmospheric pressure. The ions drift across the interface chamber and ions arriving in the vicinity of the interface orifice (see Figure 2.1) are entrained by N_2 gas escaping through the orifice into the vacuum chamber which contains the triple quadrupole mass spectrometer. There the ions can be mass separated and detected or mass selected with the first quadrupole Q1 exposed to collision induced dissociation (CID) in Q2 and the ionic products detected with Q3, (*25*).

The electrospray ions were obtained with 10^{-5} - 10^{-4} mol/L solutions of the metal salts, generally the soluble MCl_2 or $M(NO_3)_2$, in methanol. For the M^{2+} hydrates, 1 to 5% by weight water was added to the methanol when the hydrate clusters were to be observed. To generate the DMSO, DMF or other clusters, the ligands were added to methanol solutions where the metal salts were dissolved in. Typically, 10^{-3} - 10^{-2} M of the ligand solutions in methanol were used with or without the water addition. The solution flow-rate was kept at 10 μL/min and the electrospray capillary was held at +9000 V.

One particular advantage of the ions-from-solution method is the rapidity with which one can examine different systems. Solutions are easily prepared, and one can change from Co^{2+} to Zn^{2+}, say, by simply replacing the solutions in the microsyringe; this change takes only a minute or two, and within about another minute one already observes the new ion with the mass spectrometer operating under identical conditions.

RESULTS AND DISCUSSION

(a) Features of Electrospray-Generated Multiply-Charged Metal Ion Mass Spectra.

The electrospray chamber **3**, Figure 2.1, contains solvent vapor, generally methanol and water each at some 5 torr. The singly-charged M^+ ions under these conditions, see Chapter 2 and (*17*), form clusters $M^+(H_2O)_a$, $M^+(CH_3OH)_b$, $M^+(H_2O)_a(CH_3OH)_b$, where the average value of (a + b) is typically quite high (~10). The ions drift across the interface chamber, **7**, and ions arriving in the vicinity of the orifice **9** (OR) are entrained by N_2 gas escaping through the orifice into the vacuum chamber. The direct expansion of this gas mixture into vacuum leads to a low temperature molecular and ion beam.

Although the functions of the interface gas have been described in the experimental section of Chapter 2, in view of the following discussions the thermal declustering taking place in the interface chamber needs to be considered in detail. The interface gas is ultrapure N_2, but contained a known (typically 2 ppm) concentration of H_2O. Under these very dry conditions rapid declustering of the M^+ clusters occurs and hydration equilibria, eq 4.1, are established at much lower n values. One can demonstrate that such equilibration is expected, as shown below. The rate constants k_f for the forward clustering of low n clusters, see eq 4.1, are expected (*26*) to be governed by bimolecular collision rates $k_f \approx 1 \times 10^{-9}$ molecules^{-1} cm^3 s^{-1}, due to the high pressure of third-body gas (N_2). The 2 ppm H_2O in the ~700 torr interface gas, corresponds to ~1.4 mtorr, and a half-life of 10^{-5} s can then be estimated for forward clustering of low n clusters. The declustering rate constants k_r can also be evaluated (27) from available equilibrium constants, $K_{n-1,n}$, and $K_{n-1,n} = k_f/k_r$. The unimolecular k_r values for clusters of high n are very large (*27*), and lead to very short half-lives. Therefore, the equilibria (n-1,n) are expected to become established within less than 100 μs residence time in the interface chamber.

In the absence of any water in the interface region complete thermal declustering would have been expected for all analytes. However, because of the 2 ppm H_2O in the interface gas

the extent of dehydration of the incoming ions depends on the hydrate binding energies in $M^+(H_2O)_n$. Hydrates with binding energies higher than ~ 15 kcal/mol under these conditions can not be fully declustered (*27*). Furthermore, when solutions of alkali metal salts are electrosprayed the hydrates rather than the methanol solvated ions are observed, see for example Figure 2.7 and related discussions. Due to the preference of alkali metal ions for H_2O (*1,2*), an exchange of the original ligands CH_3OH for H_2O occurs in the interface region. Under the present conditions of water pressure and interface temperature the observed relative intensities of the hydrated metal ions represent equilibria cluster distributions; more details are given in the following section.

With the TAGA atmospheric pressure-vacuum interface arrangement (Chapter 2) further declustering can be induced past the interface orifice, 9 in Figure 2.1. In the gas jet on the vacuum side of the interface orifice, declustering occurs due to collisional excitation of the ions as they drift in the electrical field through the neutral gas jet. The extent of declustering can be varied by changing the electrical potentials on the electrodes , CB and Q_0 (see Figure 2.1), in the jet region. When the voltages of the OR, CB, and Q_0 electrodes are kept the same no declustering takes place in this region. In that case, the intensities of the detected ions represent the cluster distribution equilibria as established in the interface chamber. On the other hand, by lowering the potentials of the CB and Q_0 electrodes relatively to OR, the cluster distribution is shifted towards lower n values, see eq 4.1.

As with singly charged metal ions, methanol solutions of M^{II} salts also produced metal hydrates, $M^{2+}(H_2O)_n$, upon electrospray ionization. A condition for the M^{II} metal hydrates to be detected was that the second ionization potential of the metal had to be less than ~18 eV. For Be ($I.E.^{II}$ = 18.2 eV) and Cu ($I.E.^{II}$ = 20.3 eV) only the clusters $M^+OH(H_2O)_n$ were observed instead. Also, no triply charged hydrates $M^{3+}(H_2O)_n$ could be observed with the M^{III} salts for any of the metals listed above, under experimental conditions where most of the M^{II} salts led to abundant hydrates, $M^{2+}(H_2O)_n$. The charge reduction mechanism for the Cu^{2+}, Be^{2+} and M^{3+} hydrates has been considered in detail at a later section.

A typical mass spectrum obtained by electrospraying 10^{-4} M $CoBr_2$ in MeOH, with 1% H_2O at 10 μL/min is shown in Figure 4.1. Apart from the metal hydrates, $Co^{2+}(H_2O)_n$, three other major groups of metal ion-solvent clusters were detected, $Co^{2+}(CH_3OH)(H_2O)_n$, $Co^{2+}(CH_3OH)_2(H_2O)_n$, and $Co^{2+}(CH_3OH)_3(H_2O)_n$. The only charge-reduced species detected was $Co^{+}OH(H_2O)$. The ions shown in Figure 4.1 represent more than 95% of all the cobalt related ions detected and identified under the present experimental conditions. Although the cluster distribution, and the type of metal ion-methanol-water clusters may vary between metals, the M^{II} metal ions were mostly detected as the type of clusters shown in Figure 4.1. The yield and the distribution of the charge reduced clusters depended on the value of the second I.E. of the metal, and also on the electric fields in the jet region of the atmospheric pressure-vacuum interface, see following sections.

From the analytical standpoint the type of spectra shown in Figure 4.1 are not very promising, either in terms of specificity or sensitivity. However, by proper selection of ligands and experimental conditions the situation can be improved considerably.

Electrospray can produce a large variety of M^{2+} ion-ligand complexes, by proper choice of concentrations in the electrosprayed solution and of pressure of ligand vapor in the electrospray and interface chambers. Of all the ligands investigated so far (see Introduction) DMSO gave the best results both for the doubly and triply charged metal ions. In addition DMSO retards charge reduction of the triply charged clusters. An electrospray mass spectrum, obtained from a 10^{-4} M solution of $CoBr_2$ in MeOH with 10^{-2} M DMSO, at 10 μL/min, is shown in Figure 4.2A. This spectrum was obtained under identical conditions to that of Figure 4.1. A large increase in sensitivity is obtained due to the signal related to M^{2+} ions being concentrated only into a few mass values. As with water the DMSO cluster distribution varied between different metals, but in general the total ionization was concentrated in only a few m/z values. The background $Co^{2+}(DMSO)_4$ signal (*m/z* 185.5) was some 10^3 counts/s when neat methanol was run through the system. Extrapolating from the data of Figure 4.2A a $Co^{2+}(DMSO)_4$ signal 3 times higher than that of the background can

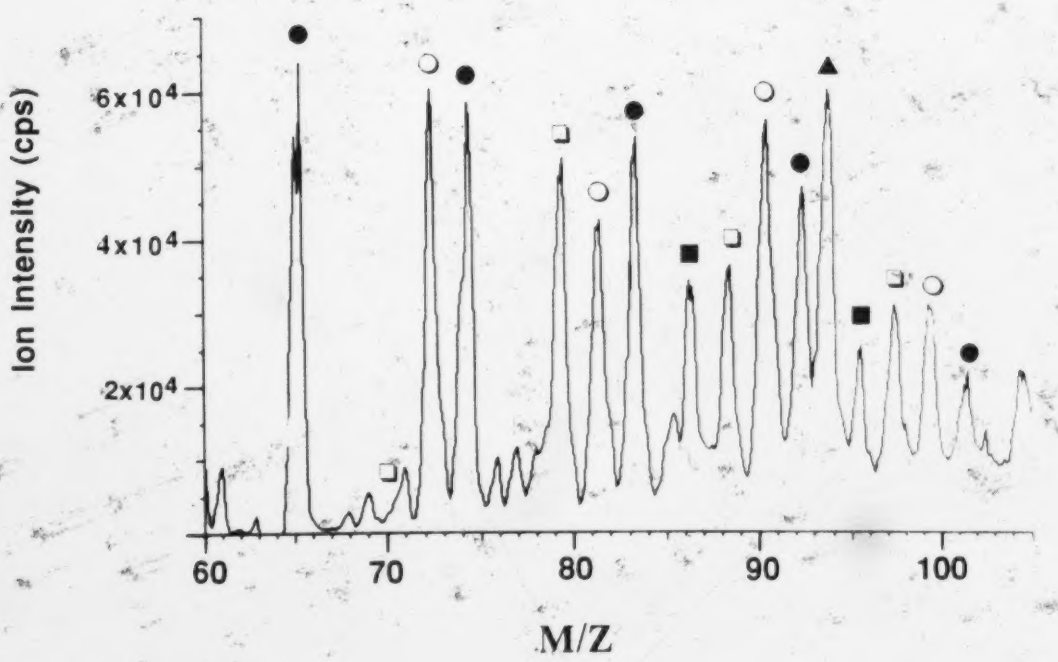

$Co^{2+}(H_2O)_n$ (●)	n=4	(m/z 65.5)*
	n=5	(m/z 74.5)
	n=6	(m/z 83.5)
	n=7	(m/z 92.5)
	n=8	(m/z 101.5)

$Co^{2+}(CH_3OH)(H_2O)_n$ (○)	n=3	(m/z 72.5)	$Co^{2+}(CH_3OH)_2(H_2O)_n$ (❑)	n=1	(m/z 70.5)
	n=4	(m/z 81.5)		n=2	(m/z 79.5)
	n=5	(m/z 90.5)		n=3	(m/z 88.5)
	n=6	(m/z 99.5)		n=4	(m/z 97.5)
$Co^{2+}(CH_3OH)_3(H_2O)_n$ (■)	n=1	(m/z 86.5)	$Co^{+}OH(H_2O)$ (▲)		(m/z 94.5)
	n=2	(m/z 95.5)			

Figure 4.1. Electrospray mass spectrum of 10^{-4} M $CoBr_2$ in MeOH, with 1% H_2O at 10 μL/min. Electrospray tip at 9 kV, voltage difference between the OR and CB electrodes, see Figure 2.1,was 22 V. * Overlap with $(CH_3OH)_2H^+$, m/z 65.

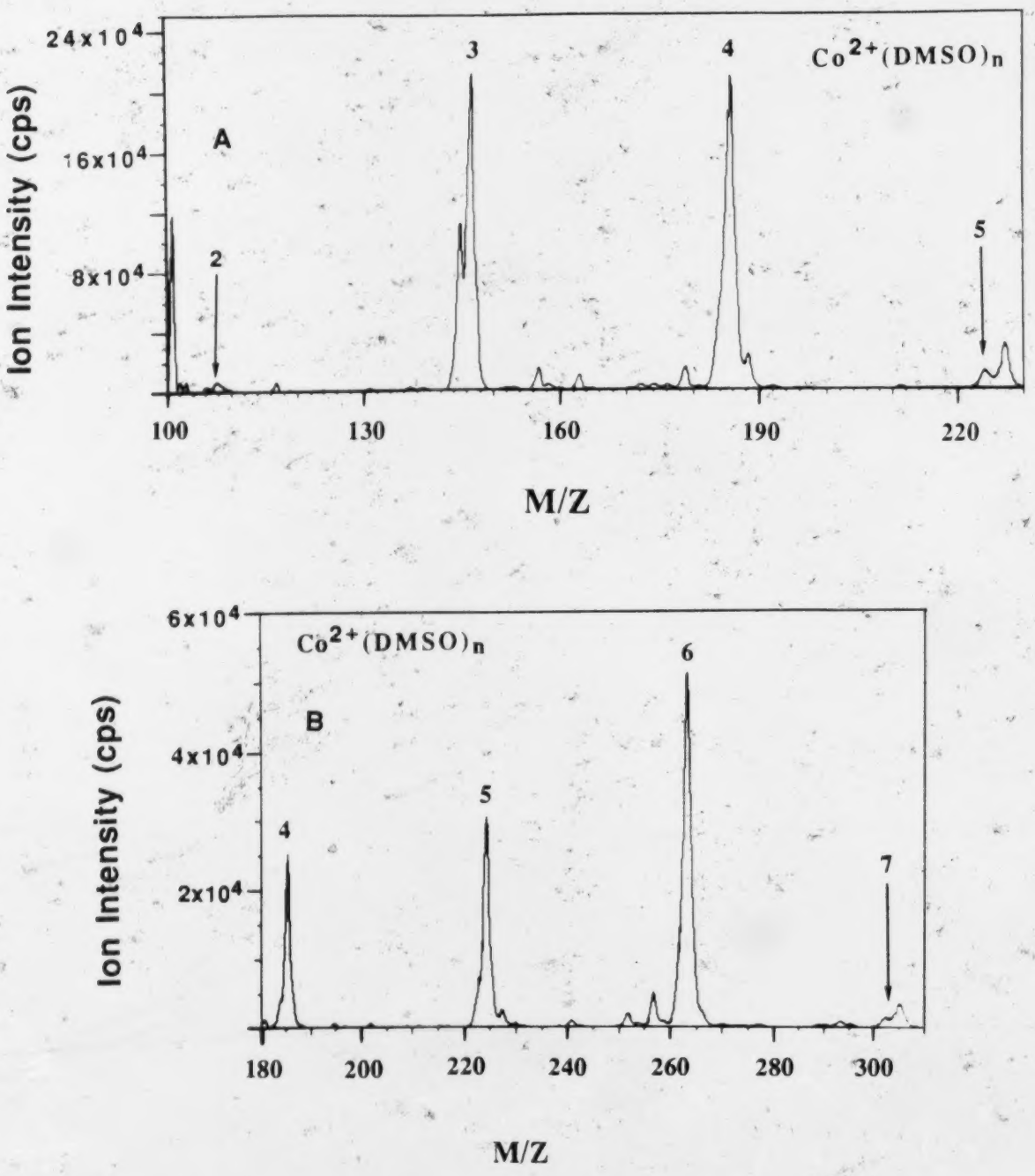

Figure 4.2. (A) Electrospray mass spectrum of 10^{-4} M $CoBr_2$ in MeOH, with 10^{-2} M DMSO, at 10 μL/min. Electrospray tip at 9 kV, voltage difference between the OR and CB electrodes, see Figure 2.1,was 22 V. (B) Same as in A but OR to CB voltage difference has been reduced to 5 V. The annotated peaks denote the numbers of DMSO ligands, n, clustered to Co^{2+}.

be obtained from 1 x 10^{-6} M concentrations. Under single ion monitoring conditions detection requires ≈5 s, which for a 10 μL/min solution flow-rate corresponds to a detection limit of 8 x 10^{-13} mol of analyte in solution.

If the TAGA interface conditions, voltages applied to OR, and CB, are not chosen carefully high n clusters, see eq 4.1, are observed with all ligands. High degree of clustering is invariably accompanied with loss in sensitivity, and spectral cleanness, see for example Figure 4.2B. Under these conditions the analyte related ions were clusters containing not only DMSO but also a large number of water and methanol molecules and were therefore spread over many masses. Part of the sensitivity loss in this case could also be due to poor ion transmission with the ion lens potentials used.

(b) Metal Ion Hydration Equilibria Measurements.

So far electrospray has been operated only at atmospheric pressure (*16,17*). Thermal ion-hydrate equilibria studies depend on mass spectrometric determination of the relative ion-hydrate ratios at equilibrium (*5*). Such determinations are difficult when the ions are formed and sampled into the vacuum from atmospheric pressure. Cooling, due to the adiabatic free jet expansion of the gas plus ions past the sampling orifice into the mass spectrometer vacuum chamber, can lead to uncontrolled growth of the clusters. However with the present experimental setup this was not a limiting factor (*22,23*), and equilibrium populations for metal hydration, eq 4.2, and other ligand equilibria could be determined.

$$M^{2+}(H_2O)_{n-1,n} + H_2O = M^{2+}(H_2O)_n \qquad (4.2)$$

The evaluation of sequential binding free energies $\Delta G^{o}_{n,n-1}$ was thus possible, and quantitative data are presented in what follows.

In these studies the interface chamber rather than the ionization region was used to create conditions where simple ion-molecule equilibria occur, for which the equilibrium constants could be determined by measuring ion intensity ratios with the mass spectrometer.

In order to check the reliability of the present experimental setup in determining metal ion-ligand binding energies, previously determined (*4b*) equilibria involving the hydration of Li^+, Na^+, K^+, and Rb^+, were measured. As before (*2,4,5*), the equilibrium constants were defined by eq 4.3, where I_n stands for the mass spectrometrically measured ion intensity of

$$K_{n-1,n} = \frac{I_n}{I_{n-1}P_{H_2O}} \qquad (4.3)$$

$$\Delta G^\circ_{n-1,n} = -RT \ln K_{n-1,n} \qquad (4.4)$$

the ion cluster with n water molecules. The water pressures used were typically 2×10^{-6} atmospheres, corresponding to the 2 ppm impurity water content in the N_2 curtain gas. The free energies $\Delta G^\circ_{n-1,n}$ are then evaluated via eq 4.4. Estimated $-\Delta G^\circ_{n-1,n}$ values for M^+ hydrates are given in Table 4.1. Also given for comparison are the results from the previous measurements (*4b*), which are more accurate since they were measured at low total pressures where ion sampling presents much less of a problem (*2,4,5*). The relative ion intensities I_n, observed in the present work, are illustrated in Figure 4.3. The ion distributions observed with the two methods were very similar; substantial ion ratio differences occured only when small ion intensities entered the ion ratio I_n/I_{n-1}. Thus at the low end of the distribution, the lowest n hydrate shown has generally higher intensity in the present results relative to the accurate data (*4b*). At the high end of the hydrates, the highest n hydrate has again a higher intensity than predicted by the previous work. These ratio errors show up in the evaluated $-\Delta G^\circ_{n-1,n}$ given in Table 4.1. The values obtained from the high intensity ions in the middle of the distribution are in very good agreement with the previous results (*4b*), while the $-\Delta G^\circ_{n-1,n}$ at the low end of the distribution is too small and that at the high end of the distribution is too high. Discrepancies at the low end of the distribution are assumed to be due to dissociation of the higher clusters in the vacuum of the mass analysis system, while those on the high end are probably due to a small extent of non-equilibrium cluster growth due to cooling in the gas jet

Table 4.1 Thermochemical Data[a] for Reactions:

$$M^{+z}(H_2O)_{n-1} + H_2O = M^{+z}(H_2O)_n \text{ where } z = 1 \text{ or } 2.$$

$-\Delta G^{o}_{n-1,n}$	Li^+	Na^+	K^+	Rb^+
0, 1			9.0 (11.4)[b]	9.4 (9.6)[b]
1,2		10.0 (13.2)[b]	9.2 (8.9)	7.2 (7.0)
2,3	10.0 (13)[b]	9.4 (9.3)	6.6 (6.3)	6.0 (5.0)
3,4	7.8 (7.5)	6.4 (6.3)	5.9 (4.4)	
4,5	5.5 (4.5)			

	Mg^{2+}	Ca^{2+}	Sr^{2+}	Mn^{2+}	Co^{2+}
7,8	8.4				
8,9	8.2	8.0	(8.0)[c]	8.3	
9,10	8.2	7.7	(7.3)[c]	8.2	8.5
10,11	7.4	7.2	7.2	7.6	7.7
11,12	7.2	7.0	6.9	7.1	7.3

[a] All values in kcal/mol for 300°K, standard state 1 atm. Evaluated from ion intensity distributions (see for example Figure 4.3). $p(H_2O) = 2 \times 10^{-6}$ atm. $-\Delta H_{n-1,n}$ estimates can be obtained by adding 6.9 kcal/mol to corresponding to values of $-\Delta G^{o}_{n-1,n}$. For example, $-\Delta H^{o}_{7,8}(Mg^{2+}) = 15.3$ kcal/mol. This is evaluated using $\Delta G^o = \Delta H^o - T\Delta S^o$ and assuming $\Delta S^{o}_{n-1,n} = 23$ cal/degree·mol (*2,4,5,22*).

[b] More accurate results in brackets from previous work (*4b*), where ion sampling was performed at low pressure.

[c] The identity of the $M^{2+}(H_2O)_n$ was checked by means of CID, i.e. only loss of H_2O should be observed. The m/z = 125, which corresponds to $Sr^{2+}(H_2O)_9$, contained also an extraneous ion which is probably $H^+(H_2O)_2(CH_3OH)_1(N_2)_2$ indicated by observed losses of m/z = 28 and 32. The intensity of the $Sr^{2+}(H_2O)_9$ ion is therefore lower than that reported in Figure 4.3 and the ΔG^o data for [8,9] and [9,10] are less reliable.

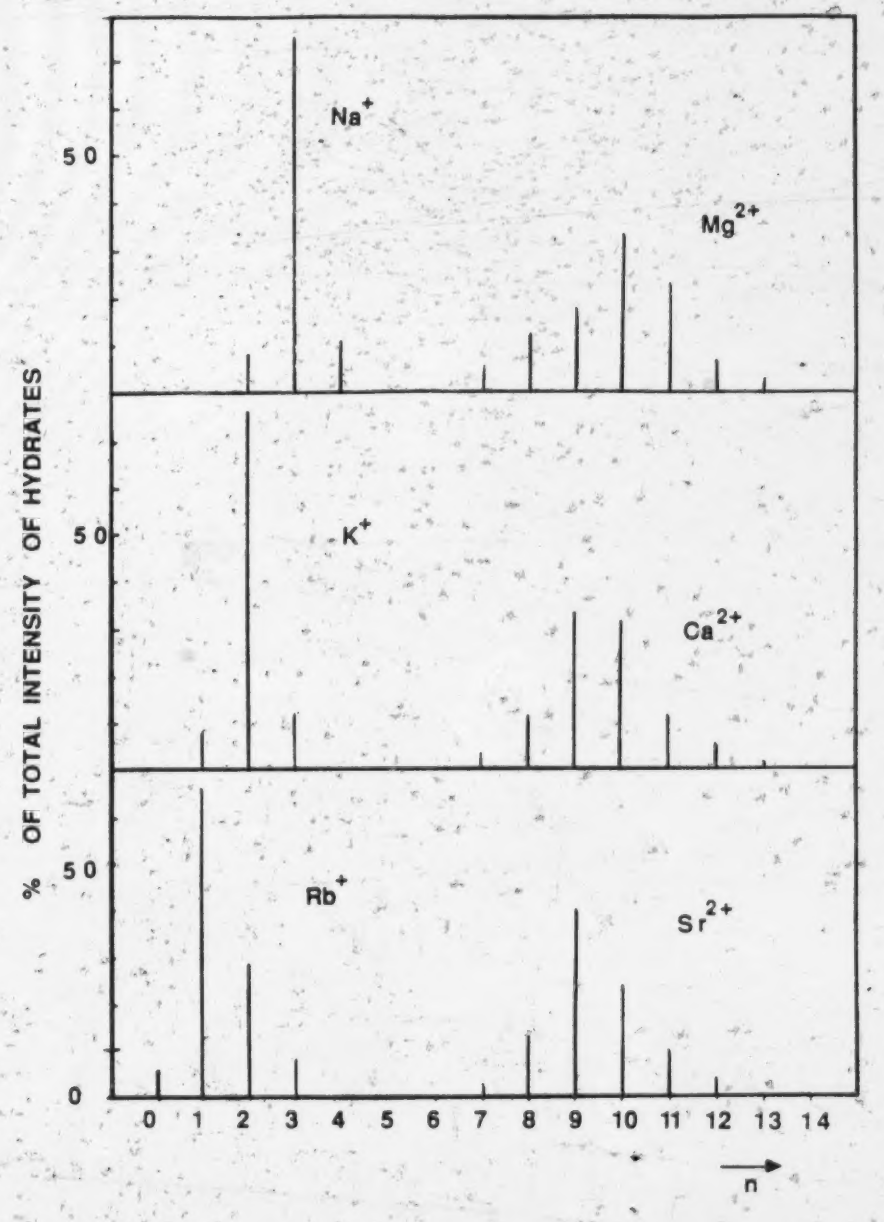

Figure 4.3. Relative intensities of alkali cation hydrates $M^+(H_2O)_n$ and isoelectronic alkaline earth hydrates $M^{2+}(H_2O)_n$, observed with the quadrupole mass spectrometer. Hydrates are in thermodynamic equilibrium in the interface chamber at 300K and water pressure 2×10^{-6} atm.

(*28*). This type of error was also encountered at times in the previous low pressure work before measurements of the time resolved equilibria were initiated (*29*). Good data could still be obtained without time resolution by using only the high intensity ions and changing reaction conditions, i.e., ligand pressure and reaction temperature, to shift the equilibria towards conditions where clusters with a given desired value of n dominate. This is also possible with the present system. The interface chamber is provided with heaters and the temperature can be changed. The ligand pressure can also be changed although over much narrower limits than in the previous work (*2,5*).

Conditions were also created for observation of hydration equilibria of doubly charged metal ions, eq 4.2. Shown in Figure 4.3 are equilibrium distribution for the M^{2+} hydrates of the alkaline earths Mg^{2+}, Ca^{2+}, and Sr^{2+}. The $\Delta G^{\circ}_{n-1,n}$ values obtained from these distributions are given in Table 4.1. As expected the observed $M^{2+}(H_2O)_n$ species are shifted to much higher n values compared to the isoelectronic $M^{+}(H_2O)_n$, see Figure 4.3. Thus, the distribution for Ca^{2+} peaks at $n \approx 10$ while that for K^{+} has a maximum at $n = 2$. The distributions for the M^{2+} ions are much broader than those for the isoelectronic M^{+}. Undoubtedly, this is due to the larger number of water molecules present in the $M^{2+}(H_2O)_n$ case. Distributions for $M^{+}(H_2O)_n$, where n is high due to higher H_2O pressure or low temperature, are also broad (*4b*).

The $M^{+}(H_2O)_n$ distribution shifts significantly to lower n as M^{+} is changed from Li^{+} to Rb^{+}, i.e., with increasing ion size. A shift towards lower n is observed also for the isoelectronic M^{2+}, however that shift is very much smaller. Again, this is not to be attributed to smaller effects of radius for the isoelectronic M^{2+} but to the high average value of n for the $M^{2+}(H_2O)_n$ involved. The effect of ion radius is small also for $M^{+}(H_2O)_n$ at high n, see Figure 6 in Dzidic (*4b*).

The equilibrium intensities of the transition metal hydrates $Mn^{2+}(H_2O)_n$ and $Co^{2+}(H_2O)_n$ were measured with the same technique and the resulting $\Delta G^{\circ}_{n-1,n}$ values are given in Table 4.1. The values are similar to those for the alkaline earth M^{2+}. Undoubtedly, this

similarity is due to the high hydration number of the ions. However, some chemical features can be found. The hydration exothermicities of Ca^{2+}, Mn^{2+} and Co^{2+} are seen to increase somewhat in this order, Table 4.1. This change is expected, since the ion crystal radii are known to decrease in the same order.

While the thermodynamic data for $M^{2+}(H_2O)_n$ at high n are of some interest, clearly much more interesting from a chemical standpoint are the inner shell interactions from n = 0 to n = 6 for H_2O as well as for a host of other ligands. These will depend strongly on specific electronic differences between the individual M^{2+}. Since the binding energies to M^{2+} ions for inner shell ligands like H_2O are expected to be in the 40-80 kcal/mol range, it is clear that inner shell equilibria measurements will require very high temperatures and a radical redesign of the apparatus. An alternative is to use collision induced dissociation in the triple quadupole, and such experiments are described in the following section.

Information on relative ligand binding energies in the inner shell can be obtained from the determination of ligand exchange reactions and equilibria:

$$M^{2+}(L)_n + bB = M^{2+}(B)_b + nL \qquad (4.5)$$

which can be set up in the interface chamber. Quantitative studies are to be contucted in the future; here a few qualitative observations are noted. It was found for ions such as Co^{2+} and Ni^{2+} that the ligands dimethyl sulfoxide (DMSO), dimethylformamide (DMF), pyridine, and polydentate oxy and amino coordinating compounds, always displace water molecules from the inner shell. The much stronger binding for these ligands indicated by the above results follows binding orders observed in aqueous solution (*30*).

(c) Collision Induced Dissociation (CID) Mass Spectra of $M^{2+}(L)_n$ and $M^{3+}(L)_n$ Complexes. Ligand Loss versus Charge Reduction.

I. $M^{2+}(L)_n$ Complexes.

As described in preceding sections, a variety of M^{2+} ion-ligand complexes can be produced by proper choice of concentrations in the electrosprayed solution and pressure of ligand vapor in the electrospray and interface chambers. Endothermic reactions of these complexes, mass selected with the first quadrupole Q1, can be induced by collisions in Q2 with collision gas Ar, and the ionic products analysed by scanning Q3, a technique described in detail elsewhere (*25*). Apart from the expected simple ligand loss reaction, eq 4.6, upon

$$M^{2+}(L)_n = M^{2+}(L)_k + (n-k)L \qquad (4.6)$$

CID of the metal ion-ligand compexes, the present studies indicated a number of alternative reaction channels which become competitive with the simple ligand loss under certain conditions. The CID mass spectrum of $Mn^{2+}(H_2O)_6$ is shown in Figure 4.4A. Observed ion products are the lower hydrates down to $Mn^{2+}(H_2O)_3$, which means simple dissociations occur from n = 6 to 4. Shown in Figure 4.4B is the CID spectrum of $Mn^{2+}(H_2O)_4$ These results show that the dissociation from the vibrationally excited (by collisions) n = 3 ion may involve simple H_2O loss in competition with the more abundant charge reduction reaction, eq 4.7, leading to $Mn^{+}OH(H_2O)$. Results for Ca^{2+} are shown in Figure 4.5. These data

$$M^{2+}(H_2O)_n = M^{+}OH(H_2O)_{n-2} + H_3O^{+} \qquad (4.7)$$

demonstrate that the H_3O^{+} forming reduction reaction 4.7 sets in at n = 2, i.e., lower than for Mn^{2+}. It was found that $Ba^{2+}(H_2O)_n$ could be cleanly dissociated by H_2O loss down to the naked Ba^{2+}. On the other hand, for $Ni^{2+}(H_2O)_n$ branching into charge reduction, eq 4.7, occurred already at n = 4, see Figure 4.6. Evidently, the $Ni^{2+}(H_2O)_4$ undergoes both charge reduction leading to $Ni^{+}OH(H_2O)_2 + H_3O^{+}$ and simple ligand loss to $Ni^{2+}(H_2O)_3$.

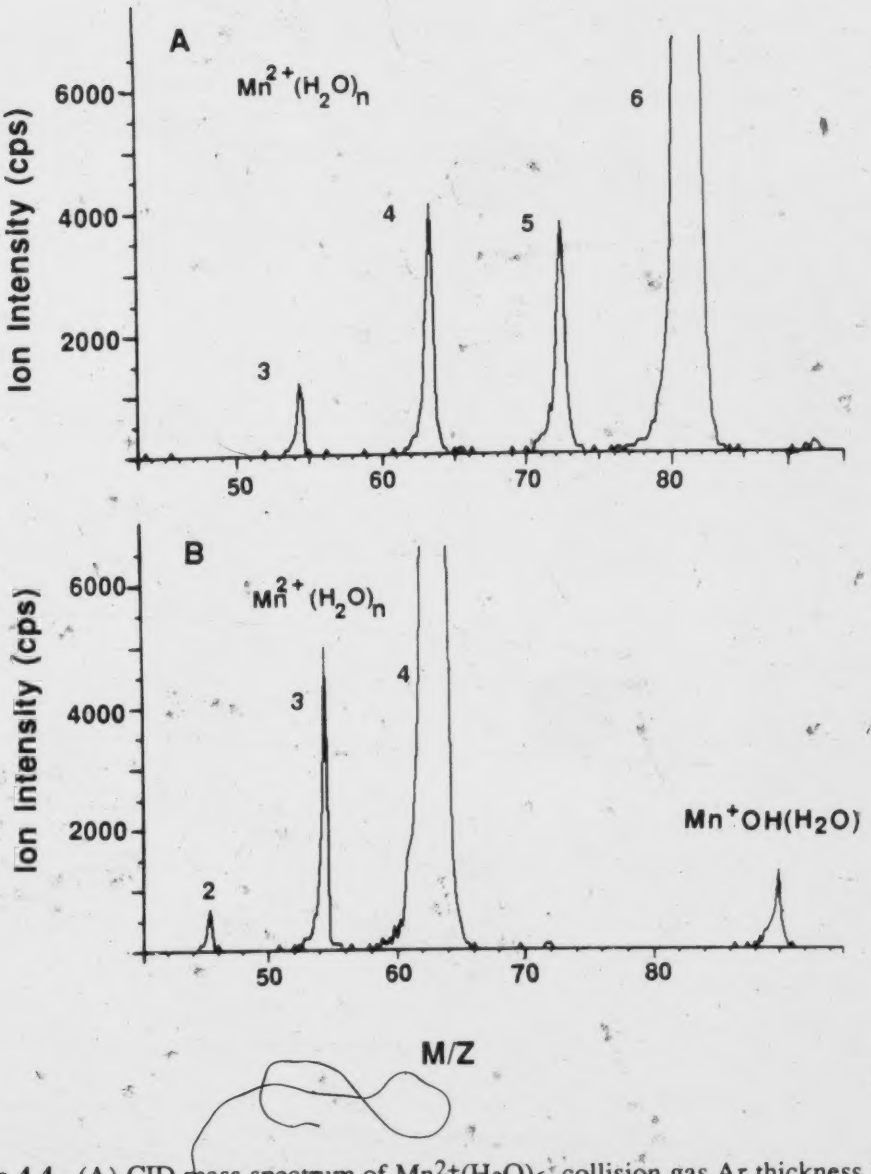

Figure 4.4. (A) CID mass spectrum of $Mn^{2+}(H_2O)_6$, collision gas Ar thickness in Q2: 4 x 10^{13} molecules/cm^2. Nominal centre-of-mass energy 7.9 eV (182 kcal/mol). Intensity of $Mn^{2+}(H_2O)_6$, 5.3 x 10^4 cps. Simple loss of H_2O down to $Mn^{2+}(H_2O)_3$ is observed. (B) CID of $Mn^{2+}(H_2O)_4$. Results indicate competitive reactions: charge reduction $Mn^{2+}(H_2O)_3$ = $Mn^{+}OH(H_2O)$ + H_3O^{+}, and simple ligand loss $Mn^{2+}(H_2O)_3$ = $Mn^{2+}(H_2O)_2$ + H_2O. Production of H_3O^{+} was observed also, but ion not shown.

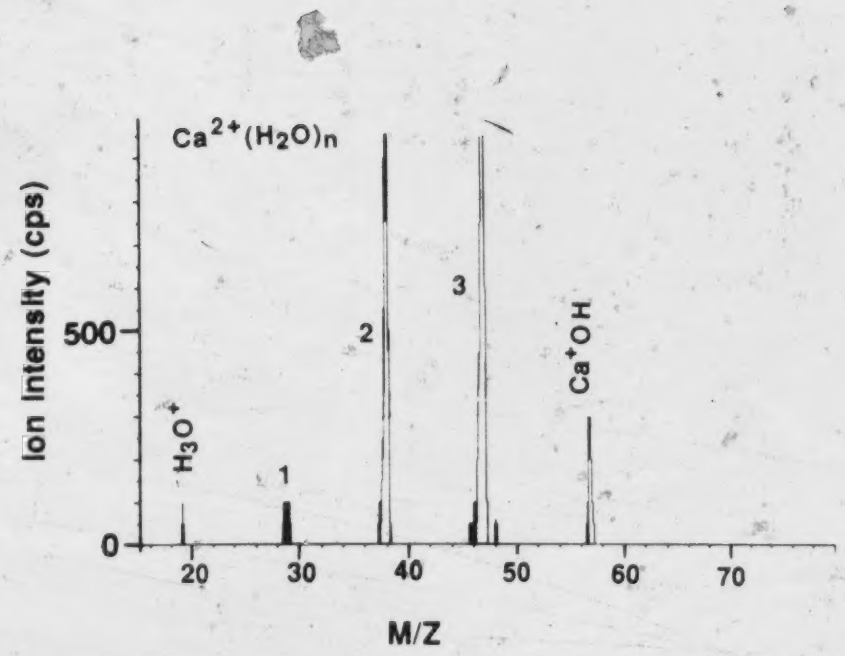

Figure 4.5. CID mass spectrum of $Ca^{2+}(H_2O)_3$. Competitive reactions $Ca^{2+}(H_2O)_2 = CaOH^+ + (H_3O)^+$, and $Ca^{2+}(H_2O)_2 = Ca^{2+}(H_2O)_1 + H_2O$ occur at n = 2, i.e., lower than n = 3 for Mn^{2+} hydrates.

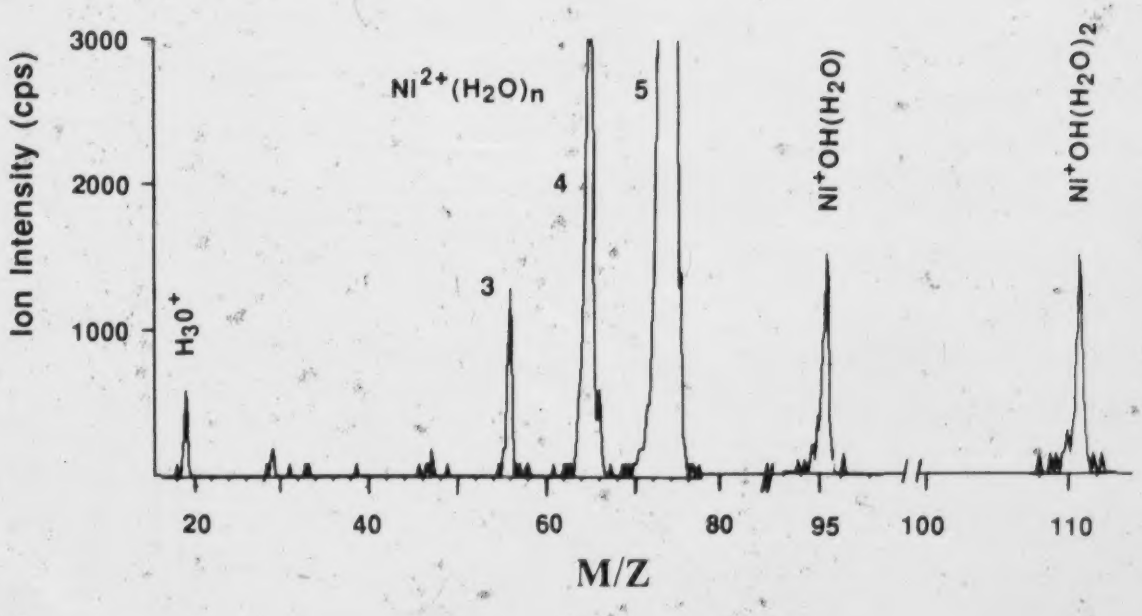

Figure 4.6. CID mass spectrum of $Ni^{2+}(H_2O)_5$. The singly charged ions $Ni^+OH(H_2O)_2$ and $(H_3O)^+$ are due to charge reduction of $Ni^{2+}(H_2O)_4$, i.e., charge reduction occurs at n = 4.

The present findings imply that simple ligand loss occurs at high n. However at some low value of n the charge reduction reaction, eq 4.7, becomes competitive with simple ligand loss, eq 4.6. The tendency for such a process to occur may be expected to increase as the ionization energy difference [I.E.(M^+) - I.E.(L)] increases.

The hydrate number n at which charge reduction, eq 4.7, becomes competitive with H_2O loss, is given in Table 4.2 for the alkaline earths and the first row transition metals that were examined.. Also included in the table with the notation n > 15 are Cu^{2+} and Be^{2+}. These entries are based on the observation that only singly charged $M^+OH(H_2O)_n$ ions were obtained for these ions, when solutions of the M^{2+} salts were electrosprayed. Thus, the charge reduction for these species is very facile and occurs either during the escape from the charged droplets or in the gas phase of the electrospray or interface chamber. The ionization energies I.E.(M^+) are also given in Table 4.2. For the alkaline earths a clear trend of n with I.E.(M^+) is observed, Charge reduction occurs at lower n as I.E.(M^+) decreases. Thus for Ba^{2+} simple H_2O loss occurs down to the bare Ba^{2+} ion. For the first row transition metals, there is also a close correlation of n with I.E.(M^+). Only Fe^{2+} is somewhat out of line.

The energy $\Delta H^{\dagger}_7$ required for the charge reduction reaction, eq 4.7, can be deduced from the thermochemical cycle shown in eq 4.8. $\Delta H_{n,0}(M^{2+})$ is the energy for

$$\Delta H^{\dagger}_7 = \Delta H_{n,0}(M^{2+}) - I.E(M^+) - D(M^+OH) - \Delta H_{n-2,0}(M^+OH) + \Delta H_9 + E_{cou} \qquad (4.8)$$

dissociation of $n(H_2O)$ from $M^{2+}(H_2O)_n$, D stands for bond dissociation energy, $\Delta H_{n-2}(M^+OH)$ is the dissociation energy for $(n-2)H_2O$ molecules from $M^+OH(H_2O)_{n-2}$, ΔH_9 is defined in eq 4.9, and E_{cou} is the coulomb energy corresponding to the energy released as kinetic energy of H_3O^+ and $MOH^+(H_2O)_{n2}$ due to the coulombic repulsion.

$$H_2O + H_2O = H_3O^+ + OH + e \qquad \Delta H_9 = 264.5 \text{ kcal/mol } (31), \qquad (4.9)$$

At the value of n which charge reduction competes with simple ligand loss reaction, eq 4.10,

Table 4.2 Ligand Number at which Charge Reduction from M^{2+} to M^{+} occurs in Preference to Neutral Ligand Expulsion.

Ion	L	I.E.(L)[a]	n[b]	I.E.(M^{+})(eV)
Be^{2+}	H_2O	12.6	> 15[c]	18.2
Mg^{2+}	H_2O	12.6	3	15.0
Ca^{2+}	H_2O	12.6	2	11.9
Sr^{2+}	H_2O	12.6	2	11.0
Ba^{2+}	H_2O	12.6	0	10.0
Mn^{2+}	H_2O	12.6	3	15.6
Fe^{2+}	H_2O	12.6	~4.5[e]	16.2
Co^{2+}	H_2O	12.6	4	17.1
Ni^{2+}	H_2O	12.6	4	18.2
Cu^{2+}	H_2O	12.6	> 15[c]	20.3
Zn^{2+}	H_2O	12.6	~5	18.0
Mn^{2+}	DMF	9.1	< 1[d]	15.6
Cu^{2+}	DMF	9.1	3	20.3
Cu^{2+}	DMSO	9.0	3	20.3
Mg^{2+},Mn^{2+}, Co^{2+},Cu^{2+}	NH_3	10.2	> 15[c]	

a Ionization energy of ligand in eV (*31*).

b $M^{2+}(L)_n$ is the complex for which both simple loss of ligand and charge reduction, see equations 4.6 and 4.7, occur competitively on CID.

c Based on observations that doubly charged ions M^{2+} could not be produced by electrospray when this ligand was present in solution or in the vapors of electrospray or interface chamber.

d Lowest ion observed on CID of $Mn^{2+}(DMF)_n$ was $M_n^{2+}(DMF)$.

e The choice of n = 4.5 was made on the basis that some $Fe^{+}OH(H_2O)_3$ was observed which gives n = 5, while relatively high intensities of $Fe^{2+}(H_2O)_4$ and $Fe^{+}OH(H_2O)_2$ were also observed which implied n = 4.

$$M^{2+}(H_2O)_n = M^{2+}(H_2O)_{n-1} + H_2O \qquad (4.10)$$

in the CID experiment one can make the approximation,

$$\Delta H^{\dagger}_{10} \text{ (or } \Delta H_{n,n-1}) = \Delta H^{\dagger}_{7} \qquad (4.11)$$

Since $\Delta H_{n,0} = \Delta H_{n,n-1} + \Delta H_{n-1,0}$, then $\Delta H^{\dagger}_{10}$ can be written as $\Delta H_{n,n-1} = \Delta H_{n,0} - \Delta H_{n-1,0}$. Also, it will be assumed that the activation energy for the reverse reaction of (4.10) is a negligible fraction of the thermochemical enthalpy change, so $\Delta H^{\dagger}_{10} \approx \Delta H_{10}$. Therefore by substitution of eq 4.11 into eq 4.8, and rearranging one obtains,

$$\Delta H_{n-1,0}\,(M^{2+}) = \text{I.E.}(M^{+}) + D(M^{+}OH) + \Delta H_{n-2,0}\,(M^{+}OH) - \Delta H_9 - E_{cou} \qquad (4.12)$$

For $Co^{2+}(H_2O)_4$, where the two processes compete, i.e., n = 4 , sufficient thermo-chemical data are available to obtain the crude numerical estimate:

$$\Delta H_{3,0}\,(Co^{2+}) \approx 181 \text{ kcal/mol} \qquad (4.13)$$

$$\Delta H_{3,0} / 3 \approx 60 \text{ kcal/mol}$$

for the average binding energy of the first three H_2O molecules to Co^{2+}. The estimate, eq 4.13, was obtained with: I.E.(Co^{+}) =394 kcal/mol; $D(Co^{+}OH)$ = 71 kcal/mol, Magnera *et al.* (*32*); $\Delta H_{2,0}\,(Co^{+}OH)$ = 60 kcal/mol, arbitrary estimate; ΔH_6 = 264.5 kcal/mol evaluated with data from Lias (*31*); E_{cou} = 80 kcal/mol, where the initial distance of the two positive charges was taken as 0.4 nm.

Values in the 60 kcal/mol range for inner shell H_2O molecules appear reasonable. The evaluation of eq 4.12 could be improved. Hydrate binding energies to $Co^{+}OH$ could be determined with the CID technique (*33*) while the coulombic term could be measured by applying a retarding voltage to the third quadrupole Q3.

An examination of eq 4.12 shows that I.E.(M^+) is only one of the terms that determine at what hydrate number n will charge reduction occur. Large binding energies of H_2O to M^{2+} will delay the onset of charge reduction, while large binding energies of H_2O to M^+OH will accelerate it. The endothermicity of $\Delta H_{n,0}$ (M^{2+}) - ΔH_{n-2} (M^+OH) increases with n, and therefore only doubly charged ions for which I.E.(M^+) is large, can undergo charge reduction at high n. The regular decrease of n with decrease of I.E.(M^+) for the alkaline earths, see Table 4.2, indicates that the terms I.E.(M^+) and D(M^+OH), both expected to decrease from Mg to Ba, are dominant. For the transition metal series in Table 4.2, a very close correlation of n with I.E.(M^+) need not be present, since the I.E.(M^+) differences are smaller and very regular changes of the other larger terms, like D(M^+OH) and $\Delta H_{n,0}$ (M^{2+}), need not occur.

Replacing H_2O with other ligands may increase or decrease the tendency for charge reduction. For example, NH_3 and pyridine (C_5H_5N) increase the tendency for reduction while ligands like dimethyl sulfoxide (DMSO) and dimethylformamide (DMF) decrease it, see Table 4.2.

Considering first the nitrogen ligands, it is easy to show on the basis of thermochemical arguments, analogous to those used to evaluate $\Delta H_7^{\dagger}$, that charge reduction may be favoured. The major difference occurs in the energetics of the reactions equivalent to eq 4.9.

$$NH_3 + NH_3 = NH_4^+ + NH_2 + e \qquad \Delta H = 203.9 \text{ kcal/mol} \qquad (4.14)$$

$$NH_3 + H_2O = NH_4^+ + OH + e \qquad \Delta H = 214.9 \text{ kcal/mol} \qquad (4.15)$$

$$C_5H_5N + H_2O = C_5H_5NH^+ + OH + e \qquad \Delta H = 210.0 \text{ kcal/mol} \qquad (4.16)$$

Note that these endothermicities are substantially lower than ΔH_9 = 264.5 kcal/mol. Although the reaction, eq 4.15, where OH rather than NH_2 is involved, is more endothermic, this endothermicity will be compensated by the expected greater exothermicity of the formation of M^+OH relative to M^+NH_2.

The reactions actually observed with nitrogen containing ligands were fairly complex. Thus, no doubly charged Mn^{2+} could be observed when NH_3 at ppm levels was added to the interface gas. The $Mn^{2+}(H_2O)_n$ were replaced in the presence of NH_3, with $Mn^{+}OH(NH_3)_k$ and $NH_4^{+}(NH_3)_n$ ions. On the other hand, $Ni^{2+}(NH_3)_4(H_2O)_n$ could be "prepared" by adding traces of NH_3 (actually 10^{-4}M ammonium acetate) to 10^{-4}M $Ni(NO_3)_2$ in methanol solution. From these limited experiments, it would appear that when NH_3 is present in the inner shell as tetraamino complex, charge reduction does not occur, but when it is in the outer shell, it can cause charge reduction.

For pyridine, Py, somewhat different observations were made. In one case, Ni^{2+}, doubly charged ions, i.e., $Ni^{2+}(Py)_4(H_2O)_n$, were observed. For Co^{2+} only $CoOH^{+}(Py)_3(H_2O)_n$ ions were found, yet in both cases 10^{-4}M Py was added to the methanol solution. It appears that both ammonia and pyridine can increase the tendency for charge reduction but the chemistry is richer and requires further study.

The ligands DMF and DMSO lead to a much later onset of charge reduction, see Table 4.2. Thus, replacement of H_2O with DMSO or DMF increases the stability of $M^{2+}(L)_n$. Cu^{2+} ions which could not be produced as hydrates were observed as $Cu^{2+}(L)_n$ when the above ligands were added to the solution. Charge reduction at a low n values was also observed with these ligands. This is demonstrated in Figure 4.7 for $Cu^{2+}(DMSO)_n$. While simple ligand loss occured at higher n, at n = 3 the charge reduction reaction, eq 4.17,

$$Cu^{2+}(DMSO)_3 = Cu^{+}(DMSO)_2 + DMSO^{+} \qquad (4.17)$$

becomes dominant. Notice that the reduction reaction in this case is simple charge transfer to the ligand (i.e. electron transfer from ligand to metal) rather than the intra-cluster proton transfer type, eq 4.7. The reason that the Cu hydrates could not be observed can be explained on the basis of reactions 4.18, and 4.19.

$$Cu^{2+}(H_2O)_n = Cu^{+}(H_2O)_{n-1} + H_2O^{+} \qquad (4.18)$$

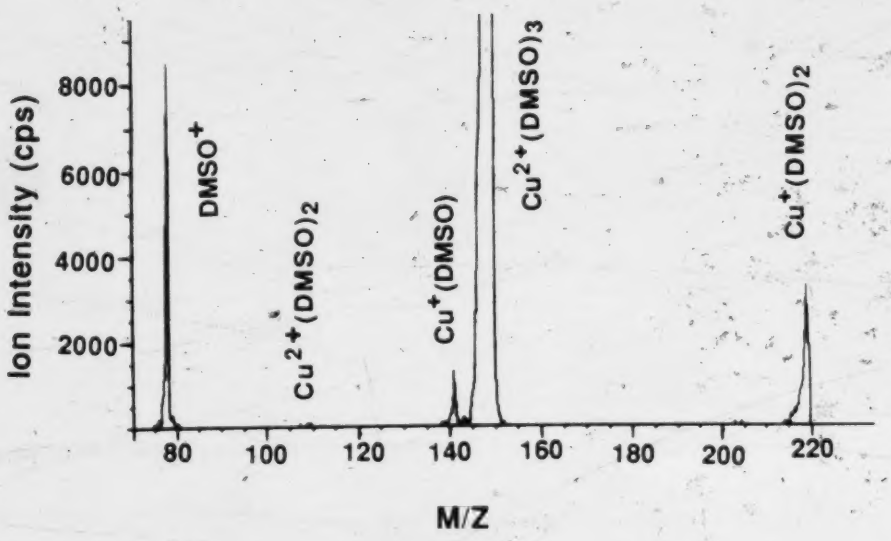

Figure 4.7. CID mass specrum of $Cu^{2+}(DMSO)_3$. Charge reduction occurs at n = 2 by charge transfer to DMSO.

$$Cu^{2+}(H_2O)_n = Cu^{+}OH(H_2O)_{n-2} + H_3O^{+} \qquad (4.19)$$

The simple charge transfer reaction, eq 4.18, requires more energy than the hydroxide reaction, forming hydronium ions, eq 4.19. This is expected because the reaction 4.20:

$$H_2O^{+} + H_2O = H_3O^{+} + OH \qquad \Delta H_{20} = -26 \text{ kcal/mol} \qquad (4.20)$$

is exothermic, and the energy released on forming $Cu^{+}OH$ is larger than the energy released on forming $Cu^{+}(H_2O)$.

For aprotic ligands like DMSO and DMF, the combination of the reaction equivalent to eq 4.20 with the reaction forming $M^{+}OH$, is expected to be less exothermic and these ligands are therefore less prone to intra cluster proton transfer charge reduction, and therefore they "protect" the double charge.

II. $M^{3+}(L)_n$ Complexes.

Ions $M^{3+}(L)_n$, where L stands for some specified ligand, were observed for M = Sc, Y, La, Ce, Nd, Sm and Co. The positions of these elements M in the periodic table, and the values of the second and third ionization potentials are given in Figure 4.8.

No triple charged hydrates $M^{3+}(H_2O)_n$ could be observed with the M^{III} salts for any of the metals listed above, under experimental conditions where M^{II} salts had led to abundant hydrates $M^{2+}(H_2O)_n$. The species observed with the M^{III} salts were the charge reduced forms $M^{2+}OH(H_2O)_n$.

The third ionization energies of all the metals used were all above 19 eV, see Figure 4.8. It was shown above that the alkaline earths and the M^{II} salts of the first row transition metals produced doubly charged hydrates, $M^{2+}(H_2O)_n$, upon electrospray, when the second ionization potential was less than ~18 eV. For Be ($I.E.^{II}$ = 18.2 eV) and Cu ($I.E.^{II}$ = 20.3 eV) only the species $M^{+}OH(H_2O)_n$ were observed. Thus, for both the M^{II} and the M^{III}

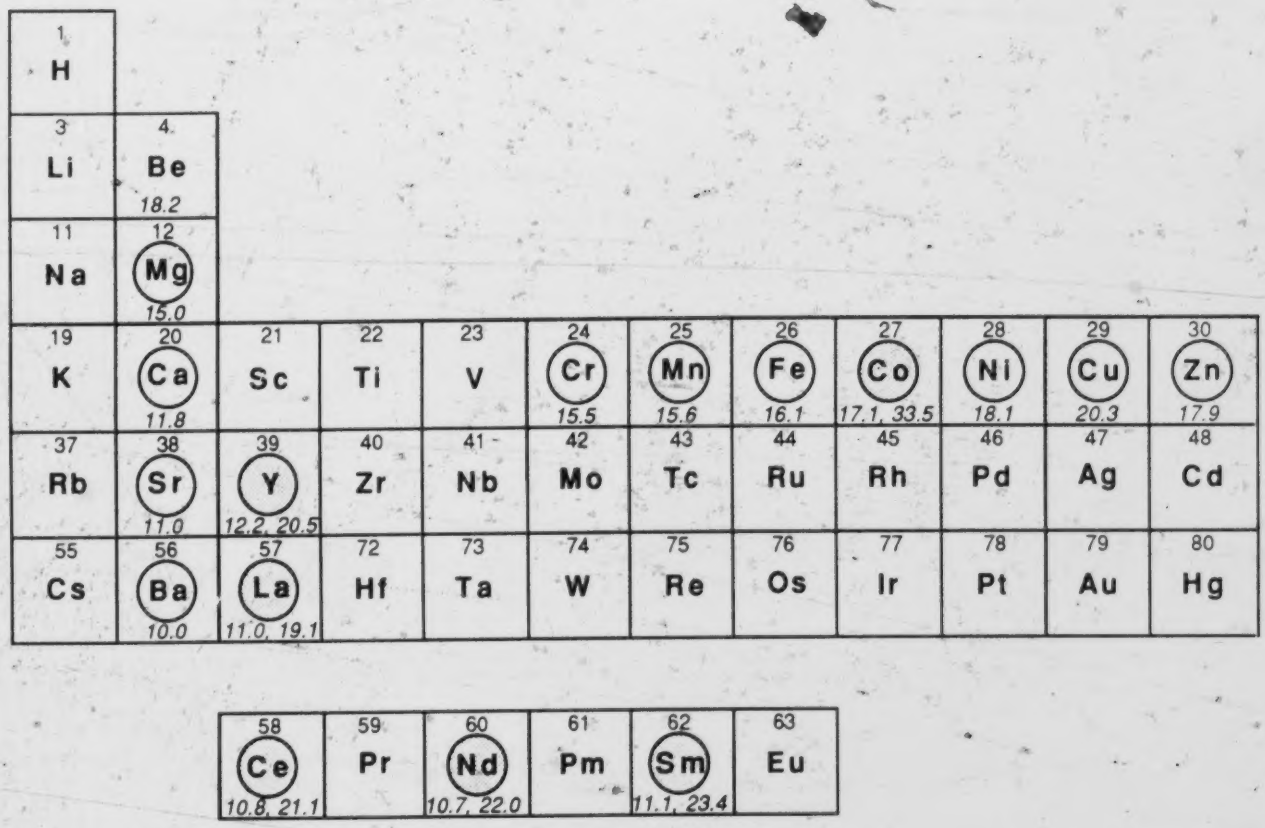

Figure 4.8. Elements whose M^{II} salts led to $M^{2+}(L)_n$ shown in small circles. Elements whose M^{III} salts led to $M^{3+}(L)_n$ shown with shadowed circles. These led also to doubly charged ions. Second Ionization Energies and third Ionization Energies given in eV.

species, the M^{2+} or M^{3+} hydrates can be observed only when the second or third I.E. is less than ~18 eV.

The CID daughter spectrum with Ar collision gas in Q2 for the $M^{2+}OH(H_2O)_6$ ion from Yttrium is shown in Figure 4.9. Successive losses of H_2O leading to n = 2 are the only reactions observed. Similar results were obtained also for the other M^{III}.

Triple charged ions, $M^{3+}(DMSO)_n$ and $M^{3+}(DMF)_n$, were obtained with solutions to which 10^{-3} M DMSO or DMF was added. The actual populations under mild conditions (low voltage difference (~5 to 10 V) between the OR and CB electrodes) were difficult to find, presumably because the ions were clusters containing not only DMSO (or DMF) but also a large number of water and some methanol molecules, and were therefore spread over many m/z values. The detected $M^{3+}(L)_n$ were obtained with CID ≈ 20 to 25 V, between OR and CB electrodes in the acceleration region ahead of Q1. This led to $M^{3+}(DMSO)_n$ with n from 4-8 for M = Y, La, Ce, Nd, Sm. This result establishes that, for these ions, DMSO is much more strongly held in the inner shell of the ion than water or methanol. Similar results were obtained with DMF although only Y and La were examined with this ligand.

The CID spectrum with Ar collision gas in Q2 for $La^{3+}(DMSO)_6$ is shown in Figure 4.10. Successive losses of DMSO are observed down to n = 3. Similar CID results were obtained for the other $M^{3+}(DMSO)_n$ ions.

In addition to $M^{3+}(DMSO)_n$, abundant doubly charged ions of the general type $M^{2+}X(DMSO)_n$ were also present. X^- was most often the counter ion of the salt used, i.e., Cl^- for chlorides, NO_3^- for nitrates or some accidental anionic impurity. Thus an X of mass 59 was traced to be due to the acetato complex formed due to the presence of $CH_3CO_2^-$ impurity at the ~10^{-6} M level. Deliberate addition of sodium acetate at a 10^{-5} M level led to an increase of the intensities of those ions containing the acetate ligand factors of 3-4. The $CH_3CO_2^-$ species is well known to lead to acetato complexes in aqueous solution.

$M^{2+}X(DMSO)_n$ ions, where X^- was OH^- or CH_3O^-, were also often found to be present. The CID spectrum of $La^{3+}(DMSO)$ in Figure 4.10 accidentally provides an example for the

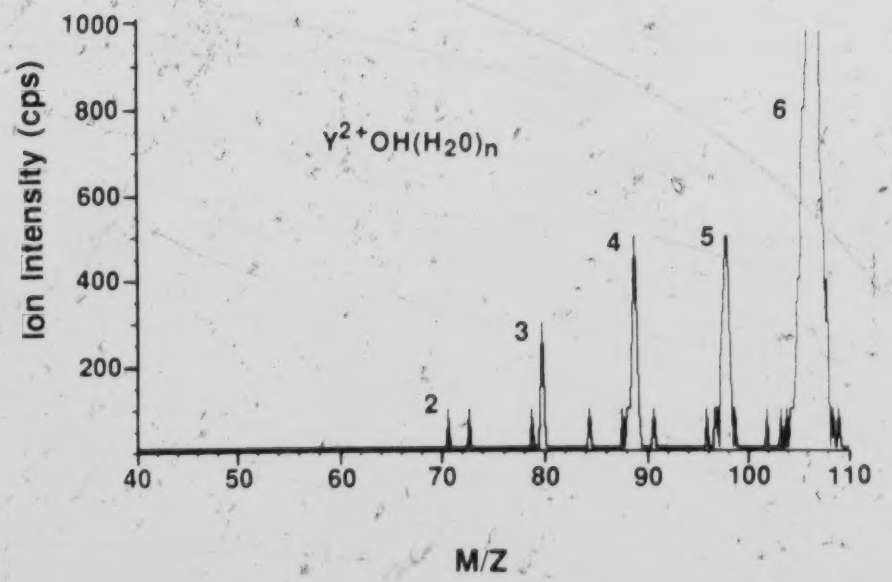

Figure 4.9. CID mass spectrum of $Y^{2+}OH(H_2O)_6$ showing successive losses of H_2O down to n = 2. Collision gas Ar.

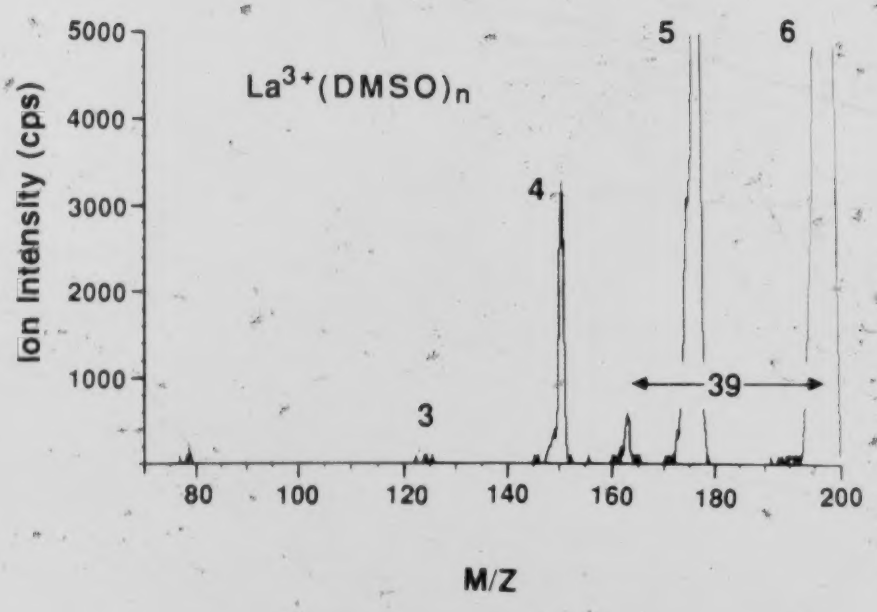

Figure 4.10. CID mass spectrum of $La^{3+}(DMSO)_6$ showing successive DMSO (MW = 78) losses at m/z = 26 intervals down to $La^{3+}(DMSO)_3$. The small peak m/z = 39 units down from the parent ion is due to loss of DMSO from extraneous doubly charged parent ion $La^{2+}OCH_3(DMSO)_3$ of same m/z = 202 as $La^{3+}(DMSO)_6$.

presence of CH_3O^-, due to a parent ion of the series $La^{2+}OCH_3(DMSO)_n$. The spacings between the main daughter ions in Figure 4.10 are m/z = 26, which corresponds to loss of DMSO (MW = 78) from a triply charged ion, i.e., from $La^{3+}(DMSO)_6$. A much smaller daughter peak occuring m/z = 39 units below the parent corresponds to loss of DMSO from a doubly charged ion. The m/z value of this doubly charged ion, m/z = 202, is the same as that of $La^{3+}(DMSO)_6$, and the doubly charged ion fits the assignment: $La^{2+}OCH_3(DMSO)_3$. Ions of the series $La^{2+}OCH_3(DMSO)_n$ where no m/z coincidences occur, were also identified. The results in Figure 4.10 do however indicate the value of the triple quadrupole CID for the identification of the ion clusters.

Suitable multidentate ligands may be expected to protect the core ion even more from intracluster charge reduction reactions. For example, the triply charged Co^{3+}(Sepulchrate) ion, see Structure I, was observed in the gas phase (*23,24*), even though the third ionization energy of Co, I.E.^{III}Co = 33.5 eV is some 10 eV higher than the third ionization energies of the other species of the present work. The Co^{3+}(sepulchrate) species, observed under mild conditions, carried a distribution of water molecules with n = 5 to 10 peaking at n = 7. This additional hydration, even though there is already a stabilization by six nitrogen ligands, illustrates the power of the triple charge. Also observed, under mild conditions and in greater abundance, were the charge reduced ions $Co^{2+}(Sep\text{-}H)(H_2O)_n$. This structure, rather than $Co^{2+}OHSep(H_2O)_{n-1}$, is chosen to represent the ion since CID of the ion hydrates led to $Co^{2+}(Sep\text{-}H)$. This result is also expected on general grounds, since H_2O and thus OH has no access to the central ion which is "protected" by the sepulchrate. Evidently, the presence of the triple charge makes the hydrogens in the two outer NH groups very acidic and, in the presence of H_2O in the outer region, charge reduction occurs by proton transfer to H_2O.

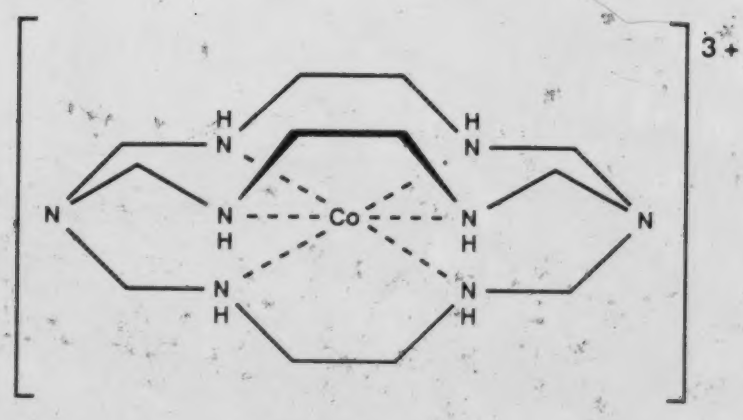

STRUCTURE I

CONCLUSIONS

Hydrates and many other metal ion-ligand complexes of doubly and triply charged metal ions, $M^{2+}(L)_n$ and $M^{3+}(L)_n$, can be produced by electrospray ionization and detected by mass spectrometry. L may be added to the electrosprayed solution or to the gas phase, i.e. electrospray chamber.

When the second ionization energy of the M^{II} is higher than ~18 eV, and the third ionization energy higher than ~23 eV for the M^{III}, the charge reduced species are generated instead. Changing the nature of the ligand may increase the stability of the M^{2+} and/or M^{3+} towards charge reduction and vice versa. For example, NH_3 and pyridine accelerate charge reduction relative to H_2O while DMSO, and DMF delay it. Multidentate polycyclic ligands with suitable cavities to accommodate the triply charged ion lead to triply charged species even when the third ionization energy is as high as 34 eV. Proper selection of ligands and experimental conditions can provide good sensitivity and specificity for metal detection. Although the results so far are mostly qualitative, they are of considerable interest. The preference of different ligands for different metals, and the variety of clusters formed, adds an additional dimension to the specificity of the technique, especially when tandem mass spectrometry is utilized for detection. Systematic studies are now underway in Dr. Kebarle's laboratory exploring the analytical potential of this technique for detection of metal ions.

The results described here also illustrate the extensive studies of the gas phase ion chemistry of M^{2+} ions that are possible with $M^{2+}(L)_n$ produced by electrospray and mass spectrometric apparatus of the type used. Extensions of the apparatus, such as photodissociation of the ion clusters in the triple quadrupole with a dye laser, as used by Michl *et al.* (*32*) for singly charged ions, should be feasible since most of the transition metal M^{2+} complexes are colored. Construction of an ion beam source consisting of a size-reduced electrospray and interface chamber, for crossed beam studies, should also be feasible. Mass analyzed ion beams of 10^5 ions/s should easily be obtainable with such a beam source.

REFERENCES

1. Bowers, M. T., Ed. *Gas Phase Ion Chemistry*. Academic Press: New York, 1979; v. 1-3.
2. Keesee, R.G.; Castleman A.W. *J. Phys. Chem. Ref. Data* **1988**, *15*, 1011.
3. Maier, J. P. Ed. *Ion and Cluster Ion Spectroscopy and Structure*. Elsevier, 1989.
4. (a) Hogg, A. M.; Kebarle, P. *J. Chem. Phys.* **1965**, *43*, 449. (b) Dzidic, I.; Kebarle, P. *J. Phys. Chem.* **1970**, *74*, 1466.
5. Kebarle, P. *Ann. Rev. Phys. Chem.* **1977**, *28*, 445.
6. (a) Kraemer, W. P.; Diercksen, G. H. F. *Chem. Phys. Lett.* **1970**, *5*, 463. (b) Diercksen, G. H. F.; Kraemer, W. P. Theoret. *Chim. Acta (Berl.)* **1972**, 387. (c) Kishenmacher, H.; Popkie, H.; Clementi, E. *J. Chem. Phys.* **1973**, *59*, 5842.
7. Chandrasekhar, J.; Spellmeyer, D. C.; Jorgensen, W. L. *J. Am. Chem. Soc.* **1984**, *106*, 903.
8. Barber, M.; Bordoli, R. S.; Sedgewick, R. D.; Tyler, A. N. *J. Chem. Soc. Chem. Commun.* **1981**, *198*, 325.
9. (a) Spears, K. G.; Fehsenfeld, F. C. *J. Chem. Phys.* **1972**, *56*, 5698. Spears, K. G.; Fehsenfeld, F. C.; McFarland, M.; Ferguson, E. E. *J. Chem. Phys.* **1972**, *56*, 2562. (b) Tonkyn, R.; Weisshaar, J. C. *J. Am. Chem. Soc.* **1988**, *108*, 7128. (c) Buchner, S. W.; Freiser, B.S. *J. Am. Chem. Soc.* **1987**, *109*, 1247. Huang, Y.; Freiser, B.S. *J. Am. Chem. Soc.* **1988**, *110*, 4434.
10. (a) Sunner, J. A.; Morales, A.; Kebarle, P. *Int. J. Mass Spectrom. Ion Proc.* **1988**, *86*, 169. (b) Sunner, J. A.; Kulatunga, R.; Kebarle, P. *Anal. Chem.* **1988**, *58*, 2009.
11. Pelzer, G.; De Pauer, E.; Viet Dung, D.; Marien, J. *J. Phys. Chem.* **1984**, *88*, 5065.
12. Vestal, M. *Anal. Chem.* **1984**, *56*, 2590.

13. Schmelzeisen-Redeker, G.; Bütfering, L.; Röllgen, F. W. *Int. J. of Mass Spectrom. Ion Proc.* **1989**, *90*, 139.

14. (a) Alexander, A.J.; Kebarle, P. *Anal. Chem.* **1986**, *58*, 471. (b) Alexander, A.J.; Kebarle, P. (unpublished work).

15. (a) Chan, K. W. S.; Cook, K. D. *J. Am. Chem. Soc.* **1982**, *104*, 5031. (b) Callahan, J. H.; Hool, K.; Raynolds, J. D.; Cook, K. D. *Anal. Chem.* **1988**, *60*, 714.

16. (a) Yamashita, M.; Fenn, J. B. *J. Phys. Chem.* **1984**, *88*, 4451. (b) *Ibid.* **1984**, *88*, 4671. (c) Whitehouse, C. M.; Dreyer, R. N.; Yamashita, M.; Fenn, J. B. *Anal. Chem.* **1985**, *57*, 675. (d) Wong, S. F.; Meng, C. K.; Fenn, J. B. *J. Phys. Chem.* **1988**, *92*, 546.

17. Ikonomou, M. G.; Blades, A. T.; Kebarle, P. *Anal. Chem.* **1990**, *62*, 957.

18. Mann, M.; Meng, C. K.; Fenn, J. B. *Anal. Chem.* **1989**, *61*, 1702.

19. (a) Smith, R. D.;Loo, J. A.; Edmonts, C. G.; Barinaga, C. J.; Udseth, H. R. *Anal. Chem.* **1990**, *62*, 882. (b) Loo, J. A.; Edmonts, C. G.; Udseth, H. R.; Smith, R. D. *Anal. Chem.* **1990**, *62*, 693.

20. Covey, T. R.; Bonner, R. F.; Shushan, B. I.; Henion, J. D. *Rapid Commun. in Mass Spectrom.* **1988**, *2*, 249.

21. Jayaweera, P.; Blades, A. T.; Ikonomou, M. G.; Kebarle, P. *J. Am. Chem. Soc.* **1990**, *112*, 2452.

22. Blades, A. T.; Jayaweera, P.; Ikonomou, M. G.; Kebarle, P. *J. Chem. Phys.* **1990**, *92*, 5900.

23. Blades, A. T.; Jayaweera, P.; Ikonomou, M. G.;Kebarle, P. *Int. J. Mass Spectrom. Ion Proc.* (in press).

24. Blades, A. T.; Jayaweera, P.; Ikonomou, M. G.;Kebarle, P. *Int. J. Mass Spectrom. Ion Proc.* (in press).

25. (a) Douglas, D. J. *J. Phys. Chem.* **1985**, *86*, 185. (b) Dawson, P. H.; French, J. B. ; Buckely, J. A.; Douglas, D. J.; Simmons, D. *Org. Mass Spectrom.* **1985**, *17*, 205. (c) *Ibid.* **1985**, *17*, 212. (d) Reid, N. M.; Buckley, J. A.; French, J. B.; Poon, C. C. *Adv. Mass Spectrom.* **1979**, 8B, 1843.

26. Lau, Y. K. ; Ikuta, S.; Kebarle, P. *J. Am. Chem. Soc.* **1982**, *104*, 1462.

27. Sunner, J.; Nicol, G.; Kebarle, P. *Anal. Chem.* **1988**, *60*, 1300 (see Appendix I).

28. Searcy, J. R. *J. Chem. Phys.* **1975**, *63*, 4114.

29. Kebarle, P. Pulsed Electron High Pressure Mass Spectrometer. *In Techniques for the Study of Ion Molecule Reactions;* Farrar, J. M.; Saunders, W. Jr., Eds.; John Wiley and Sons; New York, 1988.

30. Jorgensen, C. K. *Inorganic Complexes*; Academic Press: New York, 1963.

31. Lias, S. G.; Bartmess, J. E.; Liebman, J. F.; Holmes, J. L.; Levin, R. D.; Malard, W. G. *J. Phys. Chem. Refer. Data* **1988**, *17*, Supplement No. 1.

32. Magnera, T. F.; David, D.E.; Stulik, D.; Orth, R. G.; Finkman, H. T.; Michl, J. *J. Am. Chem. Soc.* **1989**, *111*, 4100; and 5036.

33. Jayaweera, P.; Blades, A. T.; Kebarle, P. (in preparation)

CHAPTER 5

Characterization of the Reaction Products of Deoxyguanosine with the Anticancer Agent BFNU and BFNU-1,1,1',1''-d4 in Different Buffers by HPLC/Atmospheric Pressure Ionization-Tandem Mass Spectrometry*

* A version of this Chapter has been published: Ikonomou, M. G.; Naghipur, A.; Lown, J. W.; Kebarle, P. *Biomed. Envir. Mass Spectrom.* **1990**, *19*, 434-446. Naghipur, A.; Ikonomou, M. G.; Kebarle, P.; Lown, J. W. *J. Am. Chem. Soc.* **1990**, *112*, 3178-3187.

INTRODUCTION

a. Action of Haloethylnitrosoureas on DNA Bases.

(2-Halbethyl)nitrosoureas (HENUs), structure I, including 1,3-bis(2-chloroethyl)-1-nitrosourea (BCNU); 1,3-bis(2-fluoroethyl)-1-nitrosourea (BFNU); 1-(2-chloroethyl)-3-cyclohexyl-1-nitrosourea (CCNU); 1-(2-chloroethyl)-3-(4-methylcyclohexyl)-1-nitrosourea (MeCCNU), and chlorozotocin have an established place in the clinical treatment of a range of human malignancies, including Hodgkin's disease, Burkitt's lymphoma and cerebral neoplasms (*1-3*). HENUs decompose spontaneously under physiological conditions to give rise to electrophiles which react with sensitive cellular macromolecules (*1,2,4*). Several lines of evidence indicate that DNA is one of the principal cell targets (*1,2*) and specific lesions have been identified (*4b,5*). These include alkylation of both base and phosphate residues of the nucleotides (*5f*), interstrand cross-linking (*5a,b*) and single strand breaks (*5f*). Studies of the biological pharmacology of the HENUs support the view that the critical and lethal lesions are associated with alkylation of the DNA bases including certain interstrand cross-links (*5a,b,g*). Determining the mechanism of reaction of HENUs with DNA bases is essential in order to understand the details of the mechanism of action of these valuable clinical agents.

STRUCTURE I

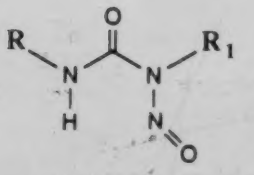

$R=R_1 = CH_2CH_2Cl$	[BCNU]
$R=R_1 = CH_2CH_2F$	[BFNU]
$R= C_6H_{11}$, $R_1=CH_2CH_2Cl$	[CCNU]
$R= 4CH_3C_6H_{10}$, $R_1= CH_2CH_2Cl$	[MeCCNU]
R= glucosamino, $R_1= CH_2CH_2Cl$	[chlorozotocin]

In this Chapter Liquid Chromatography-Tandem Mass Spectrometric (HPLC/MS/MS) procedures and methods used to characterize the products of the reaction of BFNU (Structure I) and BFNU-1,1,1',1' d_4 (**1**, structure II) with the DNA base, deoxyguanosine (**2**, structure II), under various *in vitro* experimental conditions, are described.

The HPLC/MS/MS analysis described in the present work has provided evidence which confirms a proposed mechanism for the *in vitro* alkylation of the DNA base deoxyguanosine by the anticancer agent BFNU. In brief, the proposed mechanism (*6*) suggests a transfer of the fluoroethyl group of BFNU to the N_7 position of guanosine. Furthermore, within the fluoroethyl group a shift of the F atom to the neighboring carbon is expected to occur (*6*). For the dideutero labelled fluoroethyl this F atom shift leads to an apparent shift of the deuterium atoms from position β to the fluorine, see structure II(**1**) to position α to the fluorine, see structure II(**3**). A short description of the proposed mechanism is outlined in Appendix 5-I.

The identification of the structure II(**3**) and some additional observations have ruled out a number of possible pathways (*7-9*) and have assisted in the resolution of a long standing controversy concerning the marked sequence and site selectivity of the reactions of HENU with DNA (*6*).

STRUCTURE II

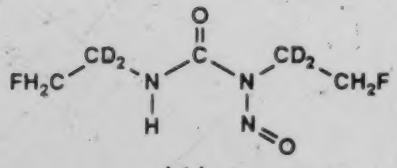

(1)

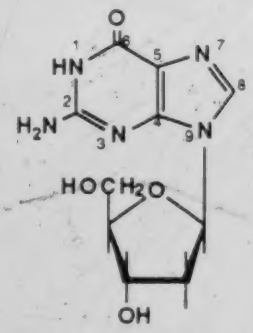

(2)

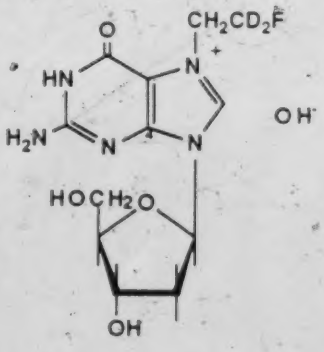

(3)

b. Description of LC/MS/MS Methodology Used to Identify the Reaction Products.

The technique of HPLC/MS has developed rapidly in recent years and at present is one of the most powerful analytical techniques in chemical analysis of mixtures (*10*). The specificity

of High Performance Liquid Chromatographic peaks containing unresolved components that nonspecific detectors cannot differentiate is increased by orders of magnitude when HPLC is coupled with mass spectrometry. An additional dimension in specificity is provided when HPLC is combined with tandem mass spectrometry (MS/MS). The sensitivity of the mass spectrometer can also be superior to other HPLC detectors. Some of the successful HPLC/MS applications to the analysis of nucleosides include the characterization of molecular products from the irradiation of a model nucleic acid (*11*), the detection of modified nucleosides in enzymatic digests of tRNA (*12*), and the analysis of a series of standard nucleoside solutions (*13*).

Nebulization of the HPLC effluent into an atmospheric pressure ionization (API) source is used in one of the commercially available HPLC/MS interfaces and its potential has been demonstrated in a number of applications (*11,14-16*). The HPLC effluent is vaporized in a heated nebulizer (*11,14,15*) by passing the liquid through a heated capillary and entraining the vapor and liquid droplets escaping the capillary tip with heated N_2 gas at atmospheric pressure. The resulting gas mixture is then exposed to API (*18*). The gasified analytes, all of which are nitrogen bases M in the present case, are ionized by protonation with reagent ions NH_4^+ produced by an electric gas discharge in the presence of NH_3 originating from the LC buffer. The protonation reaction 5.1 is of relatively low exothermicity and therefore

$$NH_4^+ + M = MH^+ + NH_3 \qquad (5.1)$$

fragmentation of MH^+ is generally not expected. In some cases however, depending on interface conditions (mostly nebulizing temperature), structurally significant fragment ions can be observed.

The API-formed ions contained in this atmospheric gas mixture are transferred to vacuum and mass analysis is obtained by simple scans of quadrupole 1 (Q_1) of the triple quadrupole mass spectrometer.

When tandem mass spectrometry (MS/MS) is employed structural information for the MH^+ ion (or other parent ions), that is usually non-existent or lost in the background of conventional mass spectra, can be obtained by collision-activated decomposition (CAD) (*19*). In this technique the ion mass-selected by the first quadrupole Q_1 and accelerated by a given potential V is exposed to collisions with a gas (commonly Ar) in a second quadrupole ,Q_2, which is operated so as to transmit all ions. The fragment ions produced by the collisional breakup of MH^+ and undecomposed MH^+ are mass analyzed in a third quadrupole, Q_3. The resulting CAD spectrum can be used for the deduction of structural features of MH^+ in a manner similar to that used for the interpretation of electron-impact and chemical ionization mass spectra (*19*).

In the present study, a triple quadrupole instrument employing the type of interface described above was used to characterize products of the reaction of deoxyguanosine with BFNU and BFNU-1,1,1',1'-d_4. The products of all reactions were hydrolyzed prior to HPLC/MS/MS analysis in order to release the modified bases from the deoxyguanosine nucleosides. General procedures for identifying the products of these reactions involved: (a) comparison of the chromatographic data with those of authentic samples, (b) detailed examination of the reconstructed ion chromatograms and API mass spectra for specific ions expected for each of the species, and (c) acquisition of CAD daughter ion mass spectra of MH^+ during elution of the component of interest.

EXPERIMENTAL SECTION

a. Reaction of Deoxyguanosine with BFNU.

Equimolar amounts of BFNU and deoxyguanosine were dissolved in dimethyl sulfoxide (0.2 mL) and tris(hydroxymethyl)aminomethane (TRIS) buffer 50 mM, pH 7.1 (0.8 mL) or sodium cacodylate buffer 50 mM, pH 7.1 (0.8 mL) was added to produce a final concentration of 0.12 M BFNU and 0.12 M deoxyguanosine. Some 5 to 10 times lower concentrations were used when BFNU-1,1,1',1'-d_4 was allowed to react with deoxyguanosine. Reactions were also performed in the presence of KBr containing 1.2 M KBr, [detailed experimental documentation is presented elsewhere (6)]. Reaction mixtures were incubated at 37°C for 24 h, and diluted with H_2O; then the DMSO was removed by lyophilization. Modified bases were released from the deoxyguanosine nucleosides by hydrolysis by 1.0 M HCl for 60 min at 100°C. Hydrolysates were neutralized with 1 M KOH to pH = 7.0 and the resulting solution was lyophilized. The residues, without further purification, were dissolved in water and 100 μL aliquots were injected for HPLC/MS and/or HPLC/MS/MS analysis. In each individual case enough water was added to the residue until a satisfactory concentration for the components of interest was obtained. It will be evident from the data presented in the results and discussion section that the components of interest present in the various reaction mixtures varied significantly in relative concentration depending on reaction conditions. This judgement was based on UV data and observed MH^+ abundances in related runs. The criteria for satisfactory aliquot concentration involved good chromatographic separation accompanied by highest possible MH^+ intensity for the mixture components of interest in a particular experiment.

b. Chromatography

The HPLC system consisted of a Waters model 510 LC pump (Waters Associates, Milford, MA) and a Rheodyne model 7125 injection valve with a 100-μL sample loop. The LC column was reversed-phase Whatman 4.6 mm x 25 cm Partisil 5 ODS-3 (Whatman,

Clifton, NJ) connected to a Waters model 441 fixed-wavelength UV detector (254 nm). HPLC chromatograms were recorded on a linear 800 series recorder (Lineman, CA). The eluent flow rate was maintained at 0.8 mL/min with a mobile phase of 10% methanol in 0.1 *M* ammonium acetate buffered to pH 4.35 with acetic acid. The exit of the UV detector was connected directly to a heated nebulizer LC/MS interface (SCIEX, Thornhill, ON).

c. Mass Spectrometry

HPLC/MS and HPLC/MS/MS analyses were performed with a SCIEX TAGA 6000E triple quadrupole mass spectrometer equipped with an atmospheric pressure ion source (API) and a heated nebulizer LC/MS interface. A schematic of the triple quadrupole instrument is shown in Figure 5.1.

In the present work a much improved design of the heated nebulizer, based on the version provided by SCIEX and described by Henion et al (*14,15*), was used. The new design (*17*) provided much more stable operation and gave good ion signal stability without loss of sensitivity which proved essential for the success of the present analysis.

Eluent, at flow rates of 0.8 mL/min, was continuously introduced into the API under either LC/MS or LC/MS/MS conditions. Typical interface operating conditions were: nebulizer heater temperature, 535 °C; nebulization pressure, 720 kPa; makeup flow rate, 4.0 L/min. In addition, air at atmospheric pressure enters the ion source at a flow rate of 12 L/min by an air pump connected to the plenum chamber (also used to remove the vaporized mobile phase). The interface dry nitrogen gas flow was kept at 200 mL/min. These conditions were also used in the flow injection experiments.

The mass spectrometer was operated in the positive-ion mode, since high sensitivity is expected for the analytes under investigation [nitrogen containing bases (*18*)] in this mode. The API reagent ions generated in the reaction zone from the HPLC effluent are NH_4^+ clusters with water, methanol, and ammonia molecules. Under LC/MS conditions, conventional positive ion mass spectra were obtained with quadrupole 1 (Q_1) in the mass

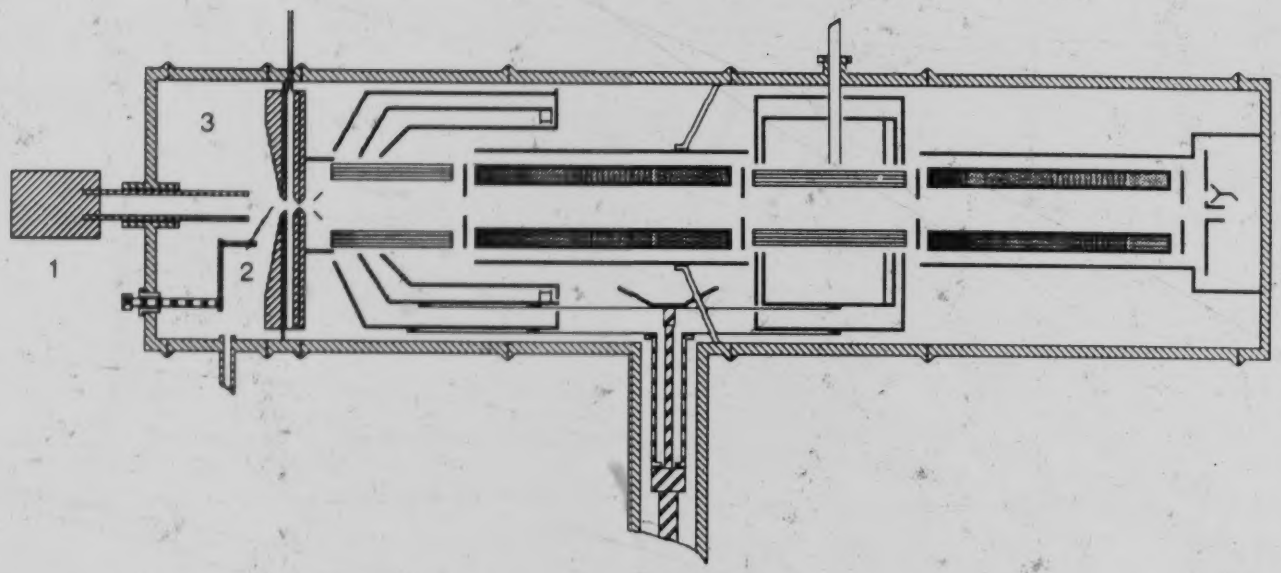

Figure 5.1. Schematic of the triple quadrupole mass spectrometer: (1) heated nebulizer; (2) ionizing needle; (3) atmospheric pressure ion source chamber. Descriptions of the remaining components are given in Figure 2.1.

filter mode with a resolution of 300 and with quadrupole 3 (Q_3) in the total ion mode. The typical scan rate was 0.2 s/decade, and the m/z 60-350 range was scanned by Q_1. Both data acquisition and analysis are under software control. Background-subtracted spectra were plotted after averaging 4-8 scans (depending on chromatographic peak width) associated with the maximum of a specific peak in the reconstructed ion chromatogram, and subtracting an average background spectrum (see for example reconstructed ion chromatograms in Results and Discussion). The background spectrum was obtained by averaging a combination of 6-12 scans taken just before and after elution of the HPLC peak of interest. The reconstructed ion chromatograms presented in the following section do not incorporate correction or smoothing of the raw data. LC/MS/MS experiments were undertaken by operating the mass spectrometer in the CAD daughter ion mode, using argon as the collision gas in Q_2 (effective target thickness was about 3×10^{14} atoms cm^{-2}, and the laboratory-frame collision energy was 48 eV). Unit resolution (full width at half maximum = 0.6 daltons) was maintained across the mass range scanned by Q_3 in all LC/MS/MS experiments. The interface conditions were identical with those of the LC/API-MS experiments. CAD spectra were obtained by averaging 5-10 scans taken during elution of the component of interest. A minimum of $\approx 5 \times 10^4$ cps parent ion (MH^+) intensity was required for obtaining reproducible relative intensities of the major daughter ions.

Both the interface and the mass spectrometer were checked daily by running a buffered 10^{-5} *M* adenosine solution through the system while keeping all interface and MS parameters constant. This precaution was necessary to ensure that optimum conditions for signal stability and sensitivity were met.

RESULTS AND DISCUSSION.

a. API and CAD Mass Spectra of Authentic 7-(2'-Hydroxyethyl)guanine and 7-(2'-Haloethyl)guanine Samples.

The above type of compounds are expected to result from the reaction of deoxyguanosine with BFNU. Analysis of the standard mixtures of authentic haloethylguanine derivatives was undertaken for the following reasons: (a) to establish HPLC retention times for each of the species, (b) to obtain characteristic LC/API-MS and CAD spectra of these analytes, and (c) to ascertain whether this LC/MS method is sensitive enough to analyze the low levels of product expected from some of the deoxyguanosine / BFNU reaction(s).

A comparison of the UV chromatogram with the LC/MS reconstructed ion chromatograms obtained from the LC separation of three synthetically prepared guanine derivatives is shown in Figure 5.2. The UV trace in Figure 5.2A was obtained from on-column injection of 1 nmol each of 7-(2'-hydroxyethyl)guanine, 7-(2'-fluoroethyl)-guanine, and 7-(2'-chloroethyl)guanine. Figure 5.2B gives the reconstructed ion chromatograms obtained from the LC/MS analysis of this standard mixture. The MH^+ ion of 7-(2'-fluoroethyl)guanine occurs at m/z = 198. The background intensity observed at that m/z was $\approx 10^4$ cps in this experiment. Extrapolating from the count rate of this ion in Figure 5.2B, it is evident that this analyte can be easily detected at a 100 pmol level (assumed signal to noise ratio ≈ 2) in the scanning mode. Much better detection limits (≈ 20 pmol) could be obtained when the mass spectrometer was operated in the single ion monitoring mode (SIM).

The positive ion API mass spectrum of authentic 7-(2'-fluoroethyl)guanine obtained under LC/MS conditions is shown in Figure 5.3A. Four significant ions which are crucial in this work, and will be referred to repeatedly throughout, are clearly seen in the spectrum. These are the protonated molecular ion **MH^+** at m/z 198 and fragment ions at **m/z 178** corresponding to loss of HF from MH^+, **m/z 166** corresponding to loss of CHF from MH^+, and **m/z 152**, which corresponds to the mass of the protonated guanine base and thus a nominal loss of C_2H_3F from MH^+. Fragment ions of exactly the same masses are also

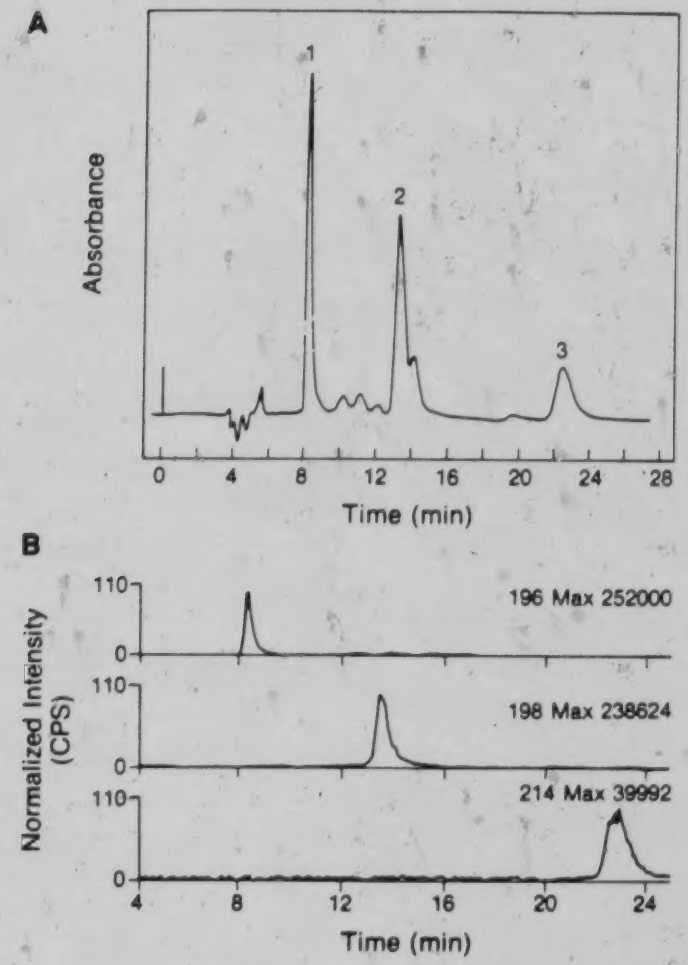

Figure 5.2. (A) HPLC/UV (254 nm) chromatogram of a standard mixture (authentic compounds were dissolved in 10% MeOH, 0.1 M NH_4Ac) of 1 nmol each of 7-(2'-hydroxy ethyl)guanine (peak 1), 7-(2'-fluoroethyl)guanine (peak 2), 7-(2'-chloroethyl)guanine (peak 3). (B) Reconstructed ion chromatograms for peaks corresponding to 7-(2'-hydroxyethyl)-guanine (MH^+, m/z 196), 7-(2'-fluoroethyl)guanine (MH^+, m/z 198), 7-(2'-chloroethyl)-guanine (MH^+, m/z 214). Actual ion counts per second also given in Figure.

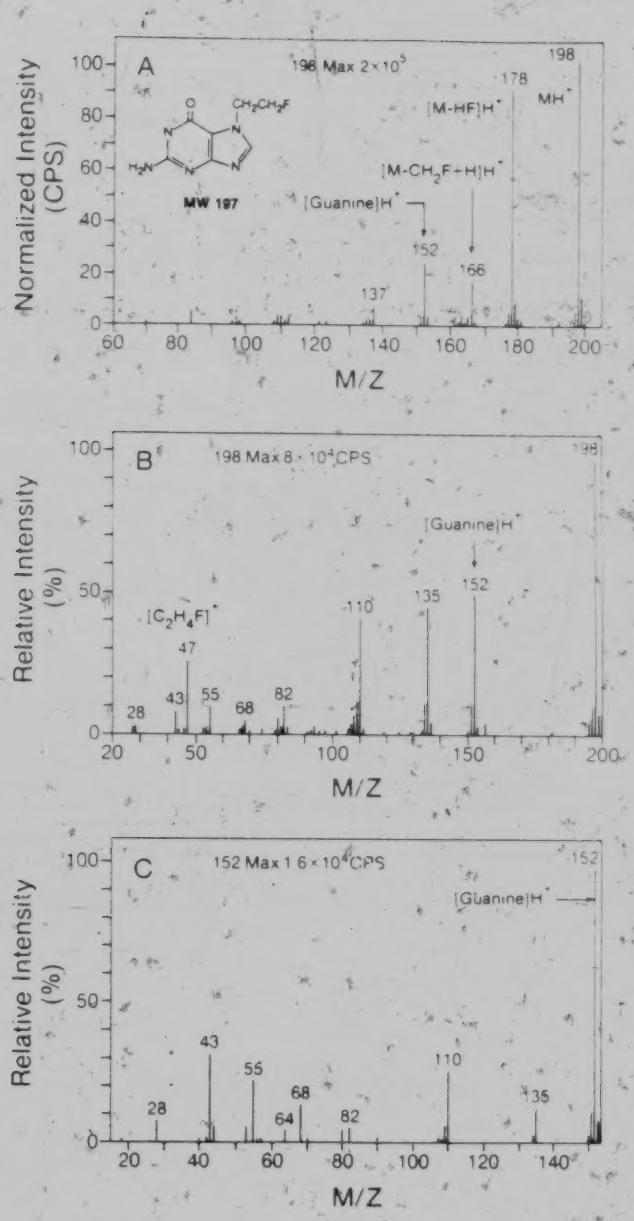

Figure 5.3. (A) Positive ion API mass spectrum of authentic 7-(2'-fluoroethyl)guanine after background subtraction obtained under LC/MS conditions at 13.5 min (elution time of this derivative). (B) LC/MS/MS CAD daughter ion spectrum of protonated 7-(2'-fluoroethyl) guanine (MH^+, m/z 198). (C) LC/MS/MS CAD daughter ion spectrum of protonated guanine $(BH + H)^+$, m/z 152 obtained from flow injection analysis of an authentic sample of 10 nmol guanine dissolved in H_2O.

present, although at different relative abundances, in the LC/API mass spectra (not shown) of the other two authentic compounds, 7-(2'-hydroxyethyl)guanine and 7-(2'-chloroethyl)-guanine.

The mechanisms by which the ions m/z 178, 166 and 152 originate need to be discussed. In a separate experiment, the MH^+ ion was obtained from standard solutions of 7-(2'-fluoroethyl)guanine by using not a heated nebulizer but electrospray as the interface to the mass spectrometer. Electrospray is a very mild form of ionization with which ions present in solution are transferred to the gas phase at ambient temperature (*20*). With this technique, only one ion, MH^+, was observed. This experiment shows that the fragments m/z 178, 166 and 152 are probably due to the high temperature associated with the nebulizer.

Two alternatives can be considered: pyrolysis of MH^+ to yield the ions m/z 178, 166 and 152 or pyrolysis of neutral M in the heated nebulizer followed by API protonation of the neutral pyrolysis products. As a guide to decomposition of vibrationally excited MH^+ one can use the MS/MS collision activated decomposition (CAD) fragment spectrum of MH^+, see Figure 5.3B. This spectrum was obtained with MH^+ produced with the heated nebulizer, but essentially identical spectra were obtained with electrospray-generated MH^+. The m/z 152 ion is seen to be the only important high-mass fragment, and m/z 178 and 166 are completely absent. The formation of m/z 152 from MH^+ corresponds to production of the stable neutral product fluoroethylene, and this decomposition can be considered likely. On the other hand, the m/z 166 corresponds to formation of CHF, a high-energy product, and this decomposition pathway is very unlikely for vibrationally excited MH^+, an expectation that agrees with the absence of 166 from the MH^+ CAD spectrum.

The above results suggest that the ion at m/z 166, and probably also m/z 178 in the LC/API mass spectrum (Figure 5.3A), are not due to pyrolytic decomposition of MH^+ but are due to pyrolysis of neutral M in the hot zones of the nebulizer. The ion at m/z 178 could be due to loss of HF from the neutral M, followed by protonation of the neutral reaction product in the API source. Similarly, the ion at m/z 166 could be due to cleavage of the ethyl C-C

bond and formation of CH_2F and an ($M\text{-}CH_2F$) free radical that subsequently abstracts an H atom from gas molecules such as CH_3OH (buffer component). The product of this reaction will be 7-methylguanine. Protonation of this product in the API source would then lead to m/z 166, which can be designated as $(M\text{-}CH_2F + H)H^+$. The pyrolytic cleavage of the $CH_2\text{-}CH_2F$ bond in 7-(2'-fluoroethyl)guanine can be justified. The two radicals CH_2F and ($M\text{-}CH_2F$) that result are both stabilized by resonance. Therefore a bond dissociation energy of ≈ 60 kcal/mol could be expected (Appendix 5-II). The temperature of the gas in the nebulizer is below 500°C, but wall temperatures close to 550°C could be present. With these estimates one can show that the bond cleavage could occur within the short (≈ 0.1 s) contact time in the nebulizer (see Appendix 5-II).

Some if not all of the m/z 152 could also be due to pyrolytic loss of the CH_2CH_2F radical from M, followed by H atom abstraction, from gas molecules like CH_3OH, leading to guanine and API protonation of the guanine (see Appendix 5-III). The resulting ion m/z 152 can be designated $(M - C_2H_4F + H)H^+$ also as BH_2^+. (*21*)

Although the pyrolysis products available from the heated nebulizer were sufficient to provide structural information of the protonated molecular ion, CAD daughter ion spectra of MH^+ (m/z 198), obtained under LC/MS/MS conditions, Figure 5.3B, also yielded several ions suitable for the structural confirmation of MH^+. These were m/z 152 corresponding to $(MH^+ - C_2H_4F + H)$, and m/z 47, representing $[CH_2CH_2F]^+$. The ion appearing at m/z 152 in this case (CAD conditions) must form by a McCloskey-type mechanism (*21*, Appendix 5-III) where the C-N bond cleavage in MH^+ is accompanied by hydrogen atom transfer. The hydrogen atom here is probably transferred from the ethyl group to the guanine base while the proton (and thus the positive charge) stays with the higher proton affinity base. Most of the remaining ions in this spectrum originate from the decomposition of the base moiety (protonated guanine, m/z 152). This was confirmed by obtaining CAD daughter ion spectra of m/z 152 from an authentic sample of guanine under standard LC/MS/MS conditions, Figure 5.3C. The ions at m/z 152,135,110,80 and 68 in the CAD spectrum of MH^+, Figure

5.3B, are also present in the CAD spectrum of authentic guanine (BH_2^+), Figure 5.3C, and can be assigned as due to sequential loss of H_2NCN from m/z 152 (m/z 110, 68) and successive losses of NH_3 and C_3NH_5 from m/z 152 (m/z 135, 80).

The only ion in the CAD spectrum of MH^+ that is not present in the CAD spectrum of authentic guanine (BH_2^+) has m/z 47, which corresponds to $[CH_2CH_2F]^+$. This ion, which must be due to the fluoroethyl group in MH^+, proved useful as shown in the subsequent discussion.

b. Characterization of 7-(2'-Fluoroethyl)guanine and 7-(2'-Hydroxyethyl)-guanine Resulting from the Reaction of Deoxyguanosine with BFNU in TRIS.

Identification and characterization of 7-(2'-fluoroethyl)guanine in the products of this reaction established whether or not alkylation of the DNA base by BFNU takes place under the present experimental conditions. The analytical work to be described led also to the finding that 7-(2'-hydroxyethyl)guanine is present in the products of this reaction. Neither BFNU in the absence of deoxyguanosine nor synthetically prepared 7-(2'-fluoroethyl)guanosine in the absence of BFNU were found to undergo fluoride for hydroxide exchange (*6*). The 7-(2'-hydroxyethyl)guanine is thus a product of the alkylation reaction of deoxyguanosine by BFNU. This result is of special significance since it indicates the presence of intermediates in the reaction which are expected on the basis of the proposed mechanism for the alkylation of DNA bases by BFNU (*6*).

The in vitro reaction of deoxyguanosine with BFNU under the conditions reported in the Experimental Section led to a number of products which were separated using high performance liquid chromatography (Figure 5.4A). Comparing the UV peaks to those of the standard mixture (Figure 5.2A), assignments of corresponding peaks were made. These peak assignments were confirmed from the reconstructed ion chromatograms and API mass spectra obtained from the HPLC/MS analysis of the reaction products. The search for

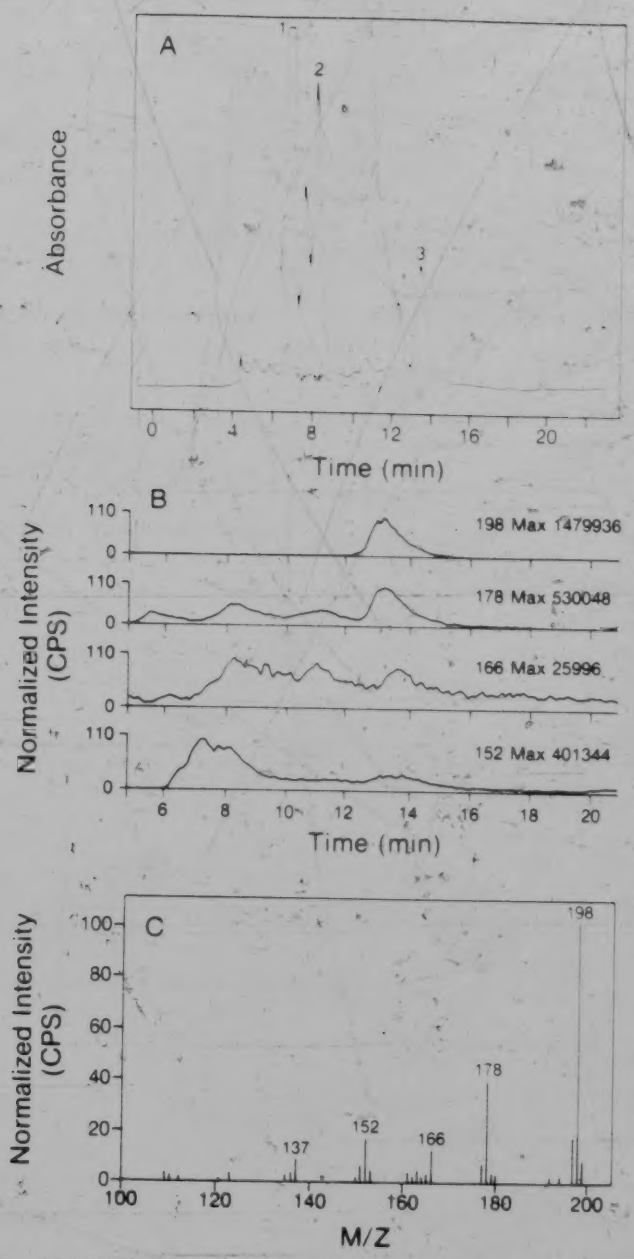

Figure 5.4. (A) HPLC/UV (254 nm) chromatogram of the products resulting from the reaction of BFNU with deoxyguanosine in TRIS buffer at pH 7.1 followed by hydrolysis. Numbered peaks correspond to compounds that were characterized from their mass spectra: peak 1, guanine; peak 2, 7-(2'-hydroxyethyl)guanine; peak 3, 7-(2'-fluoroethyl)guanine. (B) Reconstructed ion chromatogram for peaks corresponding to MH^+ (m/z 198) and characteristic fragments m/z 178, 166, and 152 of 7-(2'-fluoroethyl)guanine all showing ion maxima at the correct retention time, 13.5 min. (C) Background subtracted LC/API mass spectrum deduced from the peak maxima at 13.5 min, shown in (B).

7-(2'-fluoroethyl)guanine was carried out by examining the reconstructed ion chromatograms for ion maxima of expected ions whose elution time coincided with the assigned peak in the UV chromatogram. Reconstructed single ion chromatograms for ions m/z 198, 178, 166, and 152 expected from 7-(2'-fluoroethyl)guanine, see preceding section, are shown in Figure 5.3B. All four ions indicate distinct maxima at the expected retention time (13.5 min) for this compound, see Figures 5.2, 5.3. A background subtracted API mass spectrum deduced from the peak maxima at 13.5 min is shown in Figure 5.4C. This spectrum is very close to that of authentic 7-(2'-fluoroethyl)guanine, see Figure 5.3A. Although all the ions of interest, m/z 198, 178, 166 and 152, are present at significant abundances in this spectrum (Figure 5.4C) their relative abundances are not identical to those in Figure 5.3A. Minor discrepancies of this type can be expected on retrieval of a spectrum from an LC peak particularly when pyrolysis effects are important (see above). It should be noted that the UV chromatogram, Figure 5.4A, shows only compounds with UV absorption. The presence of a number of additional components with no UV absorption with a variety of retention times was indicated from the reconstructed ion chromatograms and it is the interference of such compounds that adds extraneous peaks or leads to oversubtraction of legitimate peaks in the background correction procedure. Nevertheless, in cases where the fragment ions are not clearly marked in the LC/API background subtracted spectrum due to the above mentioned interferences, LC/MS/MS analysis provided the required specificity. All the ions in the CAD spectrum represent the selected compound of interest, provided that the resolution of Q_1 in the triple quadrupole system is high enough.

The presence of 7-(2'-fluoroethyl)guanine was further confirmed, apart from the evidence provided from the LC/API-MS analysis, from the LC/MS/MS spectrum of MH^+, m/z 198, eluting at 13.5 min. The CAD daughter ion mass spectrum of MH^+, m/z 198, (not shown) exhibited fragment ions identical to those of the authentic compound, Figure 5.3B.

Applying experimental procedures identical to those outlined above, and using the same criteria, the presence of 7-(2'-hydroxyethyl)guanine amongst the reaction products was also

confirmed, (for more details see Table 5.1). Based on UV peak areas 7-(2'-fluoroethyl)-guanine and 7-(2'-hydroxyethyl)guanine were found to be present in approximately equal amounts in the reaction products.

c. Characterization of Dideuterated 7-(2'-Fluoroethyl)guanine Resulting from the Reaction of BFNU 1,1,1',1'-d_4 with Deoxyguanosine in TRIS.

Isotopic labelling experiments of BFNU-1,1,1',1'-d_4 reacting with deoxyguanosine were carried out in order to obtain specificity on the site of alkylation of the DNA base. The products of the reaction were separated by HPLC and analyzed by UV, LC/MS, and LC/MS/MS by a procedure similar to that outlined in the preceding sections. The main analytical objective was to identify fluoroethylguanine and other related species in the products of this reaction. The number and the specific location of the deuterium atoms on these species was of primary importance. Identification of (2'-fluoro-2',2',-dideuteroethyl)-N7-guanine among the reaction products provided the key evidence in support of one proposed mechanism of alkylation of DNA bases by anticancer alkylators (*6*). Formation of this species provides strong evidence that the C-F bond is broken and subsequently reformed in the reaction of BFNU with deoxyguanosine.

Since the deuterium content and thus the m/z value of the protonated molecular ion was not known, a search for ion maxima at the retention time 13.5 min corresponding to 7-(2'-fluoroethyl)guanine was carried out. From the selected set of reconstructed ion chromatograms shown in Figure 5.5A, it is evident that the ions at m/z 200, 180 and 166 have characteristic maxima at the correct retention time. The ion at m/z 200 is assigned to the protonated molecular ion MH^+, indicating the presence of two deuterium atoms in this derivative. The LC/API mass spectrum, Figure 5.5B, obtained at 13.5 min retention time, shows an isolated m/z 200 peak confirming the presence of only molecules containing two deuterium atoms. This retention time of dideuterated fluoroethylguanine was the same as that of the authentic 7-(2'-fluoroethyl)guanine sample, indicating that the fluoroethyl chain was

Table 5.1. Guanosine Modification by BFNU or BFNU-1,1,1',1'-d4. Hydroxyethyl-N-dG and haloethyl-N7-dG products analyzed by HPLC/MS and HPLC/MS/MS.[a]

Reaction and conditions	$HOCH_2CH_2$-N7- G[j] MH^+ (m/z 196)	$HOCHDCH_2$-N7- G[j] MH^+ (m/z 197)	$HOCD_2CH_2$-N7- G[j] MH^+ (m/z 198)	$F\text{-}CH_2CH_2$-N7- G[j] MH^+ (m/z 198)	$F\text{-}CHDCH_2$-N7- G[j] MH^+ (m/z 199)	$F\text{-}CD_2CH_2$-N7- G[j] MH^+ (m/z 200)	$Br\text{-}CH_2CH_2$-N7- G[j] MH^+ (m/z 258, 260)	$BrCHDCH_2$-N7- G[j] MH^+ (m/z 259, 261)
1. BFNU with dG in TRIS	b,c			b,c				
2. BFNU-1,1,1',1'-d4 with dG in TRIS	d,e	d,e	d,e	trace[d,e,i]	d,e	b,c		
3. BFNU with dG and excess KBr in TRIS	b,c			b,c			b,c	
4. BFNU-1,1,1',1'-d4 with dG and excess KBr in TRIS	d,e	d,e	d,e	d,e,i	d,e	b,c		e,h
5. BFNU with dG in cacodylate	b,c			b,c				
6. BFNU-1,1,1',1'-d4 with dG in cacodylate	d,e	d,e,f	d,e,g		d,e	b,c		
7. BFNU with dG and excess KBr in cacolydate	b,c			b,c			b,c	
8. BFNU-1,1,1',1'-d4 with dG and excess KBr in cacodylate	d,e	d,e	d,e	trace[d,e,i]	trace[d,e,i]	b,c		e,h

a. Products after hydrolysis with 1 N HCl.

b. Presence confirmed from reconstructed single ion chromatograms of MH^+ and specific fragments $(M\text{-}HX)H^+$, $(M\text{-}CH_2X + H)H^+$ and protonated guanine $(BH + H)^+$.

c. Additional structural information obtained by characterizing CAD daughter ion spectra of MH^+.

d. Presence deduced from reconstructed ion chromatograms of MH^+ at expected elution time. Supporting fragments cannot be assigned due to high degree of isotopic overlap.

e. MH^+ signal intensity is not sufficiently strong to obtain reliable CAD daughter ion spectra.

f. CAD daughter ion spectra indicate that there is only one deuterium present and it is located on the ethyl chain.

g. CAD daughter ion spectra indicate that one deuterium is located on the ethyl chain and the other on the base.

h. Presence confirmed by the isotopic pattern of MH^+ and the strong presence of m/z 179 indicating loss of HBr from MH^+.

i. Reconstructed ion chromatograms of MH^+ peaks are very weak in intensity therefore the identification of this species is tentative.

j. G: Guanine.

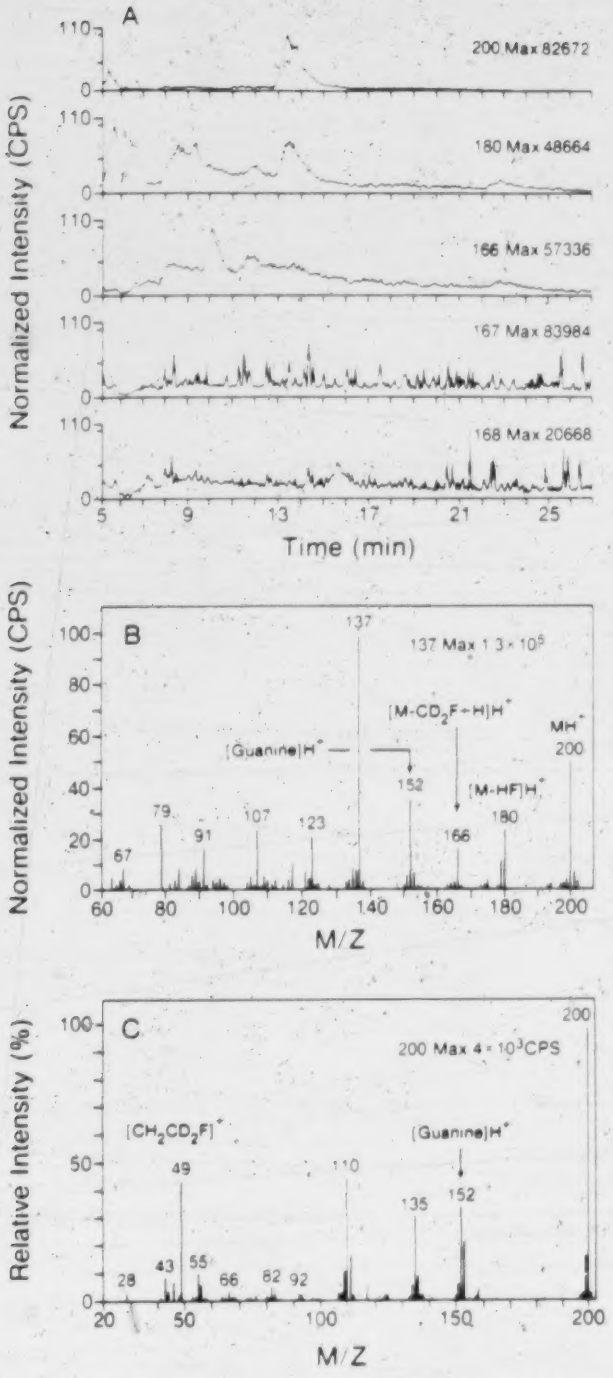

Figure 5.5. (A) Reconstructed ion chromatograms for peaks corresponding to MH^+ (m/z 200) and characteristic fragments m/z 180 and 166 of dideuterated 7-(2-fluoroethyl)guanine, all indicating ion maxima at the correct retention time of 13.5 min. Reconstructed ion chromatograms for m/z 167 and 168 are also plotted in this figure demonstrating the background like behavior of these ions. No distinct maxima are indicated at the retention time of interest, 13.5 min. (B) Background subtracted LC/API mass spectrum deduced from the peak maxima at 13.5 min, shown in (A). (C) LC/MS/MS CAD daughter ion spectrum of m/z 200, MH^+ of dideuterated 7-(2'-fluoroethyl)guanine) obtained at 13.5 min.

probably attached to the N7 position of guanine and that the fluorine atom was probably located on the C_2-position of the ethyl chain.

The mass spectral analysis of nebulized authentic 7-(2'-fluoroethyl)guanine (see preceding sections) showed that the ion at m/z 152 corresponded to protonated guanine. This ion is also present in Figure 5.5B, while m/z 153 and 154 are negligible. This shows that there was no deuterium on the protonated guanine and confirmed that both deuterium atoms were on the fluoroethyl group. Furthermore, the absence of m/z 153 and 154 showed that no deuterium was transferred from the fluoroethyl group to the guanine moiety in the nebulizer-produced LC/API mass spectrum.

Further confirmation that the fluoroethyl group was dideuterated was obtained from the LC/MS/MS CAD daughter ion spectrum of m/z 200 taken at the correct (13.5 min) retention time, shown in Figure 5.5C. This spectrum contains a prominent peak at m/z 49. In the CAD spectrum of MH^+ m/z 198 obtained from authentic 7-(2'-fluoroethyl)guanine, the prominent peak was m/z 47 (see Figure 5.3B), and this peak was identified as $[CH_2\text{-}CH_2F]^+$. The shift of that peak to m/z 49 in Figure 5.5C shows that the fluoroethyl group was now dideuterated.

The ion at m/z 180, see Figure 5.5B, corresponds to loss of HF from m/z 200. Since HF was preferentially eliminated instead of DF, and since such reactions are most likely 1,2-eliminations, the two deuterium atoms were probably on the same carbon atom as the fluorine.

The ion at m/z 166 in Figure 5.5B is clearly due to a process analogous to that giving rise to the ion of the same mass obtained from authentic 7-(2'-fluoroethyl)guanine, see Figure 5.3A. As pointed out in the preceding discussion, it is unlikely that this ion is due to fragmentation of MH^+ m/z 198, since that would lead to a neutral product CHF which is of high energy. The observation of the same mass, m/z 166, from the dideuterated compound confirms this conclusion, since the ion resulting from a cleavage reaction from the dideuterated MH^+ should have contained a minimum of one deuterium atom for a neutral loss

of CDF or two deuterium atoms for the neutral loss of CHF. Since no deuterium atoms are present in m/z 166, some of the hydrogen in m/z 166 is of foreign origin, *i.e.*, due to a bimolecular reaction. The neutral group lost then is not CHF but CH_2F (CDF and CD_2F, respectively, from the dideuterated compound). The clean loss of CD_2F from the dideuterated compound provides strong evidence that both deuterium atoms are on the α-carbon, *i.e.*, that the fluoroethyl group is CH_2CD_2F. In the section dealing with mass spectral data for authentic 7-(2'-fluoroethyl)guanine (= M), evidence was presented to support the view that losses of CH_2F occur from M due to pyrolysis of neutral M in the nebulizer, and that the resulting neutral (M - CH_2F) radical picks up a hydrogen atom by a bimolecular hydrogen abstraction reaction. The resulting (M - CH_2F + H) species becomes protonated in the API region and is detected as (M - CH_2F + H)H^+, m/z 166. The presence of a lone m/z 166 peak without deuterium satellites in the nebulizer spectrum of the dideuterated compound, shown in Figure 5.5B, is consistent with this mechanism [where m/z 166 is now (M - CD_2F + H)H^+], and provides further confirmation for its validity. However, it should be noted that the proof of structure of the 7-(2'-fluoro-2',2'-dideuteroethyl)guanine is not dependent on the exact mechanism by which the ions are formed. The pyrolysis of M merely represents the most probable mechanism. Finally, the lack of any maxima in the selected ion traces for ions m/z 167 and 168 at 13.5 min (see Figure 5.5A) further verifies the assignment of the deuterium atoms α to the fluorine. One deuterium β to the fluorine and one α would have resulted in a maximum for m/z 167 at 13.5 min, representing the (M - CHDF + H)H^+ ion formed by an identical mechanism to that discussed for m/z 166. Similarly, the presence of two deuterium atoms β to the fluorine would have indicated a maximum for m/z 168 at 13.5 min, since the (M - CH_2F + H)H^+ ion would have been expected to form.

In order to ensure that the data presented in this section were reproducible, two reactions of deoxyguanosine with BFNU-1,1,1',1'-d_4 were performed and five aliquots of each reaction product were analyzed by HPLC/MS. The presence of 7-(2'-fluoro-2',2'-dideutero-ethyl)guanine was confirmed every time. This procedure was necessary since significant

variations in the relative intensities of the ions m/z 180, 179 (probably representing (M - DF)H^+, see Figure 5.5B) and 166 were observed from one experiment to the other. The ion at m/z 137 in Figure 5.5B is a background ion that has not been subtracted upon retrieving this spectrum from the ion chromatogram.

In addition to dideuterated 7-(2'-fluoroethyl)guanine, five other distinct species were detected and identified in the products of this reaction by employing the same experimental procedures and criteria outlined above. The results of these experiments are summarized in Table 5.1. Amongst the fluoro-derivatives presented in expt.# 2 of Table 5.1, m/z 200, corresponding to (F-CD_2CH_2-N7-guanine)H^+, was some 10 times higher in intensity than m/z 199 (monodeuterated fluoro-derivative) while only a trace of m/z 198 ([F-CH_2CH_2-N7-guanosine]H^+) was detected.

Earlier mass spectra (*22a*) of dideutero(2-chloroethyl)guanine obtained from BCNU-2,2,2',2'-d_4 and deoxyguanosine were interpreted to indicate that the deuteration of the ethyl group was CD_2CH_2Cl, *i.e.*, corresponding to rearrangement as found in the present work using BFNU-1,1,1',1'-d_4. The deuterium assignment (*22a*) was based on a comparison of the electron impact (EI) mass spectrum of the deuterated derivative with that of authentic undeuterated (2-chloroethyl)guanine. In general, EI spectra are not well suited to providing a definite assignment of the position of deuterium atoms unless an EI spectrum of the authentic deuterated compound is available. Hydrogen or even carbon scrambling can occur in the excited molecular radical ion, which leads to loss of positional information for labeled atoms. These rearrangement processes have unfavorable entropy transition states but are of lower energy than, and can compete with, the more direct dissociation and cleavage processes that retain positional information for the label. For examples involving studies of systems with some relevance to the present case, see Nibbering (*22b,c,d*). In the EI study (*22a*), neither of the two major fragmentations provide unambiguous proof of the position of the deuterium. Only a lower abundance loss of CH_2Cl in the undeuterated isomer ion is seen to remain as a loss of CH_2Cl in the deuterated isomer. This peak, if one assumes absence of prior

scrambling, indicates the CD_2CH_2Cl structure. In the present study, as was discussed earlier, the fragments of the (2-haloethyl)guanines are produced by thermal decomposition of the neutral molecule and then ionized by protonation with a weak protonating agent. No deuterium scrambling is expected to occur for these low-energy processes, and the data provided multiple confirmation for the equivalent rearrangement corresponding to BFNU-1,1,1',1'-d_4 and leading to CH_2CD_2X.

d. Characterization of 7-(2'-Bromoethyl)guanine Resulting from the Reaction of Deoxyguanosine with BFNU in TRIS and in the Presence of KBr.

This section describes how 7-(2'-bromoethyl)guanine was shown to be a product of the reaction of deoxyguanosine with BFNU in the presence of KBr. Separate halide exchange experiments (*6*), where KBr in the presence of phase transfer catalyst was used, have shown that neither 1,3-bis(2-fluoroethyl)urea (BFU) nor BFNU exchanges fluoride for bromide under these conditions. 7-(2'-bromoethyl)guanine must therefore be a product associated with the alkylation reaction. Its formation is expected on the basis of the proposed mechanism for the alkylation of DNA bases by BFNU (*6*). Therefore, the present findings constitute a further verification of the proposed mechanism.

The search for bromoethylguanine derivatives was carried out by examining reconstructed ion chromatograms, obtained from the HPLC/MS analysis of the above reaction products, for ion maxima corresponding to expected pseudo-molecular ion(s) and specific fragments. Although there was no standard available to confirm the HPLC retention time of 7-(2'-bromoethyl)guanine, the reconstructed ion chromatograms, Figure 5.6A, the background subtracted spectrum obtained at 28.5 min after injection time, Figure 5.6B, and the CAD spectra of m/z 258 also obtained at 28.5 min, provide evidence for the presence of this derivative in the products of this reaction.

It is shown in Figure 5.6A that ions m/z 258, 260 and 178 maximize in intensity at the same retention time, 28.5 min. The peak at m/z 258 with the bromine isotope at m/z 260 is

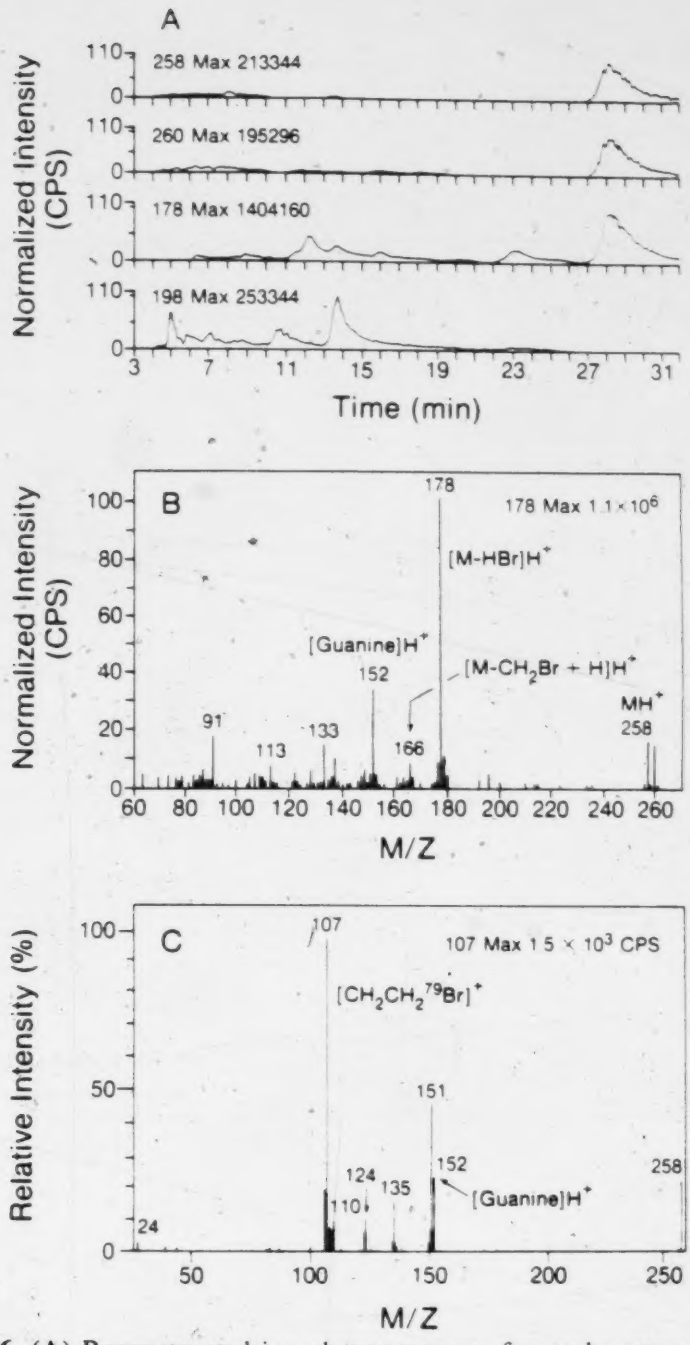

Figure 5.6. (A) Reconstructed ion chromatograms for peaks corresponding to MH^+ (m/z 258 and 260) and characteristic fragment m/z 178 of 7-(2'-bromoethyl)guanine, all showing distinct ion maxima at 28.5 min. The trace of m/z 198 , MH^+ of 7-(2'-fluoroethyl)guanine, is also ploted in this Figure. (B) Background subtracted LC/API mass spectrum deduced from the peak maxima at 28.5 min, shown in (A). (C) LC/MS/MS CAD daughter ion spectrum of m/z 258, MH^+ of 7-(2'-bromoethyl)guanine obtained at 28.5 min.

assigned to the MH^+ of bromoethylguanine (M), while the peak at m/z 178 represents loss of HBr from MH^+. Proof for the existence of a bromoethyl group in this derivative is obtained from the LC/MS/MS CAD daughter ion spectrum of m/z 258 taken at 28.5 min retention time, shown in Figure 5.6C. This spectrum contains a prominent peak at m/z 107. This peak is assigned to the $(CH_2CH_2{}^{79}Br)^+$ fragment from MH^+. The m/z 107 peak is shifted to m/z 109, identified as $(CH_2CH_2{}^{81}Br)^+$, when CAD on m/z 260 (isotope of m/z 258) is performed. The haloethyl ion $(CH_2CH_2X)^+$ is a prominent peak in the CAD spectra of all the authentic 7-(2'-haloethyl)guanines investigated in this work (X=F,Cl), therefore the presence of a corresponding peak in this spectrum clearly accounts for a bromoethyl group in this derivative.

Additional structural information for the MH^+ ion is available from the LC/API background subtracted spectrum deduced from the peak maxima at 28.5 min, Figure 5.6B. The isotopic pattern of MH^+ and the ions carrying important structural information, m/z 178, 166, and 152, are clearly marked in this spectrum. The ion at m/z/166 corresponds to loss of CHBr from MH^+ while m/z 152,which is assigned to the mass of protonated guanine base, corresponds to loss of C_2H_3Br from MH^+. These ions are believed to have formed by a process analogous to the one discussed for the authentic 7-(2'-fluoroethyl)guanine sample. The m/z 178, 166, and 152 ions are characteristic LC/API-MS fragments of 7–(2'-haloethyl)-guanine's and are associated with the fragmentation of the haloethyl group, see preceding sections. Therefore their presence in the API spectrum of Figure 5.6B suggests that the haloethyl chain of this derivative is of similar structure, *i.e.*, with Br in the C_2 position. If Br were in the C_1 position, fragment ions at m/z 244 and 246, representing $(MH^+ - CH_3 + H)$, would have been expected. There is no evidence for such fragments in Figure 5.6B nor in the reconstructed ion chromatograms of m/z 244 and 246 (not shown) at 28.5 min. Instead, the prominent fragment ion is m/z 166, representing $(M - CH_2Br + H)H^+$. The extraneous ions m/z 91,113,133, and 136 in Figure 5.6B must be background ions that have not been

totally subtracted upon retrieving this spectrum from the ion chromatogram. No distinct maxima (at 28.5 min) were observed in the reconstructed ion chromatograms of these ions.

The information available from the mass spectrometric data, *i.e.*, the isotopic pattern of the MH^+ ion, the presence of a bromoethyl group in M, and the similar fragmentation of MH^+ (under LC/API-MS conditions) to that of the 7-(2'-haloethyl)guanines, provided confirmation of the 7-(2'-bromoethyl)guanine structure.

The presence of 7-(2'-bromoethyl)guanine in the products of the reaction, suggests that fluorine from BFNU is replaced by bromine, in the reaction complex. Since 7-(2'-fluoroethyl)guanine is also present in the reaction products, the substitution is only partial. Evidence for the presence of the fluoro-derivative is provided from the reconstructed ion chromatograms of m/z 198 and 178 in Figure 5.6A. The distinct maxima of m/z 198, MH^+ of 7-(2'-fluoroethyl)guanine, together with that of m/z 178, representing loss of HF from MH^+, at 13.5 min (expected elution time for this component), confirm the presence of this species. Complete identification was provided from the API and CAD daughter ion spectra of m/z 198 (not shown), see Table 5.1. 7-(2'-hydroxyethyl)guanine was also identified as one of the products of this reaction, see Table 5.1. The approximate relative yield of the three derivatives (bromo, fluoro, and hydroxy) in the reaction products under the present conditions is 10:3:4 respectively (determined from UV peak areas).

The haloethyl $(CH_2CH_2X)^+$ ion and protonated guanine, m/z 152, are prominent peaks in the CAD daughter ion spectra of all the 7-(2'-haloethyl)guanines (X=F,CL,Br) investigated in this work. However, the shift in intensity of the m/z 152 peak to m/z 151, representing $(MH^+ - C_2H_4{}^{79}Br)$, in the CAD daughter ion spectrum of the bromo-derivative (Figure 5.6C) is somewhat unexpected and needs to be discussed, see Appendix 5-III.

e. Characterization of Monodeuterated 7-(2'-Bromoethyl)guanine, the Only Bromo-Derivative Product, Resulting from the Reactions of Deoxyguanosine with BFNU 1,1,1',1'-d_4 in TRIS in the Presence of KBr.

Of primary concern among the products of this reaction, as analysed by HPLC/API-MS, were any 7-(2'-bromoethyl)guanines (deuterated or not). Their presence would establish whether or not halide transfer takes place during alkylation of deoxyguanosine by BFNU-d_4 in TRIS and in the presence of KBr. The results of this analysis, and especially the identification of the mono-deuterated bromo-derivative and the high abundance of the dideuterated fluoro-derivative, have a direct bearing on the proposed mechanism for modification of DNA bases. They provide evidence for a diazoalkane intermediate during base modification (*6*).

A search for deuterated 7-(2'-bromoethyl)guanines was carried out by examining the reconstructed ion chromatograms, around 28.5 min, for ions representing MH^+ of a dideuterated species (m/z 260, 262), for MH^+ of mono-deuterated species (m/z 259, 261), for MH^+ of non-deuterated species (m/z 258,260), and characteristic fragments of all of these. Examination of the spectra of Figure 5.7A indicates that only the traces for m/z 259 and m/z 179 show distinct maxima at around 28.5 min. A background-subtracted LC/API mass spectrum deduced from the peak maximum at 28.5 min is shown in Figure 5.7B. The important ions in this spectrum are m/z 259,261, and 179; the other ions at m/z 174,186, and 228 are background ions that have not been totally subtracted from the ion chromatographic peak. The peak at m/z 259 with the bromine isotope at m/z 261 is assigned to MH^+ of mono-deuterated 7-(2'-bromoethyl)guanine, while the peak at m/z 179 represents loss of HBr from MH^+ (m/z 259,261). The elution time of these species is the same as that of 7-(2'-bromoethyl)guanine (28.5 min, see preceding section), consistent with an identical configuration for the molecule. Although the data presented so far strongly indicate the presence of mono-deuterated 7-(2'-bromoethyl)guanine in the products of this reaction, they are not specific enough to propose a location for the deuterium atom. Collection of more detailed structural

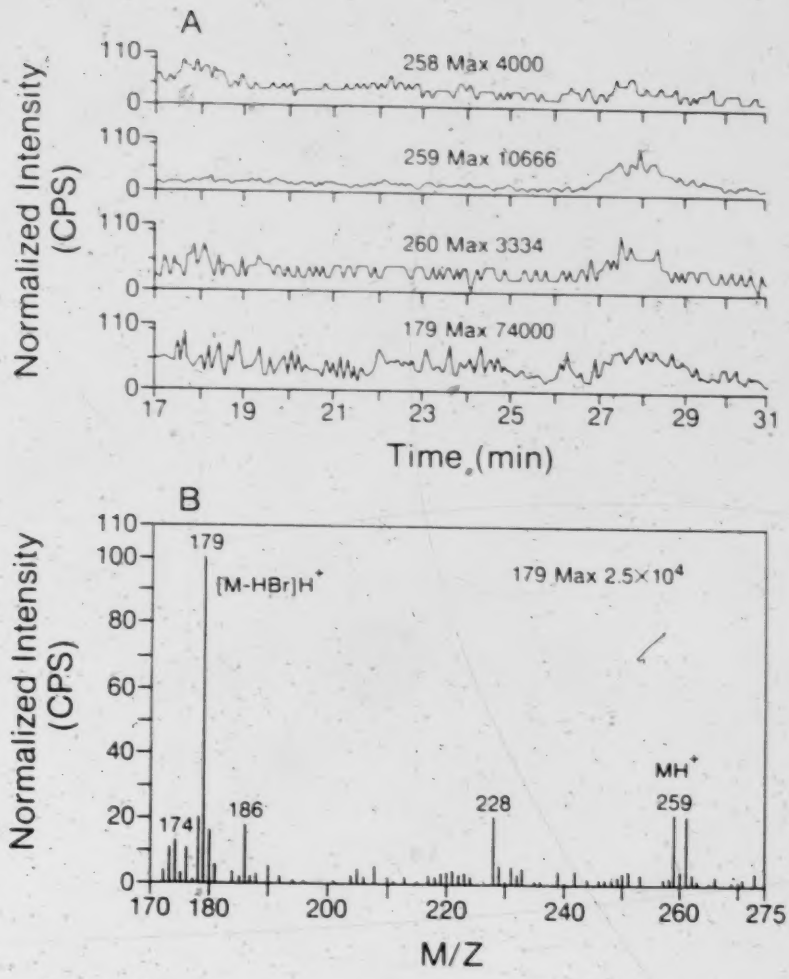

Figure 5.7. (A) Reconstructed ion chromatograms for peaks corresponding to non-deuterated 7-(2'-bromoethyl)guanine (MH^+, m/z 258), mono-deuterated 7-(2'-bromoethyl)-guanine (MH^+, m/z 259), dideuterated 7-(2'-bromoethyl)guanine (MH^+, m/z 260), and characteristic fragment ion m/z 179 represending HBr loss from MH^+ of the mono-deuterated species (m/z 259). (B) Background subtracted LC/API mass spectrum deduced from the peak maxima at 28.5 min, shown in (A).

information was not possible for the following reasons. The intensity of MH^+ is below the required count rate (> 5 x 10^4 cps) for reliable and reproducible CAD analysis. Also, acquisition of a more complete API mass spectrum (Figure 5.7B), covering the lower mass range, is not practical since the ions of interest are barely above the ion background.

The chromatographic time profiles of m/z 258 (MH^+ of non-deuterated bromo-derivative) and 260 (MH^+ of deuterated bromo-derivative) are plotted in Figure 5.7A. The trace of m/z 258 shows no maximum at approximately 28.5 min, indicating that there is no non-deuterated bromo-derivative present. The very small maximum for m/z 260 is not sufficient to account for the presence of a dideuterated derivative, especially when the m/z 262 trace (not shown) exhibited no maximum at ≈ 28.5 min. None of these ions is of appreciable intensity in the LC/API mass spectrum, see Figure 5.7B.

Although mono-deuterated 7-(2'-bromoethyl)guanine is of low concentration, dideuterated 7-(2'-fluoroethyl)guanine is a major component of the products of this reaction. Reconstructed ion chromatograms (not shown) of m/z 200 (MH^+) and m/z 180 (MH^+ - HF), characteristic ions of the dideuterated fluoro derivative, indicated intense maxima at the expected retention time of 13.5 min. The higher abundance of the fluoro-derivative suggests that the bromide exchange is not favorable in the presence of deuterium during modification of the DNA base.

Apart from mono-deuterated 7-(2'-bromoethyl)guanine and 7-(2'-fluoro-2',2'-dideutero-ethyl)guanine a number of other distinct species were detected and identified in the products of this reaction by employing the same experimental procedures and criteria that have been discussed in proceeding sections. The results of these experiments are summarized in Table 5.1, expt. # 4.

f. Characterization of 7-(2'-Hydroxyethyl)guanine and 7-(2'-Haloethyl)-guanines and their Deuterium-Labeled Counterparts from the Reactions of Deoxyguanosine with BFNU or BFNU 1,1,1',1'-d_4 in Different Buffers.

Having determined that the key individual products of the base modification could be separated and identified and the deuterium labels located within them, a systematic study of the reactions was undertaken. The conditions varied according to the presence or absence of deuterium labeling in the substrate, or of competing external halide ion, and the nature of the buffer, *i.e.*, nucleophilic (TRIS) or non-nucleophilic. The experiments performed here were similar to those of the four previous sections. The only difference between the two sets of experiments was that the reactions were carried out in sodium cacodylate instead of TRIS. HPLC/MS/MS analysis of the products of reactions **5** to **8** (see Table 5.1) led to the detection and identification of a number of important species, according to the reaction conditions, which have been summarized in Table 5.1. Similarly, the experimental procedures, conditions, and criteria used to identify these products were identical with those discussed in previous sections. However, quantifying these products poses severe problems, including differences in solubility of the deglycosidated modified bases and the difficulty of HPLC/MS detection of low concentration components eluting next to very high concentration components, as well as the coelution of isotopic components. Several approaches to these problems were investigated, and techniques were devised to give reproducible approximate relative yields of products; see Appendix 5-IV for details.

Based on the findings of these experiments, the general conclusion is that identical products are obtained when either TRIS or sodium cacodylate buffer is used.

CONCLUSION

The present study provides a demonstration of the unique capability of the present HPLC/API-MS technique when used for the identification of minor nonvolatile components of interest, present in complex mixtures. Sensitive detection (pmol to nmol range) of 7-(2'-haloethyl)guanines has been demonstrated. LC/API mass spectra of these guanine derivatives were seen to provide intense pseudo-molecular ion peaks and a number of intense fragment ion peaks. Fragment ions obtained from the LC/API-MS analysis alone provide significant structural information and permit identification of most of the species of interest. In cases where MS/MS was employed, additional fragmentation (not available in the LC/API spectra) was observed which was essential for structural elucidation of the components of interest. However loss of sensitivity associated with the MS/MS technique constrained CAD data acquisition to cases where the parent ion was of relatively high abundance.

The results obtained from the HPLC/API-MS and HPLC/MS/MS analysis of the products of reactions **1** to **8** (Table 5.1) provided means for discrimination between some alternative mechanisms of DNA base modification by clinical anticancer alkylators (HENU's). A mechanism that involves a molecular rearrangement, during formation of the critical lesions 7-(2'-fluoroethyl)guanosine and 7-(2'-hydroxyethyl)guanosine proceeding, via a diazoalkane intermediate, has been proposed (*6*).

APPENDIX 5-I. Outline of Proposed Mechanism of DNA Base Modification by the Anticancer Alkylator BFNU.

The results of the isotopic labeling experiments with BFNU-1,1,1',1'-d_4 reacting with deoxyguanosine, analyzed by HPLC/MS/MS, confirm transfer of the 2-fluoroethyl group to the N7 position of guanine with complete rearrangement of the two deuterium atoms from their initial position β to the fluorine in BFNU-d_4 to positions α to the fluorine in the nucleoside adduct.

Several lines of evidence implicate formation of tetrahedral intermediates from HENUs resulting from reversible addition of a DNA base nucleophile to the nitrosourea carbonyl group (**1**, Scheme I) (*23-25*). The initially formed tetrahedral intermediate (**2**, Scheme I) undergoes rearrangement (*25c*). This involves formation of a tetrahedral intermediate by addition of the guanosine O^6 to the carbonyl group of the iminourea of the HENU, to give (**3**, Scheme II) followed by ring closure to form the nitrosooxazolidine (**4**, Scheme II). Considering this proposal in the light of the present results it is clear that the deuterium labeling studies prove conclusively that the C-F bond is broken and subsequently reformed in the reaction of BFNU and guanosine. Formation of the N-nitrosooxazolidine (**4**, Scheme II) and attack at position 5 of the heterocycle by nucleophiles on the neighboring bases, *e.g.* at G-N7 leads to the rearranged diazoic acid (**5**, Scheme II). In the absence of an adjacent base in a complementary strand of DNA the intermediate can hydrolyze to HOEt-N7dG or react with fluoride ion within the solvent cage to form FEt-N7dG, see (**3**, Structure II). It has been demonstrated independently that the halogen group in 7-(2-haloEt)dG derivatives are not subject to hydrolysis to HOEt-N7dG (*26*), so the above competing mechanisms provide a plausible explanation for the observed formation of $HOCD_2CH_2$-N7dG together with FCD_2CH_2-N7dG.

Moreover the halide exchange experiments, in which a 10 molar excess of KBr is present during the reaction of BFNU with deoxyguanosine, result in formation of BrEt-N7-dG. By contrast no such halide exchange occurs on FEt-N7-dG directly or even in the presence of

18-crown-6 to enhance the nucleophilicity of the bromide ion. This supports the suggestion of a labile species (the diazoic acid) subject to effective competitive nucleophilic substitution by Br^-. Supporting evidence for the intermediacy of the $HON{=}N\text{-}CH_2CH_2\text{-}N7\text{-}dG$ intermediate **5** is obtained by the detection of $BrCHDCH_2N7\text{-}dG$ (*i.e.* bearing only one deuterium adjacent to bromine) in the KBr exchange reaction with BENU-1,1,1',1'-d_4.

The mechanism shown in Scheme II (**3**, **4**, **5**) has the merit that it correctly predicts the positions of the deuterium labels observed in the present study.

SCHEME I

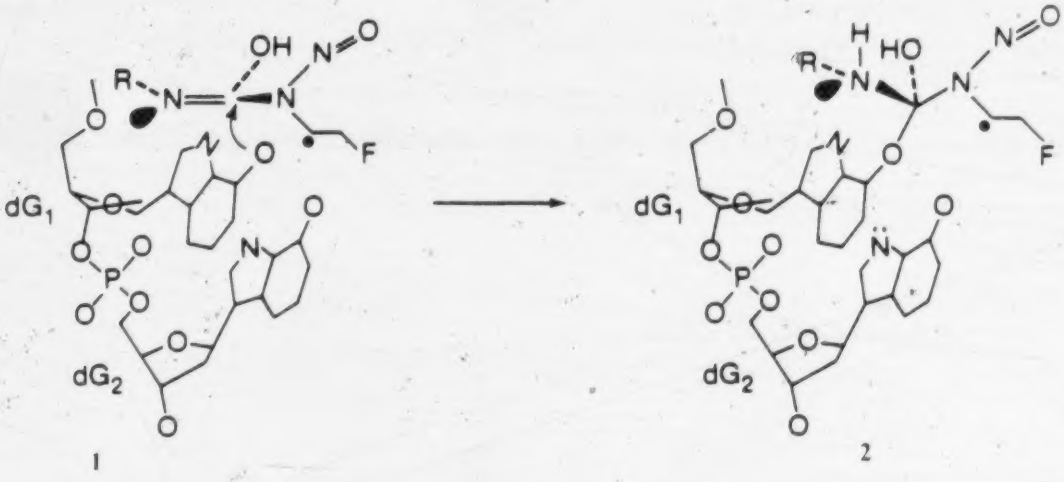

1 2

SCHEME II

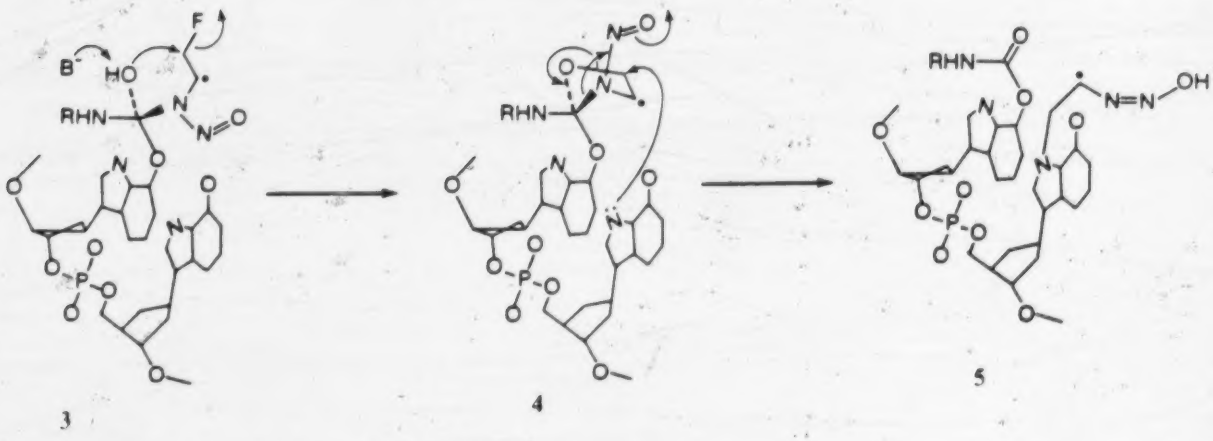

3 4 5

• designates the position of the deuterium atoms.

APPENDIX 5-II. Calculation of Reaction Time Required for the CH_2-CH_2F Pyrolytic Bond Cleavage.

A reaction time of 0.5 s is evaluated for 5% decomposition of 7-(2'-fluoroethyl)guanine with the assumption that the pre-exponential factor is $A = 10^{15}$ s^{-1} (see Table X1.5 S.W. Benson, *The Foundations of Chemical Kinetics*; McGraw Hill, 1960); the activation energy E_A = 60 kcal/mol and the temperature is 550 °C.

APPENDIX 5-III. CAD Spectral Characteristics of Protonated 7-(2'-haloethyl)guanines and Pathways of $(BH + H)^+$ Formation from 7-(2'-haloethyl)guanines Under LC/API-MS Conditions.

Close inspection of the LC/MS/MS CAD spectra of the three 7-(2'-haloethyl)guanine derivatives (Figure 5.3B for the fluoro, Figure 5.8 for the chloro, and Figure 5.6C for the bromo species) reveals some interesting trends. As pointed out in the preceding discussion, CAD of all three MH^+ species have a prominent peak at m/z 152 corresponding to loss of C_2H_3X from MH^+. This is a rearrangement process in which one hydrogen from the C_2H_4X group is transferred to the protonated guanine moiety and the resulting ion is the protonated guanine. McCloskey and coworkers (*21*) have observed that protonated mononucleosides MH^+ undergo a cleavage of the C_1'-N_9 glycosylic bond (see structure II) accompanied by transfer of a hydrogen atom from the sugar to the protonated nucleic base. The resulting protonated base, which they designated as $(BH+H)^+$ was a major ion in the CI, FAB and MS/MS spectra of all investigated nucleosides. Protonated nucleic acid bases, $(BH+H)^+$, always represent the base peak in the CAD spectra of all investigated nucleosides (*21b*). The present results show that an analogous process also occurs for protonated nucleic acid bases where the base has been modified by an alkyl side chain (C_2H_4X). However, in this case the C_1'-N_7 bond is cleaved rather than the C_1'-N_9, and this cleavage is also accompanied by hydrogen transfer (here the hydrogen transfer is from the haloethyl chain).

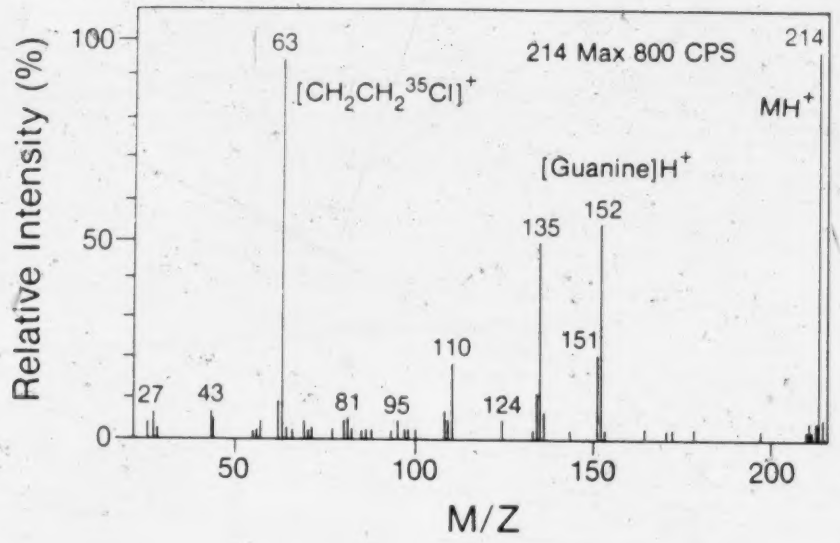

Figure 5.8. LC/MS/MS CAD daughter ion spectrum of m/z 214, MH^+ of 7-(2'-chloroethyl)guanine obtained from an authentic sample, see Figure 5.2.

The CAD spectra of the haloethylguanines also show that the rearrangement process leading to m/z 152 decreases in importance as X changes from F to Cl to Br. The m/z 152 ion decreases in relative abundance and is replaced by m/z 151, i.e. loss of neutral C_2H_4X from MH^+ and also the formation of $C_2H_4X^+$. Thus, for bromoethylguanine, see Figure 5.6C, the m/z 151 and $C_2H_4Br^+$, m/z 107, are the two major fragment ions. It is also important to note that the relative abundance of the parent ion MH^+ decreases markedly in the order: X = F,Cl, Br. Both the loss of C_2H_4X from MH^+ leading to m/z 151 and the formation of $C_2H_4X^+$ are direct cleavage processes. The increased formation of $C_2H_4X^+$ may have been expected because of the known increase of stability of the $C_2H_4X^+$ ions in the order F, Cl, Br. On the other hand, the tendency for the rearrangement leading to the m/z 152 must be decreasing in the order F, Cl, Br for reasons that are not entirely clear. The decrease of the m/z 152/151 ratio in the above order suggests that the rearrangement channel gradually switches into the direct cleavage of the C_2H_4X group.

The CAD spectra for the bromo derivative, Figure 5.6C, also provide additional confirmation of the assumed mechanism for formation of the spectra under heated nebulizer API conditions (LC/API-MS), see Results and Discussion. Comparison of the LC/API spectrum, Figure 5.6B, with the CAD spectrum shows that in the LC/API spectrum the m/z 152/151 ratio is extremely large i.e. the "rearrangement" ion, m/z 152, is present but the "direct cleavage" ion, m/z 151, is essentially absent, while the ratio reverses in the CAD spectrum.

These results demonstrate that the m/z 152 ion in the LC/API spectrum cannot be due to decomposition of vibrationally excited MH^+, since that decomposition would have led to a low m/z 152/151 ratio. Thus the LC/API ion at m/z 152 is formed by a different mechanism, i.e. probably by the pyrolysis of M to M-C_2H_4Br followed by trimolecular hydrogen abstraction and later API protonation, see Results and Discussion. The large difference in the m/z 152 and 151 ion intensities between the LC/API and CAD spectra occurs only for the

bromo derivative. It is therefore this pair of spectra that provides the best additional confirmation of the other arguments presented in the Results and Discussion.

APPENDIX 5-IV. Experimental Parameters that Cause Uncertainties in Quantifying the Reaction Products with the Present LC/MS/MS Instrumentation.

1. *Sample solubility.* Water was selected as the solvent of choice since it gave acceptable concentrations for all the components of interest present in the reaction mixture.
2. *Low concentration components eluting next to very high concentration components.*

   (a) Under these conditions low concentration components, although they are partially separated by the column, cannot be detected by UV since they elute under the "tail" of the high concentration component.

   (b) Mass spectrometric detection is also affected under these conditions. When the high concentration component reaches the ion source, it dominates the ionization during its elution time interval, and some time past that, depending on its concentration. Analytes that elute within one minute or so after the high concentration component are suppressed in detection sensitivity due to proton competition in the ion source with this residual high concentration component. This introduces an uncertainty in quantifying such components in the reaction products. The eluate affected most by this problem is the hydroxy derivative which elutes only one minute after the "giant" guanine peak, R.T. = 7.2 min (see Figure 5.4A for corresponding example).

   (c) Alternative experiments that were performed to overcome this problem involved:

   (i) The API source under standard HPLC/MS conditions is "cleaned" by an air pump at a rate of ≈ 12 L/min. This air flow rate was increased to 30 L/min from the time of injection up to and including the elution of the high concentration component guanine with R.T. of 7.2 min (see UV chromatogram on Figure

5.4A). Once the high concentration peak has eluted the flow rate was reduced to 12 L/min and was maintained at that rate for the remainder of the HPLC/MS run.

Although this procedure improved the hydroxy derivative(s) results somewhat, it introduced an additional problem. While the source was pumped at 30 L/min for 8 min its temperature, and in general the interface temperature, was reduced by some 50°C. Since there are no methods presently available to keep the source temperature constant during this first 8 min, components eluting right after this time interval are exposed to a much cooler source than the ones eluting some 30 min after injection, when the source is very "hot" since it is continuously heated by the nebulizer (T_{NEB} = 535°C).

Because the sensitivity of the heated nebulizer/API interface is based mostly on the vapor pressure of the components analyzed, and since a relatively hot source is needed for optimum sensitivity, it follows from the procedure above that all components of the HPLC mixture are ionized by conditions which might be optimum for some of them but far from optimum for others.

(ii) A second approach was to connect the HPLC eluent to the heated nebulizer right after the high concentration guanine peak (at 7.2 min) had eluted. Although this procedure removed some of the guanine interferences on the hydroxy derivative peak, it introduced a high degree of signal intensity variation for this component between consecutive runs of the same mixture. This is because the heated nebulizer/API interface requires a minute or so to reach a stable operational condition, and therefore data collected during this time are not very reproducible. Since the hydroxy derivative(s) elute during this time the above procedure was not very effective for reliable quantitation of this mixture component.

(iii) A third approach was to use HPLC to pre-separate the components of interest from a particular sample, and then combine and analyze these eluates under HPLC/MS conditions. In this experiment 10 consecutive 100 μL injections of a

particular mixture were made at 0.8 mL/min flow rate and the 8 to 20 min eluent was collected in a single vial. Some 9.6 mL of solution (buffer and sample) was collected from the 10 injections. This volume was lyophilized and the resulting solid required some 500 μL of H_2O to be fully dissolved (most of the H_2O was needed to dissolve the NH_4Ac from the buffer). Then, 100 μL of this solution was injected for HPLC/MS analysis. Although this procedure removed a large part of the high concentration components (not important for this study), and although it increased the concentration of the components of interest by a factor of two in the injected volume, it was very time consuming and ineffective for improving the detection of the very low concentration components. This is a key point, since most, if not all, of the components of interest in the deuterated samples were of very low concentration. (**NOTE:** For samples involving products of reactions performed in the presence of KBr, when sample pre-separation was needed it was applied in two steps in order to minimize sample dilution. Since the retention time of the bromo derivative was some 30 min the eluent between 20 and 29 min was not collected (no components of interest elute during this time interval) and the 29 to 32 min eluent was combined with the 8 to 20 min one.)

3. *Coelution of isotopic components.* Analysis of the reaction products of dideuterated BFNU with guanosine have indicated that the hydroxy and the fluoro derivatives are present in more than one form, *i.e.*, non-deuterated and/or monodeuterated and/or dideuterated species. Since all these species elute under one peak in the present chromatographic conditions, HPLC/MS/MS analysis is essential for their separation and identification.

Although single ion monitoring of the pseudo molecular ions of the isotopes present under a single chromatographic peak is adequate to confirm their presence, in all cases MS/MS daughter ion spectra were obtained for all these isotopes and consequently their

structures were confirmed. MS/MS experiments provided the additional high resolution separation required for the isotopic species of a single component. However, when MS/MS data are to be used for quantitation, it is important that the parent ion is of high intensity (high concentration) greater than $\approx 5 \times 10^4$ cps in order to obtain reliable and reproducible data. Significant variations in intensities are observed for low intensity daughter ions when the parent ion intensity is low. In almost all deuterated reaction mixtures the intensities of the components of interest were lower than $\approx 5 \times 10^4$ cps (except the dideuterated fluoro derivative, m/z 200) which makes their quantitation difficult and not very reliable under HPLC/MS/MS conditions.

Another uncertainty in quantifying by HPLC/MS/MS experiments is reproducibility of the experimental conditions. In order to identify the three isotopes eluting under the same peak three experiments need to be performed. To assume that identical experimental conditions exist in all three cases, parameters such as API source temperature, level of impurity present in the source during elution of the component of interest, and nebulizer performance have to be identical. However, there are no easy ways to control and define those parameters and therefore a level of uncertainty will always be present when this HPLC/MS/MS procedure is applied for quantitation. Nevertheless, if the parent ion intensities of all isotopes eluting under a single peak are of acceptable count rate, then by applying procedures 2c(ii) and/or 2c(iii) (discussed above) to HPLC/MS/MS analysis of that particular sample, reliable quantitative data can be obtained.

For most samples, provided that the concentration conditions mentioned above are met, this technique can very effectively address quantitative analytical problems similar in nature to the ones encountered in the present study.

REFERENCES

1. Ludlum, D. B. In *Cancer, a Comprehensive Treatise*; F.F. Becker, F. F., Eds.; Plenum Press: New York, 1978; p 285.
2. Wheeler, G. P. A Review of Studies on the Mechanism of Action of Nitrosoureas; American Chemical Society Symp. Series No. 30; American Chemical Society: Washington, DC, 1976.
3. (a) Weinkam, S. J.; H-S Liu, H-S. *Adv. Pharmacol. Chemother.* **1982**, *19*, pp 1-33. (b) Hemminki, K.; Ludlum, D. B. *J. Natl. Cancer Inst.* **1984**, *73*, 1021. (c) Proceedings of the 7th New Drug Symp. on Nitrosoureas. In *Cancer Treat. Ref.* **1976**, *60*, 651.
4. (a) Brundrett, R. B.; Cowens, J. W.; Colvin, M. *J. Med. Chem.* **1976**, *19*, 1958. (b) Lown, J. W. In *New Approaches to the Design of Antineoplastic Agents*; Bardos, T. J., Kaslman, T. I., Eds.; Elsevier, 1982; p 61.
5. (a) Kohn, K. W. *Cancer Res.* **1977**, *37*, 1450. (b) Lown, J. W.; McLaughlin, L. W.; Chang, Y-M. *Bio-Org. Chem.* **1978**, *7*, 97. (c) Tong, W. P.; Ludlum, D. B. *Biochem. Pharmacol.* **1979**, *28*, 1135. (d) Tong, W. P.; Kirk, M. C.; Ludlum, D. B. *Cancer Res.* **1982**, *42*, 3102. (e) Gombar, C. T.; Tong, W. P.; Ludlum, D. B. *Biochem. Biophys. Res. Commun.* **1979**, *90*, 878. (f) Lown, J. W.; McLaughlin, L. W. *Biochem. Pharmacol.* **1979**, *28*, 1631. (g) Erickson, L. C.; Bradley, M. O.; Ducore, M. J.; Ewig, R. A. G.; Kohn, K. W. *Proc. Natl. Acad. Sci. USA* **1980**, *77*, 467.
6. Naghipur, A.; Ikonomou, M. G.; Kebarle, P.; Lown, J. W. *J. Amer. Chem. Soc.* (in press).
7. (a) Hartley, J. A.; Gibson, N. W.; Kohn, K. W.; Mattes, W. B. *Cancer Res.* **1986**, *46*, 1943. (b) Mattes, W. B.; Hartley, J. A.; Kohn, K. W. *Nucleic Acids Res.* **1986**, *14*, 2971. (c) Hartley, J. A.; Lown, J. W.; Mattes, W. B.; Kohn, K. W. *Acta Oncologica* **1988**, *27*, 503. (d) Kohn, K. W.; Hartley, J. A.; Mattes, W. B.

Biochem. Pharmacol. **1988**, *37*, 1799. (e) Briscoe, W. T.; Duarte, S. P. *Biochem. Pharmacol.* **1988**, *37*, 1061. (f) Wurdeman, R. L.; Gold, B. *Chem. Res. Toxicol.* **1988**, *1*, 146. (g) Richardson, K. K.; Richardson, R. C.; Crosby, R. M.; Swenberg, J. A.; Skopek, T. R. *Proc. Natl. Acad. Sci. USA* **1987**, *84*, 344. (h) Zarbl, H.; Sukumar, S.; Arthur, A. V.; Martin-Zanca, D.; Barbacid, M. *Nature* (London) **1985**, *315*, 382.

8. (a) Buckley, N. *J. Am. Chem. Soc.* **1987**, *109*, 7918. (b) Buckley, N. J. *Org. Chem.* **1987**, 52, 484. (c) Buckley, N.; Brent, T. P. *J. Am. Chem. Soc.* **1988**, *110*, 7520.
9. Pullman, A.; Pullman, B. *Q. Rev. Biophys.* **1981**, *14*, 289.
10. Covey, T. C.; Lee, E. D.;.Bruins, A. P; Henion, J. D. *Anal. Chem.* **1986**, *58*, 1451A.
11. Alexander, A. J.; Kebarle, P.; Fuciarelli, A. F.; Raleigh, J. A. *Anal. Chem.* **1987**, *57*, 2484.
12. Edmonds, G. C.; Vestal, M. L.; McCloskey, J. A. *Nucleic Acids Res.* **1985**, *13*, 8197.
13. Esmans, E. L.; Geboes, P.; Luyten, Y.; Alderweireldt, F. C. *Biomed. Mass Spectrom.* **1985**, *12*, 241.
14. (a) Henion, J. D.; Thomson, B. A.; Dawson, P. H. *Anal. Chem.* **1982**, *54*, 451. (b) Thomson, B. A.; Danylewych-May, L. In *Proceedings of the 31st ASMS Conference on Mass Spectrometry and Allied Topics*,1983, pp 852-53.
15. Crowther, J. B.; Covey, T. R.; Silvestre, D.; Henion, J. D. *LC Mag.* **1985**, *3*, 240-254. (b) Covey, T. R.; Lee, E. D.; Henion, J. D. *Anal. Chem.* **1986**, *58*, 2453.
16. Sakairi, M.; Kambara, H. *Anal. Chem.* **1988**, *60*, 774.
17. Ikonomou, M. G.; Hogg, A. M.; Alexander, A. J.; Kebarle, P. (in preparation).
18. (a) Sunner, J.; Nicol, G.; Kebarle, P. *Anal. Chem.* **1988**, *60*, 1300. (b) Sunner, J.; Ikonomou, M. G.; Kebarle, P. *Anal. Chem.* **1988**, *60*, 1308.

19. (a) Johnson, J. V.; Yost, R. A. *Anal. Chem.* **1985**, *57*, 758A-768A. (b) Dawson, P. H.; French, J. B.; Backley, J. A.; Douglas, D. J.; Simmons, D. *Org. Mass Spectrom.* **1982**, *17*, 212. (c) *Tandem Mass Spectrometry*; McLafferty, F. W., Ed.; Wiley: New York, NY,.1983.

20. (a) Whitehouse, C. M.; Dreyer, R. N.; Yamashita, M.; Fenn, J. B. *Anal. Chem.* **1985**, *57*, 675. (b) Bruins, A. P.; Covey, T. R.; Henion, J. D. *Anal. Chem.* **1987**, *59*, 2642. (c) Chapter 2. (Ikonomou, M. G.; Blades, A. T.; Kebarle, P. *Anal. Chem.* **1990**, *67*, 957).

21. (a) Wilson, M. S.; McCloskey, J. A. *J. Amer. Chem. Soc.* **1975**, *97*, 3436. (b) Crow, F. W.; Tomer, K. B.; Gross, M. L.; McCloskey, J. A.; Bergstorm, D. A. *Anal. Biochem.* **1985**, *139*, 243.

22. (a) Parker, S.; Kirk, M. C.; Ludlum, D. B.; Koganty P. R.; Lown, J. W. *Biochem. Biophys. Res. Commun.* **1986**, *139*, 31. (b) Nibbering, N. M. M. In *High Performance Mass Spectrometry: Chemical Applications*; American Chemical Society Symp. Series No. 70; Gross, M. L. Ed.; American Chemical Society: Washington, DC, 1978; p 80. (c) Theissling, C. B.; Nibbering, N. M. M.; Boer, Th.J. de. *Adv. Mass Spect.* **1971**, *5*, 642. (d) Venema, A.; Nibbering, N. M. M.; Boer, Th.J. de. *Org. Mass Spectrom.* **1970**, *3*, 583.

23. (a) Lown, J.W., Chauhan, S.M.S., Koganty, R.R., Sapse, A-M., *J. Am. Chem. Soc.* **1984**, *106*, 6401.

24. (a) Snyder, J.K., Stock, L.M., *J. Org. Chem.* **1980**, *45*, 1990. (b) Lown, J.W., Chauhan, S.M.S., *J. Org. Chem.* **1981**, *46*, 5309.

25. (a) Buckley, N., *J. Am. Chem. Soc.* **1987**, *109*, 7918. (b) Buckley, N., *J. Org. Chem.* **1987**, *52*, 484. (c) Buckley, N., Brent, T.P., *J. Am. Chem. Soc.* **1988**, *110*, 7520.

26. (a) Tong, W.P., Ludlum, D.B., *Biochem. Pharmacol.* **1979**, *28*, 1135.

CHAPTER 6

CONCLUDING SUMMARY

a. The ESP/MS Study (Chapter 2).

In recent years electrospray ionization has received considerable attention as an ionization technique for mass spectrometry. A distinguishing feature of electrospray ionization is its ability to produce multiply charged gas phase ions from biological molecules having molecular weights up to 130,000 (*1, 2*). Applications to date have demonstrated the extraordinary potential of the technique as an interface for CZE (*2*) and capillary LC to mass spectrometry (*3*).

Most of the ESP/MS work to date (*1-3*) has emphasized specific analytical applications, although important information concerning the method was also given. The aim in the present work was to obtain somewhat more general information concerning both the physicochemical aspects of the process itself and the applicability of the method to a wide range of analytes. Factors affecting the yield of positive ions in the gas phase from electrosprayed methanol solutions of some inorganic ions and some 30 organic onium ions BH^+ from nitrogen bases B, were studied with an atmospheric pressure triple quadrupole mass spectrometer. From these investigations the following features of the ESP process were realized:

When electrospray is operated in the positive ion mode, a partial separation of positive and negative ions of electrolytes present in the solution occurs near the capillary tip and the electrosprayed droplets contain excess positive ions. At low electrolyte concentrations, 10^{-5} M or less, the ion separation can be very efficient such that the positive ions exceed the negative ions by a factor of 2 (50% yield). The ion separation yield decreases as the electrolyte concentration is increased.

For alkali ions, Ca^{2+}, NH_4^+, and organic nitrogen bases BH^+, the efficiencies of emission of positive ions of the given kind, from the droplets into the gas phase, seem to be fairly similar.

When the total electrolyte concentration in the solution is less than 10^{-4} M extremely high analyte detection sensitivities can be obtained i.e. ions in the 10^{-9} - 10^{-7} M range can be easily

detected with the mass spectrometer. The detection limit for ions BH^+ in solution can be as low as 10^{-16} moles.

Because the positive ion-negative ion separation yield decreases as the total electrolyte concentration is increased, and the emission of ions from the droplets is relatively non-selective, ionic analyte detection sensitivities decrease with increasing total electrolyte concentration in the electrosprayed solution.

The sensitivities for organic nitrogen bases B are pH dependent i.e. the detected BH^+ ion signal is approximately proportional to the BH^+ concentration in solution. However these trends are obscured when high concentrations of external electrolyte are used for the pH control.

The residence time of the average electrosprayed gas phase ions in the atmospheric gas region is ~2 x 10^{-3} seconds. Ion-molecule reactions in the gas phase such as proton transfer to stronger gas-phase base coanalyte can occur in this region, and may degrade the sensitivity of the desired analyte. This effect is important only at high analyte or buffer concentrations.

The decrease of analyte ion sensitivity at high foreign electrolyte concentration may be considered as a weakness of the method, for reverse phase HPLC applications, where buffers in the 10^{-2} M range or higher are used in order to improve the separation. However, the very high sensitivity of ESPI, which allows analytes in the 10^{-9} - 10^{-5} M range to be easily detected, means that much smaller quantities of mixtures can be used in the LC separations and the buffer concentration can be dropped accordingly to 10^{-4} - 10^{-3} M levels, where its effect on the sensitivity will be small. Considering also the low effluent flow requirement, it becomes clear that ESPI shows its greatest promise for micro LCMS applications.

The present studies have provided additional information concerning features of ESP ionization and can be useful to both ESP/MS practitioners, and to researchers developing models for ESP ionization. The effect of liquid flow rate, ion concentration, and solvent properties on the ESP generated ion current predicted by two different dynamic models on

ESP ionization (*4, 5*) are in good agreement with the trends observed in the present investigation.

b. The ESP Versus Ion Spray study (Chapter 3).

Similar systematic studies of the type performed for ESP were also performed with Ion Spray (pneumatically assisted ESP). The trends observed were similar with both spray systems. Differences between the two techniques depend mostly on their operational characteristics. For a specific application, one can choose between the two on the basis of their performance according to the requirements of the application. Properly tuned Ion Spray provides equally good and, at times depending on operational conditions, better analyte signal stability and sensitivity relative to electrospray. The pressure of 60 psi, the 5.5 kV voltage at 4 cm tip-counter electrode distance, and ≈1.5 cm off center appear to be the optimum settings for maximum analyte signal stability and sensitivity.

The large ion currents observed with Ion Spray and electrospray are due to charge separation induced by the field at the tip when the capillary is exposed to high voltages. High yields of positively charged droplets and gas phase ions $\approx 10^{-7}$ A are produced under optimal conditions. With ESP ion production quits below a certain field gradient while Ion Spray still produces ions even when there is no field between the sprayer and the counter electrode. Droplet charging, and thus ion formation, in this case is probably due to statistical charging which could be induced by nebulization alone (*4d, 6, 7*). Although Ion Spray can produce ions in the absence of any field, this mode of operation is of limited analytical significance since the analyte related ion signals are of very low sensitivity.

Ion Spray-generated ions have higher velocities in the z-direction, relative to electrospray, due to the nebulization gas current. This overcomes sensitivity limitations due to space charge and allows for higher total ion currents to be sampled via the mass spectrometer's ion sampling orifice, i.e. the atmospheric pressure vacuum interface.

Results from specially designed experimental setups, Ion Spray B and C type configurations, indicated that charge separation under zero-field conditions, nebulization only, takes place at the sprayer's tip and not during the droplets flight.

c. Multiply Charged Metal-Ion-Ligand Complexes, $M^{+z}(L)_n$, Produced in the Gas Phase by ESP Ionization (Chapter 4).

Hydrates and many other metal ion-ligand complexes of doubly ($M^{2+}(L)_n$) and triply ($M^{3+}(L)_n$) charged metal ions can be produced by electrospray ionization and detected by mass spectrometry, where M = (Mg, Ca, Sr, Ba, Mn, Fe, Co, Ni, Cu, Zn, Y, La, Ce, Nd, and Sm). The Ligand L may be added to the electrosprayed solution or to the gas phase, i.e. electrospray, chamber.

When the second ionization energy of the M^{II} is higher than ~18 eV, and higher than ~23 eV for the M^{III} respectively, the charge reduced species are generated instead. Changing the nature of the ligand may increase the stability of the M^{2+} and/or M^{3+} towards charge reduction and visa versa. For example, NH_3 and pyridine accelerate charge reduction relative to H_2O while dipolar aprotic molecules like DMSO, and DMF delay it. Multidentate polycyclic ligands with suitable cavities to accommodate the triply charged ion lead to triply charged species even when the third ionization energy is as high as 34 eV. Proper selection of ligands and experimental conditions can provide good sensitivity and specificity for metal detection. Although the results so far are mostly qualitative, they are of considerable interest. The preference of different ligands for different metals, and the variety of clusters formed, adds an additional dimension to the specificity of the technique, especially when tandem mass spectrometry is utilized for detection. Systematic studies are now underway in Kebarle's laboratory exploring the analytical potential of this technique for detection of metal ions.

The results described here also illustrate the extensive studies of the gas phase ion chemistry of M^{2+} ions that are possible with $M^{2+}(L)_n$ produced by electrospray and mass spectrometric apparatus of the type used. The energetics of the ligand binding can be studied in three regimes. At high n where the binding energies are less than ~25 kcal/mol, studies of

ion-ligand equilibria in the interface chamber can permit deduction of the energies. For lower n, energy thresholds determined by CID as a function of center-of-mass kinetic energy with the triple quadrupole, are expected to provide the data. At low n charge reduction occurs. The charge reduction reactions themselves are of interest. Estimates of the average ligand binding energies to M^{2+} can be obtained even below the charge reduction limit by CID experiments and thermochemical cycles (*8*).

d. The Combined HPLC/MS/MS Study (Chapter 5).

The products of the reaction of the anticancer agent 1,3-bis(2-fluoroethyl)-1-nitrosourea (BFNU), and of BFNU-1,1,1',1'-d_4, with the DNA base deoxyguanosine, were characterized by HPLC/MS/MS. The total effluent from the HPLC column was introduced into the API source of the triple quadrupole mass spectrometer via a heated nebulizer. The gasified mixture produced from the heated nebulizer was exposed to corona discharge ionization which led to ions generated by gas phase chemical ionization. The present study provides a demonstration of the unique capability of the present HPLC/API-MS technique when used for the identification of minor nonvolatile components of interest, present in complex mixtures. Sensitive detection (pmol to nmol range) of 7-(2'-haloethyl)guanines has been demonstrated. LC/API mass spectra of these guanine derivatives were seen to provide intense pseudo-molecular ion peaks and a number of intense fragment ion peaks. Fragment ions obtained from the LC/API-MS analysis alone provide significant structural information and permit identification of most of the species of interest. In cases where MS/MS was employed, additional fragmentation (not available in the LC/API spectra) was observed which was essential for structural elucidation of the components of interest. However loss of sensitivity associated with the MS/MS technique constrained CID data acquisition to cases where the parent ion was of relatively high abundance.

The results obtained from the HPLC/API-MS and HPLC/MS/MS analysis of the products of reactions **1** to **8** (Table 5.1) provided means for discrimination between some alternative mechanisms of DNA base modification by clinical anticancer alkylators (HENU's).

A mechanism that involves a molecular rearrangement during formation of the critical lesions 7-(2'-fluoroethyl)guanosine and 7-(2'-hydroxyethyl)guanosine proceeding via a diazoalkane intermediate has been proposed (*9*).

REFERENCES

1. Fenn, J.B.; Mann, M.; Meng, C.K.; Wong, S.F.; Whitehouse, C.M. *Mass Spectrom. Rev.* **1990**, *9*, 37.
2. Smith, R.D.; Loo, J.A.; Edmonds, C.G.; Barinaga, C.J.; Udseth, H.R. *Anal. Chem.* **1990**, *62*, 882.
3. (a) Bruins, A.P.; Covey, T.R.; Henion, J.D. *Anal. Chem.* **1987**, *59*, 2642. (b) Conboy, J.J.; Henion, J.D.; Martin, M.W.; Zweigenbaum, J.A. *Anal Chem.* **1990**, *62*, 800.
4. (a) Pfeifer, R.J.; Hendricks, C.D. *AIAA Journal* **1968**, *6*, 496. (b) Pfeifer, R.J.; Hendricks, C.D. *The Phys. of Fluids* **1967**, *10*, 2149. (c) Hendricks, C.D. *J. Colloid Sci.* **1962**, *17*, 249. (d) Hendricks, C.D. "Charging Macroscopic Particles". *In Electrostatics and Applications*; Moore, A.D., Ed.; John Willey: New York, **1973**.
5. Juhasz, P.; Kebarle, P. *Int. J. Mass Spectrom. Ion Proc.* (in press).
6. Loeb, L.B. *Science* **1945**, *102*, 573.
7. (a) Iribarne, J. V.; Thomson, B. A. *J. Chem. Phys.* **1976**, *64*, 2287. (b) Thomson, B. A.; Iribarne, J. V. *J. Chem. Phys.* **1979**, *71*, 4451. (c) Iribarne, J. V.; Dziediz, P. J.; Thomson, B. A. *Int. J. Mass Spectrom. Ion. Phys.* **1983**, *50*, 331.
8. Jayaweera, P.; Blades, A. T.; Ikonomou, M. G.; Kebarle, P. *J. Am. Chem. Soc.* **1990**, *112*, 2452. (b) Blades, A. T.; Jayaweera, P.; Ikonomou, M. G.; Kebarle, P. *J. Chem. Phys.* **1990**, *92*, 5900. (c) Blades, A. T.; Jayaweera, P.; Ikonomou, M. G.;Kebarle, P. *Int. J. Mass Spectrom. Ion Proc.* (in press). (d) Blades, A. T.; Jayaweera, P.; Ikonomou, M. G.;Kebarle, P. *Int. J. Mass Spectrom. Ion Proc.* (in press).
9. Naghipur, A.; Ikonomou, M. G.; Kebarle, P.; Lown, J. W. *J. Amer. Chem. Soc.* 1990, *112*, 3178.